MICROCOPY RESOLUTION TEST CHART

NATIONAL BUREAU OF STANDARDS-1963-

AFAL-CP-87-003   AD:

DTIC FILE COPY

Conference Proceedings for the period 8 January 1987 to 9 January 1987
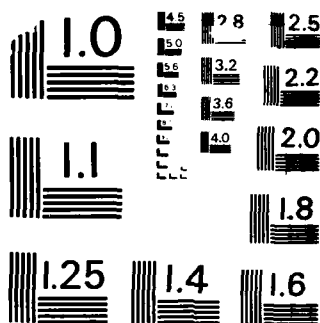
Proceedings of the Cooling, Condensation, and Storage of Hydrogen Cluster Ions Workshop

December 1987   Author:
                       Dr. J. T. Bahns

DTIC
ELECTE
MAR 1 5 1988
S   D
α-D

Approved for Public Release

AD-A189 857

Air Force Astronautics Laboratory

Air Force Space Technology Center
Space Division, Air Force Systems Command
Edwards Air Force Base,
California 93523-5000

88 3 15   026
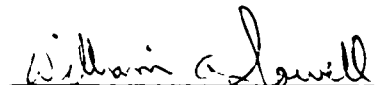
NOTICE

FOREWORD

This is the conference proceedings of the Cooling, Condensation, and Storage of Hydrogen Cluster Ions Workshop held 8-9 January 1987 at SRI International, Menlo Park, CA.

This conference proceedings has *been reviewed* and is approved for distribution in accordance with the the distribution statement on the cover and on the DD Form 1473.

WILLIAM A. SOWELL, CAPT, USAF
Project Manager

FOR THE COMMANDER

ROBERT C. CORLEY
Chief, ARIES Office

REPORT DOCUMENTATION PAGE

1a. REPORT SECURITY CLASSIFICATION Unclassified		1b. RESTRICTIVE MARKINGS *A189 857*
2a. SECURITY CLASSIFICATION AUTHORITY		3. DISTRIBUTION/AVAILABILITY OF REPORT Approved for public release. Distribution is unlimited.
2b. DECLASSIFICATION/DOWNGRADING SCHEDULE		

4. PERFORMING ORGANIZATION REPORT NUMBER(S)	5. MONITORING ORGANIZATION REPORT NUMBER(S)

6a. NAME OF PERFORMING ORGANIZATION University of Dayton Research Institute	6b. OFFICE SYMBOL (If applicable)	7a. NAME OF MONITORING ORGANIZATION Air Force Astronautics Laboratory
6c. ADDRESS (City, State and ZIP Code) Dayton, Ohio		7b. ADDRESS (City, State and ZIP Code) Edwards AFB, CA 93523-5000

8a. NAME OF FUNDING/SPONSORING ORGANIZATION	8b. OFFICE SYMBOL (If applicable)	9. PROCUREMENT INSTRUMENT IDENTIFICATION NUMBER

8c. ADDRESS (City, State and ZIP Code)	10. SOURCE OF FUNDING NOS.			
	PROGRAM ELEMENT NO.	PROJECT NO.	TASK NO.	WORK UNIT NO.
11. TITLE (Include Security Classification) Proceedings of the Cooling, Condensation, and Storage of Hydrogen Cluster Ions	61101F	2301	MI	RB

12. PERSONAL AUTHOR(S) Dr J. T. Bahns

13a. TYPE OF REPORT Conference Proceedings	13b. TIME COVERED FROM 87/1/8 TO 87/1/9	14. DATE OF REPORT (Yr., Mo., Day) 87/12	15. PAGE COUNT 331

16. SUPPLEMENTARY NOTATION

17. COSATI CODES			18. SUBJECT TERMS (Continue on reverse if necessary and identify by block number)
FIELD	GROUP	SUB. GR.	Cluster Ions, Hydrogen Cluster Ions, Antimatter, HEDM,
07	02		Antihydrogen, Propulsion, Ion Traps, Ion Cooling,
07	04		Containerless condensation

19. ABSTRACT (Continue on reverse if necessary and identify by block number)

The Cooling, Condensation, and Storage of Hydrogen Cluster Ions Workshop (CCSHCI) was held 8-9 January 1987 at SRI International, Menlo Park, CA. This workshop was conducted in order to explore the critical issues involving the "containerless" condensation of hydrogen cluster ions. The papers presented covered the areas of cluster ions, ion traps, and laser cooling.

20. DISTRIBUTION/AVAILABILITY OF ABSTRACT UNCLASSIFIED/UNLIMITED ☒ SAME AS RPT. ☐ DTIC USERS ☐	21. ABSTRACT SECURITY CLASSIFICATION Unclassified
22a. NAME OF RESPONSIBLE INDIVIDUAL WILLIAM A. SOWELL, Capt, USAF	22b. TELEPHONE NUMBER (Include Area Code) (805) 275-5561
	22c. OFFICE SYMBOL CX

DD FORM 1473, 83 APR   EDITION OF 1 JAN 73 IS OBSOLETE.

Table of Contents

Cooling and Trapping

Appendix

Preface

My personal involvement in the field of antimatter research began in late 1985 when I was asked to study the problem of laser cooling H_2, the intent being to use laser cooled molecules for growing large crystals of antihydrogen "ice". This approach was recently proposed by R. Forward (1) who was aware of a multitude of condensation pathways starting with antiprotons and positrons, that lead to bulk antimatter. In studying this problem, it soon became apparent that laser cooling molecules would be a rather difficult task that perhaps outweighed its own justification since there had been no studies performed to answer the question of how best to assemble, condense, and store antimatter in a convenient form.

In late December '85, while deliberating with W. C. Stwalley at the Iowa Laser Facility, the notion of using hydrogen cluster ions was first discussed. In the months that followed (containing numerous lengthy conversations with C. W. Larson), the feasibility of a "cluster ion approach" seemed to increase.

During June-July '86, the (UD sponsored) Hydrogen Cluster Ion Study Group (HCISG) (see appendix) solicited the help of Stwalley, Sando, and Tardy in further analyzing this approach. It was due to the highly enthusiastic efforts of this small study group, that many of the critical issues involving the "containerless" condensation of hydrogen cluster ions first came into focus. It also became clear that due to the diverse nature of the cluster ion approach, a much more rigorous analysis would be needed. It was recommended that a workshop encompassing the fields of cluster ions, ion traps, and laser cooling, be held that would further develop these ideas.

The Cooling, Condensation, and Storage of Hydrogen Cluster Ions Workshop (CCSHCI) came about as a result of the preliminary analysis done by the HCISG. For two days 18 participants and 23 invited guests reviewed those things (in the areas of cluster ions, ion traps, and laser cooling) which are known and relevant to the problem. They have also considered what needs to be known such that some of the many fascinating applications of antimatter may soon become a reality. There were numerous creative ideas presented by the participants and voluntary speakers that stimulated many a lively discussion.

Certain working assumptions have been made at the onset. With regard to the "Cluster Ion Approach" it was assumed that unlimited quantities of antiprotons, positrons, photons, anti-H atoms (and possibly molecules), will be available . . . and that we can perform the synthesis of hydrogen cluster ions under the well confined conditions of trap-like devices that use electric and/or magnetic fields to confine particles that are either charged or have an appreciable magnetic moment. Photons are preferred as third bodies. It was generally agreed by the participants that we refer to "normal" matter when communicating ideas.

1. Forward, R., Antimatter Annihilation Propulsion, AFRPL Special Report, F04611-83-C-0046/UDR-TR-55, September 1985.

J. T. Bahns -April 1987

Participants

Dr. John T. Bahns
University of Dayton Research Institute
AFAL/LKCS
Edwards AFB, Ca. 93523-5000   805-275-5656

Prof. Michael T. Bowers
Department of Chemistry
University of California
Santa Barbara, Ca. 93106   805-961-2893

Dr. Mark Crofton
C/O Charles Stevens
Bldg. 222 L329/1216
Lawrence Livermore Laboratories
7000 East Ave.
Livermore, Ca. 94550   415-422-0961

Dr. Robert L. Forward
Hughes Research
3011 Malibu Canyon Road
Malibu, Ca. 90265   213-317-5280

Prof. Gerald Gabrielse
Physics Department FM-15
University of Washington
Seattle, Wa. 98195   206-545-2401

Dr. Hanspeter Helm
Molecular Physics Dept.
SRI International
333 Ravenswood Ave.
Menlo Park, Ca. 94025   415-859-4637

Prof. William A. Lester Jr.
Lawrence Berkeley Laboratories
Mail Code 50D106
#1 Cyclotron Road
Berkeley, Ca. 94720   415-486-6722

Prof. Richard Lovelace
Applied and Engineering Physics
237 Clark Hall
Cornell University
Ithaca, N.Y. 14853   607-255-3968

Prof. Thomas J. McIlrath
Institute for Physical Science and Technology
IPST Building
University of Maryland
College Park, Md. 20742   301-454-4843

Prof. H. Harvey Michels
United Technologies Research Center
MS/72
East Hartford, Conn. 06108   203-727-7000 ext. 7489

Prof. J. Brian A. Mitchell
Department of Physics
University of Western Ontario
London, Ontario N6A3K7   519-661-2192 ext. 6448

Dr. William D. Phillips
Building 220
Room B258
NBS
Washington, DC 20234   301-975-6554

Dr. Roberta P. Saxon
PN093
SRI International
333 Ravenswood Ave.
Menlo Park, Ca. 94025   415-859-2663

Prof. Henry F. Schaefer III
Department of Chemistry
237 Hildebrand
University of California
Berkeley, Ca. 94720   415-642-1957

Prof. William C. Stwalley
Iowa Laser Facility
Department of Chemistry
University of Iowa
Iowa City, Ia. 52242   319-335-1299

Prof. John Weiner
Chemistry Department
University of Maryland
College Park, Md. 20742   301-454-6094

Dr. David J. Wineland
Time and Frequency Standards Group 524.11
National Bureau of Standards
325 Broadway
Boulder, Colo. 80303   303-497-5286

Lisa Yeh
Giaugue BG3
Department of Chemistry
University of California
Berkeley, Ca. 94720   415-486-5741

Invited Guests

Dr. Y. K. Bae
Molecular Physics Laboratory
SRI International
333 Ravenswood Ave.
Menlo Park, Ca. 94025
415-859-3814

Dr. R. Becker
University of Dayton Research Institute
KL 462
300 College Park
Dayton, Oh. 45469
513-229-3964

Dr. D. Coon
Microtronics Associates
4516 Henry St.
Pittsburgh, Pa. 15213
412-624-1727

Dr. R. Corley
AFAL/CX
Edwards AFB, Ca. 93523-5000
805-275-5623

Dr. P. C. Cosby
Molecular Physics Laboratory
SRI International
333 Ravenswood Ave.
Menlo Park, Ca. 94025
415-859-5128

Dr. D. R. Crosley
Molecular Physics Laboratory
SRI International
333 Ravenswood Ave.
Menlo Park, Ca. 94025
415-859-2395

Prof. G. Dunn
JILA
University of Colorado
Boulder, Colo. 80309-0440
303-492-7824

Prof. L. Friedman
Department of Chemistry
Brookhaven National Labs.
Upton, N.Y. 11973
516-282-4301

Dr. G. Gerber
University of Dayton Research Institute
300 College Park
Dayton, Oh. 45469-0001
513-229-3221

Dr. V. Haloulakos
McDonnell Douglas
Huntington Beach, Ca.
714-896-3456

Dr. D. L. Huestis
Molecular Physics Laboratory
SRI International
333 Ravenswood Ave.
Menlo Park, Ca. 94025
415-859-4637

Prof. T. Kalogeropoulos
Department of Physics
Syracuse University
Syracuse, N.Y. 13244-1130
315-423-3158

Prof. D. D. Konowalow
Science II
Room 241
State University of New York
Binghamton, N.Y. 13901
607-777-6788

Dr. C. W. Larson
University of Dayton Research Institute
AFAL/DYCRL/MS24
Edwards AFB, Ca. 93523-5000
805-275-5656

Dr. D. C. Lorents
Laboratory Director
Chemical Physics Laboratory
SRI International
333 Ravenswood Ave.
Menlo Park, Ca. 94025
415-859-3167

Dr. R. McFarlane
Quantum Electronics Division
Hughes Research
3011 Malibu Canyon Road
Malibu, Ca. 90265
213-317-5445

Dr. F. Mead
AFAL/LKCS/MS24
Edwards AFB, Ca. 93523-5000
805-275-5540

Prof. C. B. Moore
Department of Chemistry
B45 Hildebrand
University of California
Berkeley, Ca. 94720
415-642-6000

Maj. G. Nordley
AFAL/CX
Edwards AFB, Ca. 93523-5000
805-275-5653

Dr. E. Ottewitte
Idaho National Engineering Laboratories
P. O. Box 1625
Idaho Falls, Idaho 83401
208-526-1751

Dr. J. R. Peterson
Molecular Physics Laboratory
SRI International
333 Ravenswood Ave.
Menlo Park, Ca. 94025
415-859-6200

Maj. J. Prince
AFOSR/NP
Bolling AFB, DC 20332
Autovon 297-4908
202-627-5351

Mr. W. Roe
AFAL/XRX
Edwards AFB, Ca. 93523-5000
805-275-5206

Maj. W. Seward
AFWAL/Peoc-3
Wright-Patterson AFB, Oh. 45433
513-255-2923

Capt. W. Sowell
AFAL/CX
Edwards AFB, Ca. 93523-5000
805-275-5651

Dr. R. S. Turley
Hughes Research
3011 Malibu Canyon Road
Malibu, Ca. 90265
213-317-5622

Proceedings
of the
Cooling, Condensation, and Storage of Hydrogen Cluster Ions
Workshop

Sponsored by
The University of Dayton Research Institute

Conducted at
S R I International
Menlo Park, Ca.
January 8 & 9, 1987

Editor
J. T. Bahns

J. T. Bahns

Introduction to the Workshop on Cooling, Condensation, and Storage
of Hydrogen Cluster Ions

Introduction
to the
Workshop on Cooling, Condensation, and Storage of
Hydrogen Cluster Ions

J. T. Bahns

(University of Dayton Research Institute)
AFAL/LKCS/MS24
EAFB, Ca. 93523-5000

The central question addressed by the "cluster ion approach" is how to go from antiprotons and positrons (with negligible kinetic) to something resembling bulk antimatter (or having high energy density). There are a number of potential solutions that we are aware of: trapping H atoms in magnetic traps (1-3) (see Lovelace's report) or as spin polarized atoms (4-6); interstitial enrichment of "normal" crystalline matter with antiprotons (in naturally occurring lattice defect-ion traps) (7-8); growing crystals of hydrogen "ice" from laser-cooled hydrogen molecules (9) (see also Forward's report in these proceedings); and the growth and confinement of hydrogen cluster ions (see appendix for the Proceedings of the HCISG). Each approach has its own set of merits and disadvantages. This paper will briefly review the current status of the "cluster ion approach."

Advantages

Cluster ions are preferred as the basic form for antimatter storage for the following reasons:

1. Chemical stability: Cluster ions have binding energies that greatly exceed that of uncharged hydrogen due to the ion-induced dipole force. This higher stability is manifested as a lowering of the vapor pressure (relative to the neutral bulk solid). Hence, the constraint of low temperature is not as critical as it would be with uncharged hydrogen.

2. Easy confinement and manipulation with E & M fields: The fact that ions interact strongly with electric and magnetic fields makes them relatively easy to trap, transport, and store.

3. Large sizes: Hydrogen cluster ions (normal matter) have been produced in the laboratory with mass/charge ratios exceeding 10^6. Closely related to this advantage is the fact that stable multiply charged cluster ions may also be prepared. For example, the dipositive hydrogen clusters have been accurately calculated to exist for masses above 900 (stable tripositive ions above mass 2900) (10).

4. Radiative cooling: Hydrogen cluster ions have an extensive infrared spectrum allowing them to radiatively cool ground state internal degrees of freedom much faster than corresponding uncharged clusters.

5. Low susceptibility to accidental annihilation: Because large cluster ions can be dynamically stored and have relatively small physical dimensions, they are less susceptible to fragmentation by unavoidable background gas annihilation. It is important to consider the consequences of normal background gas annihilation on the surface of a cluster ion. If the cluster ions fragment, an avalanche could result. From known annihilation cross sections however, the high-energy products of surface annihilation on a cluster ion should just pass through the cluster and annihilate elsewhere.

6. Ion trap advantages: The use of well known ion trap technology (known for >30 yrs) should allow for relatively easy manipulation of cluster ions. Being well understood, the design of a wide variety of hybrid ion trapping structures should be possible. Some specific advantages (and flexibilities) are:

        a. Very low energy requirements for operation and storage,
        b. High vacuum compatibility,
        c. Deepest trap depths and longest confinement times,
        d. Numerous cooling techniques already demonstrated (e.g. resistive, sympathetic, and optical side band),
        e. Light weight.

7. Ion-molecule/atom association: Growth of cluster ions via ion-neutral association is desirable because of the large cross sections (>100 A^2).

Disadvantages

Because of coulomb repulsion between cluster ions, there is a limit (referred to as the space-charge limit) to the density of stored cluster ions that can be achieved (about 10^7-10^{10} ions/cm^3). It is

worth noting, however, that the use of large cluster ions may circumvent this disadvantage in two ways. First, the use of very large cluster ions ($>10^7$) would still result in high energy density even though the ion density is low. Second, the storable density of cluster ions should increase with increasing cluster ion mass to charge ratio (see discussion in appendix, p 14 &16).

Due to the space charge limit, the expected association rates in the gas phase will likely be small. Association rates have been estimated to be less than 10^5 cm^{-3} s^{-1} for the smallest cluster ions. However, these rates can (in principle) be improved by utilizing large volumes and/or large cluster ions. To overcome limitations stemming from the space charge limit, large volume storage will likely be needed. At the present time ion traps seem to be scalable to large volumes (see Wineland's report in these proceedings).

Association Channels

It is important to realize that "containerless" or "collisionless" condensation is a relatively new idea that has (until now) been without application. Three association channels have been identified for the buildup of large hydrogen cluster ions (see Stwalley's report(s) in these proceedings). Only the positive hydrogen cluster ions are worth considering due to predicted instabilities in the small negative clusters (see report by Michels). Ion atom association (A^+),

$$H_n^+ + H = H_{n+1}^+ + h\nu,$$
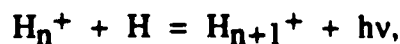
is the most desirable because it *avoids* the use of H_2. However, it may not work with the even numbered cluster ions (explained below). H_2 dimers present serious difficulties in terms of production yields, cooling of internal energy, and manipulation (or trapping) (see reports by Sando and Weiner). The threshold cluster size for this path is not known; calculations are currently underway to determine if it can be applied to the production of small clusters ($n<11$). Ion molecule association (M^+),
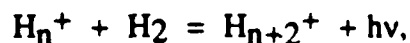
$$H_n^+ + H_2 = H_{n+2}^+ + h\nu,$$

is expected to work well for clusters above the threshold cluster size at approximately mass 29 (see Tardy's report in the appendix). The

remaining path (A^+/M^+) uses repeated alternate applications of A^+ and M^+,

a. (A^+) $H_n^+(\text{odd}) + H = H_{n+1}^+ (\text{even}) + h\nu$

b. (M^+) $H_{n+1}^+(\text{even}) + H_2 = H_{n+2}^+(\text{odd}) + H,$

depending on whether the cluster contains an even or odd number of protons. The second step (b), in going from an even to an odd cluster, is the most problematic since approximately 4.5 eV would be released into the nascent cluster ion should it be attempted via the A^+ method. This difficulty can be removed by using the M^+ process, but at the expense of having to deal with H_2.

The overall "containerless" condensation process is assumed to take place within the confines of ion trap-like devices at relatively low temperatures (<4 K) and in near perfect vacuums ($<10^5 \text{ cm}^{-3}$). The "cluster ion" approach seems valid thus far under scrutiny and is the only comprehensive plan known for the condensation of antimatter into a high energy-density form that uses current (or near term) technology. Current research is aimed at the "bottle neck" region, involving the production of the small clusters. The possibility of performing the condensation utilizing radiative association (stimulated and spontaneous) is given priority (i.e. photons preferred as third bodies). It is plausible that once sufficiently large (n>1000?) clusters have been prepared, many of the difficulties (e.g. association rates, fragmentation etc.) will tend to go away. Clustering about D^+, He^+, and heavier ions is a possibility (with some advantages) that is currently being analyzed in detail (see also Forward's report on heavy antinuclei). The difficult task of building up large cluster ions however will only need to be done once provided that the "seed" clusters are always kept for subsequent growth cycles.

References

1. Lovelace R. V. E., Mehanian C., Tommila T. J., and Lee D. M., "Magnetic Confinement of a Neutral Gas," Nature 318, 30-36 (1985).

2. Migdall A. L., Prodan J. V., Phillips W. D., Bergeman T. H., and Metcalf H. J., "First Observation of Magnetically Trapped Neutral Atoms," Phys. Rev. Lett. 54, 2596 (1985).

3. Wing W. H., "Electrostatic Trapping of Neutral Atomic Particles," Phys. Rev. Lett. 45, 631 (1980).

4. Sprik R., Walraven J. T. M., and Silvera I. F., "Compression of Spin-Polarized Hydrogen to High Density," Phys. Rev. Lett. 51, 479 (1983).

5. Hess H. F., Bell D. A., Kochanski G. P., Cline R. W., Kleppner D., and Greytak T. J., "Observation of Three-Body Recombination in Spin-Polarized Hydrogen," Phys. Rev. Lett. 51, 483 (1983).

6. Stwalley W. C., "A Hybrid Laser-Magnet Trap for Spin-Polarized Atoms," Prog. Quant. Electr. 8, 203 (1984).

7. Auret F. D., Leitch A. W. R., and Vermaak J. S., "A Deep Level Transient Spectroscopy Analysis of Electron and Hole Traps in Bulk-Grown GaAs," J. Appl Phys. 59, 158 (1985).

8. Nauka K., Goorsky M. S., Gatos H. C., and Lagowski J., "Nitrogen-Related Deep Electron Traps in Float Zone Silicon," Appl. Phys. Lett. 47, 1341 (1985).

9. Forward R. L., "Antiproton Annihilation Propulsion," AFRPL Special Publication, F04611-83-C-0046/UDR-TR-85-55, Sept. 1985.

10. Echt O., Casero R., and Soler J. M., private communication.

Robert L. Forward

Prospects for Antiproton Production and Propulsion

PROSPECTS FOR ANTIPROTON PRODUCTION AND PROPULSION

Robert L. Forward
Hughes Research Laboratories, Malibu, CA 90265

ABSTRACT

Antiproton annihilation propulsion is a new form of space propul-
sion, where milligrams of antiprotons in the form of frozen
crystals of antihydrogen are used to heat tons of reaction fluid
to high temperatures. The hot reaction fluid is exhausted from a
nozzle to produce high thrust at high exhaust velocity. This
paper summarizes the results of a continuing study to determine
the physical, engineering, and economic feasibility of antiproton
annihilation propulsion. The conclusion of the study to date is
that antiproton propulsion is feasible, but expensive. Because
the low mass of the antihydrogen fuel and its storage container
more than compensates for the high price of antiprotons, compara-
tive mission studies show that antihydrogen fuel can be cost
effective in space, where even normal chemical fuel is expensive
because its mass must be lifted into orbit before it can be used.
Antiprotons are already being generated, captured, cooled, and
stored at a number of particle physics laboratories around the
world, albeit in small quantities. This paper outlines some
ideas for improving the generation efficiency of antiprotons and
describes techniques for the cooling, trapping, long-term
storage, and effective utilization of milligram quantities of
antihydrogen for space propulsion. Converting the antiprotons
into antihydrogen is a non-trivial problem. One of the more
promising techniques involves the use of hydrogen cluster ions.
Since the formation of (anti)hydrogen from (anti)protons and
(anti)electrons through the cluster ion process will be the
subject of the rest of the papers in this workshop, it will not
be addressed in this paper.

INTRODUCTION AND SUMMARY

In antiproton annihilation propulsion, milligrams of antihydrogen
will be used to heat tons of reaction fluid to high temperatures.
The hot reaction fluid will then be exhausted from a nozzle to
produce high thrust at high exhaust velocity (100 to 350 km/s).
Antiprotons are the preferred form of antimatter for propulsion.
Unlike antielectrons (positrons), antiprotons do not completely
convert into gamma rays upon annihilation. Instead, two-thirds
of the annihilation energy is emitted as charged particles
(pions) whose kinetic energy can be converted into thrust by
interaction with a magnetic field nozzle or a working fluid.

Picogram quantities of antiprotons are already being generated,
captured, cooled, and stored in magnetic storage rings at a
number of particle physics laboratories around the world. The
facility at CERN in Switzerland[1] has been producing picograms of
antiprotons per day since 1982. The facility at Fermilab in the
USA[2] came on line in 1985, but there are no plans to decelerate

the antiprotons to subrelativistic energies. The facility at IHEP in Novosibirsk, USSR[3,4] is still in the planning stage.

As is shown in Figure 1, normal matter protons are accelerated to relativistic velocities in a proton synchrotron accelerator until their kinetic energy (26 to 120 GeV) is many times greater than their rest mass energy (1 GeV). The high energy proton beam is sent into a heavy metal target where the kinetic energy is converted into a spray of photons and particle-antiparticle pairs, a small fraction (<5%) of which are proton-antiproton pairs. A fraction (<30%) of the relativistic antiprotons (3 to 50 GeV) are at a small enough angle to be brought to a focus by a magnetic focusing lens. Of these, a very small fraction (<1%) have the proper momentum to be captured by a magnetic ring. The pulses of captured antiprotons are debunched and cooled using rf fields, then decelerated to subrelativistic energies (<50 to 300 MeV) where they are further cooled, accumulated, and stored for hours or days at a time until they are needed for high energy proton-antiproton collision experiments or low energy antiproton annihilation experiments.
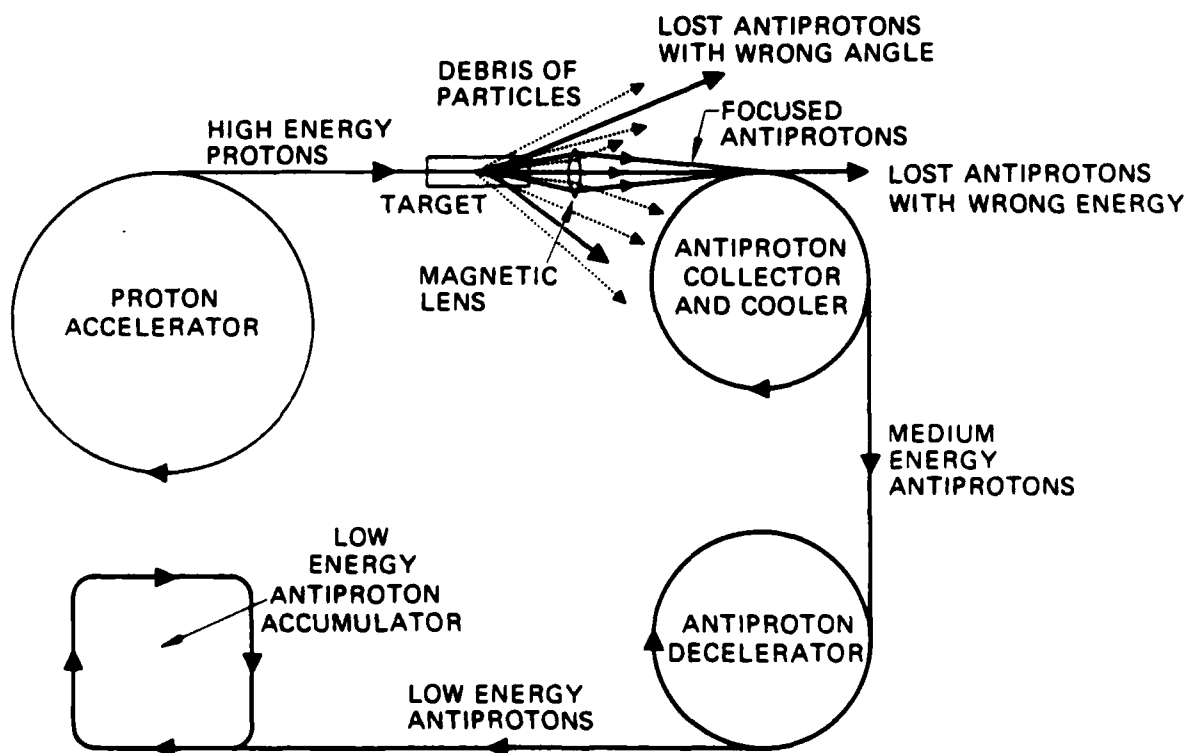
Fig. 1. Present method for collecting antiprotons.

We will assume the reader is aware of this ongoing work on the production of antiprotons at the various particle physics laboratories around the world. In this paper we will concentrate on the less well known techniques for using antiprotons for propulsion, improving the antiproton production efficiency from picograms per day to milligrams per day, briefly discuss the problems of turning the antiprotons into antihydrogen, and then show how the antihydrogen can be held for long periods of time in relatively compact storage traps until ready for use.

ANTIHYDROGEN PROPULSION

It has long been realized that antimatter would be a valuable propulsion energy source because it allows for the complete conversion of mass to energy. Early studies of the concept by Sänger[5] assumed that the antimatter would be in the form of positrons, which interact with electrons to produce 0.511 MeV gamma rays. The antiproton is more suitable than the positron for propulsion systems. The annihilation of an antiproton with a proton does <u>not</u> produce gamma rays immediately. Instead, the products of the annihilation are from three to seven pions. On the average there are 3.0 charged and 1.5 neutral pions.[6] As is shown schematically in Figure 2, the neutral pions have a lifetime of only 90 as and almost immediately convert into two high energy (200 MeV) gamma rays. The charged pions have a normal half-life of 26 ns, but because they are moving at 94% the speed of light, their lives are lengthened to 70 ns. Thus, they travel an average of 21 m before they decay.
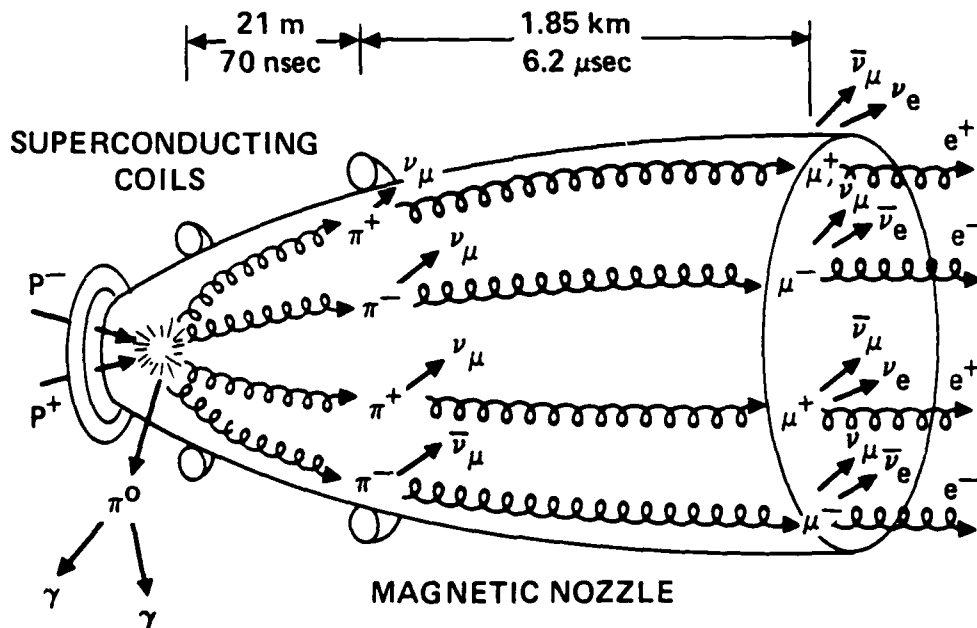
Fig. 2. Schematic of an idealized antiproton rocket.

13

This interaction length is long enough that either magnetic
fields can be used to redirect the isotropic microexplosion into
a directed flow of charged pions to provide thrust or the charged
pions can be used to heat reaction mass. Even after the charged
pions decay, they decay into energetic charged muons, which have
even longer lifetimes and interaction lengths for further conver-
sion into thrust. The charged muons then decay into energetic
charged electrons and positrons, which can be utilized to obtain
more thrust. Thus, if milligrams of antiprotons could be made
and stored, then, according to known physical principles, they
can be used as a highly efficient propulsion energy source.

Because of the extreme difficulty in obtaining significant
quantities of antimatter, the idea of an antimatter rocket has
usually been relegated to the category of "science fiction".
Recent progress in particle physics on methods for obtaining
intense antiproton beams, however, has caused those in the space
propulsion community to take another look at the concept of
antimatter propulsion to see if the concept can be removed from
the "science fiction" category to the "technically difficult and
very costly" category, at which point the military services or
NASA could begin considering its use. The last seven years have
seen the presentation of a number of papers on antimatter propul-
sion,[7-14] A study was also recently undertaken to determine the
physical, engineering, and economic feasibility of antiproton
powered propulsion.[15] The conclusion of the study was that anti-
hydrogen propulsion was feasible, but expensive.

ANTIMATTER PROPULSION MISSIONS

The availability of antimatter as an energy source for space
propulsion will revolutionize space travel. Many of the present
assumptions that are implicit in the design of a mission will no
longer be valid, and mission designers will have to develop a new
set of assumptions to replace them. For example, the concept of
mass ratio and staging mass fractions plays an important part in
the present design of missions. Once a mission has been defined,
there is a certain characteristic velocity V for that mission and
once the fuel is chosen, there is a fixed exhaust velocity v
available from that fuel. The total mission mass ratio R is then
automatically determined by the relation:

$$R = \frac{m_v + m_p}{m_v} = e^{V/v}$$

where m_v is the mass of the empty vehicle (including payload)
delivered to the destination and m_p is the mass of the
propellant exhausted at velocity v. Thus, every different
mission with a different characteristic velocity requires a
different mass ratio and a different vehicle design. Also, if
the mission characteristic velocity exceeds five times the
exhaust velocity, the mass ratio becomes greater than 100, and
there is a tendency to say that the mission is "impossible".

With antimatter powered rockets, the exhaust velocity can be tailored to match the mission characteristic velocity, thus minimizing the mass ratio and mission cost. It has long been known[16] that the mass ratio of an optimized antimatter rocket never exceeds 5:1, and mass ratios that minimize total mission cost are typically 2.5:1 for _any_ mission characteristic velocity[13]. Since the amount of reaction mass needed remains a constant, the _same_ vehicle can be used for all missions, with the only difference being the amount of antimatter used. With anti- matter rockets, mission trajectories will no longer be modified Hohmann transfers, but nearly straight lines. Manned missions to Mars will no longer take years of time, but months of time[14], with significant savings in vehicle and ground support costs.

Research on antiproton annihilation propulsion technology is admittedly very high risk. The extremely high payoff in fast, efficient space propulsion, however, makes it worthwhile to spend a significant amount of effort to determine the feasibility of the concept. In addition, there seems to be a paucity of alter- nate propulsion concepts that can achieve the same results of high propulsion efficiency, low system mass, comparatively low cost, and short mission times.

IMPROVING ANTIPROTON PRODUCTION EFFICIENCIES

There are a number of obvious ways to improve the efficiency of antiproton production over the present methods. It should be realized that the present production facilities were designed under a number of restrictions. They had to use existing proton accelerators, fit onto the existing sites, and not use up too much time on the main research machine. In our recent study[15] a good part of our effort was to determine the reasons behind the low efficiencies of the present facilities. Some of the low efficiencies are inherent, such as the number of antiprotons per proton from a target. Most of the other low efficiencies are just artifacts of the particular choices forced on the particular facility, and there are obvious ways to improve these efficiencies by large factors.

When the present facilities for generating antiprotons[1-4] were constructed, they had to use existing proton accelerators avail- able at the site. The operating energies of these accelerators are known to be far from optimum for efficient production of antiprotons. It can be shown[15] that the maximum energy effic- iency production rate occurs for an incident proton energy of 200 GeV and is 0.085 antiprotons/proton. This antiproton produc- tion rate is 2 times the production at the Fermilab energy of 120 GeV and 20 times the production at the CERN energy of 26 GeV. Although the number of antiprotons produced continues to increase as the incident proton energy is increased, above 200 GeV the gain in antiproton annihilation energy obtainable is not enough to offset the increased proton energy required.

IMPROVING ACCELERATOR EFFICIENCY

The present machines that are used for accelerating protons to
relativistic speeds are synchrotrons. The synchrotron provides
the particle physicist with high-energy protons at a very
precisely known energy. It is the ideal tool for the study of
elementary particle physics. The average current that the
synchrotron can handle is small, however, and the energy
efficiency is only a few percent. The linear accelerator or
linac is an alternate machine for producing high-energy protons
that can handle high average currents and has high energy
efficiency. By using the alternating gradient focusing concept,
it has become possible to accelerate high current beams to very
high energies. The energy limit is economic, not technical. It
is known that machines can be built to handle peak currents of
over 250 mA, since that has been demonstrated in the first
section of the linac injector at Fermilab, which is the only
section where current limitations would occur. Acceleration to
higher energies only requires more rf acceleration sections.

With the availability of new high efficiency (75%) klystrons, the
ac "wallplug" power to proton beam power efficiencies of a linac
could exceed 50%. The Chalk River, Canada linac program[7] has
been studying 100% duty factor linacs, with the goal of producing
a linac capable of of 300 mA <u>average</u> current at 1 GeV (0.3 GW
beam power) for use in an accelerator breeder. The acceleration
limit of a linac (the energy increase per meter) is determined by
the sparking limit in the cavity. The sparking limit is
inversely proportional to the wavelength. Present 200 MHz
machines usually operate at 1 MeV/m but there are designs for
higher frequency machines that will operate at 5 MeV/m. A
5 MeV/m linac for generating a 200 GeV proton beam would be 40 km
long. This is a little longer than the 28 km LEP ring presently
under construction at CERN and 1/5th the size of the 200 km
Supercollider being proposed as the next large particle accel-
erator in the USA. If run at a power level of 10 GW, the proton
current required would be only 50 mA. By separating out the
antiprotons coming from the target and dumping the remaining
particles into an electronuclear breeder reactor loaded with
unenriched uranium, such a factory would require no outside power
source and would essentially be turning depleted uranium into
plutonium and antiprotons.

IMPROVING ANGULAR CAPTURE EFFICIENCY

The present angular capture efficiencies of the magnetic lens
collection systems are already quite good, with up to 30% of the
antiprotons collected and directed into the aperture of the
collecting ring. The present designs, however, were optimized
for the antiproton energies expected at the particular facility
and the particular conditions in the target area. All of the
studies to date have assumed that only a single, on-axis lens
would be used to capture the antiprotons. Because the anti-
protons are being emitted over a wide angle, this immediately

16

leads to the requirement of a short focal length for the lens so it can capture these wide angle antiprotons. Research needs to be done on the feasibility and comparative merits of an array of lenses. Since each lens has to capture only the antiprotons in a small portion of the emitted beam solid angle, the focal length requirements can be relaxed, making the lens design easier. The support hardware for the lenses will cause interception losses, however, and realistic tradeoff studies need to be done between the number of lenses and the lens design parameters. If a multiple lens approach looks desirable, then invention is needed on low-loss devices for separating the wide angle antiproton beam into multiple beams to minimize the interception losses of the multiple lens hardware.

Present magnetic lens designs, such as the lithium lens[18], require the antiproton beam to pass through the material of the lens. This causes significant losses in the antiproton spectrum. This is not true for the magnetic quadrupole lens, but it does not focus well in all orientations. New lens concepts are needed with low loss and good focusing. Another method for construction of a magnetic lens similar to that of the lithium lens would be to carry the current for the lens in a cylinder of ionized plasma[19] instead of lithium metal. The problem of current or beam heating of the lens would be gone and it is likely that absorption of the antiprotons in the lens would be less. A plasma lens would also have problems, such as the various plasma instabilities that would be driven by the high currents needed.

The present single magnetic lens concepts have already achieved angular capture efficiencies of 30% or greater and there are many ideas for new lens concepts with greatly improved performance. It is reasonable to expect that after modest investment in invention, engineering, and testing, there should be new magnetic lens designs capable of capture angles of 60 mrad and capture efficiencies of 85% or greater.

IMPROVING MOMENTUM CAPTURE EFFICIENCY

When the antiprotons come from the target, they have a wide spread in momentum as well as angle. It is this wide spread in antiproton momentum and the difficulty of making an antiproton collection ring with a wide momentum acceptance that leads to the extremely low inefficiencies in present antiproton "factories". For example, at CERN, the present momentum acceptance in the Antiproton Accumulator is only $dp/p=1.5\%$. For a peak momentum of 5 GeV/c, this translates into a momentum bite of only 0.05 GeV/c. Thus, only 1% of the 5 GeV/c half-width of the antiproton momentum spectrum is captured. If we assume that an antiproton factory has an incident proton beam at 200 GeV energy and a 60 mrad angular acceptance, then the flux of antiprotons per proton per unit antiproton momentum is shown in Figure 3.[20] The antiproton flux peaks at 12.5 GeV/c antiproton momentum and spreads from 1 GeV/c to 50 GeV/c, with a half-width of 22 GeV/c. The present state-of-the-art in collection rings for antiprotons

17

is a momentum acceptance of about 6%. Even if this could be raised to 8%, the momentum bite at an antiproton momentum of 12.5 GeV/c would still be only 1 GeV/c and would capture only 4.5% of the antiprotons.
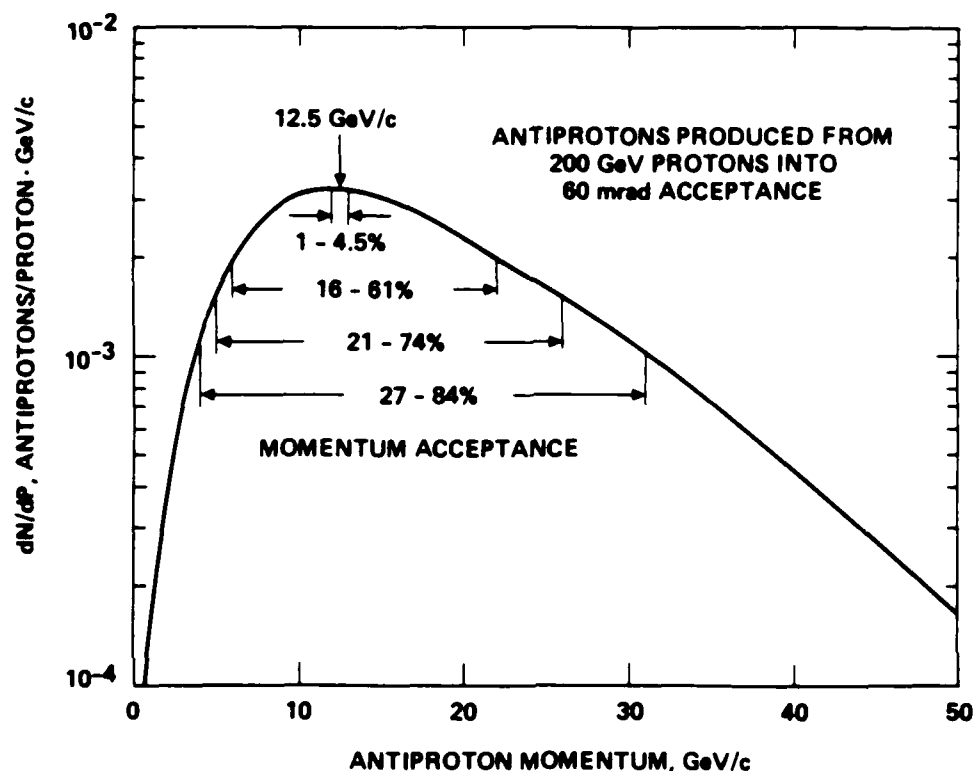
Fig. 3.   Antiprotons vs. momentum spread.

The obvious solution is to build a multiplicity of rings. They would be identical copies and share the same tunnel (since tunnel costs are a major portion of the cost of a ring). Each ring would have the strength of the magnetic fields in its bending magnets set at a different level to keep a different antiproton momentum circulating through its vacuum pipe. If each ring could handle a momentum bite of 1 GeV/c, then as we see in Figure 3, 16 rings could capture 61% of the antiproton momentum spectrum and 27 rings could capture 84% of the antiprotons.

Separating the antiproton beam into different momentum buckets should not be difficult. A magnetic focusing lens has chromatic aberration. Antiprotons with different momenta come to a focus at different distances from the focusing lens. A string of diverter magnets can deflect the different antiproton momenta in different directions, where they can be channeled to the proper collecting ring.

SYSTEM EFFICIENCY ESTIMATES

From the previous sections we can see that there are a number of ways to improve the efficiency of antiproton production over the present techniques. The first obvious improvement is to use a higher proton energy so that more antiprotons are produced in the target. As is shown in Table 1, by going to 200 GeV, the number of antiprotons produced can be increased by a factor of 20 from the 3.8×10^{-3} $\bar{p}/p$ at CERN to 8.5×10^{-2} $\bar{p}/p$. The present magnetic lenses are relatively efficient in capturing the resulting antiprotons in angle. Yet by improving the design and going to multiple lens collectors, we should be able to improve the angular capture efficiency by a factor of 3 or 4 to 85%.

Another place where improvement can be made is in the momentum capture efficiency. The single ring collectors at CERN[1], Fermilab[2], and IHEP[3,4] are severely limited by difficulties with matching the ring acceptances to the lens emittances. With a large enough tunnel and enough money to build copies of the collectors, each tuned to accept a different momentum range, it should be possible to improve the capture efficiencies significantly. Whether it will be possible to go from the present few percent to a desirable 85% is unknown.

There are many losses as the antiproton beam is generated, collected, and switched around from one device to another. The handling efficiencies in the present facilities are not bad, but improvement in this area is also needed. As we can see from Table 1, if all these efficiencies can be achieved, the total production efficiency of antiprotons can be raised from the present 4×10^{-7} $\bar{p}/p$ at CERN by more than five orders of magnitude to 5×10^{-2} $\bar{p}/p$.

Table 1. Antiproton Production Efficiencies

	CERN	Fermilab	Goal
Incident Proton Energy (GeV)	26	120	200
Generation Efficiency ($\bar{p}/p$)	0.4%	4.7%	8.5%
Angular Capture Efficiency	20%	30%	85%
Momentum Capture Efficiency	1%	1.2%	85%
Handling Efficiency (est.)	5%	18%	80%
Total Prod. Efficiency ($\bar{p}/p$)	4×10^{-7}	3×10^{-5}	5×10^{-2}

TRAPPING OF ANTIPROTONS

The present method for storing antiprotons uses magnetic storage rings, which keep the antiprotons circling in a beam at some fixed momentum. These large, heavy, magnetic storage rings are obviously unsuitable for propulsion applications. A number of experimenters have proposed to decelerate the antiproton ions down to almost zero velocity and put them into a Penning trap.

The first to accomplish this feat was a group led by Prof. G. Gabrielse from the University of Washington,[21] who has a paper describing their experiment elsewhere in these proceedings. They used a cryogenic Penning trap modified by thinning the center portion of one of the cap electrodes down to about 0.25 mm. This thin portion was used to degrade the energy in a pulse of anti-protons extracted from the low energy antiproton ring (LEAR) at CERN. The velocity of the antiprotons was brought down to nearly zero so the antiprotons could be captured in the trap. The intention of the group is to return to CERN in 1987 to trap just a few antiprotons and measure the mass of the antiproton to high precision. A group led by M. Hynes at Los Alamos National Lab-oratory is more ambitious[22]. They are fabricating a radio frequency quadrupole (RFQ) decelerator that will decelerate a beam dump of antiprotons from LEAR down to the trap energy and deposit up to 10^{10} antiprotons in their Penning trap.

CONVERSION OF ANTIPROTONS TO ANTIHYDROGEN

For propulsion applications it would be desirable to minimize the size and mass of the antimatter container. To do this it will be necessary to store the antiprotons as some form of antihydrogen rather than as antiproton ions. The first step is to convert the antiprotons into atomic antihydrogen by adding a positron. A straightforward approach to the production of antihydrogen from these trapped antiprotons would be to convert the Penning trap into one that would hold and cool both positive and negative ions. A simple example is the rf Paul trap, which can hold both antiprotons and positrons, and cool them until their relative velocities are low enough that the conversion to antihydrogen takes place naturally. The use of rf modulation or laser radiation to enhance the various reactions needs to be studied. Also, the effectiveness of magnetic fields or laser beams[23] to trap and manipulate the neutral antihydrogen atoms and ions needs to be determined.

CLUSTER ION FORMATION OF ANTIHYDROGEN ICE

The objective of this workshop is to study the feasibility of the growth of amorphous or crystalline antihydrogen through the cluster ion process. The important feature of the cluster ion process is that the growing cluster always maintains a charge and thus can easily be kept in an electromagnetic trap. It is hoped that macroscopic crystals can be grown in this fashion, since it will certainly be simpler than trying to grow neutral anti-

hydrogen ice crystals using laser trapping and cooling[23] or some other yet-to-be-discovered process.

Since other reports in this workshop proceedings will cover the cluster ion growth and cooling processes in considerable detail, I will not include a discussion here, but will assume that the growth has been successful and that we have made macroscopic amorphous or crystalline balls of antihydrogen ice. The antihydrogen ice should be generated at very low temperatures (<2 K) to prevent evaporation loss and should be large enough to scatter infrared light so their position can be determined. The resulting ice particles will mass from nanograms (10^5 J of equivalent energy) to milligrams (10^{11} J of equivalent energy).

LEVITATION OF ANTIHYDROGEN ICE

The techniques for the formation of solid antihydrogen may turn out to be relatively simple. More likely, however, the effort may require large, heavy, complex equipment requiring large amounts of power. Once the small microcrystals or larger ice balls of antihydrogen ice are formed, however, they can be transferred to a compact, lightweight, storage and transport system that uses simple magnetic or electric traps for levitation. The magnetic susceptibility of molecular hydrogen depends upon its state. The orthohydrogen molecule has both of its protons with their magnetic moments pointing in the same direction, so it has a positive magnetic moment. The para-hydrogen molecule has its two protons and its two electrons with their spins oriented in opposite directions so the particle spins cancel out. This gives the parahydrogen molecule a negative or diamagnetic susceptibility. Diamagnetic substances are attracted to the minimum in a magnetic field. Even with a purely static magnetic field, the configuration is stable, unlike levitation systems based on repulsion of paramagnetic or ferromagnetic materials, which are unstable.

The magnetic susceptibility of solid parahydrogen has not yet been measured. The theoretical prediction of the magnetic susceptibility of a one-gram formula weight of molecular hydrogen is -3.98×10^{-6} cgs units.[24] This is to be compared to a value of -6.0×10^{-6} cgs for graphite. There have been many demonstrations of the stable levitation of grams of graphite using nonsuperconducting magnets. In one example, a ring shaped rotor weighing 3.843 g and containing only 0.933 g of graphite was levitated in the 0.2 cm gap between two opposed ring shaped room temperature permanent magnets with a magnetic field of 11,600 G.[25]

One configuration for a magnetic trap that would be compatible with a cryogenically cooled vacuum chamber would be a pair of superconducting rings carrying opposed persistent currents. This passive magnetic levitation technique is the preferred suspension method since it would be safer than any active levitation technique, as well as making the storage and transport container extremely simple, compact, and independent of electric power.

21

An alternate method of levitating antihydrogen ice is to use active electrostatic levitation between two servo-controlled electrically charged plates. The ice particles need to be slightly charged. This can be accomplished either by charging the ice positive by addition of extra positrons or charging it negative by driving off the positrons with ultraviolet light. One example of such an electrostatic trap has been constructed at the Jet Propulsion Laboratory.[26] The trap has levitated a 20-mg ball of water ice in the one gee field of the earth. The density of water at 1.0 g/cc is 13 times that of antihydrogen ice at 0.0763 g/cc. Thus, the present JPL trap with its present voltage levels could levitate a 1.5-mg ball of antihydrogen ice of the same size, surface area, and surface charge at a vehicle acceleration of 13 gees.

STORAGE OF ANTIHYDROGEN ICE

As has been shown in previous sections, it should be possible to form and levitate antihydrogen ice. Since laser cooling[23] will leave the antihydrogen at a temperature well below 1 K, the antihydrogen ice will start out cold. The vapor pressure of antihydrogen[27] at 1 K is only 8.3×10^{-39} Torr, so if kept below this temperature there is essentially no sublimation. The vapor pressure rises exponentially with the inverse of the temperature, however, so at 2 K it has risen to 4×10^{-18} Torr, where the sublimation rate is about 1000 (anti)molecules per second from a milligram-sized ball, while at 4 K it is 2×10^{-7} Torr, where sublimation is rapid. To keep the sublimation rate of the anti-hydrogen down to controllable levels, its temperature should be kept below 2 K. The walls of the storage and transport container should also be cooled to well below liquid helium temperatures to keep the walls from outgassing. New, continuously operating rotary paramagnetic salt refrigerators in a compact package are now available[28] that can pump 1.8 W at 1.8 K, so the mass of these antimatter "fuel tanks" should not be a problem.

Even if the antihydrogen and the walls are kept cold, there will always be a few stray antihydrogen molecules leaving the ice ball and annihilating on the container walls, while there will also be a few stray outgassing hydrogen molecules or other normal molecules knocked off the container walls by those annihilation processes or cosmic rays that would drift across the chamber to annihilate on the surface of the antihydrogen. Each molecular annihilation event will produce on the average six 200 MeV gamma rays, six 250 MeV charged pions, and four 0.511 MeV gammas from the annihilation of the positrons and electrons.

For 200 MeV gamma rays, the attenuation coefficient in matter is roughly constant at 0.1 cm^2/g. Since the density of antihydrogen is 0.0763 gm/cm^3, the attenuation per unit path length is only 0.0076/cm. Thus, instead of causing intense local heating, most of the gamma rays would pass right through a milligram sized iceball and continue on through the container wall to deposit their energy in the outside shield. Only 74 fJ or 460 keV of

energy is deposited in the antihydrogen iceball. For the 250 MeV charged pions, the stopping power is essentially flat at 15 MeV/(g/cm^2). The charged pions will leave only 55 fJ or 340 keV of energy in the antihydrogen and deposit most of their energy outside. Thus, an annihilation that takes place on the surface of an antihydrogen iceball will only deposit 0.5 pJ of energy, or a picowatt heat input for two annihilations/second.

Obtaining a better estimate of the real vapor pressure inside a cryogenically cooled chamber will require research. We have evidence that the vacuums must be fairly good since a single positron has been kept in a 4.2 K Penning trap for a month.[29] But the annihilation cross section for a free positron and a bound electron at these very low energies is not known well enough to establish a firm lower bound on the vacuum level in the trap. Plans are presently underway[21] to trap a few antiprotons from the Low Energy Antiproton Ring at CERN in a cryogenically cooled Penning trap in order to measure the antiproton mass to high accuracy. If the antiprotons survive in these traps for long periods of time, then this should also provide estimates of the residual vapor pressure in these traps.

Despite all precautions, some heat will get to the antihydrogen ice and methods must be found to remove that heat without physically contacting the antihydrogen. One possibility is to use radiation cooling to the container walls. Cluster ions, because of their complex structure have a complex infrared spectrum. This should aid in cooling the cluster during formation. One essential aspect of cluster ion research should be the measurement of the infrared spectra as a function of cluster ion size and composition. This data can then be used to determine whether radiation cooling will be sufficient to keep the antihydrogen cold, or whether some more active form of cooling[15] will be needed.

EXTRACTION OF ANTIMATTER FROM STORAGE

There are a number of techniques for extracting the antihydrogen from the storage trap and directing it into the rocket engine under control. If the antihydrogen is in the form of an electrostatically suspended ball many milligrams in size, then the antiprotons can be extracted from the ice ball by irradiating the ice with ultraviolet, driving off the positrons, extracting the excess antiprotons by field emission with a high intensity electric field, then directing them to the thrust chamber.[10]

It might be more desirable to form the antihydrogen as a cloud of charged microcrystals, each crystal a microgram in mass and containing the energy equivalent of 20 kg of chemical fuel. Then, using a directed beam of ultraviolet light to drive off a few more positrons, an individual microcrystal could be preferentially extracted from the microcrystal cloud using electric fields, and directed down a vacuum line[30] to the thrust chamber. Since the position of the charged microcrystal in the injection

line can be sensed, mechanical shutters can allow the passage of the microcrystal without breaking the storage chamber vacuum.

CONCLUSION

Our major conclusion about antihydrogen propulsion is that the concept is physically feasible, but expensive. Yet, despite the high cost of antimatter, it may be a cost effective fuel in space where any fuel is expensive. There is very high risk in the development of antiproton annihilation propulsion. The major uncertainties seem to be in the production and capture of the antiprotons at high efficiency, and the conversion of antiprotons into frozen antihydrogen without excessive losses. The storage problems look tractable. It is important to remember that many of the problems of capturing, cooling, slowing, trapping, and storing of (anti)protons and (anti)hydrogen can be done as low cost student thesis topics using normal protons and hydrogen.

ACKNOWLEDGEMENTS

REFERENCES

1. E. Jones, S. van der Meer, R. Rohner, J.C. Schnuriger, and T.R. Sherwood, "Antiproton production and collection for the CERN antiproton accumulator," IEEE Trans. Nuclear Sci. **NS-30**, 2778-2780 (August 1983).

2. J. Peoples, "The Fermilab antiproton source," IEEE Trans. Nuclear Sci. **NS-30**, 1970-1975 (August 1983).

3. A.I. Ageyev, et al., "The IHEP accelerating and storage complex (UNK) status report," pp. 60-70, Proc. 11th Conf. on High Energy Accelerators, Geneva, Switzerland (1980).

4. T. Vsevolozhskaya, et al., "Antiproton source for the accelerator-storage complex UNK-IHEP," Fermilab Report FN-353 8000.00 (June 1981), a translation of INP Preprint 80-182 (December 1980).

5. E. Sänger, "The theory of photon rockets," Ing. Arch. **21**, 213 (1953). [In German.]

6. M.R. Clover, R.M. DeVries, N.J. DiGiacomo, and Y. Yariv, "Low energy antiproton-nucleus interactions," Phys. Rev. **C26**, 2138-2151 (1982).

7.   R.L. Forward, "Interstellar flight systems," AIAA Paper 80-0823, AIAA International Meeting, Baltimore, MD (1980).

8.   R.L. Forward, "Antimatter propulsion," J. Brit. Interplanetary Soc. 35, 391-395 (1982).

9.   B.N. Cassenti, "Design considerations for relativistic anti-matter rockets," J. Brit. Interplanetary Soc. 35, 396-404 (1982).

10.   D.L. Morgan, "Concepts for the design of an antimatter annihilation rocket," J. Brit. Interplanetary Soc. 35, 405-412 (1982).

11.   G. Vulpetti, "A propulsion-oriented synthesis of the antiproton-nucleon annihilation experimental results," J. Brit. Interplanetary Soc. 37, 124-134 (1984).

12.   R.L. Forward, "Antiproton annihilation propulsion," J. Propulsion and Power 1, 370-374 (1985).

13.   R.L. Forward, B.N. Cassenti, and D. Miller, "Cost comparison of chemical and antihydrogen propulsion systems for high Delta-V missions," AIAA Paper 85-1455, 21st Joint Prop. Conf., Monterey, CA (8-10 July 1985).

14.   S.D. Howe, M.V. Hynes, R.E. Prael, and J.D. Stewart, "Potential applicability of the Los Alamos antiproton research program to advanced propulsion," 15th Int. Symp. on Space Tech. and Science, Tokyo, Japan (19-23 May 1986).

15.   R.L. Forward, Antiproton Annihilation Propulsion, AFRPL TR-85-034, Final Report on Contract F04611-83-C-0046, Order RI-32901 with AF Rocket Propulsion Lab, LKC, Edwards AFB, CA 93523-5000 (September 1985).

16.   L.R. Shepherd, "Interstellar flight," J. Brit. Interplanetary Soc. 11, 149-167 (1952).

17.   H.J.C. Kouts, Chairman, Proceedings of an Information Meeting on Accelerator Breeding, Brookhaven National Laboratory, Upton, New York, (18-19 Jan 1977).

18.   B.F. Bayanov, et al, "The antiproton target station on the basis of lithium lenses," Proc. 11th Int. Conf. High Energy Accelerators, Geneva, pp. 362-368 (1980).

19.   Pisin Chen, J.J. Su, T. Katsouleas, S. Wilkes, and J.M. Dawson, "Plasma focusing for high energy beams," Preprint SLAC-PUB-4049 (August 1986).

20.   C. Hojvat and A. Van Ginneken, "Calculation of antiproton yields for the Fermilab antiproton source," Nucl. Instr. & Methods 206, 67-83 (1983).

21. G. Gabrielse, et al., "First capture of antiprotons in a Penning trap: a kiloelectronvolt source," Phys. Rev. Lett. 27, 2504-2507 (17 November 1986).

22. M.V. Hynes and L.C. Campbell, "Physics with bottled antiprotons," pp. 201-210, **Proc. 1st Workshop on Antimatter Physics at Low Energy**, B.E. Bonner and L.S. Pinsky, ed., Fermilab, Batavia, IL (10-12 April 1986).

23. S. Chu, J.E. Bjorkholm, A. Askin, and A. Cable, "Experimental observation of optically trapped atoms," Phys. Rev. Lett. 57, 314-317 (1986).

24. R.C. Weast, **CRC Handbook of Chemistry and Physics**, 63rd Edition, (CRC Press, 1983), p. E-119.

25. R.D. Waldron, "Diamagnetic levitation using pyrolytic graphite," Rev. Sci. Instr. 37, 29-34 (1966).

26. W-K Rhim, M.M. Saffren, and D.D. Elleman, **Material Processing in the Reduced Gravity Environment of Space**, G.E. Rindone, ed., (Elsevier, 1982), p. 115.

27. J.C. Mullins, W.T. Ziegler, and B.S. Kirk, "The thermo-dynamic properties of parahydrogen from 1 to 22 K," Georgia Institute of Technology, Atlanta, Georgia, Technical Report No. 1, Project No. A-593, Contract No. CST-7339 with National Bureau of Standards, Boulder, Colorado (1 November 1961).

28. Y. Hakuraku and H. Ogata, "A rotary magnetic refrigerator for superfluid helium production," J. Appl. Phys. 60, 3266-3268 (1 November 1986).

29. G. Gabrielse, University of Washington, personal communication.

30. Ronald K. Goodman and Angus L. Hunt, "Ammonia-pellet generation system for the Baseball II-T target plasma experiment," Rev. Sci. Inst. 48, 176 (1977).

Roberta P. Saxon

Overview of Hydrogen Clusters

OVERVIEW OF HYDROGEN CLUSTERS

Roberta P. Saxon

Chemical Physics Laboratory
SRI International
Menlo Park, California 94025

Abstract

Equilibrium geometries and energetics of the ground states of hydrogen cluster ions obtained from theoretical calculations are reviewed. Possible roles of excited states in promoting association reactions to form H_n^+ by H atom addition are considered and available information for H_3^+ electronic states is surveyed.

Introduction

As indicated in other reports in this volume, concentration and "containerless" storage of antimatter are among the significant issues that will have to be addressed to realize the tremendous potential of antimatter fuel for high-thrust propulsion. The leading approach to address this problem involves the use of cluster ions. Singly charged hydrogen cluster ions up to fairly large masses have been observed by mass spectrometry and the storage of charged particles in ion traps for long periods of time has already been demonstrated. (Taking advantage of the symmetry between antimatter and matter, this paper will be phrased exclusively in terms of ordinary matter.)

To examine the concept of the use of hydrogen cluster ions, a workshop chaired by John Bahns was held at the University of Iowa in July, 1986. As described in the report of that workshop[1], applying RRKM theory to the addition of H_2 to H_n^+ and making assumptions about the normal modes of large clusters, Tardy predicts that clusters larger than a certain size (n~30) will be stabilized by radiative emission. Thus the bottleneck for the formation of large clusters is the stabilization of small clusters.

This paper, therefore, will be limited to a review of the properties and formation of small cluster ions. In particular, we will focus on the equilibrium geometries and energetics of small cluster ions, which have been obtained primarily from theoretical calculations. In addition, we will discuss association reactions to form H_n^+, examining the possible role of electronically excited states in promoting such reactions.

H_n^+ and H_n^- Ground States

Of the numerous theoretical papers on hydrogen ion clusters in the literature, the three most recent and comprehensive treatments[2-4] are reviewed here. Wright and Borkman[2] have obtained optimized geometries for H_n^+ for n between 3 and 9 at the self-consistent field (SCF) and unrestricted Hartree Fock (UHF) level using a double zeta (DZ) basis set. Hirao and Yamabe[3] have optimized positive and negative clusters for odd values of n between 3 and 13, also at the SCF level, using a somewhat larger basis set, the standard 4-31G augmented by one p and two diffuse s functions. Finally, Yamaguchi, Gaw, and Schaefer[4] have performed optimizations for H_n^+ for n odd between 3 and 9, using both the SCF and singles and doubles configuration interaction (SDCI) methods with DZ and double zeta plus polarization (DZP) basis sets. The DZP/SDCI results of Yamaguchi et al. are expected to provide the most reliable results.

A consistent qualitative picture of the positive cluster ions emerges from these three studies. As shown in Fig. 1, the odd positive cluster ions can be characterized as an H_3^+ triangle surrounded by H_2 molecules. For n=5,7,9, the molecules are located off the vertices and perpendicular to the plane of the H_3^+. In the larger species, H_2 molecules are added above and below the H_3^+ plane, parallel to it, as well. From Ref. 2, the even positive clusters have the same form, replacing one H_2 of the next larger odd n cluster by a single H.

Characterization of the odd clusters as $H_3^+(H_2)_m$ becomes more applicable as the cluster size increases. As discussed by Schaefer in greater detail in another report in this volume, H_5^+ shows significant deviations from unperturbed H_3^+ and H_2 bond lengths and frequencies. Comparisons of the bond lengths determined at the same level of theory by different workers show maximum discrepancies of 0.03Å. The interfragment distance was found to be the most sensitive to the level of theory used in the optimization. For H_5^+, DZ/SDCI and DZP/SDCI results[4] for this bond length differed by 0.4Å.

While an appealing qualitative picture of the negatively charged cluster ions for odd n between 3 and 13 may also be drawn[3], because, as discussed by Michels at this conference, they are not predicted to be stable when zero point vibration is taken into account and because H_2^- is not a stable species, they will not be considered further.

Calculated dissociation energies for removal of H_2 from H_n^+ for odd n and removal of H from even numbered clusters are shown in Table I. The DZP/SDCI values are observed to be in excellent

agreement with the recent experimental results of Beuhler, Ehrenson and Friedman[5]. We may use the remaining data in Table I to calibrate the DZ/SDCI results of Ref. 2 for the even numbered clusters. While there is uncertainty in the numerical value of the energy, we would expect the prediction of the stability of these clusters to be substantiated. Observation of the H_4^+ ion by mass spectrometry has been reported[6] by Kirchner, Gilbert, and Bowers. (The report by Bowers at this conference of the observation of significant quantities of H_6^+ raised the question of the existence of a different form of the ion than that treated to date theoretically.)

Table I. Dissociation energies in kcal/m.

$$H_n^+ \rightarrow H_{n-2}^+ + H_2$$

	Ref. 2 DZ/SDCI	Ref. 4 DZ/SDCI	Ref. 4 DZP/SDCI	Ref. 5 Expt.	Ref. 7 Expt.
H_5^+	3.0	3.7	6.9	6.6	9.6
H_7^+	2.0	3.0	3.4	3.1	4.1
H_9^+	1.2	2.6	3.3		3.8
H_{11}^+	2.4				

$$H_n^+ \rightarrow H_{n-1}^+ + H$$

H_4^+	1.5
H_6^+	1.2
H_8^+	1.0

Association Reactions

Of the various types of association reactions enumerated for the buildup of hydrogen clusters[1], the addition of hydrogen atoms, $H + H_n^+ \rightarrow H_{n+1}^+$, is considered to be among the most promising since it would not require the formation of cold H_2. In this paper, we examine the addition of H to H_2^+ to form H_3^+.[2] Even this seemingly simple reaction exhibits significant complications. Chief among them is the existence of the competing charge transfer reaction, $H + H_2^+ \rightarrow H^+ + H_2$, which is exoergic by 2 eV. One proposal to promote the desired

association reaction is through the technique of transition state spectroscopy, indicated schematically in Fig. 2, in which the initial collision complex is pumped to an excited electronic state that would then radiate spontaneously or by stimulation to the stable ground state. Use of this approach requires a knowledge of the excited electronic states of H_3^+.

To our knowledge, the only survey in the literature of numerous electronic states of H_3^+ is that of Schaad and Hicks[8], who carried out a variational calculation directly from exponents optimized at each point without using SCF orbitals. Their results for singlet states restricted to D_{3h}, i.e. equilateral triangle, symmetry are reproduced in Fig. 3. They reported only one excited bound state, the $^3\Sigma_u^+$. This state has been confirmed by the calculations of Ahlrichs, Votava, and Zirz[9], who used a more conventional approach.

Information on the two lowest singlet surfaces of H_3^+ is available from the work of Preston and Tully[10] and Bauschlicher et al.[11], who were interested in treating the charge transfer dynamics. The results are complicated by the presence of a crossing seam, a line in multidimensional space where the surfaces cross. They can best be understood by the cuts through the potential surfaces illustrated in Figs. 4 and 5, where the potentials are given as functions of one H-H distance with the third H fixed at a specified distance. When the third particle is infinitely far away (Fig. 4), the two surfaces cross. For closer distances (Fig. 5), there is an avoided crossing and finally curves that bear no resemblance to the original H_2 and H_2^+ are obtained. The points at H-H distance 2.0 a_o in the last frame correspond to the first two potential curves in Fig. 3 at the corresponding distance. The resulting adiabatic potential surfaces are reproduced in Fig. 6. The lowest surface correlates asymptotically to $H^+ + H_2$, while the second state connects to $H + H_2^+$, the initial channel of the hydrogen association reaction.

The transition state spectroscopy suggestion (Fig.2), from which we started, may need to be transformed to, for example, an approach based on non-resonant Raman scattering on the upper surface of that fraction of the incoming flux that has made the transition to the lower surface. Pursuing this approach would require knowledge of the electronic transition moments between the surfaces as a function of geometry, which can be calculated quite accurately with present methods, and considerable further analysis. Almost no information exists for the excited states of the larger cluster ions, which will surely be even more complicated.

Concluding Remarks

Up to this time, little work has been devoted to non-collisional stabilization in association reactions. Thus many interesting and challenging problems remain. As this brief survey for H_3^+ may have illustrated, some of the information needed to begin the analysis has already been obtained in other contexts. Furthermore, present theoretical and experimental methods can contribute far more if we focus directly on the association reaction problem. I look forward to a great deal of interesting work in the coming years.

References

1. J. T. Bahns, ed. Hydrogen Cluster Ion Study Group Report (University of Iowa 6/30-7/11/86).
2. L. R. Wright and R. F. Borkman, J. Chem. Phys. 77, 1938 (1982).
3. K. Hirao and S. Yamabe, Chem. Phys. 80, 237 (1983).
4. Y. Yamaguchi, J. F. Gaw, and H. F. Schaefer, J. Chem. Phys. 78, 4074 (1983).
5. R. J. Buehler, S. Ehrenson, and L. Friedman, J. Chem. Phys. 79, 5982 (1983).
6. N. J. Kirchner, J. R. Gilbert, and M. T. Bowers, Chem. Phys. Lett. 106, 7 (1984).
7. K. Hiraoka and P. Kebarle, J. Chem. Phys. 62, 2267 (1975).
8. L. J. Schaad and W. V. Hicks, J. Chem. Phys. 61, 1934 (1974).
9. R. Ahlrichs, C. Votava, and C. Zirz, J. Chem. Phys. 66, 2771 (1977).
10. R. K. Preston and J. C. Tully, J. Chem. Phys. 54, 4297 (1971).
11. C. W. Bauschlicher, S. V. O'Neil, R. K. Preston, and H. F. Schaefer, J. Chem. Phys. 59, 1286 (1973).
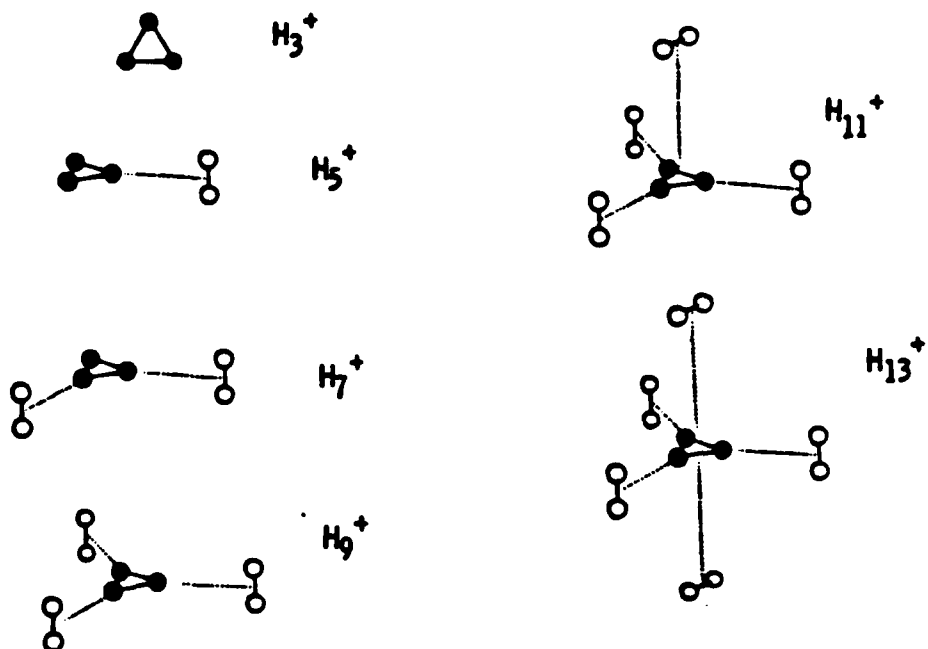
FIG. 1. Schematic diagram of equilibrium geometries of
ground states of positive hydrogen cluster ions.
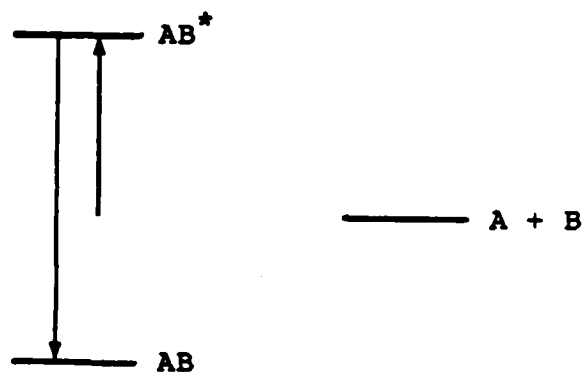
FIG. 2. Schematic diagram of stabilization of
association reaction by transition state spectroscopy
approach.
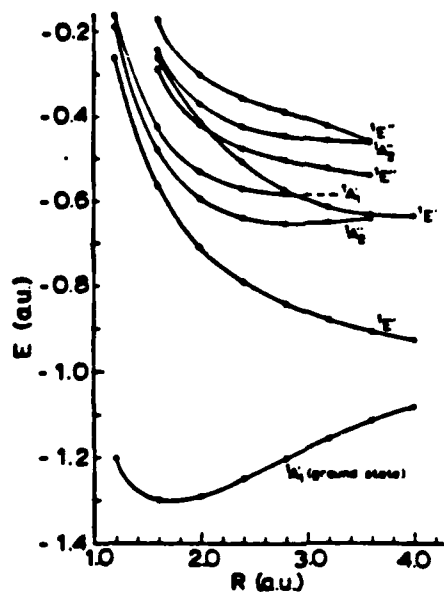
FIG. 3. Singlet states of H_3^+ in D_{3h} geometry calculated by Schaad and Hicks (Ref. 8)
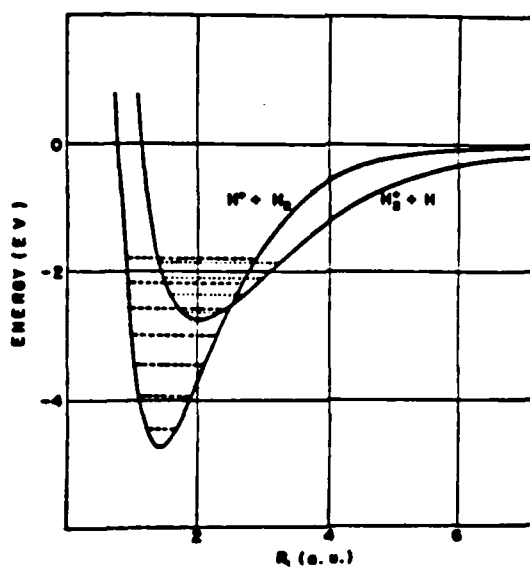
FIG. 4. Cut through the two lowest singlet potential surfaces for collinear H_3^+ for one H infinitely removed from the other two, whose separation is given by R_1. (From Preston and Tully, Ref. 10)
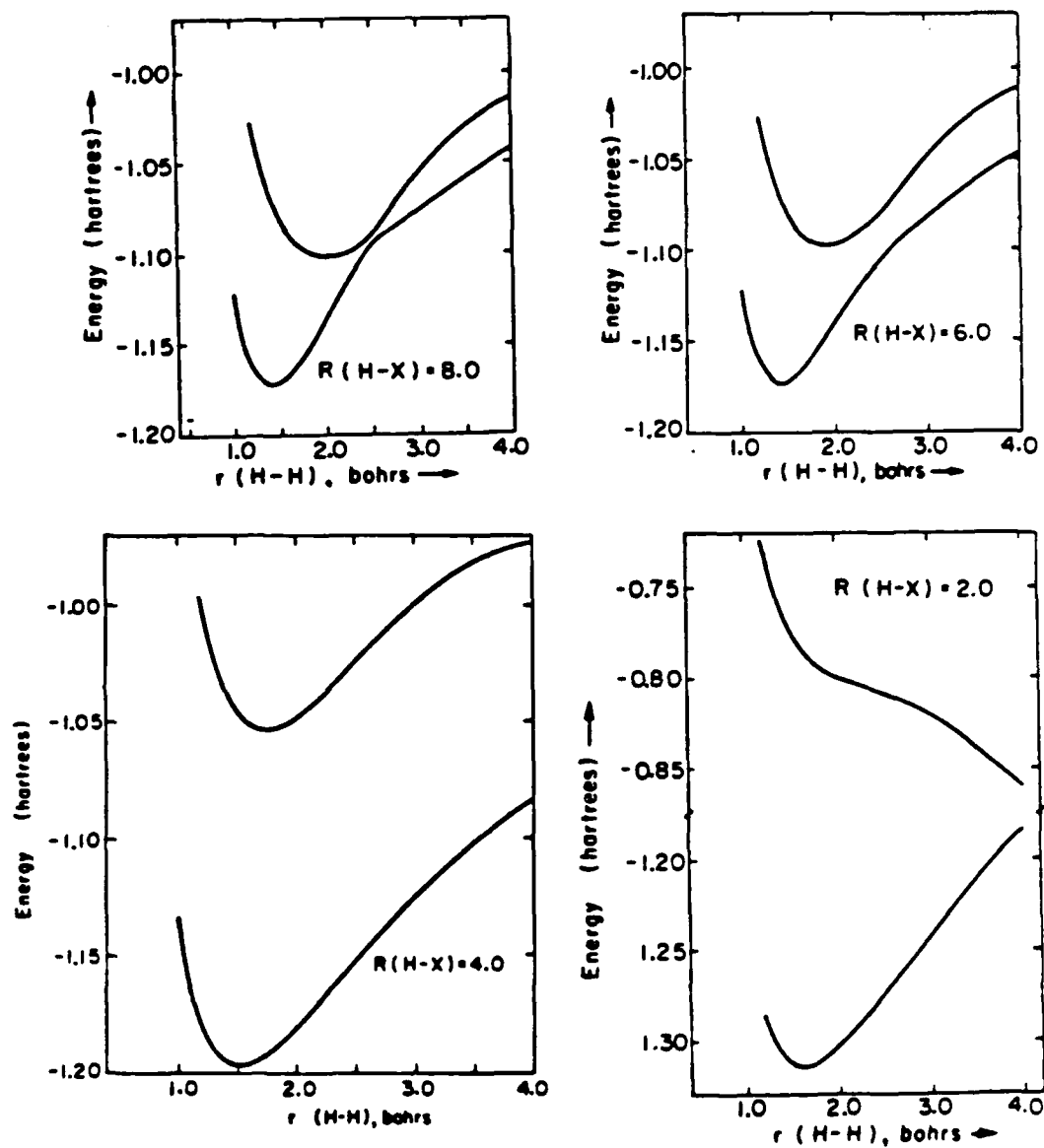
FIG. 5. Cut through the two lowest singlet potential surfaces in C_{2v} geometry for given distance of third H from other two (labeled as R(H-X)). (From Bauschlicher et al. Ref. 11)

First excited $^1A_1$ potential surface
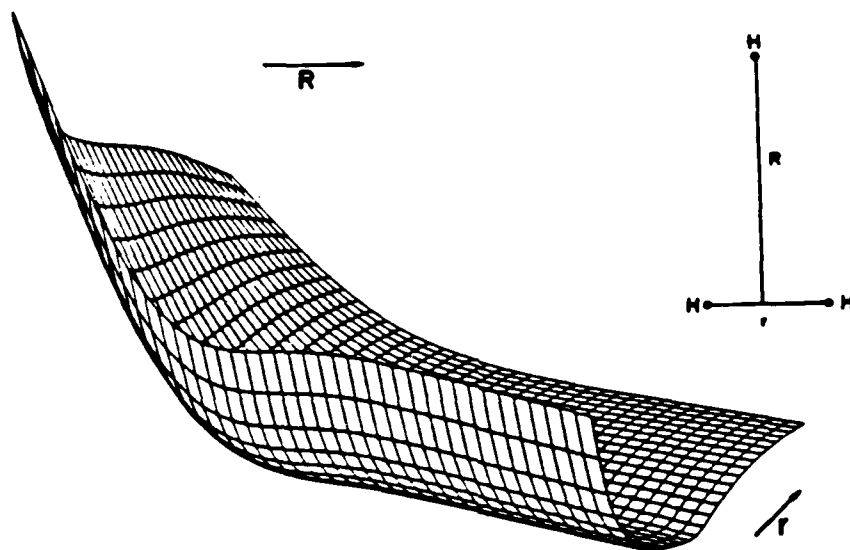
Lowest $^1A_1$ potential surface
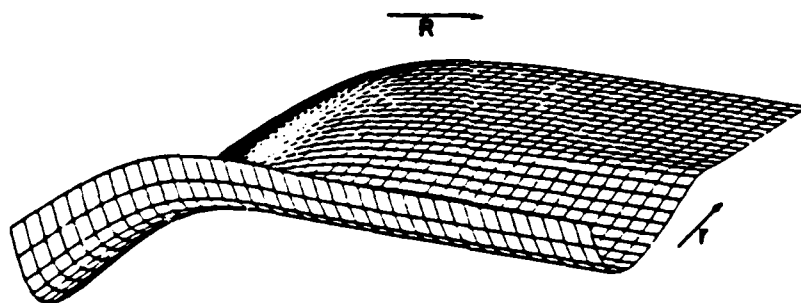
FIG. 6. Perspective plot of the two lowest $^1A_1$ potential surfaces of H_3^+. (From Bauschlicher et al. Ref. 11)

William C. Stwalley

Large Hydrogen Cluster Ions

Large Hydrogen Cluster Ions

William C. Stwalley
Iowa Laser Facility and
Departments of Chemistry and of Physics and Astronomy
University of Iowa
Iowa City, Iowa 52242-1294

This article summarizes the concept of growth/fragmentation cycles for large hydrogen cluster ions in an ion trap. The various possible collisional processes are listed and briefly discussed with emphasis on the positive ion growth and fragmentation processes.

I. Introduction

The Air Force has identified antimatter propulsion as a possible "enabling" technology for a variety of important space missions. Thus it has begun funding basic research with the ultimate goal of producing an antiproton propulsion system if such a system is in fact feasible. For such a system, antiprotons must be produced, slowed to low energy and condensed to a high density form suitable for propulsion applications, which exist even at the milligram or microgram level. Dr. Forward has reviewed this topic in these proceedings.[1]

Note that since matter-antimatter annihilation releases a great deal of energy, the condensation to the bulk high density form must be done under "containerless" and "collisionless" conditions, i.e. there must be no collisions of condensed antimatter with walls or even background gas molecules made of ordinary matter.

A leading concept to span this gap from slowed antiprotons to bulk antimatter is the cluster ion approach which Dr. Bahns has reviewed for these proceedings.[2] Additional material may be found in the Proceedings of the Hydrogen Cluster Ion Study Group.[3] This approach assumes antiprotons and positrons can be efficiently recombined to form antihydrogen atoms and that these atoms can be cooled, moved and trapped using lasers and magnetic fields. It also employs the relatively well-defined ion trap technology (used in the new generation of "atomic clocks" and reviewed by Dr. Wineland in these proceedings[4]).

For simplicity, I will discuss ordinary matter rather than antimatter. Our goal is ultimately to synthesize H_N^+ ($N \geq 10^{17}$) starting from cold H^+, e^- and H. I note in passing that this cluster ion technology may be of interest in many other contexts besides antimatter propulsion, energy storage and directed energy beams. For example, the ordinary matter cluster ions may be useful for directed energy and laser amplifier applications, and as precursors for a H_N neutral beam for directed energy or magnetic or inertial confinement fusion applications.

II. The Growth/Fragmentation Cycle

The schematic diagram of a growth/fragmentation cycle for large hydrogen cluster ions in an ion trap is summarized schematically in Figure 1. Suppose we have a large ion I_1 (the definition of large will be discussed below) consisting of, for example, 1000 protons and 999 electrtons. Can we grow this cluster in the ion trap in the <u>complete</u> absence of wall or background gas collisions to an ion I_2 consisting of, for example, 10,000 protons and 9,999 electrons? Then can we fragment this larger ion into two smaller ions I_3 and I_4 each larger than our initial large ion I_1? If so, then the problem of storing bulk quantities of antimatter (antiprotons and positrons) as antihydrogen cluster ions[1] reduces to the problem of forming a single such I_1 ion (a "seed crystal", although, of course, the ion may in fact not be crystalline).

Figure 1. Schematic diagram of a growth/fragmentation cycle for a large hydrogen cluster ion I_1 (see text).
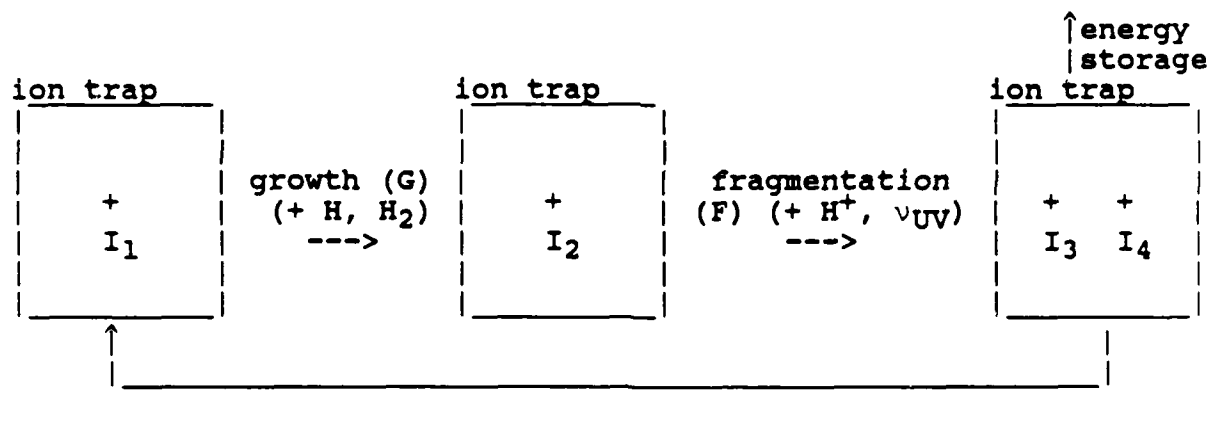
To begin to answer these questions, let us first note (Table I.) the very limited number of reactants we have at our disposal for our growth and fragmentation of bulk cluster ions from a "seed crystal" ion under containerless/collisionless conditions. Certainly H^+ and e^- are available. H is probably available via stimulated recombination, although production rates may be a problem. Most useful photons (ν) are available, at least using pulsed lasers. The formation of internally cold H_2 will be difficult, particularly if one insists on a reasonable efficiency. H^- will be exceedingly difficult to form and will henceforth be ignored. Let us now turn to the cases of positive and negative cluster ions separately.

III. Positive Ions

The collisional processes of interest are given in Tables II

Table I. Reactants available for growth and fragmentation of large hydrogen cluster ions.

probable	questionable
H^+	H_2
e^-	H^-
H	
ν	

and III, for H_N^+ ions with odd and even numbers of protons, respectively. The collisional processes are categorized as G (growth), F (fragmentation) and L (loss) processes. Note that the growth processes employing H atoms should work well for N odd, but not for N even. Indeed the process of growth by H atom addition is limited by the competition between processes 3a. and 3b. in Table III. A cluster cannot be considered "large" for the purposes of this discussion unless the rate for 3a. in Table III significantly exceeds the rate for 3b. in Table III. My purely intuitive _guess_ is that this will require N ~ 10^{3-4}. Clearly some fundamental research is needed to establish this. It certainly should happen for some finite value of N, however.

Table II. Collisional processes involving H_N^+ ions with N odd ($H_N^+ \simeq H_3^+(H_2)_{(N-3)/2}$)

1.	$H^+ + H_N^+$	$\rightarrow [H_{N+1}^{+2}]^+ \rightarrow 2\ H_{\sim N/2}^+$	F
2.	$e^- + H_N^+$	$\rightarrow [H_N] \rightarrow 2\ H_{\sim N/2}$	L
3.	$H + H_N^+$	$\rightarrow [H_{N+1}^+]^* \rightarrow H_{N+1}^+ + \nu_{IR}$	G
4. a.	$\nu_{IR} + H_N^+ \rightarrow H_{N-2}^+ + H_2$		L
b.	$\nu_{UV} + H_N^+ \rightarrow [H_N^{+2}] + e^- \rightarrow 2\ H_{\sim N/2}^+ + e^-$		F
5.	$H_2 + H_N^+$	$\rightarrow [H_{N+2}^+]^* \rightarrow H_{N+2}^+ + \nu_{IR}$	G

If internally cold H_2 can somehow be produced, then process 5. in Table II can be used for the growth process. This greatly relaxes the size needed for efficient growth. D. C. Tardy in Reference 3 has estimated that for cold hydrogen cluster ions, photo-emission (3. a. in Table III) and H_2 desorption (3. b. in Table

Table III. Collisional processes involving H_N^+ ions with N even
($H_N^+ \cong H_3^+(H_2)_{(N-4)/2}H$)

1.	$H^+ + H_N^+$	$\rightarrow [H_{N\mp1}^{+2}]^\dagger \rightarrow 2\, H_{\sim N/2}^+$	F
2.	$e^- + H_N^+$	$\rightarrow [H_N] \rightarrow 2\, H_{\sim n/2}$	L
3. a.	$H + H_N^+$	$\rightarrow [H_{N+1}^+]^\dagger \rightarrow H_{N+1}^+ + \nu_{IR}$	G
b.		$\rightarrow H_{n-1}^+ + H_2$	L
4. a.	$\nu_{IR} + H_N^+ \rightarrow H_{N-2}^+ + H_2$		L
b.	$\nu_{UV} + H_N^+ \rightarrow [H_N^{+2}] + e^- \rightarrow 2\, H_{\sim N/2}^+ + e^-$		F
5.	$H_2 + H_N^+ \rightarrow [H_{N+2}^+]^\dagger \rightarrow H_{N+2}^+ + \nu_{IR}$		G

III) are competitive for N $\cong$ 27. He also has estimated that if
the cluster ion has the rather modest internal energy of 1000
cm^{-1}, the different rates are competitive at N $\cong$ 37. Clearly
then the growth process alluded to in Section I. requires either
H atom addition to very large (N ~ 10^{3-4}) clusters or the more
problematical addition of cold H_2 to somewhat smaller clusters (N
$\cong$ 27-37). Nevertheless, it does appear likely that for some
cluster size, growth is feasible.

With regard to fragmentation, the possible processes are 1.
and 4. b. in Tables II and III. However, process 4. b. does in-
clude production of an e^-. In the case of antimatter, such a
process would release an unacceptably large amount of energy (un-
less the corresponding positron could somehow be collected).
Thus the proton impact processes (1. in Tables II and III) are to
be favored, although there is no experimental verification of
such processes at this time.

IV. Negative Ions

The negative ions H_N^- may not be stable in many instances.[4]
Moreover, the H_N^- collisional processes, enumerated in Table IV,
are not as favorable as those given above for positive ions in
Tables II and III. In particular, loss by detachment (3. b. and
5. b.) may well compete with growth (3. a. and 5. a.). In addi-
tion it is not clear that many of the small H_N^- ions are stable
(see e.g. the contribution by H. Michels to those proceedings[5]),
so producing a large H_N^- ion may be very difficult.

V. Summary

There are many potentially interesting processes involving
large cluster ions of hydrogen and very little current informa-
tion. Examination of the potential growth and fragmentation

Table IV. Collisional processes involving H_N^-.

1.	a.	$H^+ + H_N^- \rightarrow H_N + H$	L
	b.	$\rightarrow H_{N-1} + H_2$	L
2.		$e^- + H_N^- \rightarrow [H_N^{-2}]^\dagger \rightarrow 2\ H_{N/2}^-$	F
3.	a.	$H + H_N^- \rightarrow [H_{N+1}^-]^\dagger \rightarrow H_{N+1}^- + \nu_{IR}$	G
	b.	$\rightarrow H_{N+1} + e^-$	L
4.	a.	$\nu_{IR} + H_N^- \rightarrow H_N + e^-$	L
	b.	$\rightarrow H_{N-2}^- + H_2$	L
5.	a.	$H_2 + H_N^- \rightarrow [H_{N+2}^-]^\dagger \rightarrow H_{N+2}^- + \nu_{IR}$	G
	b.	$\rightarrow H_{N+2} + e^-$	L

processes, especially for the positive ions, would seem to be a particularly appropriate study for research.

References

1. R. Forward, "Prospects for Antiproton Production and Propulsion", in these proceedings.

2. J. T. Bahns, "Introduction to the Workshop on Cooling, Condensation and Storage of Hydrogen Cluster Ions", in these proceedings.

3. J. T. Bahns, editor, <u>Proceedings of the Hydrogen Cluster Ion Study Group</u> (1986).

4. D. Wineland, "Ion Traps", in these proceedings.

5. H. Michels, "Electronic Structure and Stability of Small Cation and Anion Hydrogen Clusters", in these proceedings.

John Weiner

Associative Two-Body Condensation in Laser-Cooled Sodium and Hydrogen

Associative Two-Body Condensation in Laser-Cooled
Sodium and Hydrogen

John Weiner
Department of Chemistry
University of Maryland
College Park, Maryland 20742

ABSTRACT

This report summarizes our understanding of two-body asso-
ciative ionization and radiative association in sodium atom
collisions and hydrogen atom collisions. We examine the feasabi-
lity of using these processes to promote condensation into
polyatomic clusters without recourse to collisional relaxation.

INTRODUCTION

The first part of this report will summarize what we know
about the dynamics of associative ionization collisions between
Na atoms and contrast these findings to what we might expect in
the H + H system. We will then discuss the possible consequences
of very cold collisions on the product ion dimer internal state
distribution. In the second part we discuss our calculations of
radiative association in an ensemble of very cold sodium atoms
and show that, unless some stimulated process is invoked, the
product vibrational state distribution is likely to be broad.

I. ASSOCIATIVE IONIZATION

A. Total Rate Constants

My research group first undertook to measure accurately
associative ionization (AI) rate constants in alkali systems so
as to gauge their importance relative to other inelastic pro-
cesses. The results of these studies[1-4] demonstrate three impor-
tant points: (1) rate constants for

$$Na(3s) + Na^*(np) \rightarrow Na_2^+ + e: \ 5 < n < 15 \qquad (1)$$
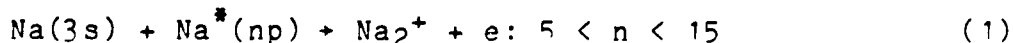
are large, ranging from 3×10^{-10} to a maximum of 2×10^{-9} cm^3 sec^{-1}
at n=11. (2) Rate constants increase rapidly with principal quan-
tum number to a maximum between n=9-11, after which they gra-
dually decline. Reference 1 compares these findings to a theory
advanced by Janev[5] and Duman[6]. Agreement was fair, but theory
and experiment appeared to be diverging at higher n. Recently
Boulmer and Weiner[4] extended these results to n=27 and measured
rate constants involving s and d as well as p excited orbitals.
These new results (see Fig. 1) clearly demonstrate that the dyna-
mical picture implicit in the theory proposed by Janev and Duman
is inadequate to account for the observations. (3) The rate
constant for AI between two excited Na atoms,

$$Na(3p^2P_{3/2}) + Na(3p^2P_{3/2}) \rightarrow Na_2^+ + e \qquad (2)$$

is surprisingly small (1.1×10^{-11} cm^3 sec^{-1}) compared to those of process (1). Reaction (2) is important because of the role it plays in initiation of laser-triggered alkali vapor plasmas and because earlier studies had reported wildly different numbers for the AI rate coefficient. The work by Gallagher and Huennekens[7] in a high-pressure cell and our own work in crossed beams[2,3] are the only two studies to properly consider the important effects of radiation trapping. These two determinations are in agreement to within about 25%.

B. Velocity Dependence of AI Rate Constant

The surprisingly small rate constant for (3) immediately raises the possibility of a potential barrier and suggests a study of AI as a function of collision energy. We decided to attack this problem by initiating a velocity-selected crossed beams experiment. A work station was established at the Regional Laser Lab in Philadelphia in order to take advantage of the available single-frequency ring dye laser needed to excite narrow "δ-function" velocity groups from the global velocity distribution of each Na beam. Scanning the laser frequency and measuring the Na$_2^+$ production from AI leads to a direct determination of the AI "excitation function" (probability vs. collision energy). Figure 2 shows three of the the present experimental configurations and refs. 8 - 10 report the results of the experiment. We found a strong dependence of cross section on collision velocity with a minimum at about 1.6×10^3 m sec^{-1} (0.15 eV) and a steeply rising curve on both sides of the minimum. It appeared that a single potential curve could not possibly account for this behavior, and our tentative guess was that at least two potentials, one attractive and the other repulsive, contribute significantly to the final associative ionization state. The curious shape of the excitation function was quite unexpected, and it was clear from these initial results that the range of available collision velocities had to be greatly expanded, especially toward the energy region below 80 meV. References 9 and 10 escribe recent new results where we report the determination of spin-selected[9] excitation functions for singlet and triplet manifolds over a collision energy range from 2.4 meV to 290 meV (see Fig. 3) and p-lobe alignment selected[10] excitation functions over the same energe range (see Fig. 4). Although our interpretation is still tentative in the spin-selected case, we believe that the singlet curve sharply rising above about 0.15 eV is due to the repulsive $^1\Sigma_u^-$ state while the low-energy feature peaking at about 0.6 eV on both singlet and triplet excitation function is due to a collection of attractive states. In the p-lobe selected case (Fig. 4) we have shown[11] that $^3\Sigma_u^+$ and $^1\Sigma_g^+$ are the leading contributors at high energy.

C. Internal State Distributions

The distribution of rotational and vibrational states of the product ions provide important information on the collision process in two ways: (1) the rotational energy is directly related

to the amount of orbital angular momentum available in the colli-
sion, and (2) the vibrational energy is related to the shape and
position of the electronic potential curves involved in the
transition.[12]   Reference 13 reports the results of an experiment
in which we have measured the internal state distributions of
process (2) and process (1) with n=6. As an alternate approach
to accurately measuring the energy distribution of low-energy
electrons (a very difficult task below about 0.5 eV), we have
chosen photofragment translational spectroscopy.[14,15] This tech-
nique involves photodissociation of the product ions and measure-
ment of fragment kinetic energies by time-of-flight (TOF). The
nascent Na_2^+ internal energy distribution follows directly from
the fragment recoil kinetic energy distribution. Figure 5 shows
the fragment TOF spectrum for process (1) with n=6, together with
calculated spectra obtained for various choices of model internal
state distributions. The conclusion of a rather extensive analy-
sis based on Monte Carlo simulations is that: (1) the associative
ionization probability (opacity function) falls rapidly with
internuclear distance after a separation of about 2Å; and (2) the
distribution of populated vibrational states is nonthermal,
increasing approximately linearly with vibrational level. We
find essentially the same results for process (2). In fact the
behavior of the opacity function is consistent with our earlier
study of the velocity dependence (section I.B) where, in order to
fit the high-velocity side of the excitation function, we assumed
an exponentialy decreasing form for the autoionization width and
found that the opacity function dropped essen tially to zero
beyond b≈2.3Å. It is interesting to note that although pro
cesses (1) and (2) have similar opacity functions, the overall
rate constant of (2) is only 3% of (1). Whether the disparity
in rate constants is due to widely differing Franck-Condon
overlap factors or autoionizing widths is an unresolved
question.
     An essential point emerging from these studies is that,
although associative ionization usually has a large cross sec-
tion, the internal states of the product dimer ion will not be
narrowly distributed. In fact it appears that the vibrational
distribution is controlled by the continuumbound Franck-Condon
factors for all the relevant molecular states contributing to AI.
If this is indeed the case, then AI at very slow collisions
should favor the lowest vibrational states since the
Franck-Condon overlap factors will be greatest for v"=0 of the
dimer ion. Further research is obviously required to investigate
this point futher.
     The analogous reaction in hydrogen to process (2),

$$H(2p) + H(2p) \rightarrow H_2^+ + e \tag{3}$$
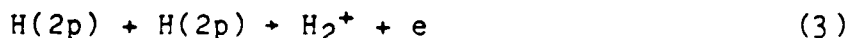
is probably not significant because the total energy is far above
the H_2^+ dissociation limit. Probably Penning ionization rather
than associative ionization would therefore dominate the
branching ratio. A more likely process is

$$H(2s) + H(4d) \rightarrow H_2^+ + e \tag{4}$$

in which only the AI channel is open. Production of H_2^+ by process (4) could be realized by an ensemble of laser-stopped hydrogen atoms immersed in Lyman-α molasses or confined in an optical trap. A second laser stimulates the $H(2p) \rightarrow H(4d)$ transition and then the AI collision proceeds as in reaction (4). As in the Na case, cold-atom collisions should favor low vibrational level population, but this has yet to be demonstrated.

II. RADIATIVE ASSOCIATION

A. INTRODUCTION

Recent developments in laser-cooling and trapping of atoms have opened the possibility of studying an entirely new regime of heavy-particle collision dynamics at ultracold temperatures. The salient features of this new regime are: (1) the heavy-particle de Broglie wavelength is much longer than the collisional interaction range, (2) the width of the translational partition function is comparable to the natural line width of the atomic resonance transition, (3) the orbital angular momentum is so low that only a few partial waves contribute to the scattering event. Thus many conventional ideas characterizing heavy-particle collision dynamics have to be re-examined. For example, in Na atom collisions the reduced mass at a temperature of 1 mK corresponds to a de Broglie wavelength of about 550 a.u. Therefore the semiclassical picture in which nuclear motion is treated as a classical particle moving in an adiabatic potential breaks down and must be replaced by a treatment fully quantal in both the nuclear and electronic motion. Narrowing of the translational energy distribution function with decreasing temperature results in a free-bound spectroscopy exhibiting lines of comparable sharpness to those normally associated with bound-bound spectroscopy. Furthermore, quantal scattering at low energy and angular momentum implies that only a few partial waves contribute to the process; and therefore, many quantum resonance features normally obscured by summation over hundreds of partial waves will be observable in the total cross section. In particular, shape resonances, in which the colliding particles are trapped behind a centrifugal barrier, may enhance the total cross section for radiative association by orders of magnitude. Cold-atom radiative collisions are important not only for their intrinsic interest as a novel bond-forming mechanism but also for the role they may play in other phenomena at low temperature such as ion or neutral cluster condensation stabilized without third-body collisions.

B. CALCULATIONS

The basic two-step pathway to radiative association is:

$$Na + Na + h\omega_1 \rightarrow Na_2^* \tag{5}$$

$$Na_2^* \rightarrow Na_2 + h\omega_2 \tag{6}$$

52

Process (5) is a free-bound laser-induced absorption to an excited state more attractive at long-range than the ground state. The very cold atoms do not have sufficient energy to escape the upper-state potential well by dissociation and are confined to bound vibrational motion until they radiatively relax to the ground dimer state. The computational task is to calculate the rate of laser-induced radiative association as a function of laser flux ϕ, absorption cross section σ_a, and atomic density, N. The rate of reaction is given by,

$$R = \sigma_a \, N \, \phi \qquad (7)$$

and we relate σ_a to the small-gain emission cross section, σ_e, by,

$$\sigma_e = \frac{\lambda^2 hA}{8\pi} \qquad (8)$$

where

$$A = \frac{64\pi^4}{3h} \cdot \frac{1}{\lambda^3} \cdot |\langle v'|\mu|\epsilon''\rangle|^2 \qquad (9)$$

and

$$\sigma_a = \sigma_e \frac{g'}{g} \left[N \sum_{j'v'} (2j+1)e^{-\epsilon''/kT}/Q_T \right] \qquad (10)$$

where Q_T is the translational partition function,

$$Q_T = \left(\frac{2\pi\mu kT}{h^2} \right)^{3/2}$$

Note that the quantity in brackets in (10) is the number of atoms that have the correct energy for the free-bound transition. After the absorption, it remains to calculate the spectrum of the bound-bound de-exictation to the internal manifold of the ground state. The spontaneous emission Einstein A coefficient is given by

$$A' = \frac{64\pi^4}{3h} \sum_{v'} \frac{1}{\lambda^3} \quad |\langle v''|\mu|v'\rangle|^2 \qquad (11)$$

and the emission cross section is

$$\sigma_e = \frac{\lambda^2}{8\pi} A' \, g(\nu)$$

where $g(\nu)$ is the Lorentz line-shape function. Figs. 6 and 7 show the normalized absorption coefficient and Einstein A spontaneous emission coefficient as a function of the frequency of the exciting laser ($h\omega_1$). In Fig. 6 the ordinate is expressed as the normalized absorption coefficient, k, from which an absolute rate can be determined by taking the product of k with the atomic density.

53

Several points are worth noting: (1) the rate of radiative association only becomes significant when the density exceeds 10^{10} atoms cm^{-3}. Below this threshold the signal is too weak to be observed. (2) The emission is considerably blue-shifted from the Na resonance line, and therefore a non-dispersive detector can measure the integrated emission without interference from the excitation line. (3) The vibrational distribution of ground-state dimers is rather broad, following the distribution of Franck-Condon factors in the X ← A sodium dimer emission.

Figure 8 shows the detailed absorption spectrum near threshold. The peaks are P and R branch transitions from the continuum of the ground state to low rotational levels of the $v'= 130$ of the excited A state. Note that at several transitions sharp resonances are clearly evident with enhancements in the total absorption rate of about two orders of magnitude.[16]

The broad distribution of external states calculated in Fig. 7 will probably be a general feature of radiative association in hydrogen as well. The appropriate states are present in the H+H system; and, taking the singlet manifold as an example, a laser tuned to the red of the H_2 (B $^1\Sigma_u^+$) dissociation limit will induce association by

$$H(2s) + H(2s) + \hbar\omega_1 \rightarrow H_2^*(B\ ^1\Sigma_u^+) \qquad (12)$$

$$H_2^* \rightarrow H_2(X\ ^1\Sigma_g^+) + \hbar\omega_2 \qquad (13)$$
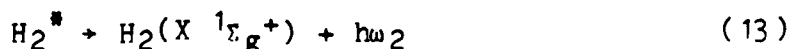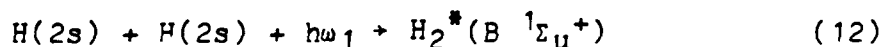
Processes (12), (13) are parallel to processes (5), (6) in sodium. The rate of radiative association in hydrogen will probably be greater over a wider spectral range of $\hbar\omega_1$ because the B state has a significant admixture of the ion pair (H^+, H^-) state, making it attractive over an even longer range than the resonant dipole-dipole interaction in sodium. The final internal state distribution of the X state, produced by spontaneous emission from the B state (equation (13)), is controlled by Franck-Condon factors and will therefore be almost certainly vibrationally hot. Stimulated emission B → X, however, could be used to direct population into low-lying vibrational states. Details of the stimulated process have not been calculated either in sodium or in hydrogen and at this writing no experiment has been performed on either system. A simplified theory of laser-induced radiative association has been worked out for sodium[16] which indicates that the overall process together with interesting quantum resonance effects should be observable.

54

REFERENCES

1. R. Bonanno, J. Boulmer, and J. Weiner, J. Phys. B 16, 3015 (1983).

2. R. Bonanno, and J. Weiner, Phys. Rev. A 28 604 (1983).

3. R. Bonanno, J. Boulmer, and J. Weiner, Commts. At. Mol. Phys. XVI, 109 (1985).

4. J. Weiner, and J. Boulmer, J. Phys. B 19, 599 (1986).

5. R. Janev and A. Mihajlov, Phys. Rev. A 21, 819 (1980).

6. E. Duman, and I. Shmatov, Sov. Phys. JETP 51, 1061 (1980).

7. J. Huennekens, and A. Gallagher, Phys. Rev. A 28, 1276 (1983).

8. M-X. Wang, M.S. deVries, J. Keller, and J. Weiner, Phys. Rev. A 32, 681 (1985).

9. M-X. Wang, J. Keller, J. Boulmer, and J. Weiner, Phys. Rev. A 35, 934 (1987).

10. M-X. Wang, J. Keller, J. Boulmer, and J. Weiner, Phys. Rev. A 34, 4497 (1986).

11. M-X. Wang and J. Weiner, Phys. Rev. A (in press).

12. J. Lorenzen, H. Morgner, W. Pussert, M.W. Ruf, and H. Hotop, Z. Phys. A 310, 141 (1983) and references cited therein.

13. J. Keller, R. Bonnano, M-X. Wang, M.S. deVries, and J. Weiner, Phys. Rev. A 33, 1612 (1986).

14. H. Helm, and R. Möller, Phys. Rev. A 27, 2493 (1983) and references cited therein.

15. C. Brechignac and Ph. Cahuzac, Chem. Phys. Lett. 112, 20 (1984).

16. H. Thorsheim, J. Weiner and P.S. Julienne (Phys. Rev. Lett. submitted).
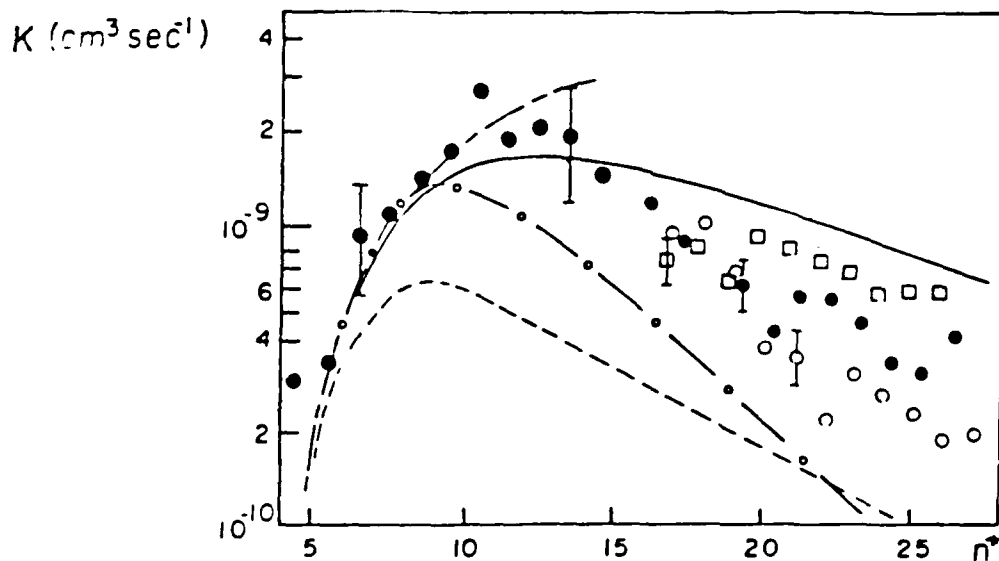
Fig. 1. Associative Ionization Rate Constant vs. Effective Quantum Number.
Data symbols: □ s levels, ● p levels, o ℓ ≥ 2 levels. Theoretical
curves: ---s levels, —— p levels, -o- ℓ ≥ 2 levels.
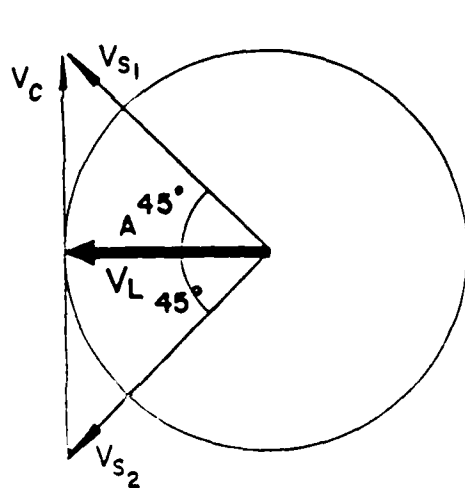
(a)

one laser beam
two sodium sources
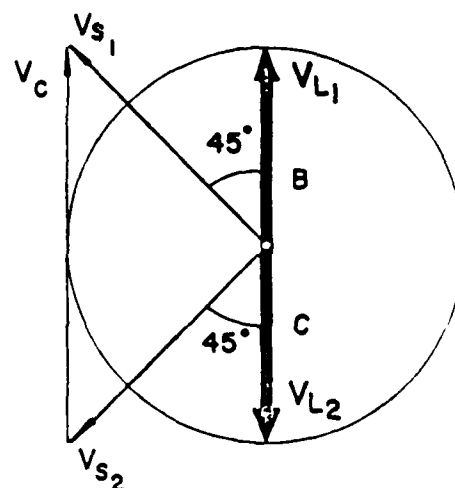
(b)

counterpropagating lasers
two sodium sources

Fig. 2. Schematic diagram of laser-beam, atomic-beam laboratory setup.
The labels V_{S_1} and V_{S_2}, refer to velocity vectors from atomic beam
sources 1 and 2, respectively. Labels V_{L_1} and V_{L_2} denote the laser-
selected velocity component of each atmoic beam. Labels A, B, C are
the laser propagation paths used in these experiments, and V_C is the
collision velocity.

56

COLLISION ENERGY (eV)

CROSS SECTION (ARB. UNITS)

COLLISION VELOCITY (10^3 MS^{-1})
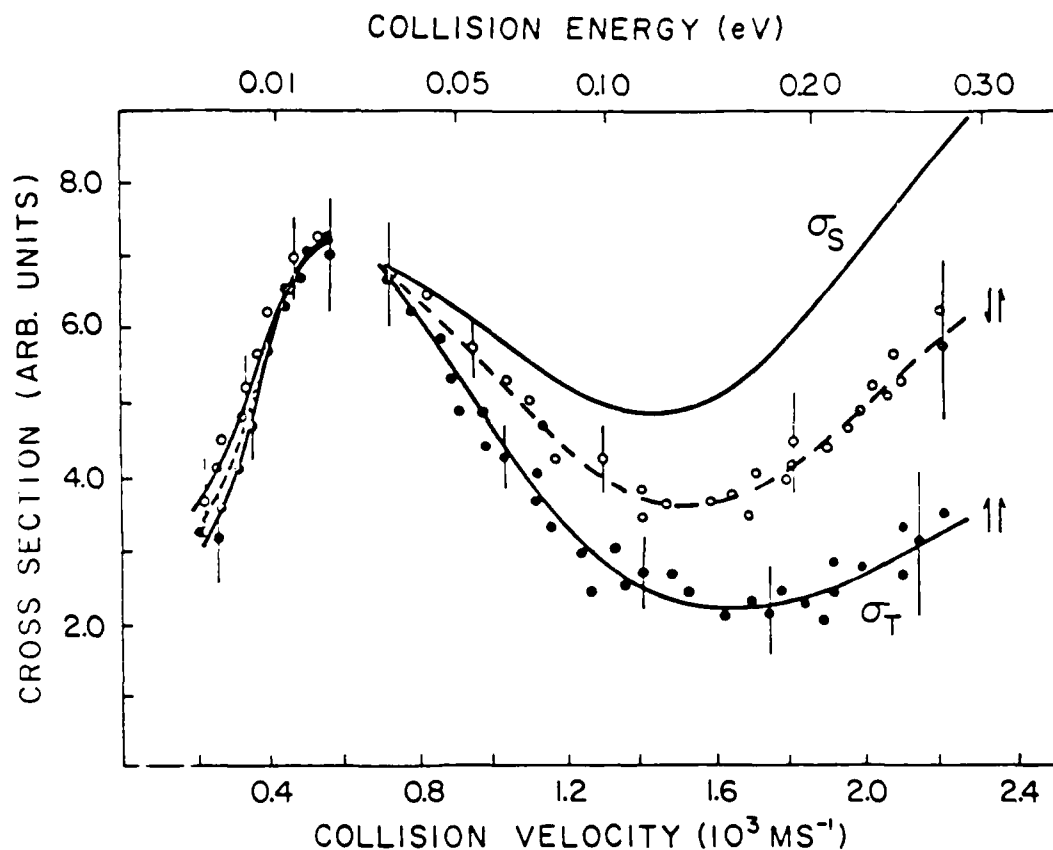
Fig. 3. Excitation function for spin-selected associative ionization (AI). Spin labels ↑↑ and ↑↓ correspond to laboratory spin orientations. Singlet and triplet excitation functions are labeled by σ_S and σ_T respectively.

CROSS SECTION (ARB. UNITS)

AVERAGE COLLISION VELOCITY (ms^{-1})
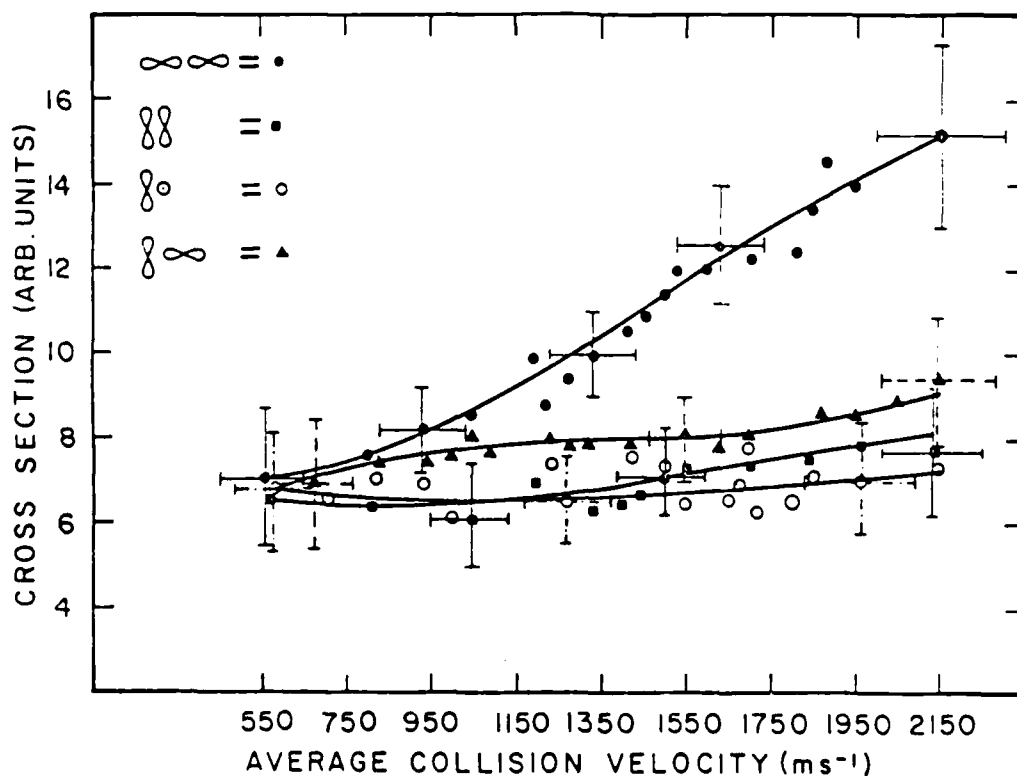
Fig. 4. AI cross sections as a function of average collision velocity for four different combinations of linear polarization. Note the dramatic increase in cross section of axial-axial approach with increasing velocity.

57
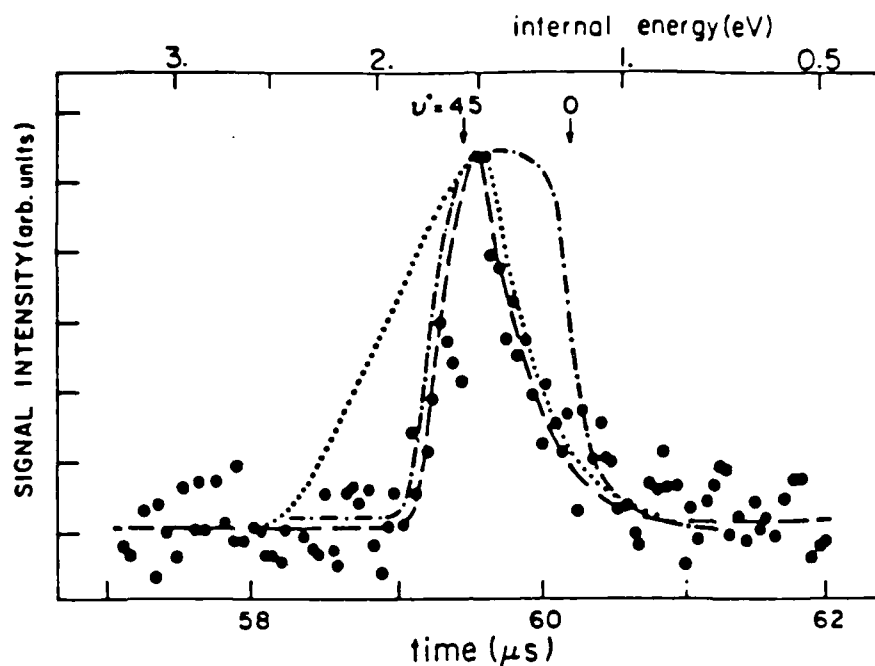
Fig. 5. Forward photofragment spectrum (large solid circles) together with
three different simulations. ···, impact parameter b=5 and only v"=0
populated. -·-·-·, b=0 and all vibrational levels equally populated.
- - -, b=2 and vibrational population linear with v" level. Latter
choice is best fit to measured spectrum. Note that -·-·-· is displaced
slightly to the right for clarity. The left edge is almost congruent
with - - -.
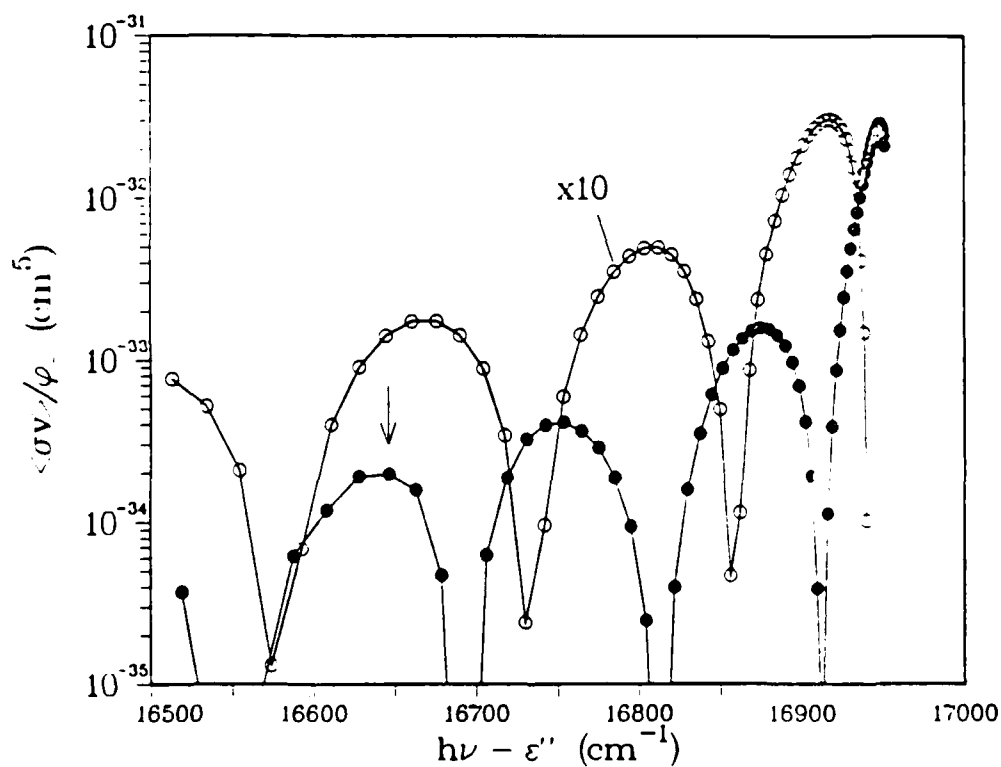
Fig. 6. Free-bound normalized absorption coefficient as a function of laser
frequency ($\hbar\omega_1$). $^1\Sigma_g \leftrightarrow {}^1\Sigma_u$, solid circles. $^3\Sigma_g \leftrightarrow {}^3\Sigma_u$, open circles.
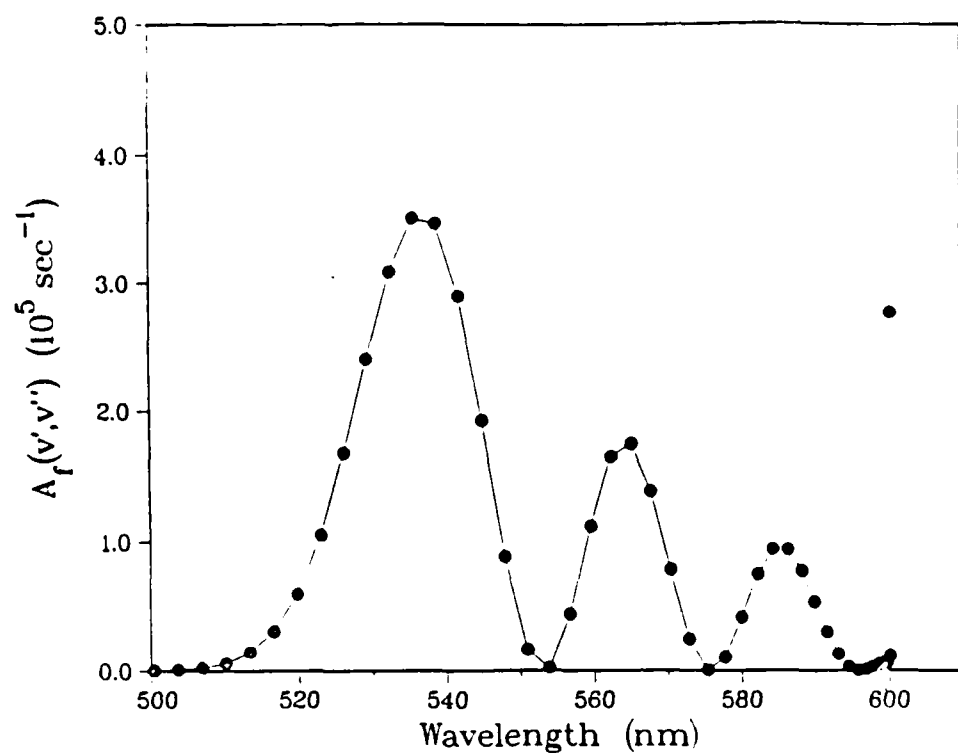
Fig. 7. Round-Round $^1\Sigma_u$ → $^1\Sigma_g$ emission spectrum from v'=107.
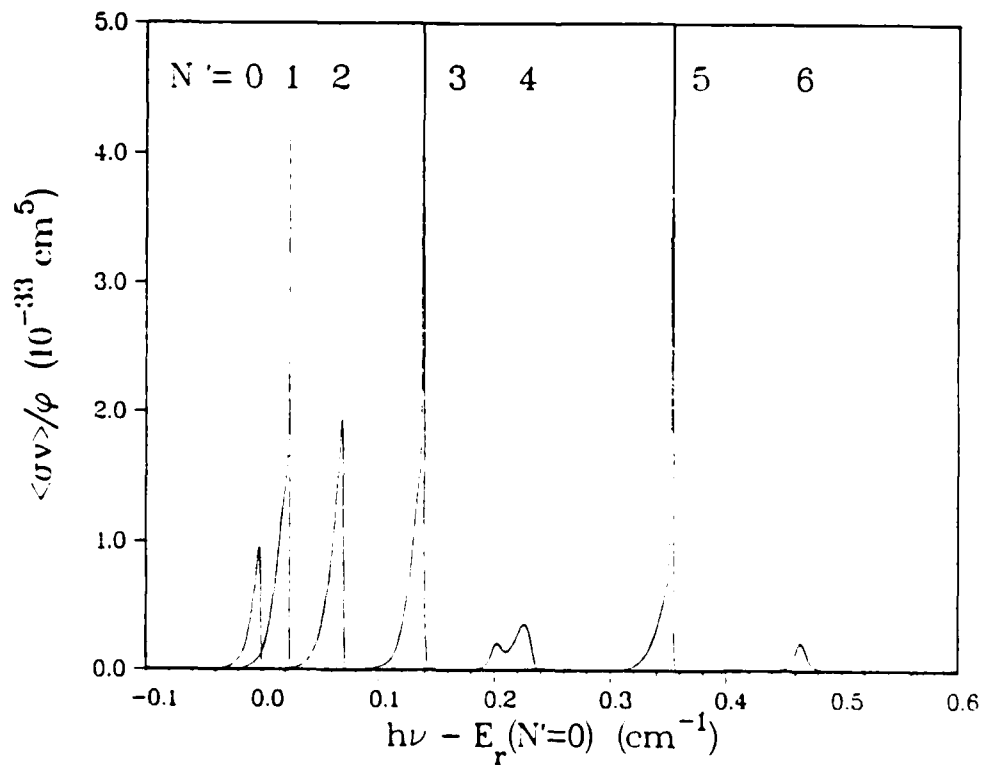
Fig. 8. Detail of $^1\Sigma_g$ → $^1\Sigma_u$ absorption spectrum showing P,R branch progression and resonances.

59

Michael T. Bowers

Formation and Reactivity of Small Hydrogen Cluster Ions

61

Formation and Reactivity of Small Hydrogen Cluster Ions

Michael T. Bowers
Department of Chemistry
University of California
Santa Barbara, CA 93106

ABSTRACT

A specially designed coaxial drift tube type ion source has been utilized to generate ionic hydrogen clusters. The cluster mass spectrum is dominated by odd clusters (H_5^+, H_7^+, H_9^+...) in line with past studies on hydrogen ion clusters. For the first time, however, even cluster ions are formed with relative intensities $H_6^+>>H_8^+>H_{10}^+>H_4^+$. The observation of a relatively intense H_6^+ peak ($H_6^+/H_5^+ \approx 0.05$) was unexpected. The peak at nominal mass 6 was confirmed to be H_6^+ and not H_4D^+ by high resolution analysis. A number of possible formation mechanisms are proposed. The most likely is reaction of H_3^+ or H_5^+ with metastable electronically excited H_3^* or H_5^*. The odd ions H_5^+, H_7^+ and H_9^+ lose H_2 in metastable reactions. Theory indicates that a nascent H_9^{+*} cluster formed from $H_7^+ + H_2$ collisions accounts for the H_9^+ metastable. The H_5^+ ion is shown to lose H_2 via tunneling through rotational barriers. The H_7^+ system is intermediate.

INTRODUCTION

The question of the feasibility of antimatter propulsion has been dealt with by Forward[1] and will not be considered further here. Also, the questions surrounding the suitability of hydrogen ion clusters as potential storage media for antimatter has been addressed previously[2] and elsewhere in this report and won't be dealt with here. What will be dealt with are some results on the formation and reactivity of small hydrogen ion clusters recently obtained in our laboratory at UC Santa Barbara.[3,4] Our interest in these species has been stimulated primarily by their fundamental importance. Because of the relatively small number of electrons, rather sophisticated calculations can be done,[5] the details of which are commented on elsewhere in this report. One important consequence of these calculations is the series of stable structures that have been predicted for even (H_4^+, H_6^+ etc.) and odd (H_5^+, H_7^+, etc.) clusters. A cartoon summarizing these stable structures is given in Fig. 1.

The paper will be organized as follows. The experimental method will be briefly summarized. Next a results and discussion section will be presented that highlights the important findings

63

LOWEST ENERGY CONFIGURATIONS
SUGGESTED BY THEORY:

EVEN CLUSTERS	ODD CLUSTERS

H_4^+

H_5^+

H_6^+

H_7^+

H_8^+

H_9^+

H_{10}^+ ?

H_{11}^+ ?
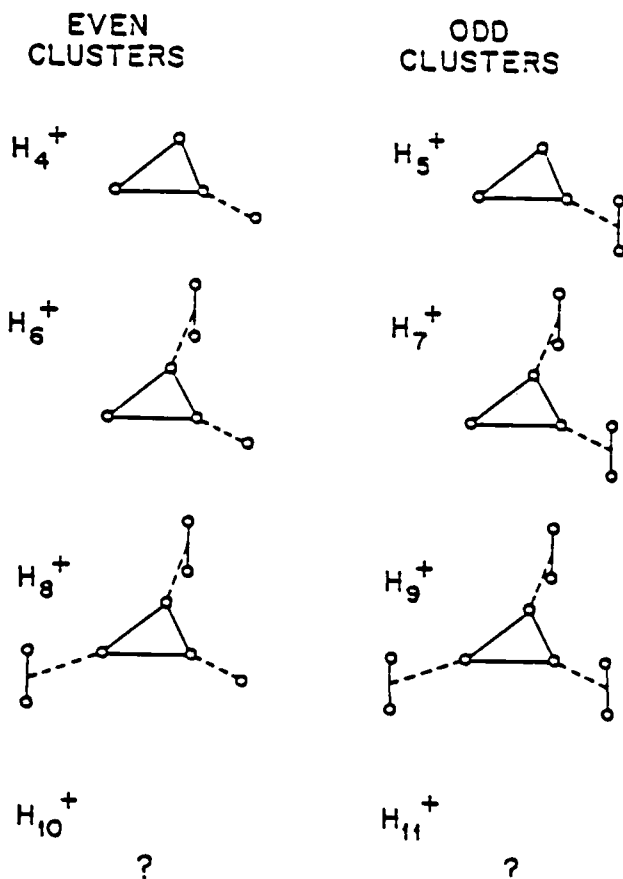
Fig. 1

in both even and odd clusters. A section will then be included
that lists some of the important measurements that need to be
accomplished.

EXPERIMENTAL

The experiments were performed on a VG Analytical ZAB-2F
double focusing reverse geometry mass spectrometer (Fig. 2)[6]
Ions were formed by electron impact in a specially designed
temperature and pressure variable drift source. The experimental
details have been fully discussed in the literature[3,4] and will
only be briefly summarized here. In all instances the
temperature was maintained at 85 K and the H_2 pressure between
0.3 and 0.5 torr. Ionization occurred by electron impact using
500 eV electrons. Under these conditions the electron beam
penetrated the entire ion source from the electron entrance hole
to the ion exit slit.
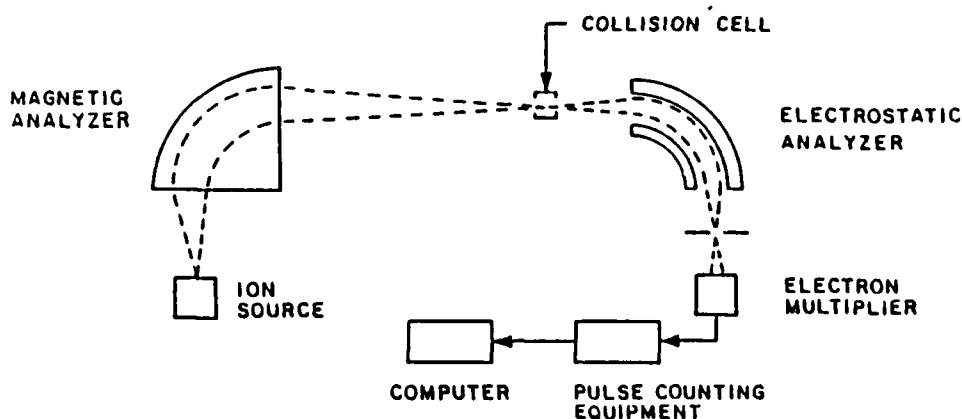
Fig. 2: Schematic of the instrument used to
obtain the data discussed in this paper.

RESULTS AND DISCUSSION

A mass spectrum of species emitted from the ion source
under typical conditions is given in Fig. 3. The spectrum is
dominated by the odd cluster species H_3^+, H_5^+, H_7^+ and H_9^+. The
only significant even mass intensity is at mass 6. The
discussion will be separated into two parts: first we will
discuss the odd clusters and then the even clusters.

A. H_5^+, H_7^+, H_9^+ and H_{11}^+

The dominant cluster intensities observed can be explained
by the following reactions in the ion source:

$$\underline{\Delta H, eV}$$

$$H_2 + e^- \longrightarrow H_2^+ + 2e^- \qquad +15.43 \qquad (1a)$$

$$H_2^+ + H_2 \longrightarrow H_3^+ + H \qquad -1.7 \qquad (1b)$$

$$H_3^+ + 2H_2 \longrightarrow H_5^+ + H_2 \qquad -0.29 \qquad (1c)$$

$$H_5^+ + 2H_2 \longrightarrow H_7^+ + H_2 \qquad -0.13 \qquad (1d)$$
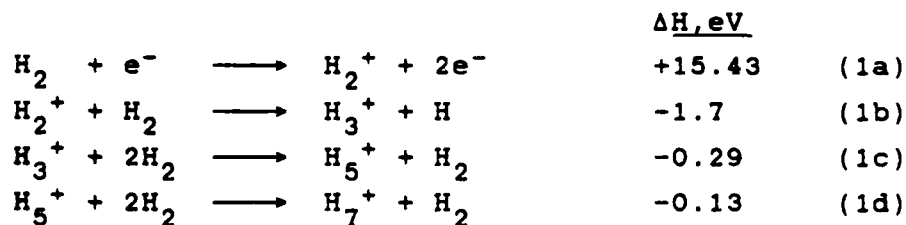
It is apparently not possible to stabilize the H_4^+ intermediate
in reaction (1b) and consequently H_4^+ is not observed. These
results are qualitatively consistent with previous experimental
studies.[7] One interesting point can be made by comparing the
intensities of H_5^+, H_7^+ and H_9^+ to H_{11}^+. Only a very small drop

65
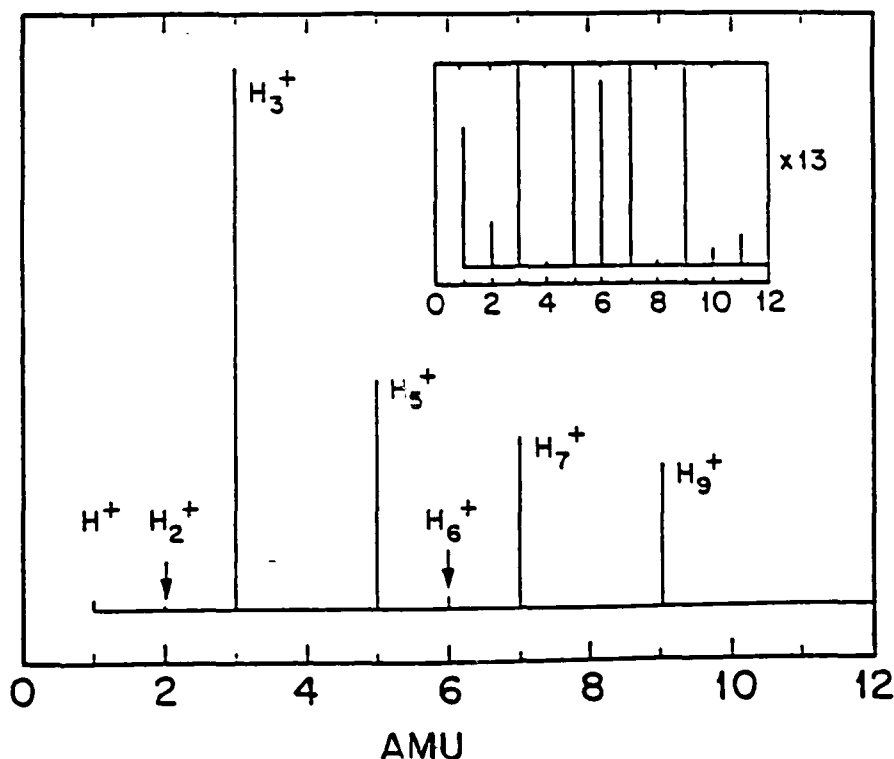
Fig. 3: Mass spectrum of positive ions exiting the ion source
at hydrogen pressures of 0.5 torr. The very small
peaks at nominal mass 4, 8 and 10 are primarily H_2D^+,
H_6D^+ and H_9D^+ but very small amounts of H_4^+, H_8^+ and
H_{10}^+ are also found.

in intensity is observed between H_5^+ and H_9^+ but a precipitous
drop is observed for H_{11}^+. This can be rationalized by reference
to the structures in Fig. 1. Once all of the corners of the H_3^+
core are occupied by H_2-molecules, addition of the next H_2-
molecule must occur at an energetically less favorable site
(probably above or below the plane of the H_3^+ core). This
observation has the consequence that the formation of H_{11}^+
presents a kinetic bottleneck in building larger size H_n^+
clusters starting from H_3^+. In order to estimate the magnitude
of this problem the rate constants for the varying clustering
steps would have to be measured. These are currently not known.
     One of the important aspects of hydrogen ion clustering is
the theoretical model used to describe the kinetics. Our group
has pioneered the statistical phase space theory of ion-neutral
association reactions.[8] This theory has not as yet been
applied to hydrogen clustering. We have, however, applied it to
the calculation of the kinetic energy distribution expected from
the spontaneous dissociation of nascent hydrogen ion collision
complexes. For example:

$$H_5^+ + H_2 \xrightarrow{k_f} (H_7^+)^* \tag{2a}$$

$$(H_7^+)^* \xrightarrow{k_b} H_5^+ + H_2 \tag{2b}$$

$$(H_7^+)^* + H_2 \xrightarrow{k_s} H_7^+ + H_2 \tag{2c}$$
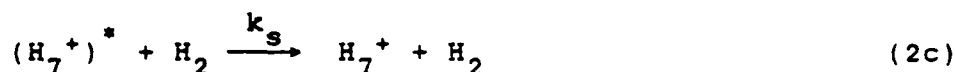
The reaction sequence (2) is a specific example of the general energy transfer mechanism responsible for ion neutral clustering.[8] The theory calculates the (E,J) distribution of the $(H_7^+)^*$. In the association kinetics the values of k_f, k_b and k_s are computed. However, an interesting test of the theory is obtained by calculating the kinetic energy distribution of H_5^+ + H_2 generated from spontaneous dissociation of nascent $(H_7^+)^*$. The data and theoretical predictions for H_9^+, H_7^+ and H_5^+ spontaneously losing H_2 are given in Fig. 4.

Fig. 4

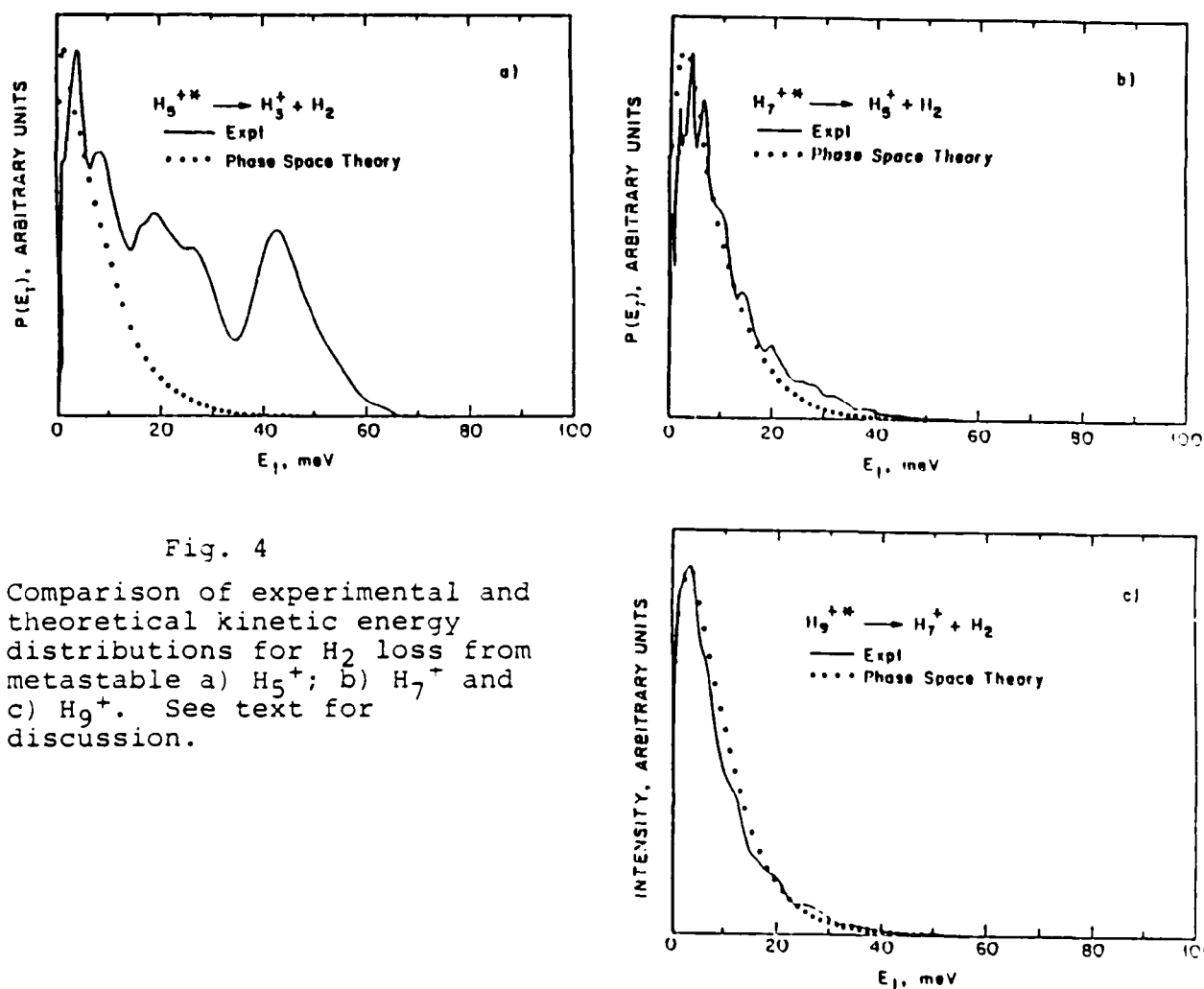Comparison of experimental and theoretical kinetic energy distributions for H_2 loss from metastable a) H_5^+; b) H_7^+ and c) H_9^+. See text for discussion.

It is apparent from Fig. 4 that for H_9^+ excellent agreement between theory and experiment is obtained. This result verifies the ion-induced dipole potential used in the theory is appropriate, as is the overall formalism. Theory also predicts the overall shape of the H_7^+ distribution but does not predict the structure. For H_5^+, very poor agreement between theory and experiment is obtained. The reason for the poor agreement with H_5^+ is that vibrational predissociation is no longer the dissociation mechanism. The H_5^+ data are well fit by a combination of phase space theory and JWKB tunneling through centrifugal barriers.[3] The details are beyond the scope of this paper. The calculations did confirm that the potential surfaces generated by Ahlrichs[48] are accurate until very high total angular momentum states are considered. The structure in the H_7^+ kinetic energy distribution is presumed due to tunneling although calculations were not done to confirm it.

B. H_4^+, H_6^+, H_8^+ and H_{10}^+

No even hydrogen cluster had been unambiguously observed until recent measurements in our group showed H_4^+ could be formed from collisional dissociation of H_5^+ ions.[9] Hence, we were very surprised at the very large H_6^+ peak apparent in the mass spectrum of Fig. 3. This observation was specially surprising since only a tiny peak was observed at nominal mass 4. Hence, clustering of H_2 to either H_4^+ or H_2D^+ could not be the source for the peak at mass 6. In order to establish the isotopic identity of the peak a high mass resolution scan was done. The results are given in Fig. 5.
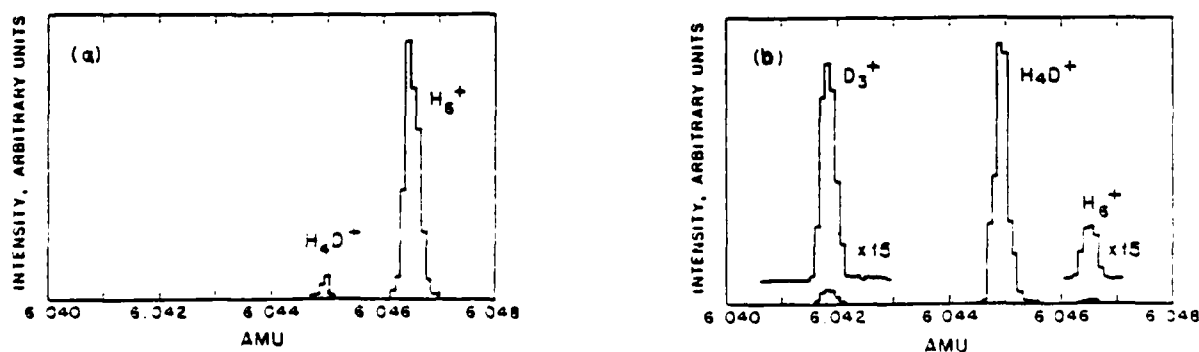
Fig. 5:   High resolution spectra of the peak at nominal mass 6:
a) in research grade H_2, corresponding to the mass
spectrum in Fig. 3; b) with a trace of D_2 added.

In pure research grade H_2, the dominant peak at mass 6 (95%) is identified at the exact mass expected for H_6^+. A small (5%) contribution is due to H_4D^+. This assignment is confirmed by the addition of a trace amount of D_2 to the H_2 resulting in the H_4D^+

peak dominating the isotopic distribution (Fig. 5b).

The immediate question arises as to the origin of the H_6^+ ion. This point is discussed in some detail elsewhere.[4] The most likely candidates are given in reactions 3:

$$H_3^+ + H_3^* \longrightarrow H_6^+ + H \qquad (3a)$$

$$H_5^+ + H_3^* \longrightarrow H_6^+ + H_2 \qquad (3b)$$

$$H_3^+ + H_5^* \longrightarrow H_6^+ + H_2 \qquad (3c)$$
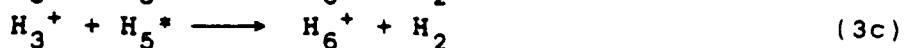
Electronically excited metastable H_3^* has been shown to be long lived,[10] and hence H_5^* may also be long lived. The H_3^* and H_5^* molecules are probably formed by recombination of electrons with $H_3^+(v>0)$, H_5^+, H_7^+ etc. in the ion source. The coaxial nature of the source, Fig. 6, supports this mechanism because low energy electrons and cluster ions are slowly drifting in an opposite direction in a narrow cone in the center of the cell.

FIELD GUARD DRIFT RINGS
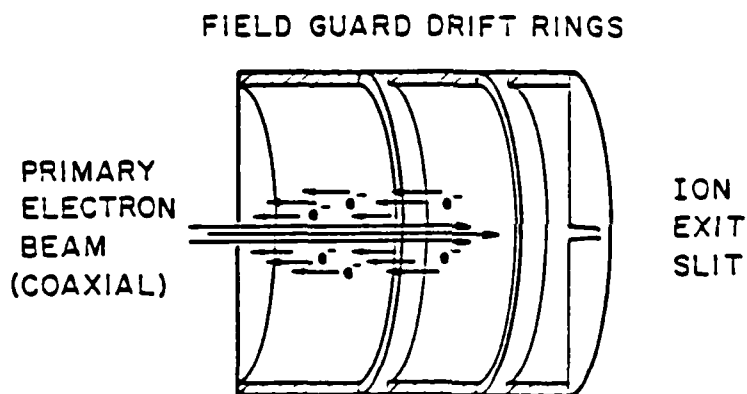
Fig. 6: Cutaway view of the ion source. The 500 eV electron beam enters from the left. Scattered electrons drift right to left while positive ions drift left to right.

Additional experiments must be done to confirm this mechanism. If correct, it may have important implications for antimatter clustering.

Collision induced dissociation (CID) is a useful method for deriving information on ion structures. The CID spectra of H_6^+ and H_7^+ are given in Fig. 7. The H_7^+ CID spectrum is dominated by loss of H_2 to form H_5^+ (~95%) with loss of two H_2 molecules to form H_3^+ providing most of the rest of the product ion current (4%). Noteworthy, however, is the formation of small amounts of H_4^+ and H_6^+.

The CID spectrum of H_6^+ is qualitatively much different. The loss of H to form H_5^+ is about as probable as the loss of H_2 to form H_4^+. Perhaps surprising is the facile loss of both H and H_2 (or H_3?) to form large amounts of H_3^+. Both this fact and the necessarily exotic mechanism for formation of H_6^+ indicate that possibly the H_6^+ ions formed and detected in our system may

$H_6^+ \xrightarrow[\text{He}]{} H_{5,4,3,2,1}^+$ a)

$H_7^+ \xrightarrow[\text{He}]{} H_{6,5,4,3,2,1}^+$ b)

x 200

AMU

AMU
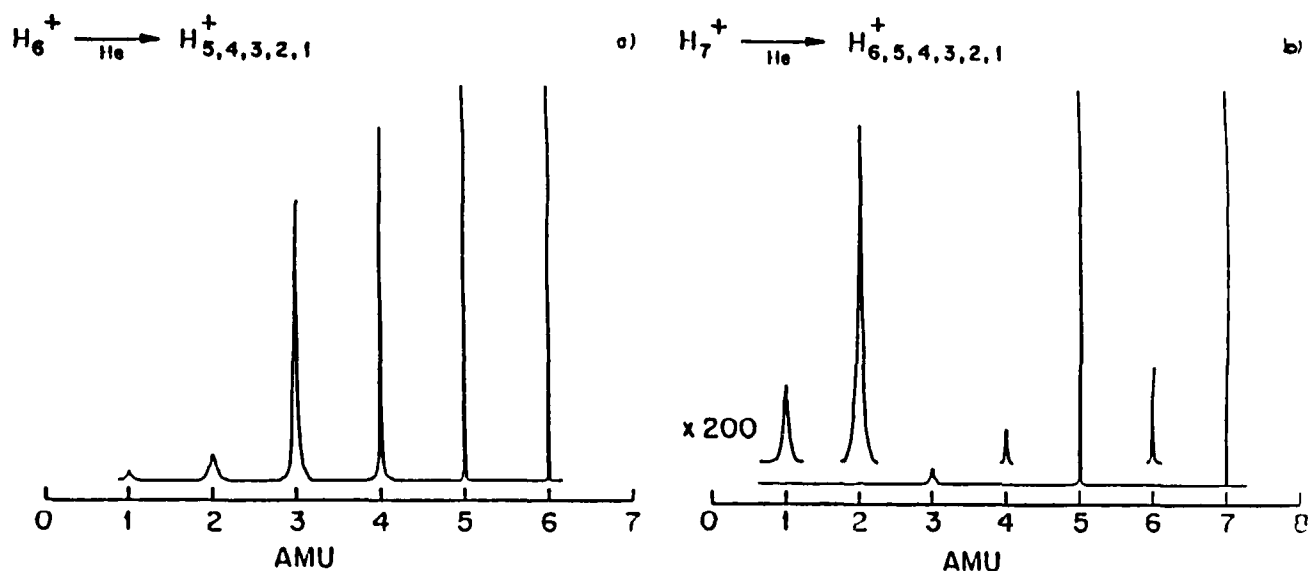
Fig. 7. Collision induced dissociation spectra of a) H_6^+ and
b) H_7^+. Note that H and H_2 are lost from H_6^+ with
nearly equal probability while H_2 loss from H_7^+ is
approximately 1000 times more probable than H loss.

not be the structure indicated in Fig. 1, although there is not
conclusive evidence one way or the other. Some high level
calculations, including electronic excited states, should be done
on this system.

The presence of a strong H_6^+ peak in the mass spectrum
indicates that the ligand switching reaction 4 is very slow:

$$H_6^+ + H_2 \longrightarrow H_7^+ + H \qquad\qquad (4)$$

since the average H_6^+ ion undergoes hundreds of collisions before
it exits the ion source. If we are dealing with ground state
H_6^+, shown in Fig. 1, then $D_0^0(H_5^+ - H) \gg D_0^0(H_5^+ - H_2)$. Again
good theoretical calculations should be done to confirm or
contradict this prediction.

Work that Needs to Be Done

Throughout the text a number of suggestions have been made
for further work. These, and others, will be listed here.

1. The temperature dependence of the following association
rate constants must be measured:

$$H^+ + H_2 + M \longrightarrow H_3^+ + M$$
$$H_3^+ + H_2 + M \longrightarrow H_5^+ + M$$
$$H_9^+ + H_2 + M \longrightarrow H_{11}^+ + M$$
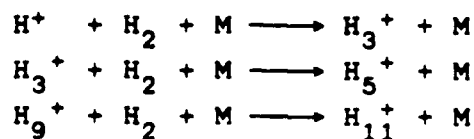
Isotopic variations should also be measured as these
are of fundamental interest and will be important for
confirming the theoretical model. These should
include:

$$H^+ + D_2 + M \longrightarrow HD_2^+ + M$$

$$D^+ + H_2 + M \longrightarrow DH_2^+ + M$$

$$H^+ + HD + M \longrightarrow H_2D^+ + M$$

$$H_3^+ + D_2 + M \longrightarrow H_3D_2^+ + M$$

$$D_3^+ + H_2 + M \longrightarrow D_3H_2^+ + M$$
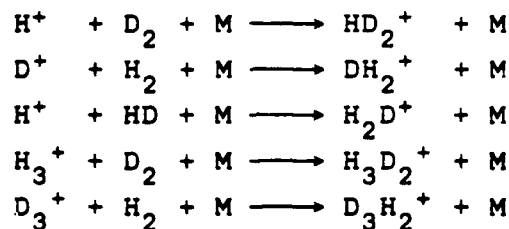
All of these experiments, with the exception of H_3^+ +
H_2 + M $\longrightarrow$ H_5^+ + M will require an instrument that
injects the reactant ion into a differentially pumped
drift tube ion source containing the neutral reactant.
Such a device has been designed at UC Santa Barbara and
will be constructed within the next year.

2. Statistical theory calculations should be done on each
   of the systems listed in 1. The simplest of these can
   be initiated in the absence of experiment and can be
   used to estimate the required source pressures and
   temperatures for successful experiments to be
   performed.

3. The mechanism of formation of H_6^+ should be pursued.
   Ultimately this may require the construction of a
   dedicated crossed beam machine. Initially, however, we
   can alter the source conditions to test the proposed
   mechanism. One suggestion made at the workshop was to
   add small quantities of a thermal electron scavenger
   (SF_6 or CCl_4). We can also accurately measure the H_6^+
   arrival time distribution at the detector in a pulsed
   experiment to see how it compares to H_3^+ and H_5^+.

4. Serious theoretical effort should be put into
   calculating the structure and stability of H_6^+ in both
   the ground and low lying excited states.

5. Measurements of the rates of association of different
   cluster ions with H atoms need to be made. An
   instrument dedicated to these experiments will have to
   be designed and built.

REFERENCES

1. R. Forward, University of Dayton Research Institute, Report # UDR-TR-85-55 and FO4611-83-C-0046, (September 1985).

2. Proceedings of the Hydrogen Cluster Ion Study Group, J.T. Bahns organizer, University of Dayton Research Institute, (Summer 1986).

3. N.J. Kirchner and M.T. Bowers, J. Phys. Chem., (in press).

4. N.J. Kirchner and M.T. Bowers, J. Chem. Phys., (in press).

5. See, for example, a) W.I. Salmon and R.D. Poshusta, J. Chem. Phys., 59, 4867 (1973); b) R. Ahlrichs, Theor. Chim. Acta (Berlin), 39, 149 (1975); c) U. Yamaguchi, J.F. Gaw and H.F. Schaeffer, J. Chem. Phys., 78, 4074 (1983); d) L.R. Wright and R.F. Borkman, J. Chem. Phys., 77, 1938 (1982).

6. For details, see P.A.M. van Koppen, P.R. Kemper, A.J. Illies and M.T. Bowers, Int. J. Mass Spectrom. Ion Phys., 54, 265 (1983).

7. See, for example, a) F. Kirchner, Z. Naturforsch, Teil A18, 879 (1963); b) A. van Deurson and J. Reuss, Int. J. Mass Spectrom. Ion Phys., 11, 483 (1973); c) M. Saporaschenko, J. Chem. Phys., 42, 2760 (1965); d) A. van Lumig and J. Reuss, Int. J. Mass Spectrom. Ion Phys., 27, 197 (1978). See also Ref. 4c for a review.

8. L. Bass, W.J. Chesnavich and M.T. Bowers, J. Am. Chem. Soc., 101, 5493 (1979); P.A.M. van Koppen, M.F. Jarrold, M.T. Bowers, L. Bass and K.R. Jennings, J. Chem. Phys., 81, 288 (1984).

9. N.J. Kirchner, J.R. Gilbert and M.T. Bowers, Chem. Phys. Lett., 106, 7 (1984).

10. J.F. Garvey and A. Kupperman, Chem. Phys. Lett., 107, 491 (1984).

Yukio Yamaguchi, Jeffrey F. Gaw, Richard B. Remington, and
Henry F. Schaefer III

The H_5^+ Potential Energy Hypersurface

The H_5^+ Potential Energy Hypersurface.
Characterization of Ten Distinct
Energetically Low-Lying Stationary Points

Yukio Yamaguchi, Jeffrey F. Gaw, Richard B. Remington,
and Henry F. Schaefer III

Department of Chemistry and Lawrence Berkeley Laboratory
University of California
Berkeley, California 94720

Abstract

Ab initio molecular electronic structure theory has been
used in an attempt to characterize the low-lying stationary
points on the H_5^+ potential energy hypersurface. Three distinct
levels of theory have been used: the self-consistent-field (SCF)
method, configuration interaction (CI) including all single and
double excitations, and full configuration interaction. Four
different basis sets were used: double zeta (DZ), double zeta
plus polarization (DZP), an extended basis set designated H
(6s2p/4s2p) and a second extended basis set designated H
(8s3p/6s3p). The higher levels of theory are in agreement that
the only minimum for H_5^+ is a C_{2v} structure, with three other
stationary points (of D_{2d}, C_{2v}, and D_{2h} symmetries) lying less
than one kcal/mole higher in energy. The predicted dissociation
energy D_0 is 5.5 kcal/mole, which is estimated to be about one
kcal/mole less than the exact D_0. Furthermore, there are six
other stationary points lying less than 8 kcal/mole above the
minimum. Vibrational frequencies, dipole moments, and infrared
intensities for each of the ten stationary points have been
predicted at several different levels of theory. From the
perspective of quantum chemistry, the H_5^+ system is very
attractive as a candidate for the study of the vibrational
dynamics of weakly bound systems.

Table 1.   Total energies and geometrical structures for the H_5^+ global minimum (Structure 1) at eleven different levels of theory

| Level of Theory	DZ	DZP	(4s2p)	(6s3p)	DZ	DZ	DZP	DZP	(4s2p)	(4s2p)	(6s3p)
	SCF	SCF	SCF	SCF	CISD	Full CI	CISD	Full CI	CISD	Full CI	CISD
Energy in Hartrees	-2.407823	-2.434670	-2.441263	-2.442128	-2.462310	-2.463153	-2.509874	-2.511426	-2.520609	-2.522444	-2.523150
R(A)	1.7510	1.5375	1.5468	1.5456	1.7131	1.7091	1.2622	1.2287	1.2831	1.2466	1.3387
d(A)	0.7406	0.7464	0.7496	0.7490	0.7562	0.7573	0.7608	0.7636	0.7672	0.7705	0.7640
r_1(A)	0.8697	0.9028	0.9102	0.9098	0.8822	0.8833	0.9759	0.9921	0.9817	0.9988	0.9606
r_2(A)	0.8276	0.8250	0.8310	0.8297	0.8369	0.8373	0.8035	0.8003	0.8131	0.8098	0.8174
α (degrees)	56.82	54.38	54.32	54.26	56.63	56.58	48.62	47.57	48.93	47.83	50.36

Figure labels: r_1, r_2, α, R, d
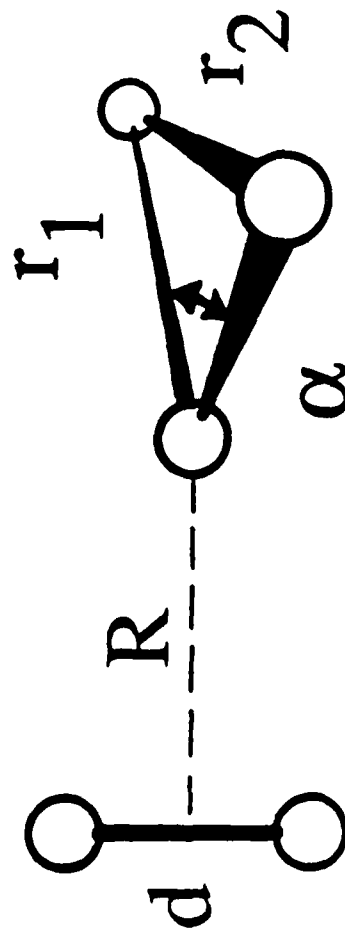
Table 11. Harmonic vibrational frequencies (in cm^{-1}) for ten conformers of H_5^+ at the DZP Full CI level of theory.

Conformer	1	2	3	4	5	6	7	8	9	10
Symmetry	C_{2v}	D_{2d}	C_{2v}	D_{2h}	C_{2v}	C_{2v}	C_{2v}	C_{2v}	C_s	C_{3v}
Planarity	No	No	Yes	Yes	No	Yes	Yes	Yes	No	No
ω_1	4198(A_1)	4067(A_1)	4221(A_1)	4086(A_g)	4424(A_1)	4432(A_1)	4431(A_1)	4486(A_1)	4490(A')	4516(A_1)
ω_2	3824(A_1)	4000(B_2)	3813(A_1)	4007(B_{1u})	3592(A_1)	3528(A_1)	3593(A_1)	3573(A_1)	3577(A')	3573(A_1)
ω_3	2043(B_1)	1626(E)	2092(B_1)	1766(B_{2u})	2850(A_1)	2707(A_1)	2853(A_1)	2832(A_1)	2827(A'')	2823(E)
ω_4	1746(A_1)	1626(E)	1800(A_1)	1465(A_g)	2781(B_1)	2690(B_1)	2783(B_1)	2792(B_1)	2825(A')	2823(E)
ω_5	1300(B_2)	1464(A_1)	1145(B_2)	1348(B_{3g})	418(B_2)	531(B_2)	379(B_1)	258(A_1)	222(A')	166(A_1)
ω_6	963(B_2)	1036(E)	1118(B_1)	1243(B_{3u})	357(A_1)	374(B_1)	346(A_1)	225(B_2)	188(A')	188i(E)
ω_7	944(B_1)	1036(E)	867(B_1)	954(B_{2u})	335(B_2)	362(A_1)	319(B_2)	233i(B_1)	23(A'')	188i(E)
ω_8	478(A_1)	188(B_1)	495(A_1)	1831(A_u)	161(A_2)	394i(B_1)	1511(A_2)	2491(B_1)	2621(B_1)	194i(E)
ω_9	173(A_2)	448i(B_2)	165i(A_2)	4901(B_{1u})	398i(B_1)	395i(B_2)	398i(B_1)	260i(B_2)	2701(A')	194i(E

77

6s3p/SCF   6s3p/CISD

J. A. Montgomery, Jr. and H. H. Michels

Electronic Structure and Stability of Small Cation
and Anion Hydrogen Clusters

Electronic Structure and Stability of Small Cation and Anion Hydrogen Clusters

J. A. Montgomery, Jr. and H. H. Michels[*]
United Technologies Research Center
East Hartford, CT 06108

ABSTRACT

$\underline{\text{Ab initio}}$ calculations of the electronic structure of H_n^- and H_n^+ clusters have been carried out using accurate Gaussian basis sets and with levels of theory up to fourth-order perturbation theory (MP4) and single and double excitation configuration interaction (CISD). The odd hydrogen cation addition sequence, $H_n^+ + H_2 \rightarrow H_{n+2}^+$, appears to be thermodynamically stable for large size cluster formation. The even H_6^+ cation also exhibits surprising stability in D_{2d} symmetry. In contrast, the hydrogen anion addition sequences, $H_n^- + H \rightarrow H_{n+1}^-$ and $H_n^- + H_2 \rightarrow H_{n+2}^-$, appear to be thermoneutral or unstable.

83

INTRODUCTION

There have been numerous thermochemical and kinetics studies of weakly bound ionic clusters during the past decade[1,2]. Of particular interest are the H_n^+ cation and H_n^- anion sequences since they represent examples of the chemistry of strong chemical bonding, in H_3^+, the simplest hydrogen bonded molecular ion, in H_5^+, and the simplest atomic anion, H^-. In addition, for the first few members of these sequences, detailed <u>ab initio</u> quantum mechanical calculations of their equilibrium bond lengths and vibrational spectra can be carried out.

Very recently, the possibility of forming large H_n^+ clusters (n > 1000), that could be kept for long periods of time in a Penning trap, has been discussed[3]. Such a system is a prototype for bulk antiproton or antihydrogen storage, with uses as high energy density material or as an energy source for advanced propulsion concepts. The mechanism for formation and storage of these large cluster ions can be understood only if the thermodynamics and kinetics of the cluster growth processes are identified and analyzed in detail. It is the purpose of this paper to examine the thermodynamic stability of the first few members of the hydrogen cation and anion cluster sequences since their stability is a requirement for defining a useful association pathway for the growth of large clusters.

Numerous experiments[4,5] have measured the stability of the odd-membered hydrogen clusters that are formed by the association reaction:

$$H_n^+ + H_2 \rightarrow H_{n+2}^+ \quad ; \quad n = 3,5,7,\ldots \tag{1}$$
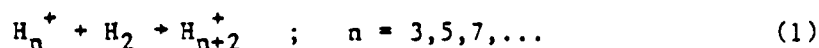
These clusters exhibit stabilization energies of approximately 3-6 kcal/mol, in good agreement with theoretical calculations[6,7]. Until recently, the even-membered hydrogen clusters had not been observed, with the exception of the suggestion of a stable H_4^+ ion formed by the attachment of a H atom to the H_3^+ ion[8]. A very recent study of the even-membered clusters[9] suggests that the H_4^+ observation could be interpreted as H_2D^+. This study also indicates a high degree of stability for H_6^+.

In contrast, the negative hydrogen ion clusters have never been observed and a recent careful search for stable or metastable H_2^- and H_3^- produced negative results[10]. There have been several theoretical studies [11,12] which support the existence of stable H_3^-, and higher clusters, but more accurate ab initio calculations[13] shed doubt on this conclusion.

The present study is limited to an analysis of the H_5^+ and H_6^+ cation and the H_3^- anion. Previous theoretical studies [6,7] of H_5^+ provide a basis for comparison with the present work and allow us to access the accuracy of our analysis of H_6^+, a system of particular interest in the hydrogen cation sequence. Our analysis of H_3^- is carried out using several basis sets and four levels of theory in order to establish the stability of this anion. This extensive study is necessary since a negative result for the stability of H_3^-, coupled with the known, unstable structure for H_2^-, precludes any simple association pathway for the growth of larger anion clusters.

THEORETICAL CONSIDERATIONS

In order to establish the thermodynamic stability of these hydrogen cluster ions, ab initio calculations were carried out to determine their electronic structure and stable geometries. Several Gaussian basis sets, with increasing flexibility, were employed in these studies and levels of theory up to single and double configuration interaction expansions (CISD) were examined. We describe these calculations separately for our studies of the anion and cation structures.

Stability of H_3^-

The most extensive study of the H_n^- anions previously reported is that by Hirao and Yamabe[13] who carried out both SCF and CISD calculations using a double-zeta plus polarization Gaussian basis set. Their results indicated that successive ion clusters were stable by 0.5-1.0 kcal/mol in this approximation but that, for the critical H_3^- anion, this stabilization energy appeared to be less than the increased zero-point energy in forming H_3^- from $H^- + H_2$.

In order to clarify this stability issue for H_3^-, we have carried out _ab initio_ calculations using three different Gaussian basis sets. The first (and smallest) basis set was the (6s1p/4s1p) construction reported by Nicolaides, et al.[14] This basis set (labeled SMALL) is a slight improvement over the 4-31G plus polarization (double-zeta plus polarization) basis set that was employed by Hirao and Yamabe[13]. A somewhat more extended basis (labeled LARGE) was then constructed by augmenting the hydrogen basis reported by Siegbahm and Liu[15] with a diffuse s-function (exponent = 0.016) and three p-functions (exponents = 0.1, 0.4, 1.6). Finally, a very large (labeled HUGE) hydrogen basis was constructed by augmenting the basis reported by Dykstra, et al[16] with a diffuse s-function (exponent = 0.014) and a diffuse p-function (exponent = 0.07).

SCF and perturbation theory calculations through the MP4 (SDTQ) level of theory were performed with each of these basis sets. CISD calculations were performed with the SMALL and LARGE basis sets. These calculations included full geometry optimization and vibrational analysis. Computational limitations allowed only a single point CISD energy calculation with the HUGE basis. All calculations were performed with the GAUSSIAN 82 system of programs[17].

The results of these calculations are summarized in Table I, which includes the H^- and H_2 constituents as well as H_3^-. Note that program limitations precluded the calculation of vibrational frequencies at the MP4 level. It is clear from Table I that the inclusion of the vibrational zero point energy is necessary to assess the stability of H_3^-. We find with every basis and level of theory that the H_3^- ion is not stable with respect to H^- and H_2. This conclusion is supported by the results of earlier theoretical work[12,13], and by the recent experimental study of Bae, Coggiola, and Peterson[10].

Stability of H_5^+ and H_6^+

In order to assess the recent calculations by Yamaguchi, et al[7] with respect to basis set convergence, an SCF study of H_5^+ was carried out with the HUGE basis. This is the first test of the possible importance of d-functions in studies of hydrogen cluster ions. The results are shown in Table II which

indicate that only a slight improvement (1 mhartree) in the optimized SCF energy is obtained by including d-functions. Our optimized geometries using the HUGE basis are in excellent agreement with the results reported by Yamaguchi, et al[7] with a somewhat smaller (8s3p/6s3p) basis. Our very accurate SCF analysis suggests that the C_{2v} structure of H_5^+, found in the earlier calculations of Yamaguchi, et al,[6] is indeed the lowest energy and most stable structure for H_5^+.

The theoretical calculations of Wright and Borkman[18] predict the most stable configuration of H_6^+ to be an H_3^+ ring with attached H and H_2 ligands (see Fig. 1). However, it is difficult to visualize a mechanism for formation of this structure under the experimental conditions reported by Kirchner and Bowers[9]. We have made some preliminary calculations on H_6^+ structures that might be formed from H_3^+ and H_3^*. Our calculations to date indicate that the Wright and Borkman structure is not the lowest energy state of this system. Instead, we find that the ground state of H_6^+ may be of D_{2d} symmetry (see Fig. 2). SCF calculations with the SMALL and LARGE basis sets indicate a lower energy for the C_s structure but more accurate MP2 calculations with the SMALL basis set show a lower energy for the D_{2d} "twisted bow-tie" structure. Vibrational analyses indicate that both of these structures represent true minima, and we estimate the C_s conformation to lie about 0.1 eV above the ground D_{2d} state. A summary of these results is given in Table III. We suggest that the D_{2d} structure may be that observed by Kirchner and Bowers, as it seems more likely to be produced from $H_3^* - H_3^+$ collisions than the C_s structure studied by Wright and Borkman[18]. Further calculations are in progress to more fully characterize the stationary points on the H_6^+ potential surface.

DISCUSSION AND RECOMMENDATIONS

The present calculations appear to rule out the formation of hydrogen anion clusters though either of the association reactions:

$$H_n^- + H \rightarrow H_{n+1}^- \qquad (2)$$

$$H_n^- + H_2 \rightarrow H_{n+2}^- \qquad (3)$$

Although previous studies by Hirao and Yamabe[13] indicate a weak stability for H_n^- clusters, up to n = 13, the non-existence of H_2^- and H_3^- precludes formation of higher clusters through either reaction (2) or (3). There remains the possibility (albeit remote) that association of H^- with a stable Rydberg state of H_3 could produce H_4^-. Further calculations are in progress to access this association pathway.

Our studies of H_5^+ indicate that triple-zeta plus polarization quality basis sets are probably adequate for quantitative studies of the hydrogen cation clusters. A more complete characterization of H_n^+ clusters is indicated to obtain quantitative results for the energetics of hydrogen atom addition. In addition, a complete IR frequency analysis should be carried out on these optimized H_n^+ structures in order to obtain a more accurate prediction of their unimolecular decomposition rates. Studies of excited state surfaces for H_n^+ should also be carried out since radiatively induced stabilization processes for cluster growth, such as

$$H_n^+ + H_2 \rightarrow \left[H_{n+2}^+\right]^* \tag{4}$$

$$\left[H_{n+2}^+\right]^* + h\nu \rightarrow H_{n+2}^+ + h\nu' \tag{5}$$
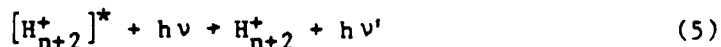
may be important.

Finally, in light of the unusual stability observed for H_6^+, more detailed studies of ion-Rydberg state association reactions should be undertaken. In particular, an accurate characterization of several geometries for H_6^+ should be carried out, including studies of the regions of the potential energy surface connecting these geometries. Such studies will shed more light on the stability question of H_6^+ in D_{2d} symmetry.

REFERENCES

1. E. E. Ferguson, F. C. Fehsenfeld and D. L. Albritton in "Gas Phase Ion Chemistry", ed. M. T. Bowers, Academic Press, NY (1979).

2. T. D. Mark and A. W. Castleman, Jr., Adv. At. Mol. Phys. $\underline{20}$, 64 (1985).

3. Proceedings of the Hydrogen Cluster Ion Study Group, ed. J. T. Bahns, University of Dayton (1986).

4. R. J. Beuhler, S. Ehrenson and L. Friedman, J. Chem. Phys. $\underline{79}$, 5982 (1983).

5. M. T. Elford, J. Chem. Phys. $\underline{79}$, 5951 (1983).

6. Y. Yamaguchi, J. F. Gaw, and H. F. Schaefer III, J. Chem. Phys. $\underline{78}$, 4074 (1983).

7. Y. Yamaguchi, J. F. Gaw, R. B. Remington and H. F. Schafer III, The H_5^+ Potential Energy Hypersurface. Characterization of Ten Distinct Energetically Low-Lying Stationary Points, J. Chem. Phys., in press.

8. N. J. Kirchner, J. R. Gilbert and M. T. Bowers, Chem. Phys. Lett. $\underline{106}$, 7 (1984).

9. N. L. Kirchner and M. T. Bowers, J. Chem. Phys. $\underline{86}$, 1301 (1987).

10. Y. K. Bae, M. J. Coggiola and J. R. Peterson, Phys. Rev. $\underline{A29}$, 2889 (1984).

11. A. M. Sapse, M. T. Rayez-Meaume, J. C. Rayez and L. J. Massa, Nature $\underline{278}$, 332 (1979).

12. J. C. Rayez, M. T. Rayez-Meaume and L. J. Massa, J. Chem. Phys. $\underline{75}$, 5393 (1981).

13. K. Hirao and S. Yamabe, Chem. Phys. $\underline{80}$, 237 (1983).

14. C. A. Nicolaides, I. D. Petsalakis and G. Theodorakopoulos, J. Chem. Phys. $\underline{81}$, 748 (1984).

15. P. Siegbahn and B. Liu, J. Chem. Phys. $\underline{68}$, 2457 (1978).

16. C. E. Dykstra, A. S. Gaylord, W. D. Gwinn, W. C. Swope and H. F. Schaefer III, J. Chem. Phys. 68, 3951 (1978).

17. W. J. Hehre, L. Radom, P. v. R. Schleyer and J. A. Pople, "Ab Initio Molecular Orbital Theory", Wiley-Interscience (1986).

18. L. R. Wright and R. F. Borkman, J. Chem. Phys. 77, 1938 (1982).

Table I. Calculated Electronic Energies and Bond Lengths for H_3^-.

Level	R1	R2	H_3^- electronic energy	H_3^- zero-pt. energy	H^- electronic energy	H_2 electronic energy	H_2 zero-pt. energy	D_e	D_o
SCF/small	0.7340	3.2120	-1.621341	0.01250	-0.487640	-1.132408	0.01046	1.29	-0.75
MP2/small	0.7451	2.8977	-1.668994	0.01277	-0.507128	-1.160181	0.01030	1.68	-0.79
MP4/small	0.7482	2.9607	-1.683973	---	-0.514803	-1.167750	---	1.42	---
CISD/small	0.7480	3.0933	-1.684610	0.01227	-0.517166	-1.168354	0.01005	1.25	-0.97
SCF/large	0.7385	3.2020	-1.622682	0.01236	-0.487785	-1.133502	0.01046	1.40	-0.50
MP2/large	0.7436	2.8129	-1.679633	0.01258	-0.514177	-1.163478	0.01032	1.98	-0.28
MP4/large	0.7473	2.8950	-1.697126	---	-0.524534	-1.170956	---	1.64	---
CISD/large	0.7469	2.9583	-1.696702	0.01216	-0.526268	-1.171560	0.01005	1.58	-0.53
SCF/huge	0.7383	3.2015	-1.622877	0.01234	-0.487887	-1.133598	0.01044	1.39	-0.51
MP2/huge	0.7438	2.7649	-1.682973	0.01257	-0.515161	-1.165762	0.01031	2.05	-0.21
MP4/huge	0.7476	2.8695	-1.699551	---	-0.524995	-1.172764	---	1.79	---
CISD/huge	0.7476	2.8695	-1.698957	---	-0.526727	-1.173376	0.01005		

Bond lengths are in angstroms, energies in hartrees,
except D_e and D_o, which are in millihartrees. R1 is the H – H
equilibrium separation, and R2 is the H_2 – H^- equilibrium separation.

As CISD is not size-consistent, the CISD D_e values are found from
$D_e(CISD) = E[R1=H_2(R_e), R2=15Å] - E[eq]$. $D_o = D_e - ZPE(H_3^-) + ZPE(H_2)$.

Table II. SCF Geometry of H_5^+ using HUGE Basis.

	This Work	Yamaguchi, et al Ref. 7
	$R_1 = 0.9092$ Å	0.9098 Å
	$R_2 = 1.5894$ Å	1.5903 Å
	$\alpha = 54.2392°$	$54.32°$
	$\beta = 27.2312°$	$27.24°$
	$E_{el} = -2.443048$ h	-2.442128 h
	$R = 1.1305$ Å	1.1290 Å
	$\alpha = 40.0724°$	$40.20°$
	$E_{el} = -2.439886$ h	-2.438910 h

C_{2v}:
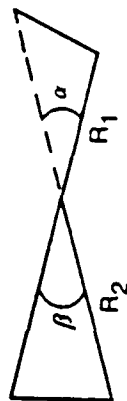
D_{2h}:
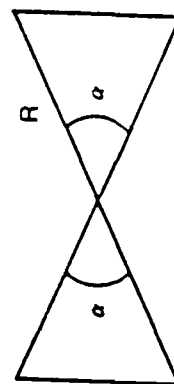
Table III. H$_6^+$ Optimized Structure

C$_s$ Symmetry

Level	R1	R2	R3	R4	R5	R6	Energy
SCF/SMALL	1.8537	0.9159	0.8474	0.8881	1.5939	0.7476	-2.941047
SCF/LARGE	1.8736	0.9068	0.8486	0.8777	1.6495	0.7454	-2.945925
MP2/SMALL							-3.003310

D$_{2d}$ Symmetry

Level	R1	R2	R3	Energy
SCF/SMALL	1.0409	1.2483	0.7795	-2.936759
SCF/LARGE	1.0421	1.2488	0.7776	-2.939731
MP2/SMALL	1.0380	1.2271	0.7873	-3.006855

D$_{2d}$ Vibrational Frequencies

	b1	e	e	b2	e	e	al	e	e	al	b2	al
SMALL	66	375	375	734	817	817	877	1230	1230	2140	3951	4042
LARGE	69	354	354	683	795	795	858	1196	1196	2072	3910	4000
MALL	69	380	380	911	788	788	1014	1235	1235	2154	3871	3949

...ths are in angstroms, energies are in hartrees, and vibrational frequencies ...numbers. Note that the b1 vibrational mode is a torsional motion about the axis of the

MICROCOPY RESOLUTION TEST CHART

NATIONAL BUREAU OF STANDARDS-1963-

FIGURE 1. H_6^+ C_s Structure.

FIGURE 2. H_6^+ D_{2d} Structure.

Hanspeter Helm

Photon-Assisted Formation and Cooling of Molecular Hydrogen

PHOTON-ASSISTED FORMATION AND COOLING OF MOLECULAR HYDROGEN

Hanspeter Helm

Molecular Physics Department
SRI International
Menlo Park, California 94025

Abstract

We discuss photon-assisted reactions for forming molecular
hydrogen ions from protons and hydrogen atoms using free-bound
absorption of the collision complex. We also discuss the possi-
bility of forming very weakly bound, electronically excited H_2^+
molecules in collisions between two electrons and two protons. A
third topic explores stimulated Raman scattering as a technique
to cool internal excitation of the molecules.

Introduction

This contribution discusses various techniques which could
assist in the controlled formation, cooling and state selection of
molecular hydrogen in a containerless environment, as may be re-
quired for antimatter molecule synthesis. The thoughts developed
in the following do rot provide a conclusive solution to the very
formidable problems associated with the formation of molecules from
the basic constituents, electrons and protons, in the gas phase.
They do however promise low-yield synthesis, and they are meant to
stimulate theoretical and experimental work along new approaches.

Three of the many aspects important in molecular hydrogen
synthesis are explored. We first discuss limitations for stimu-
lating the radiative recombination rate in proton-hydrogen atom
collisions. Then we discuss the possibility of hydrogen atom
formation in high density mixtures of electrons and protons. A
third subject regards the use of stimulated Raman-scattering to
cool and state-select molecular hydrogen.

1. Stimulated Radiative Association Reactions.

Only recently have radiative association reactions been demonstrated in the laboratory.[1] Such reactions are considered to be among those important for molecular synthesis in interstellar clouds.[2] Below we outline some of the fundamental parameters for two schemes of the photon-assisted radiative association reaction between protons and hydrogen atoms.

A. Radiative association via the $2p\sigma_u \rightarrow 1s\sigma_g$ transition of H_2^+.

Collisions of protons and ground state hydrogen atoms at low translational energies can be described as a coherent superposition of scattering events along the $1s\sigma_g$ $(X^2\Sigma_g^+)$ and $2p\sigma_u$ $(A^2\Sigma_u^+)$ potential energy curves. These two electronic states are connected in an allowed dipole transition. This transition is the origin for the bound-free photodissociation reaction of H_2^+ which has been studied extensively in the visible and near UV[3,4] (see Figure 1).
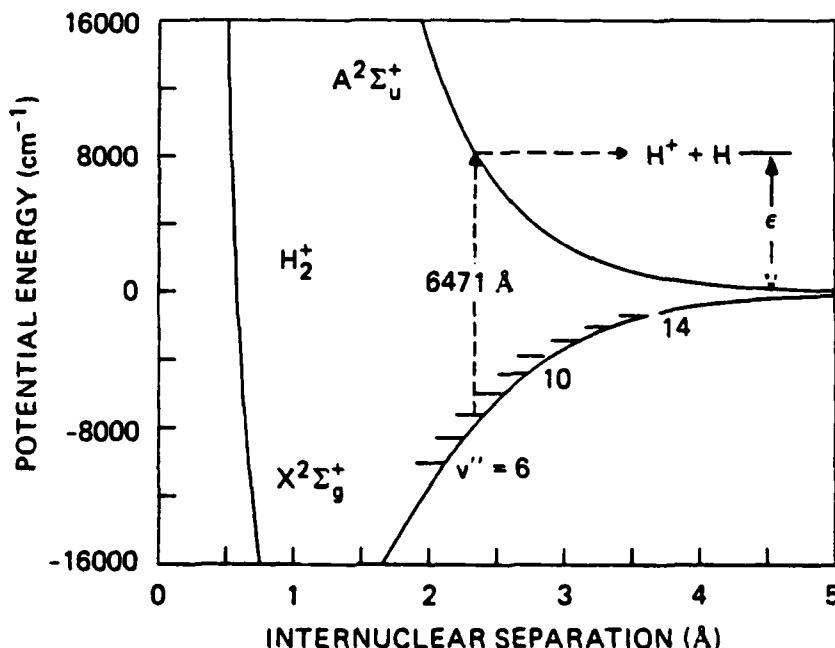
Figure 1. Photodissociation of ground-state H_2^+ in $2p\sigma_u \rightarrow 1s\sigma_g$ transition. Energy balance requires that the kinetic energy of the proton-hydrogen pair, ϵ be equal to the difference between the photon energy and the bond energy of the photodissociated rovibrational state.

98

The inverse of this process, radiative association, should occur with small probability in collisions of protons and H(1s) atoms and lead to the formation of stable H_2^+ ions. The classical turning points on the $2p\sigma_u$ potential energy curve, and hence the range of vibrational levels of H_2^+ that can be populated in such a process are determined by the collision energy. At thermal energies the turning points lie at large internuclear separation and only infrared transitions into the highest vibrational levels of the molecular ion efficiently contribute to the radiative association process. Energetic collisions are required to access the repulsive $2p\sigma_u$ curve at short enough internuclear separation to allow radiative events to reach the ground vibrational state of the molecular ion (see Figure 1).

The rate at which radiative association events occur spontaneously is determined by ratio of the lifetime for a radiative transition to the collision lifetime, that is roughly one in 10^6 collisions may spontaneously lead to the formation of a stable molecule. In principle the rate of formation can be enhanced by stimulating the emission event with a photon of energy $h\nu$, but at best an equilibrium between the population of any particular bound H_2^+ level (with a dissociation energy D) and the continuum population p + H(1s) at the energy $\varepsilon = h\nu - D$ can be enforced.

To put the problem in a quantitative perspective involving actual rates, we consider a test volume of 1 cm^3 filled with N protons and N hydrogen atoms, each at a translational energy of 5 meV. Assuming a hard sphere cross section of 1 A^2 the rate of proton-hydrogen atom collisions is $10^{-11}N^2$ sec^{-1}. At a density N = 10^6 cm^{-3} we have 10 collisions per second. Consequently at a spontaneous association rate of 1 in 10^6 collisions about one H_2^+ molecule will be formed spontaneously per day in such an environment. From Figure 1 we can judge that the most likely levels of H_2^+ populated at collision energies of 5 meV (40 cm^{-1}) are the vibrational levels v = 16 and higher.

To evaluate the efficiency of stimulating the association reaction with external photons we consider the test volume to be irradiated with a flux of P photons per second and per square

centimeter from a laser with photon energy $h\nu = 10$ meV. The photodissociation reaction of H_2^+ in high vibrational levels with these photons has a cross section on the order of 10^{-16} cm^2, giving a rate of photodissociation of $10^{-16}P$ sec^{-1}. At $P = 10^{20}$ photons/cm^2sec^1 (corresponding to 160 mW) the lifetime of H_2^+ against photodissociation becomes 100 μs. This is the time that is available to us to remove any H_2^+ molecules formed in the test volume in order to prevent them from being destroyed by photodissociation. This very high far-infrared photon flux will enhance the radiative association event according to the number of photons seen by the collision complex $p+H(1s)$. In a first estimate we assume the size of the complex to be 1 A^2. The photon flux used above gives us 10^4 photons per A^2 and per second. Assuming a collision lifetime of 0.1 ps we will have 10^{-9} photons per collision that are useful for the stimulated radiative association. This value is three orders of magnitude below the spontaneous rate, which we estimated above to be of the order of 10^{-6} per collision. From this we conclude that stimulated radiative association via the repulsive $2p\sigma_u$ state is unlikely to be useful for enhancing the rate of radiative association.

A possible alternative approach is to make use of electronically excited states of H_2^+ and we discuss such a scheme below.

B. Spontaneous Radiative Stabilization of Electronically Excited H_2^+.

Bound excited states of H_2^+ have been predicted[5] to exist which are connected in allowed electronic transitions to the high-lying vibrational levels of ground state H_2^+. In Figure 2 we show the lowest bound excited ungerade state, $2p\pi_u$, which correlates to $H^+ + H(2p)$. Predicted photon energies for transitions from the ground state to $2p\pi_u$ lie near 1200 Å. A calculation of the Frank-Condon factors for the transition $2p\pi_u \rightarrow 1s\sigma_g$ shows that a significant portion of the radiative events from the excited state to the ground state terminates at energies above the ground state dissociation limit[6] (see Figure 3). For example the transitions
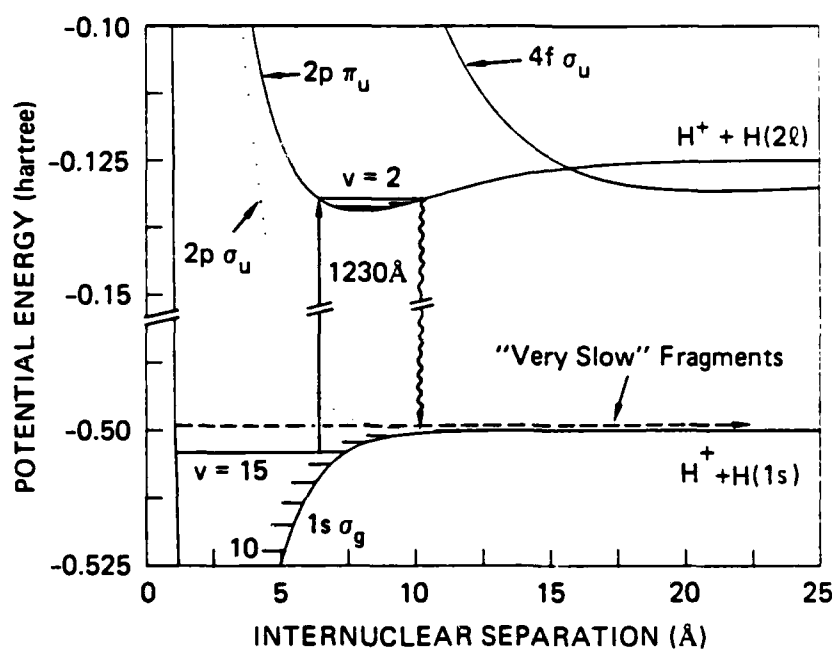
Figure 2. Photodissociation of ground state H_2^+ in $2p\pi_u \leftarrow 1s\sigma_g$ transition. Due to its equilibrium separation the excited $2p\pi_u$ state bridges the bound portion of ground state H_2^+ with the continuum of $1s\sigma_g$.
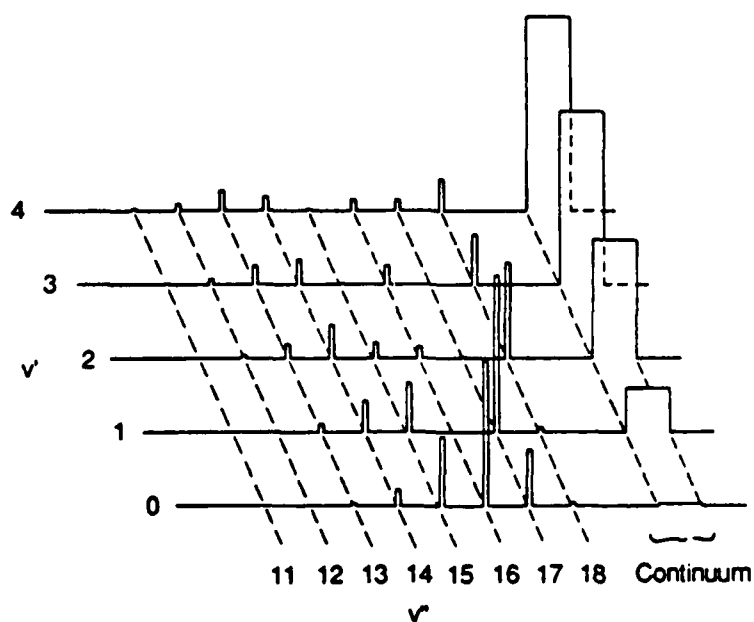
Figure 3. Franck-Condon Factors (represented by the height of the bars) for the transitions $2p\pi_u \leftarrow 1s\sigma_g$ as a function of vibrational level of ground state H_2^+. The narrow bars represent the transitions into the bound portion of the ground state. The wide bars to the right represent the portion of fluorescence terminating in the continuum of the ground electronic state. (Ref. 6).

from v = 2 of the $2p\pi_u$ state preferentially populate the vibrational levels 14 and 18 of the $1s\sigma_g$ state. However the sum of the Franck-Condon Factors for all transitions from the $2p\pi_u$ (v' = 2) state to the bound region of ground state H_2^+ accounts for only 56% of all events. The remaining 44% terminate at energies just above the dissociation limit H^+ + H(1s) in the form of Condon diffraction bands. The distribution of the transition intensities to bound levels and to the continuum is shown in Figure 3 for several vibrational levels of H_2^+ $2p\pi_u$. In Figure 4 we show the predicted distributions of translational energies of the dissociation products which arise when the transitions from the v = 2 and v = 0 vibrational levels terminate in the continuum of the ground state. It may be seen that proton-hydrogen pairs with very low center-of-mass energies are produceu preferentially in these bound-free transitions.
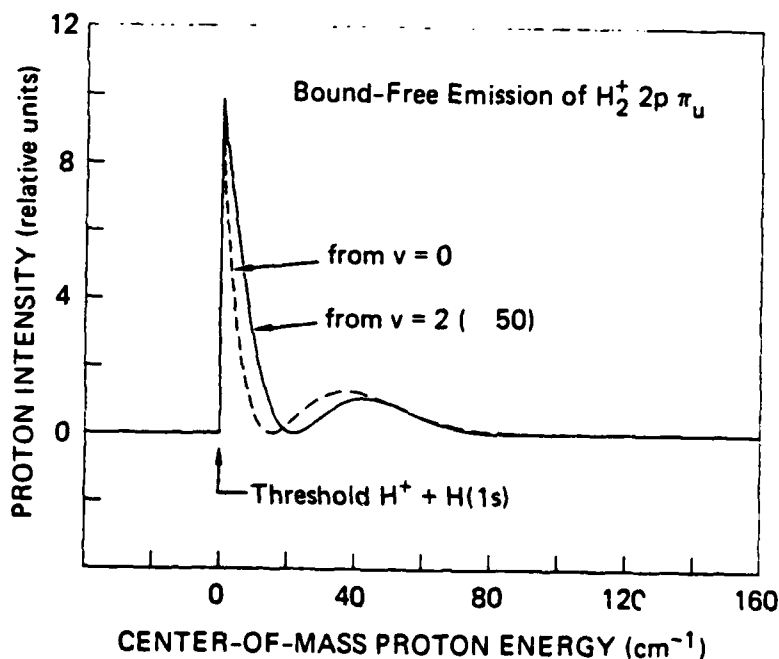
Figure 4. Kinetic energy distribution of proton-hydrogen pairs formed in spontaneous emission of $H_2^+(2p\pi_u)$. (Taken from Ref. 6).

In the spirit of the current discussion we explore the reverse process, that is the possibility of photon absorption by slow proton-hydrogen atom collision pairs, in the vicinity of the energy difference between the ground state dissociation limit and a bound vibrational level of the $2p\pi_u$ state. The free-bound cross section for this process can be significantly higher than that for the first case considered, $2p\sigma_u \rightarrow 1s\sigma_g$, since for $2p\pi_u \rightarrow 1s\sigma_g$ the transition intensity is concentrated over a very small range of continuum energies (10 meV in the example of $v = 0$ and 2 in Figure 4, of which about 50 % are concentrated within a 10 cm^{-1} bandwidth close to threshold).

Following excitation of the $2p\pi_u$ state the molecule has two dominant channels for relaxation: It may either radiate back into the continuum (and dissociate again) or into the bound vibrational levels of H_2^+. A minor loss channel for H_2^+ $2p\pi_u$ (<1%) is the infrared transition[7] to the $3d\sigma_g$ state (not shown in Figure 2).

The photon emitted in the transition from the discrete $2p\pi_u$ level to the bound levels of H_2^+ is of higher energy than that used for the excitation event. Therefore the reverse reaction which appears as a limiting factor in process A discussed above is not an issue in this scheme. The newly formed H_2^+ molecule may however be photodissociated at the excitation wavelength in a bound-free transition involving the repulsive $2p\sigma_u$ state (see Figures 1 and 2). It appears that by proper choice of the excitation wavelengths this loss channel can be minimized since the cross section for the bound-free photodissociation process $2p\sigma_u \rightarrow 1s\sigma_g$ oscillates with photon energy.[3]

A quantitative analysis of the efficiency of this process and its possible advantage over process A will have to entail a comparison of the free-bound absorption probabilities for the $2p\pi_u \rightarrow 1s\sigma_g$ and $1s\sigma_g \rightarrow 2p\sigma_u$ transitions and a spectroscopic determination the predicted bound $2p\pi_u$ levels which have eluded experimental observation to date.

2. Formation of Rydberg Molecules of H_2^+.

Excitation of the electron in H_2^+ leads to a dilution of negative charge between the protons and hence to a reduction in bonding. The strongest bonding character in the electronically excited states of H_2^+ is retained for orbitals of the type $d\sigma_g$, being 1.4 eV and .6 eV for the states arising from $H^+ + H(n = 2)$ and $H^+ + H(n = 3)$ respectively. Associated with the dilution of negative charge is an increase in the bond length of the molecule (8 and 24 a_o respectively for the two configurations mentioned above).

In the limit of high n these states converge to the repulsive Coulomb curve $H^+ + H^+$, the $d\sigma_g$ states retaining substantial bonding character in wide shallow wells.

To gain a first picture of these loosely bound H_2^+ Rydberg ions we may extrapolate what is currently known about excited states of H_2^+. In Figure 5 we show the lowest gerade states of H_2^+. To obtain potential energy curves for high n values we may scale the bond energies and bond lengths with n^{-3} and n^3 respectively. For example the equilibrium separation of the n=30 $d\sigma_g$ state of H_2^+ is expected to be of the order of 10^4 Å having a bond energy of 5 cm^{-1}. Molecules in such states can in principle be formed in long-range encounters between two protons and two electrons where one of the electrons removes the excess kinetic energy of excited H_2^+. Assuming a Poisson distribution of nearest neighbor distances we estimate that the probability for such a four particle encounter is 10^4 s-1 when electron densities of 10^{10} cm^{-3} and proton densities of 10^8 cm^{-3} are assumed. We note that these densities are in the realm of the operation parameters[8] for the merged electron-proton ring which is currently under construction at the University of Aarhus.

While the dominant loss mechanism of such loosely bound H_2^+ molecules will be via Coulomb collisions with neighboring charged particles, at least two additional removal processes have to be considered: one is the possibility of predissociation of the exited molecule into $H^+ + H(m<n)$, a second is the temporary removal of the collision complex from the region of efficient Coulomb breakup by the vibrational motion of the molecule: once formed the vibrational
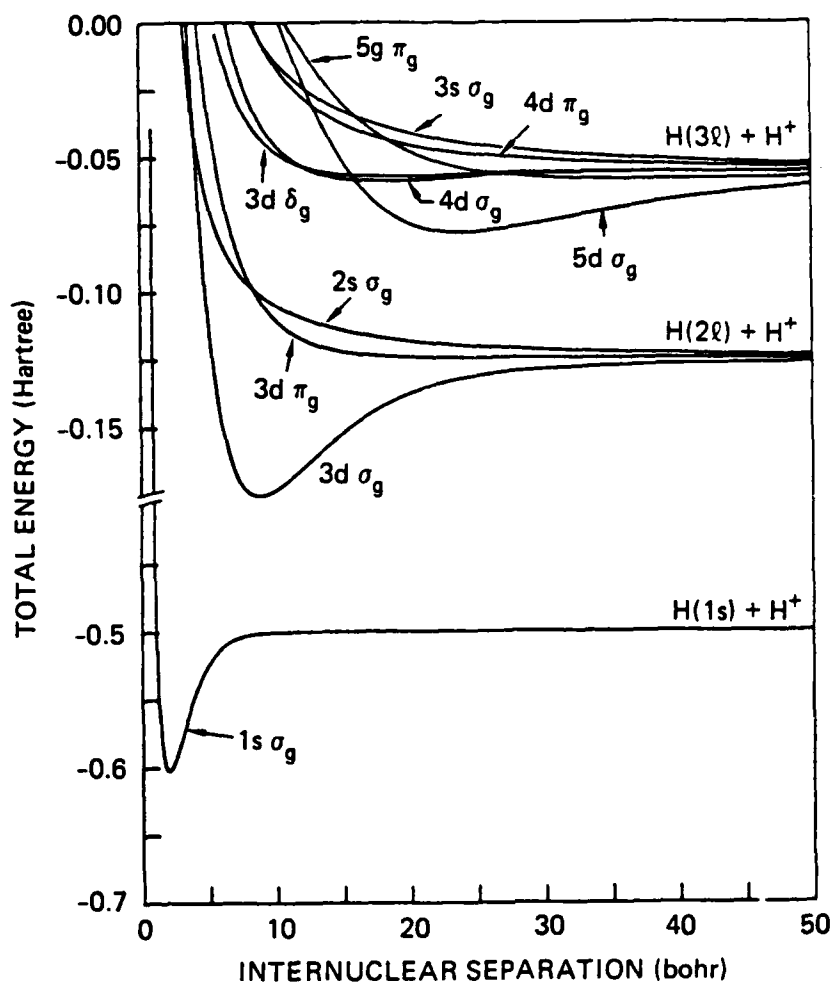
Figure 5. Lowest gerade electronic states of H_2^+. (Taken from Ref. 7).

motion of the species will pull protons together on the shallow attractive excited state potential energy curve, thus separating it in energy from the Coulomb dissociation limit. The breathing motion of vibration in highly excited H_2^+ is substantial: several thousand Å for n>20. This extreme of nuclear motion in a wide shallow potential well requires an extraordinary length of time. The classical vibration should take nanoseconds and longer. While this process will by itself not lead to the formation of stable ground state H_2^+ it may offer a substantial time window in which the excited molecules can be separated from the proton-electron beam.

3. Cooling of Hydrogen Molecules by Stimulated Raman Processes.

A very formidable problem posed in any scheme of condensing molecular hydrogen in the gas phase is the requirement of cooling internal and translational degrees of freedom of the species formed. We suggest that cooling of internal degrees of freedom in the molecule can be accomplished by stimulated Raman processes involving either virtual, continuous or real bound levels of the molecule.

This possibility is suggested by the recent report by Möhlmann [9] of the observation of Anti-Stokes Raman shifting by H_2^+ ions in a conventional Raman cell. When the irradiated area of the cell is depleted of ground state hydrogen molecules by multiphoton ionization, then Raman shifting occurs on the remaining H_2^+ ions with comparable efficiency. Evidence for this is found in the observed wavelength shifts which pinpoint the origin of the Raman process to the vibrational spacing in the molecular ion. Möhlmann's experiment was carried out at 10.6 μm, a wavelength where H_2^+ in its ground vibrational state cannot photodissociate. The virtual state involved in this Raman process has to derive its character from an electronic excitation, and it must at this wavelength be borrowed most efficiently from the $2p\sigma_u$ state which is (for $v = 0$ of the ion) 12 eV nonresonant at vertical energies.

If spontaneous stimulated Raman processes occur with high probability in the ion then they can surely be induced deliberately using two lasers tuned to wavelengths such that their photon energies differ by rovibrational spacings of the ion (or neutral) molecule. In this fashion the population in any pair of vibrational levels can be equalized. In Figure 6 we show three possible schemes for the Raman-process.

The experimental demonstration of a redistribution of vibrational and rotational energy in a species such as H_2^+ is certainly within the capabilities of current state of the art experiments.[4] To our knowledge a theoretical formulation of the Raman efficiency using as an intermediate a virtual state derived from a repulsive electronic state (such as the case for the $2p\sigma_u$ state of H_2^+) has not yet been given. The theoretical illumination of this process

106
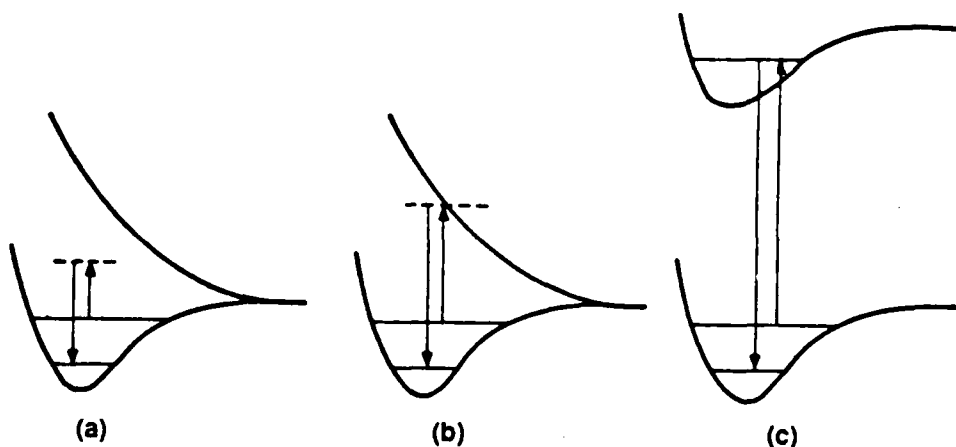
Figure 6. Stimulated Raman schemes to cool and state select molecular hydrogen. The transitions indicated in a) and b) are applicable to the case of H_2^+ and involve as intermediate a virtual and dissociative electronic state respectively. Case c) is applicable to neutral H_2 and involves as intermediate a bound discrete level in the B or C state.

would greatly aid in determining the dependence of the Raman efficiency on detuning from the intermediate state and help tailor demonstration experiments to successful operation parameters. In the case of H_2^+ the only useful intermediate state for cooling rovibrational excitation to the ground vibrational state of the ion appears to be the repulsive $2p\sigma_u$ state. In the case of the neutral hydrogen molecule, internal energy cooling with resonant Raman processes may more efficiently be achieved using as intermediate the bound levels in the $B^1\Sigma_u^+$ or $C^1\Pi_u$ states.

Conclusion

To date no experiments on controlled radiative association and cooling of molecular hydrogen have been performed. Schemes such as those discussed above may however soon be explored in high-density merged-particle beams or in long-term storage devices such as ion traps.

The low yield inherent in all H_2^+ syntheses proposed to date suggests that radically different approaches should also be subject to closer inspection. Among these should be the search for antimatter H_2^+ molecules formed directly in the antiproton production process. This certainly low probability event may yet compete, in both cost and time, with the controlled generation of H_2^+ condensation centers for antimatter clustering.

REFERENCES

1. S.E. Barlow, G.H. Dunn, and M. Schauer, Phys. Rev. Lett. 52, 902 (1984).
2. J.H. Black, A. Dalgarno, and M. Oppenheimer, Ap. J. 199, 633 (1975).
3. F. Von Busch and G. H. Dunn, Phys. Rev. A5, 1726 (1972).
4. H. Helm and P. C. Cosby, J. Chem. Phys. June 1987 (and references therein)
5. M.M. Madsen and J.M. Peek, Atomic Data 2, 171 (1971).
6. H. Helm, ICPEAC (1987) contributed paper.
7. C. Beckel, M. Shapi, and J.M. Peek, J. Chem. Phys. 59, 5288 (1973).
8. N. Bjerre, private communication.
9. G.R. Mohlmann, Chem. Phys. Lett. 115, 226 (1985).

Sheng-Yu Huang and William A. Lester, Jr.

Quantum Monte Carlo Study of the Mies Associated with
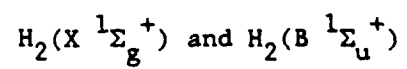
$$H_2(X\ ^1\Sigma_g^+) \text{ and } H_2(B\ ^1\Sigma_u^+)$$

QUANTUM MONTE CARLO STUDY OF THE MIES ASSOCIATED WITH
$H_2(X\ {}^1\Sigma_g^+)$ and $H_2(B\ {}^1\Sigma_u^+)$*

Sheng-Yu Huang and William A. Lester, Jr.
Department of Chemistry, University of California, Berkeley
and Materials and Molecular Research Division, Lawrence Berkeley Laboratory,
Berkeley, California 94720

Introduction

Excited states of interacting systems, that are bound in the ground state only by van der Waals forces, can interact to form strongly bound species. This is found even for systems in which only one of the fragments is excited, and is exemplified by the excimer states $He-He^*$, $Ar-Ar^*$, and $H_2-H_2^*$. Here the asterisk denotes the first excited state of the same spin symmetry as the ground state. Interest in the latter system has increased recently with the study of Nicolaides et al.[1] of the $H_2(X\ {}^1\Sigma_g^+) - H_2(B\ {}^1\Sigma_u^+)$ system because of the ionic character of the B state, which these authors label at $4.0a_0$, where charge transfer occurs, a maximum ionicity excited states (MIES). This state is of special interest because of its strong electrostatic binding with the nonreactive singlet ground state.

A model [1-3] based on MIES properties suggests that bound excited states of polyatomic systems can be formed in regions characterized by an avoided crossing with the ground state, if one of the interacting molecules can exist in a MIES. The description for $H_2-H_2^*$, where H_2^* denotes $H_2(B\ {}^1\Sigma_u^+)$ is one in which a positive ion complex H_3^+ is formed, and interacts in its ground state equilibrium geometry (equilateral triangle with $r = 1.65a_0$) with H^-. The MIES geometry corresponding to $H^+ H^-$ for the parent $H_2(B\ {}^1\Sigma_u^+)$ is the charge transfer region at $4.0a_0$. The mechanism supported by Nicolaides, Theodorakopoulos, and Petsalakis (NTP) with CI computations is one of H_3^+, which is electron deficient in the center of the triangle, interacting with H^- at a distance of roughly $4.0a_0$ above the plane of the H_3^+ triangle.

Studies of the $H_2^*-H_2$ system are in progress in this laboratory using the fixed-node quantum Monte Carlo (FNQMC) method. A brief introduction to the method follows.

Quantum Monte Carlo

Monte Carlo approaches to solving problems with many degrees of freedom are a class of statistical methods having in common the generation of "random" numbers. In the past few years, Monte Carlo approaches have seen increased application in a number of diverse fields. What we mean here by quantum Monte Carlo (QMC) is a Monte Carlo procedure which solves the Schrödinger equation. This is to be distinguished from so-called variational Monte Carlo, in

which one obtains expectation values for a *given* trial wave function.

This ability to stochastically solve the Schrödinger equation provides an alternative to conventional techniques of quantum chemistry. Early work[4] has shown that highly accurate total energies and correlation energies can be obtained by QMC. In fact, in a procedurally simple manner, accuracies exceeding those of the best *ab initio* configuration interaction calculations have been obtained.

The essence of the procedure is to simulate a quantum system by allowing it (and an ensemble of differently prepared systems) to evolve under the time-dependent Schrödinger equation in imaginary time. Excited states of the same symmetry as lower state can also be computed with the method.

By writing the imaginary-time Schrödinger equation with a shift in the zero of energy as

$$\frac{\partial \Psi(\underline{R},t)}{\partial t} = D \nabla^2 \Psi(\underline{R},t) + [E_T - V(\underline{R})]\Psi(\underline{R},T), \tag{1}$$

we see that it may be interpreted as a generalized diffusion equation. The first term on the right-hand-side is the ordinary diffusion term, while the second term is a position-dependent rate (or branching) term. For an electronic system, $D = \hbar^2/2m_e$, $\underline{R}$ is the three-N dimensional coordinate vector of the N electrons, and $V(\underline{R})$ is the Coulomb potential. Since diffusion is the continuum limit of a random walk, one may simulate Eq. (1) with the function Ψ (note, not Ψ^2) as the density of "walks". The walks undergo an exponential birth and death as given by the rate term.

The steady-state solution to Eq. (1) is the time-independent Schrödinger equation. Thus we have $\Psi(\underline{R},t) \rightarrow \phi(\underline{R})$, where ϕ is an energy eigenstate. The value of E_T at which the population of walkers is asymptotically constant gives the energy eigenvalue. Early calculations employing Eq. (1) in this way were done by Anderson on a number of one- to four-electron systems.[5]

In order to treat systems larger than two electrons, the Fermi nature of the electrons must be taken into account. The antisymmetry of the eigenfunction implies that Ψ must change sign; however, a density (e.g., of walkers) cannot be negative. The method which imposes antisymmetry, and at the same time provides efficient sampling (thereby reducing the statistical "noise"), is importance sampling with an antisymmetric trial function Ψ_T. The zeroes (nodes) of Ψ_T become absorbing boundaries for the diffusion process, which maintains the antisymmetry. The additional boundary condition that Ψ vanish at the nodes of Ψ_T is the fixed-node approximation. The magnitude of the error thus introduced depends on the accuracy of the *nodes* of $\Psi_T(\underline{R})$, and vanishes as Ψ_T approaches the true eigenfunction. To the extent that Ψ_T is a good approximation of the wave function, the true eigenfunction is almost certainly quite small near the nodes of Ψ_T. Thus one expects the fixed-node error to be small for reasonable choices of Ψ_T.

To implement importance sampling and the fixed-node approximation, Eq. (1) is multiplied on both sides by Ψ_T, and rewritten in terms of the new

probably density $f(\underline{R},t) = \Psi_T(\underline{R})\Psi(\underline{R},t)$. The resultant equation for $f(\underline{R},t)$ may be written

$$\frac{\partial f}{\partial t} = D\nabla^2 f + [E_T - E_L(\underline{R})]f - D\nabla\cdot[fF_Q(\underline{R})]. \qquad (2)$$

The local energy $E_L(\underline{R})$, and the "quantum force" $F_Q(\underline{R})$ are simple functions of Ψ_T given by

$$E_L(\underline{R}) \equiv H\Psi_T(\underline{R})/\Psi_T(\underline{R}), \qquad (3a)$$

and

$$F_Q(\underline{R}) \equiv 2\nabla\Psi_T(\underline{R})/\Psi_T(\underline{R}). \qquad (3b)$$

Equation (2), like Eq. (1) is a generalized diffusion equation, though now with the addition of a drift term due to the presence of F_Q.

In order to perform the random walk implied by Eq. (2) we use a short-time approximation to the Green's function which is used to evolve $f(\underline{R},t) \rightarrow f(R',t+\tau)$. This evolution process is iterated to large t. The Green's function becomes exact in the limit of vanishing time-step size, τ.

Progress Report on H_2-H_2^*

We have demonstrated that MCSCF wave functions as trial functions for FNQMC calculations can recover $\approx 100\%$ of the correlation energy of ground states and $\approx 95\%$ of the correlation energy of excited states.[5] Using an extended (triple zeta-plus-polarization (TZP)) basis set, MCSCF calculations were carried out for the H_4 MIES that confirmed the characteristics depicted in Fig. 1 for the C_{3v} pyramidal structure. These include the minimum energy geometry, the doubly degenerate E ground state as H separates from H_3 for $R > 3.8$ a.u., and the nondegenerate A ground state for $R < 3.8$ a.u., consistent with an E- to A-state crossing at $R = 3.8$ a.u. For C_s symmetry the avoided crossing was obtained. Figure 2 displays the results of the MCSCF pilot computations. These curves lie above those of (NTP)[1] and reflect the better capability of the *ab initio* MRD-CI wave functions compared to the compact MCSCF trial functions needed here as FNQMC trial functions. The key comparison, however, is with the FNQMC results obtained with the MCSCF functions which is presented below.

Calculations were carried out in C_{2v} symmetry for $H_2(B)$ approach to $H_2(X)$ in which these molecules are contained initially in perpendicular planes that bisect each other. Figure 3 displays this arrangement and summarizes, in accompanying Table I, the sequence of geometry changes, labeled I-VII, that carry the system from the asymptotic region to the neighborhood of the H_4 MIES configuration. Table I also contains the energy lowering associated with these steps. It is noteworthy that no energy barrier is encountered along this path.

FNQMC calculations using the MCSCF trial functions discussed in Sec. A yield ≈ 0.6-1.0 eV energy lowering compared to the results of NTP and are presented in Fig. 4. Such a large change was not anticipated and so it was important to test the validity of this finding. To this end a configuration

interaction calculation including all single and double excitations (SDCI) using the MCSCF pilot study basis set was carried out at $R = 3.4$ a.u. The energy was 0.32 eV lower than NTP's value and is consistent with the improvement expected based on studies of other systems.

Excited-state calculations provide the severest test of the FNQMC approach because of the lack of knowledge of the accuracy of the excited state trial function needed to provide a nodal description that assures orthogonality to the ground state of the same (A') symmetry (C_S). MCSCF calculations close to the pes avoided crossing suffered from root flipping. Despite the use of familiar MCSCF strategies to address the problem, it could not be resolved.

The MCSCF convergence problem had been encountered earlier for $He - H_2(B)$ but resolved by the use of an *ab initio* CI method. Interest here in using the FNQMC method led us to develop a method for trial function construction[6] that avoids the MCSCF procedure. The approach amounts to the introduction of parameter optimization in the random walk process. Using group theory a projection operator is constructed and used to constrain the wave function to have the symmetry properties of the state of interest. Another projection operator is constructed that insures orthogonality to the ground state.

Concluding Remarks

The H_2-H_2* system is a considerable theoretical and practical interest. The FNQMC has been demonstrated to yield accuracies that are achieved only with considerable difficulty using familiar *ab initio* methods. The goal of this effort is to ascertain the stability and energetics of this molecular species.

References

(1) C. A. Nicolaides, G. Theodorakopoulos, and I. D. Petsalakis, J. Chem. Phys. 80, 1705 (1984).

(2) C. A. Nicolaides and A. Dzetsis, J. Chem. Phys. 80, 1900 (1984).

(3) C. A. Nicolaides, I. D. Petsalakis, and G. Theodorakopoulos, J. Chem. Phys. 81, 748 (1984).

(4) P. J. Reynolds, D. M. Ceperley, B. J. Alder, and W. A. Lester, Jr., J. Chem. Phys. 77, 5593 (1982).

(5) R. M. Grimes, B. L. Hammond, P. J. Reynolds, and W. A. Lester, Jr., J. Chem. Phys, 85, 4749 (1986).

(6) Z. Sun, S.-Y. Huang, and W. A. Lester, Jr., *"Algorithm for Optimizing Parameters in a Quantum Monte Carlo Trial Function,"* to be published.

POTENTIAL ENERGY SURFACE CROSSING

FOR PYRAMIDAL H₄
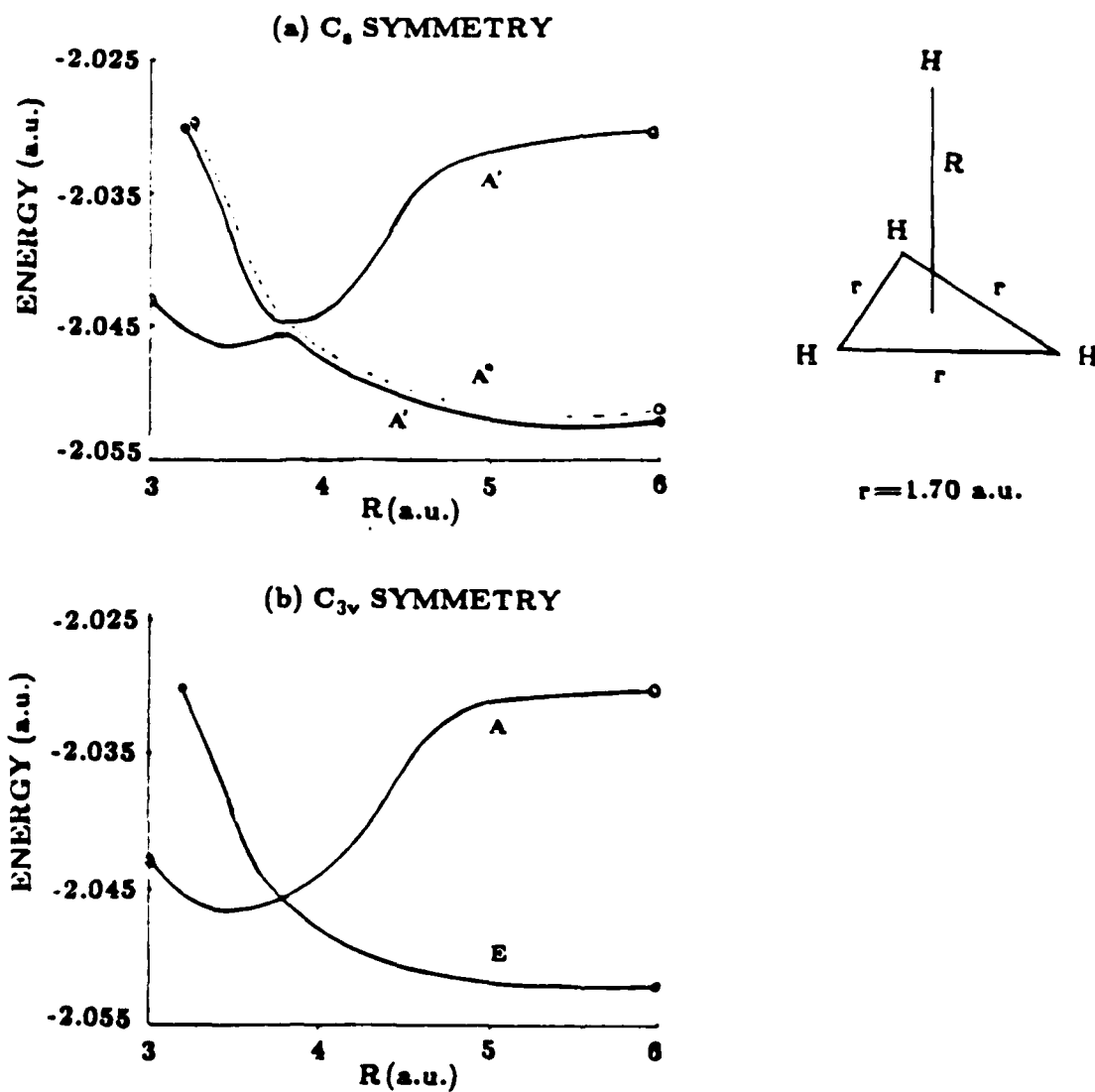
Figure 1. Ground- and excited-state H_4 potential energy curves for trigonal pyramidal geometry (a) C_s symmetry and (b) C_{3v} symmetry.
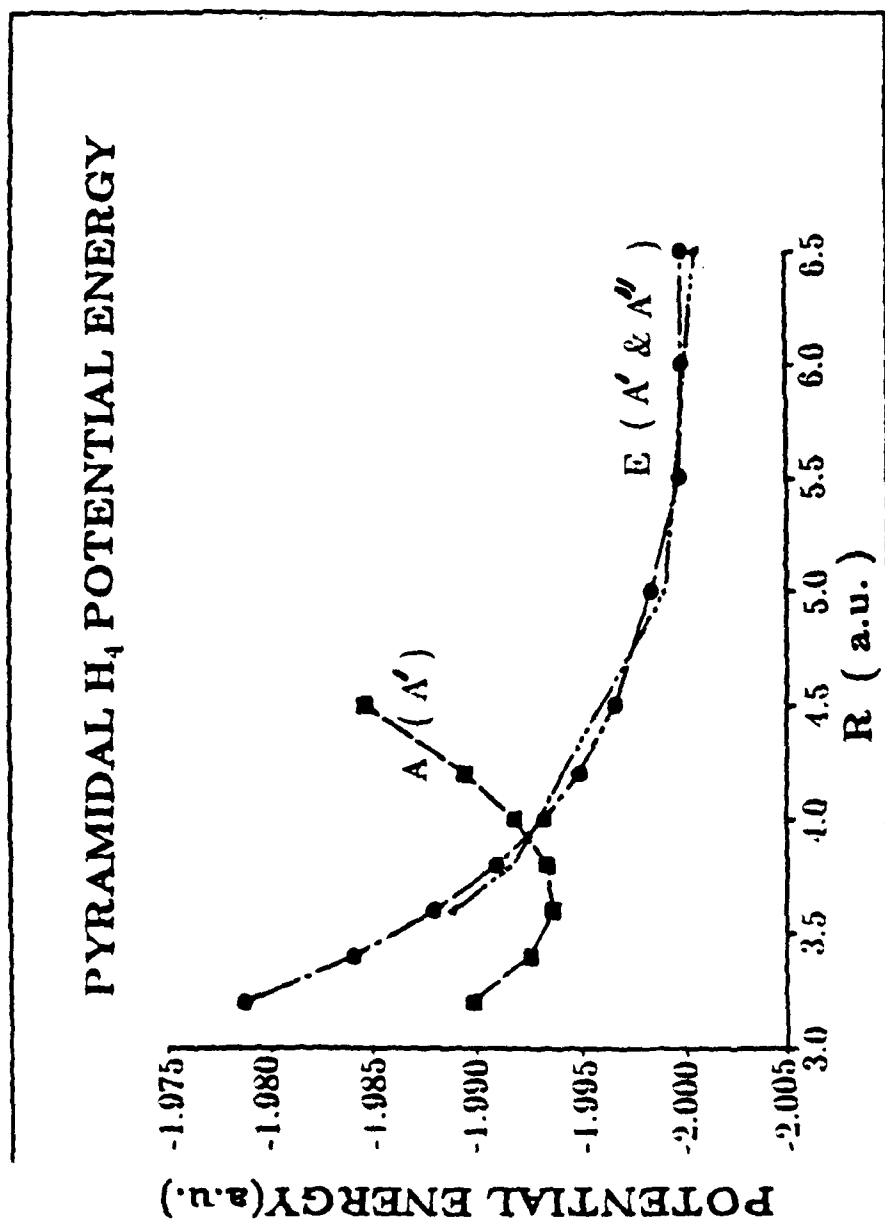
Figure 2. Potential energy curves from MCSCF trial functions for trigonal pyramidal geometry in C_{3v} symmetry. The state designations for C_s symmetry are indicated in parentheses. The lack of coincidence of the E curves reflects their calculation in lower symmetry and provides an indication of the MCSCF convergence.
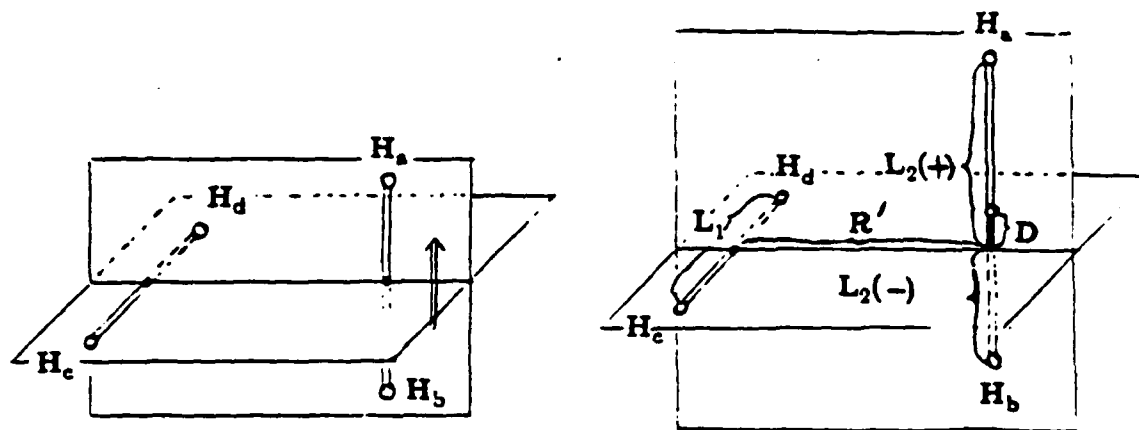
Table I. Geometries and energies for the approach of $H_2(B)$ to $H_2(X)$

step	R'	L1	L2	L2(+)	L2(-)	D	energy lowering
I	5-2.2	1.40	2.43	1.215	1.215	0	-0.91
II	2.2	1.40	2.43	1.215-1.93	1.215-0.5	0.715	-0.20
III	2.2	1.60	2.63	1.93-2.13	0.5	0.865	-0.20
IV	2.2-1.75	1.60	2.63	2.14	0.5	0.865	-1.0
V	1.75-1.55	1.60	2.73	2.23	0.5	0.915	-0.46
VI	1.55	1.60	3.13	2.23-2.63	0.5	1.115	-0.69
VII	1.50	1.70	3.23	2.63-2.73	0.5	1.165	-0.11

TOTAL ENERGY LOWERING FOR THE SEVEN STEPS IS 3.75 ev.

* Distances in a.u.; energies in ev.

R'-distance between the midpoint of $H_2(X)$ and the point where $H_2(B)$ meets the $H_2(X)$ plane.

L_1-length of $H_2(X)$.

L_2-length of $H_2(B)$.

$L_2(+)$-length of $H_2(B)$ above $H_2(X)$ plane.

$L_2(-)$-length of $H_2(B)$ below $H_2(X)$ plane.

D-magnitude of shift of $H_2(B)$ midpoint (above(+) /below(-)) plane of $H_2(X)$.

Figure 3. Geometries used to calculate the approach of $H_2(B)$ to $H_2(X)$. This figure incorporates Table I which provides detailed geometries and relative energies.

POTENTIAL ENERGY OF PYRAMIDAL H₄
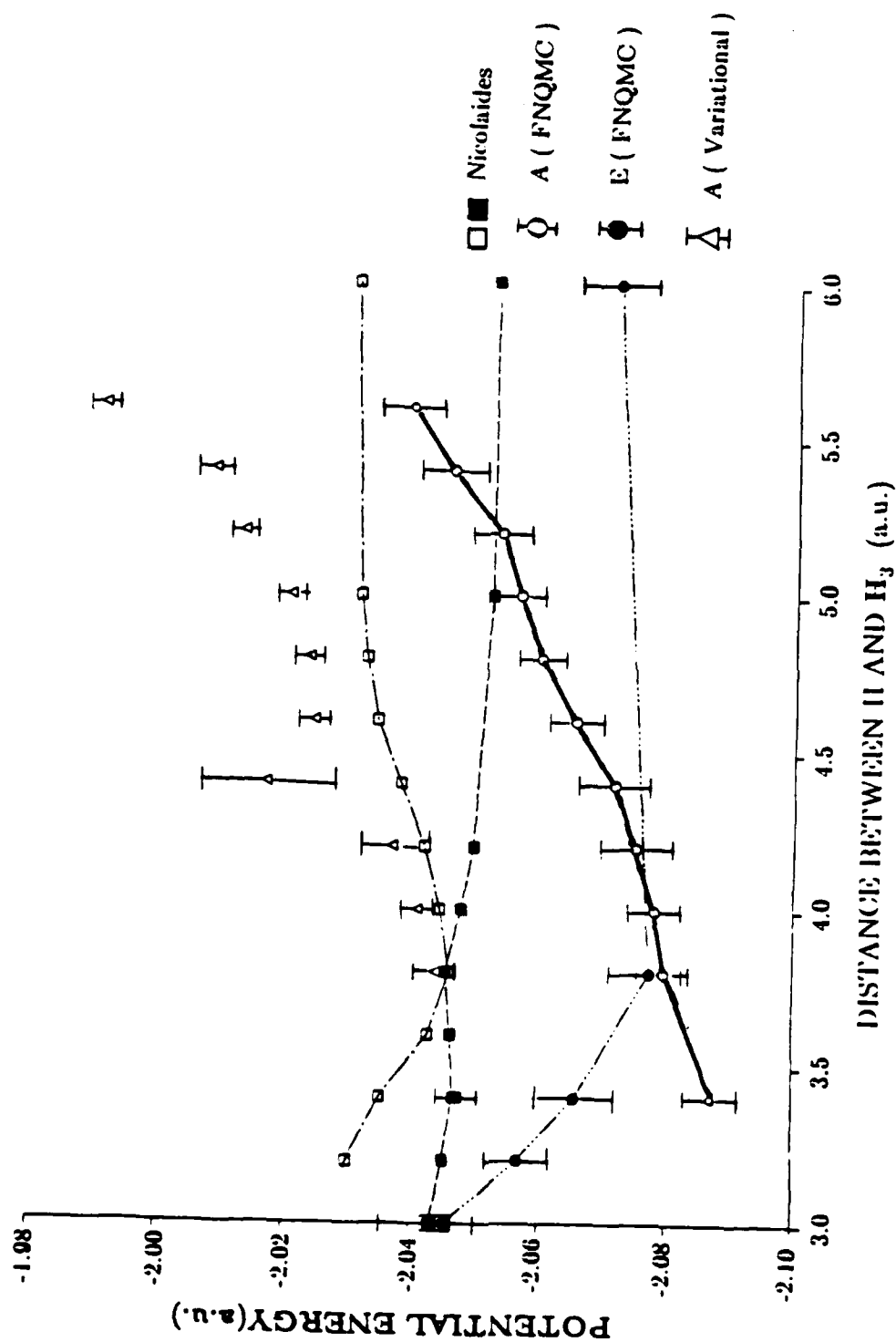
Figure 4. Potential energy of trigonal pyramidal H_4 as a function of the distance R between H and H_3. The A(variational) results were determined using a new optimization method for FNQMC trial functions, see text.

Mark Crofton

Infrared Spectroscopy of H_3^+

Infrared Spectroscopy of H_3^+

Mark Crofton/Lawrence Livermore National Laboratory

The methods and results of infrared spectroscopy of H_3^+ by Oka and others are outlined. Possible application of similar methods to the spectroscopy of hydrogenic species such as H_5^+ is discussed.

The feasibility of containerless antimatter storage as hydrogenic cluster ions depends in part upon the characteristics of the eigenstates of the individual ions and how they interact with each other. Yet these eigenstates remain, to a large extent, unknown and unstudied. Because of the rarity of stable electronically excited states for polyatomic ions and the difficulty of microwave spectroscopy on the H_n^+ species (n = 3,5,...), vibration-rotation spectroscopy is often the best or only way to obtain detailed information for these species. Such work is in its beginning stages. The two most important developments in the spectroscopy of these species were 1) the observation by Oka[1] in 1980 of the vibration-rotation spectrum of H_3^+ and 2) the more recent observation by Lee[2] of H_5^+, H_7^+, H_9^+ etc. by vibrational predissociation spectroscopy.

The primary focus of this report, as it was for the presentation at the SRI workshop, is on Oka's spectroscopic studies of H_3^+ past and present, including discussion of future plans. The author was a student of Oka from 1982-1986.

The H_3^+ molecular ion is the simplest polyatomic system, and the subject of a great many theoretical studies culminating in the extremely accurate calculations of Carney and Porter.[3,4] The other major advances in understanding of H_3^+ were a) the beam-foil induced Coulomb explosion experiment of Gaillard et al.[5] which confirmed the expected equilateral triangle structure,[6] and b) the observation by Herzberg[6] of H_3 and D_3 Rydberg spectra. Oka's observation[1] of the infrared ν_2 band of H_3^+ by a direct infrared absorption method represents the first direct spectroscopic information for this ion. A multiple-reflection dc discharge cell and a difference frequency spectrometer[7] as frequency tunable infrared source were used for the detection. The source is generated by mixing radiation of an Ar laser (ν_{Ar}) with that of a dye laser

(ν_D) in a temperature-controlled $LiNbO_3$ crystal, to produce a few microwatts of infrared radiation. The frequency $(\nu_{Ar} - \nu_D)$ is tunable from 4400 - 2300 cm-1. The source was frequency modulated and the absorption signal demodulated by phase-sensitive detection.

Since 1980 several new methods for generating and detecting ions in the infrared have been developed. The overall improvement in signal to noise ratio is two to three orders of magnitude. The new methods include use of different discharges, such as hollow cathode[8,9] and alternating current, and new modulation techniques such as current modulation and velocity modulation[10] Also, improvement in laser technology and use of source noise subtraction[11] has been important.

The information obtainable from the rotationally resolved vibrational band includes the upper and lower state molecular constants, which contain information about the molecular geometry and the molecular Hamiltonian. The molecular constants have been determined very well for the ground state and ν_2 state from a variety of studies, [12,13] with J' as high as 10. The effects of centrifugal distortion and interactions of ν_2 and ν_1 states have been analyzed. Because H_3^+ is so light, it is very important to fit the spectrum using a model which allows for higher-order effects but has a low number of adjustable parameters. Two approaches were used by Watson,[13] one using a conventional effective Hamiltonian in a Padé formulation and the other a supermatrix approach. The Padé formulation converges more rapidly and gives a better fit, especially at high J. The final fit of 111 observed H_3^+ lines and 26 ground state term values had a standard deviation of 0.065 cm-1 with 31 adjustable parameters. A fit using the potential constants as the least-squares adjustable parameters will probably constitute a better approach. Since all of these results have been published with lengthy discussions of their significance, they will not be discussed in detail here.

There has been no well-defined study of other H_3^+ vibrational states. While Carrington and coworkers[14] have been able to use Doppler-tuned ion beam laser spectroscopy to observe a rich and very complex spectrum of H_3^+ near its dissociation limit, they have not been able to analyze it in detail. Some hot band lines involving $2\nu_2$ and/or some other excited state may have been observed in the hollow cathode emission spectrum by Majewski et al.[13] At the present level of sensitivity it may well be possible to observe the $2\nu_2 \leftarrow \nu_2$ and $\nu_1 + \nu_2 \leftarrow \nu_1$ bands. This will be attempted in the near future by the Oka group.

The deuterated isotopes D_3^+, HD_2^+ and H_2D^+ have been studied also; ν_2 band[16,17] of D_3^+, ν_1,[18] ν_2[19] and ν_3[19] bands of HD_2^+ and ν_1,[20] ν_2[16,21] and ν_3[16,21] bands of H_2D^+.

While there is much useful spectroscopic work left to be done on H_3^+, other hydrogenic species H_5^+, H_7^+, H_9^+, etc. are much more poorly characterized. Some of the stretching vibrational frequencies and band structures are known from the work of Okumura, Yeh and Lee.[2] None of these bands have been rotationally resolved, probably as a result of homogeneous broadening since the upper state vibrational energy in each case is greater than the measured dissociation energies.[22,23] Rotational resolution would yield much more information concerning the geometries and dynamics of these important ions. Such resolution is likely to come in the case of H_5^+ with the observation of the relatively intense band at approximately[24,25] 1700 cm-1, which is somewhat analogous to the ν_2 band of H_3^+. The spectrum should be extremely complex[2] due to the[3] presence of three tunneling motions, each of which is expected to have a low potential barrier.[25,26] For H_7^+ and H_9^+ an even lower photon energy may be required for high resolution studies because of the lower dissociation energies. The abundant production of H_5^+, at least, is not expected to be experimentally difficult. The search for new spectra of H_3^+ and H_5^+ in solid, liquid and gaseous hydrogen plasma will be one of the main thrusts of the Oka group research effort in the near future.

[1] T. Oka, Phys. Rev. Lett. _45_, 531(1980).

[2] M. Okumura, L.I. Yeh and Y.T. Lee, J. Chem. Phys. _83_, 3705 (1985).

[3] G.D. Carney and R.N. Porter, J. Chem. Phys. _65_, 3547(1976).

[4] G.D. Carney, Mol. Phys. _39_, 723(1980).

[5] M.J. Gaillard, D.S. Gemmell, G. Goldring, I. Levine, W.J. Pietsch, J.C. Poizat, R.J. Ratkowski, J. Remillieux, Z. Veger, and B.J. Zabransky, Phys. Rev. A _17_, 1797(1978).

[6] G. Herzberg, J. Chem. Phys. _70_, 4806(1979).

[7] A. S. Pine, J. Opt. Soc. Amer. _64_, 1683(1974), and _66_, 97 (1976).

[8] S.C. Foster, A.R.W. McKellar and T.J. Sears, J. Chem. Phys. _81_, 578(1984).

[9] T. Amano, J. Opt. Soc. Am. _2B_, 790(1985).

[10] C.S. Gudeman and R.J. Saykally, Ann. Rev. Phys. Chem. _35_, 387(1984).

[11] D.J. Nesbitt, H. Petek, C.S. Gudeman, C.B. Moore, and R.J. Saykally, J. Chem. Phys. _81_, 5281(1984).

[12] J.K.G. Watson, S.C. Foster, A.R.W. McKellar, P. Bernath, T. Amano, F.S. Pan, M.W. Crofton, R.S. Altman, and T. Oka, Can. J. Phys. 62, 1875(1984).

[13] W.A. Majewski, M.D. Marshall, A.R.W. McKellar, J.W.C. Johns and J.K.G. Watson, submitted to J. Mol. Spectrosc.

[14] A. Carrington, J. Buttenshaw, and R. Kennedy, Mol. Phys. 45, 753(1982).

[15] P. Jensen and P.R. Bunker, to be published.

[16] J.T. Shy, J.W. Farley and W.H. Wing, Phys. Rev. A24, 1146 (1981).

[17] J.K.G. Watson, S.C. Foster, and A.R.W. McKellar, Can. J. Phys., in press.

[18] K.G. Lubic and T. Amano, Can. J. Phys. 62, 1886(1984).

[19] S.C. Foster, A.R.W. McKellar, and J.K.G. Watson, J. Chem. Phys. 85, 664(1986).

[20] T. Amano and J.K.G. Watson, J. Chem. Phys. 81, 2869-2871 (1984).

[21] S.C. Foster, A.R.W. McKellar, I.R. Peterkin, J.K.G. Watson, F.S. Pan, M.W. Crofton, R.S. Altman, and T. Oka, J. Chem. Phys. 84, 91(1986).

[22] R.J. Beuhler, S. Ehrenson and L. Friedman, J. Chem. Phys. 79, 5982(1983).

[23] M.T. Elford, J. Chem. Phys. 79, 5951(1983).

[24] Y. Yamaguchi, J.F. Gaw and H.F. Schaefer III, J. Chem. Phys. 78, 4074(1983).

[25] Y. Yamaguchi, private communication to T. Oka.

[26] R. Ahlrichs, Theor. Chim. Acta 39, 149(1975).

L. I. Yeh, M. Okumura, J. D. Myers, and Y. T. Lee

Vibrational Spectroscopy of the Hydrogen and Hydrated
Hydronium Cluster Ions

VIBRATIONAL SPECTROSCOPY OF THE HYDROGEN AND HYDRATED HYDRONIUM CLUSTER IONS

L. I. YEH, M. OKUMURA, J. D. MYERS, and Y. T. LEE

Materials and Chemical Sciences Division
Lawrence Berkeley Laboratory and
Department of Chemistry, University of California
Berkeley, California 94720 USA

ABSTRACT

Two series of cluster ions have been investigated in our laboratory. The hydrogen cluster ions H_n^+ (n=5,7,9,11,13,15) have been probed in the region of the H-H stretch frequency from 3800 to 4200 cm^{-1}. These hydrogen cluster ions consist of an H_3^+ core which is solvated by H_2 moieties. Upon excitation of an H-H stretch, these ions undergo vibrational predissociation losing one or more H_2 units. Absorption is monitored by detecting the fragment ions as a function of the probe frequency. Broad absorption bands were seen for these hydrogen cluster ions. The peak absorption position increased significantly with larger cluster size to H_9^+ and then remained essentially constant to H_{15}^+.

The hydrated hydronium ions $H_3O^+ \cdot (H_2O)_n$ (n=1,2,3) have been studied in a similar fashion. A probe laser was tuned from 3550 to 3800 cm^{-1} to excite an O-H stretch. The dissociation energy was much larger than the probe laser frequency. Therefore, a second laser was employed which utilized the multiphoton dissociation (MPD) process. Once again, fragment ions were monitored as a function of the probe frequency. In this series the antisymmetric and symmetric O-H stretch of the H_2O moieties was observed. Rotational structure was resolved in the antisymmetric O-H stretch band in $H_5O_2^+$ proving the power of this technique for doing high resolution infrared spectroscopy of cluster ions.

INTRODUCTION

We have recently obtained gas phase infrared absorption spectra of the mass selected hydrogen cluster ions and the hydrated hydronium cluster ions by observing the consequences of absorption of an IR photon. Previous experimental work on cluster ions have largely been limited to thermochemical, kinetic, or matrix studies. Many studies have been directed toward determining the dissociation energy of H_5^+ [1-5]. Two of the most recent studies were by Elford[6] who found it to be 5.8 ±

1.2 kcal/mole and Beuhler, Ehrenson, and Friedman[7] who reported 6.6 $\pm$ 0.3 kcal/mole. Recently, Miller[8] has reported fluorescence excitation spectra of $C_6F_6^+ \cdot X$ (X= He, Ne, Ar, N_2) with vibrational structure. Until recently, the only study on vibrational spectra of gas phase cluster ions was done by Schwarz[9,10]. In this early work, Schwarz studied both the ammoniated ammonium ions and the hydrated hydronium ions. An inherent difficulty of his technique was in determining which cluster ion was responsible for a particular absorption feature. Nonetheless, he managed to roughly assign low resolution vibrational spectra of these ions.

A considerable amount of theoretical calculations on electronic structure and vibrational frequencies have been carried out on these cluster ions. A large impetus for our experimental studies was the work done by Schaefer and coworkers. Yamaguchi, Gaw, and Schaefer[11] calculated harmonic vibrational frequencies with a semi-empirical correction factor for the hydrogen cluster ions H_n^+ (n=5,7,9). Remington, Colvin, Raine, and Schaefer[12] did similar calculations to obtain vibrational frequencies, structures, and energies for the hydrated hydronium series $H_3O^+ \cdot (H_2O)_n$ (n=1,2,3). Although the larger hydrogen cluster ions and the hydrated hydronium cluster ions can be considered as $H_3^+ \cdot (H_2)_n$ and $H_3O^+ \cdot (H_2O)_n$, one ambiguity for both $H_3^+ \cdot H_2$ and $H_3O^+ \cdot H_2O$ is whether the ground state is an asymmetric structure as implied in the above notation, or a symmetric structure ($H_2 \cdot H^+ \cdot H_2$ or $H_2O \cdot H^+ \cdot OH_2$) where the center proton is equally shared. The theoretical calculations show that for both ions, the two structures are very close in energy; for H_5^+, the asymmetric structure is lower in energy by only 0.09 kcal/mole, whereas for $H_5O_2^+$, the symmetric structure is lower in energy by 0.2 kcal/mole. These theoretical predictions on the ground state structures are not in disagreement with our experimental results. The larger cluster ions can accurately be described as an H_3^+ core solvated by H_2 moieties and as an H_3O^+ core solvated by H_2O units.

EXPERIMENTAL

The apparatus used to study these cluster ions consists of a radio frequency octopole ion trap and a tandem mass spectrometer[13]. Two different ion sources were used to study the hydrogen cluster ions. The first used a supersonic expansion of ~20 atm of ultrahigh purity hydrogen cooled to 135 K. The neutral hydrogen clusters formed from the expansion were then ionized by a Brink's type electron bombardment ionizer[14]. This process yielded the odd mass cluster ions H_n^+ (n=5,7,9,11,13,15). The other ion source used was a corona discharge source. ~200 torr of UHP hydrogen was flowed past a needle set to +1.5 kV. A corona discharge formed between this needle and the copper walls of the source which were cooled to -20C. The vibrational degrees of freedom were cooled in the high pressure drift region

to approximately room temperature. This region was followed by a supersonic expansion through a 75 μm nozzle which effectively cooled the rotational temperature. The motivation for building the corona discharge source was the lower vibrational and rotational temperature of the nascent ions as compared to the expansion followed by electron impact ionization source. The corona discharge source was the only one used in the hydrated hydronium ion series.

Once the ions are formed, they're focused and mass selected by a 60° sector magnet. They're then bent 90° to be collinear with the laser as shown in Fig. 1. An octopole rf ion trap is usually used to trap the ions and hold them while various spectroscopic interrogations are made. The ions are then released, mass filtered, and counted by a Daly-type ion counter.

Two different laser excitation schemes were employed. For the hydrogen cluster ions, the dissociation energy of the weakest bond is less than the frequency used to excite the stretch of the H_2 moiety. Thus, vibrational predissociation can be used to monitor the absorption by the cluster as a function of laser frequency. This method is ideal for our experimental apparatus due to the high detection sensitivity of the fragment ions as contrasted with the lower sensitivity using conventional absorption techniques.

The hydrated hydronium series needs a different laser scheme. Here, the dissociation energy far exceeds the vibrational quantum of an O-H stretch. Thus, a two laser set-up was necessary. The first laser excites the O-H stretch which places the ion high up in the quasicontinuum. Once in the quasicontinuum, resonant transitions are always likely in a certain frequency range for an absorption because the density of states is so high. Also, total absorption of photons is determined by the fluence of the laser (photons/area) rather than the intensity. Therefore, the second laser, which is a cw CO_2 laser , is set to a frequency and intensity where ground state absorption is negligible. Those molecular ions excited by the first laser, however, will absorb many CO_2 laser photons and dissociate. So, in this scheme, the CO_2 laser is fixed at a constant frequency and intensity for a given parent cluster ion and the fragment ions are detected as a function of the first laser's frequency.

Two different tunable infrared lasers were used in these experiments. An optical parametric oscillator (OPO) pumped by a Nd:YAG was used for the initial scanning. Although this laser had the advantage of high power, it had the disadvantage of having a broad bandwidth. The other laser used was the Burleigh F-center laser pumped by a Kr^+ laser. The F-center laser was run both with an intracavity etalon ($\Delta v \sim 3 \times 10^{-5}$ cm^{-1}) and without the etalon ($\Delta v \sim 0.5$ cm^{-1}). Spectra taken using these lasers will be compared in the next section.

RESULTS AND DISCUSSION

A. Hydrogen cluster ions

The absorption band corresponding to an H-H stretch was observed for H_n^+ (n=5,7,9,11,13,15). This work was reported previously[15,16]. In Fig. 2 is shown the absorption band for H_5^+, H_7^+, and H_9^+. These spectra were taken using the electron impact ion source and the OPO. No rotational structure was observed under these conditions. From the predicted structures, the rotational spacing in H_5^+ was expected to be ~6 cm^{-1}. Because the linewidth of the OPO was ~10 cm^{-1}, we went to the higher resolution F-center laser. No rotational structure was observed even under the conditions where we were limited by the Doppler width of the ions. Also in Fig. 2 are shown the spectra of H_7^+ and H_9^+. These larger cluster ions have multiple dissociation pathways. Although the band shapes are broad enough to cause some ambiguity in determining the band origin, it is evident that the frequency of the H-H stretch moiety increases with larger cluster size.

Fig. 3 shows the spectra obtained for H_9^+, H_{11}^+, H_{13}^+, and H_{15}^+. These peaks are also rather broad. The position of the peak maximum as a function of cluster size is plotted in Fig. 4. Although the peak maximum shifts to higher frequency with larger cluster size, the shift is quite small after H_9^+. The H-H stretch in free H_2 is not infrared allowed. The analogous motion to the H-H stretch in the hydrogen cluster ions can be seen due to the perturbation by the H_3^+ core. The three binding sites directly on the H_3^+ become filled at H_9^+. The additional H_2 units on the larger cluster units occupy sites farther removed from H_3^+. Therefore, we believe those additional H_2 moieties are too far removed from the perturbation caused by the H_3^+ core to become infrared allowed. The reason, then, that the curve in Fig. 4 levels out after H_9^+ is that the H_2 stretch excited always corresponds to one of the H_2 moieties directly bound to the H_3^+ core.

The electron impact ion source used to take the above spectra was expected to form the ions internally excited. In contrast, the corona discharge ion source should be much cooler. This difference was confirmed by the H_5^+ spectra shown in Fig. 5. The top panel shows the spectrum using the electron impact source. The shoulder on the blue side of the peak becomes markedly smaller on going to the corona discharge source. Also, the absorption becomes much narrower using the corona discharge source. These observations lend credence to the theory that the lack of observed rotational structure is due at least in part to spectral congestion.

As mentioned earlier, the symmetric $H_2 \cdot H^+ \cdot H_2$ D_{2d} structure is only 0.09 kcal/mole higher in energy than the ground state asymmetric $H_3^+ \cdot H_2$ C_{2v} structure at the full CI level with an extended basis set[16]. In fact, there are two more structures predicted to lie less than 1 kcal/mole above the lowest energy structure. These are the planar $H_3^+ \cdot H_2$ C_{2v} and the planar $H_2 \cdot H^+ \cdot H_2$ D_{2h} structures. The H_5^+ molecular ion is, as all the hydrogen cluster ions are, very floppy and as such have several structures close in energy to the ground state. These structures may in fact be barriers to different permutations of the ground state structure. It is also possible that once the zero point energy of the motion connecting the structures is included one or more of the double well potentials may give rise to a broad single well.

The frequencies of the motions connecting these structures are low. Even with the corona discharge source, these vibrations are not expected to be effectively cooled. It is these considerations which lead us to postulate that at least part of the explanation for the lack of rotational structure is spectral congestion.

Homogeneous broadening processes could also contribute. In the larger cluster ions, several H_2 moieties come off after excitation of the H-H type stretch. The fragmentation distribution is shown in Fig. 6. This indicates that the intramolecular vibrational redistribution rate must be much faster than the rate of dissociation of an H_2 unit.

B. Hydrated hydronium cluster ions

The hydrated hydronium ion $H_3O^+ \cdot (H_2O)_n$ (n=1,2,3) were studied using the F-center laser both without ($\Delta\nu \sim 0.5$ cm^{-1}) and with ($\Delta\nu \sim 3 \times 10^{-5}$ cm^{-1}) the intracavity etalon. In the case where the etalon was used, the true linewidth was limited by the motion of the ions confined in the rf octopole trap. This Doppler width was $\Delta\nu \sim 0.02$ cm^{-1}. Spectra for all three cluster ions were obtained at low resolution in the O-H stretch region.

In Fig. 7 is shown the low resolution scan of $H_5O_2^+$. Two features are seen. The band centered at 3609 cm^{-1} is assigned to the symmetric O-H stretch of an H_2O moiety. The other feature is assigned to the antisymmetric O-H stretch of an H_2O unit and has been resolved into a series of Q branches in a perpendicular band progression. Details of this and other spectra will be presented in a future paper[17].

131

ACKNOWLEDGMENT

REFERENCES

1. U. A. Arifov, S. L. Pozharov, I. G. Chernov, and Z. A. Mukhamediev, High Energy Chem. 5, 69 (1971).

2. S. L. Bennett and F. H. Field, J. Amer. Chem. Soc. 94, 8669 (1972).

3. M. T. Elford and H. B. Milloy, Aust. J. Phys. 27, 795 (1974).

4. K. Hiraoka and P. Kebarle, J. Chem. Phys. 62, 2267 (1975).

5. Rainer Johnsen, Chou-Mou Huang, and Manfred A. Biondi, J. Chem. Phys. 65, 1539 (1976).

6. M. T. Elford, J. Chem. Phys. 79, 5951 (1983).

7. R. J. Beuhler, S. Ehrenson, and L. Friedman, J. Chem. Phys. 79, 5982 (1983).

8. Richard A. Kennedy and Terry A. Miller, J. Chem. Phys. 85, 2326 (1986).

9. Harold A. Schwarz, J. Chem. Phys. 67, 5525 (1977).

10. Harold A. Schwarz, J. Chem. Phys. 72, 284 (1980).

11. Yukio Yamaguchi, Jeffrey F. Gaw, and Henry F. Schaefer III, J. Chem. Phys. 78, 4074 (1983).

12. Richard B. Remington, Michael E. Colvin, Gwen P. Raine, and Henry F. Schaefer III, unpublished results.

13. For details of the experimental apparatus, see: S. W. Bustamente, Ph.D. Thesis, University of California, Berkeley, 1983, and M. Okumura, Ph.D. Thesis, University of California, Berkeley, 1986.

14. Y. T. Lee, J. D. McDonald, Pr. R. LeBreton, and D. R. Herschbach, Rev. Sci. Instrum. 40, 1402 (1969).

15. M. Okumura, L. I. Yeh, and Y. T. Lee, J. Chem. Phys. 83, 3705 (1985).

16. L. I. Yeh, Mitchio Okumura, and Y. T. Lee in Electronic and Atomic Collisions, edited by D. C. Lorents, W. E. Meyerhof, and J. R. Peterson (Elsevier Science Publishers B.V., Netherlands, 1986), pp. 813-818.

17. Yukio Yamaguchi, Jeffrey F. Gaw, Richard B. Remington, and Henry F. Schaefer III, preprint.

18. L. I. Yeh, M. Okumura, J. D. Myers, and Y. T. Lee, unpublished results.

FIGURE CAPTIONS

Fig. 1. Schematic of the experimental apparatus.

Fig. 2. Vibrational predissociation spectra of H_5^+, H_7^+, and H_9^+ taken using the optical parametric oscillator. The ions were formed in the electron impact ion source.

Fig. 3. Vibrational predissociation spectra of H_9^+, H_{11}^+, H_{13}^+, and H_{15}^+ (from top to bottom) taken using the F-center laser. The ions were formed in the electron impact ion source.

Fig. 4. Plot of H-H stretch absorption peak frequency versus hydrogen cluster size.

Fig. 5. Comparison of OPO spectra of H_5^+ created in a a) electron impact and b)corona discharge ion source.

Fig. 6. Plot of the fragmentation branching ratios of the hydrogen cluster ions after absorption of an IR photon.

Fig. 7. Vibrational spectrum of $H_5O_2^+$ created by the corona discharge source taken with the F-center laser at ~ 0.5 cm^{-1} resolution.
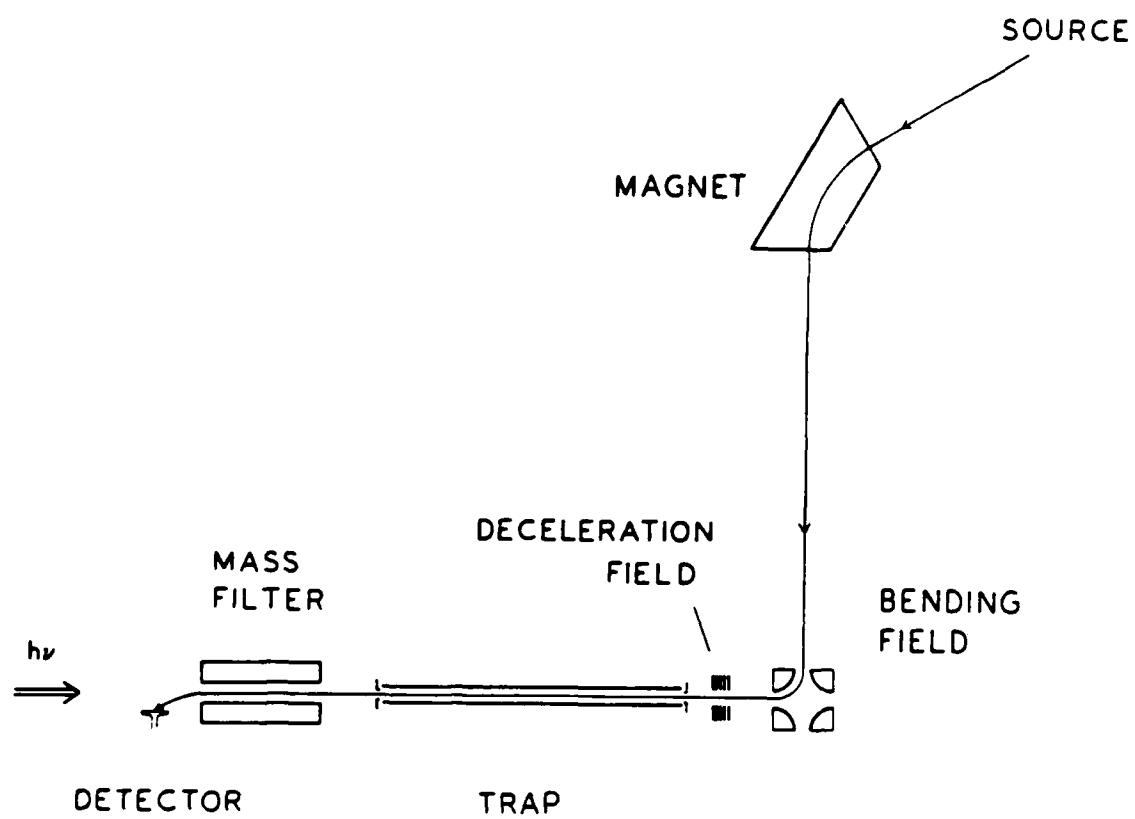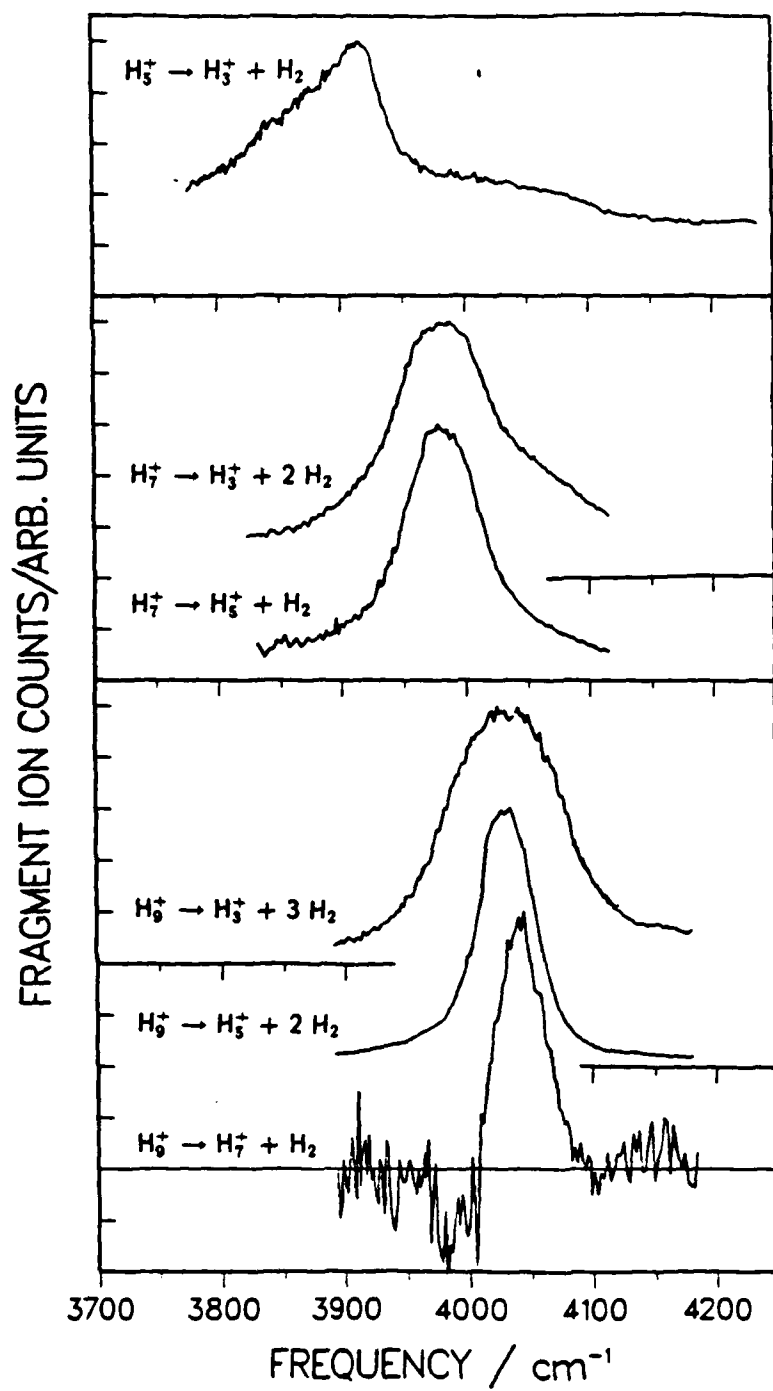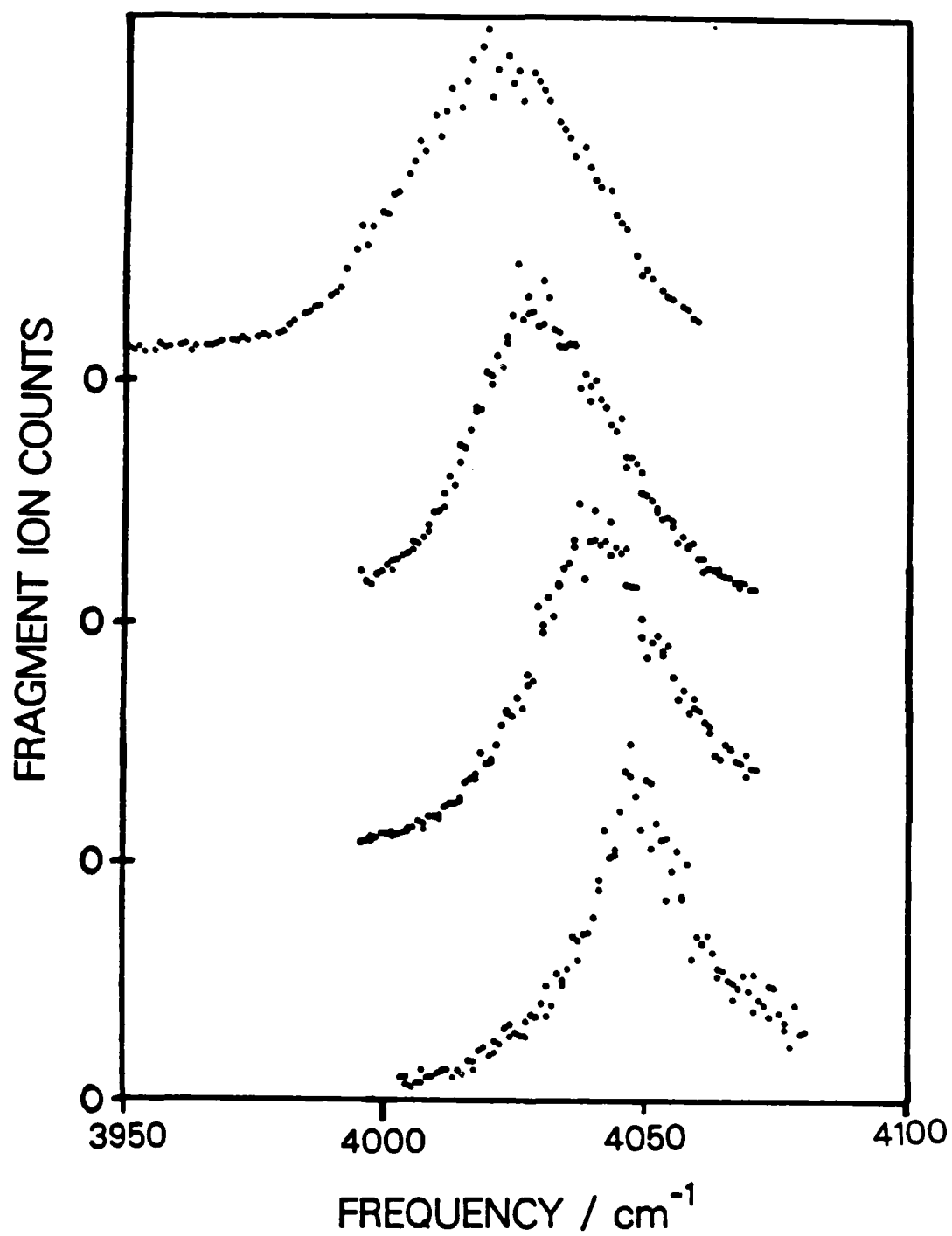
SOURCE

MAGNET

MASS
FILTER

DECELERATION
FIELD

BENDING
FIELD

hν

DETECTOR

TRAP

XBL 847-3011

Fig. 1

Fig. 2

XBL 8612-5046

FREQUENCY / cm^{-1}

XBL 8612-5034

Fig. 3

FREE H$_2$ STRETCHING FREQUENCY

H$_n^+$ PARENT CLUSTER SIZE n

PEAK POSITION / cm^{-1}

XBL 856-2796

Fig. 4

138

Fig. 5

XBL 8612-5036

H_{15}^{+}

H_{13}^{+}

H_{11}^{+}

H_{9}^{+}

H_{7}^{+}

3   5   7   9   11   13

FRAGMENT CLUSTER MASS

XBL 8612-5048

Fig. 6

140
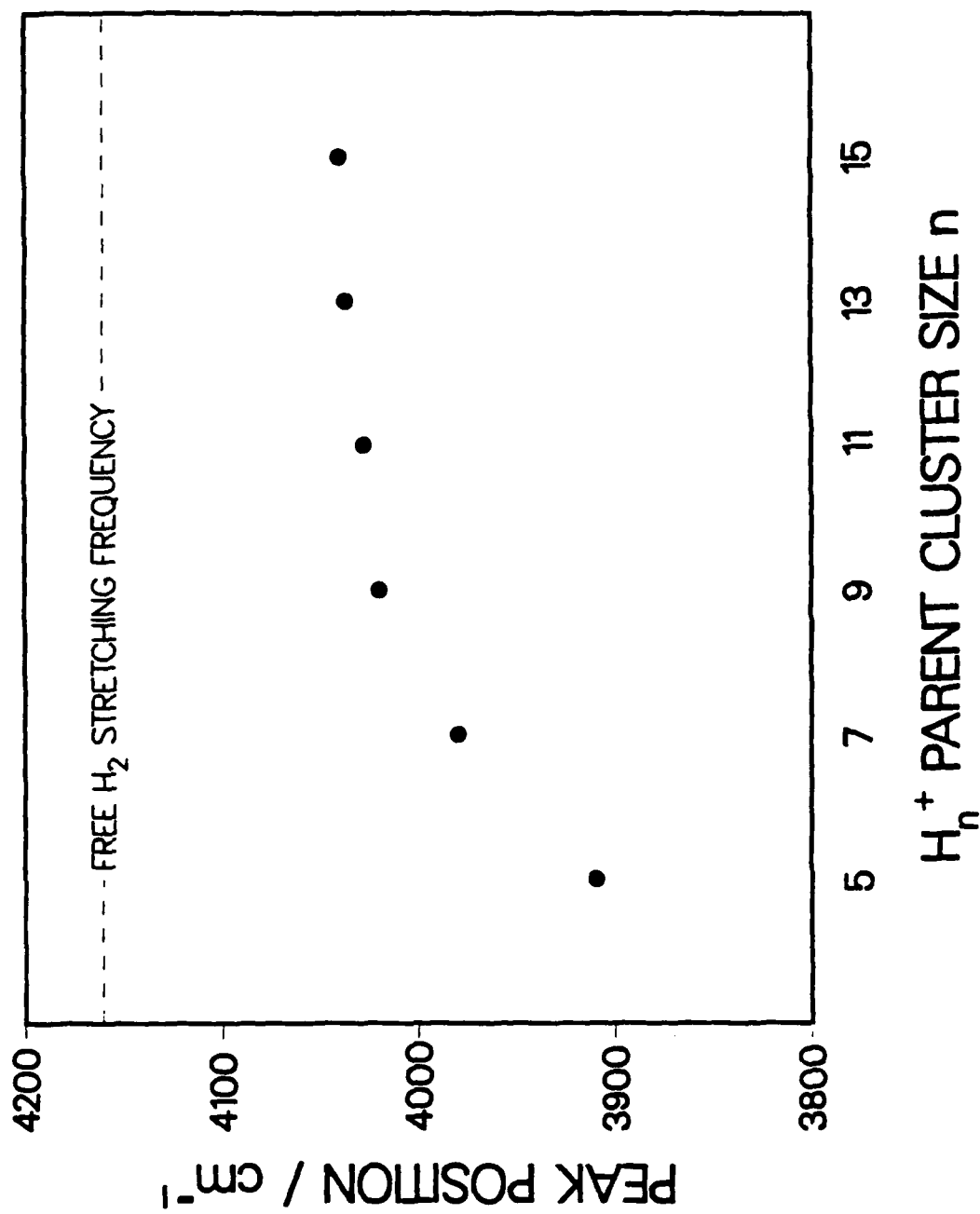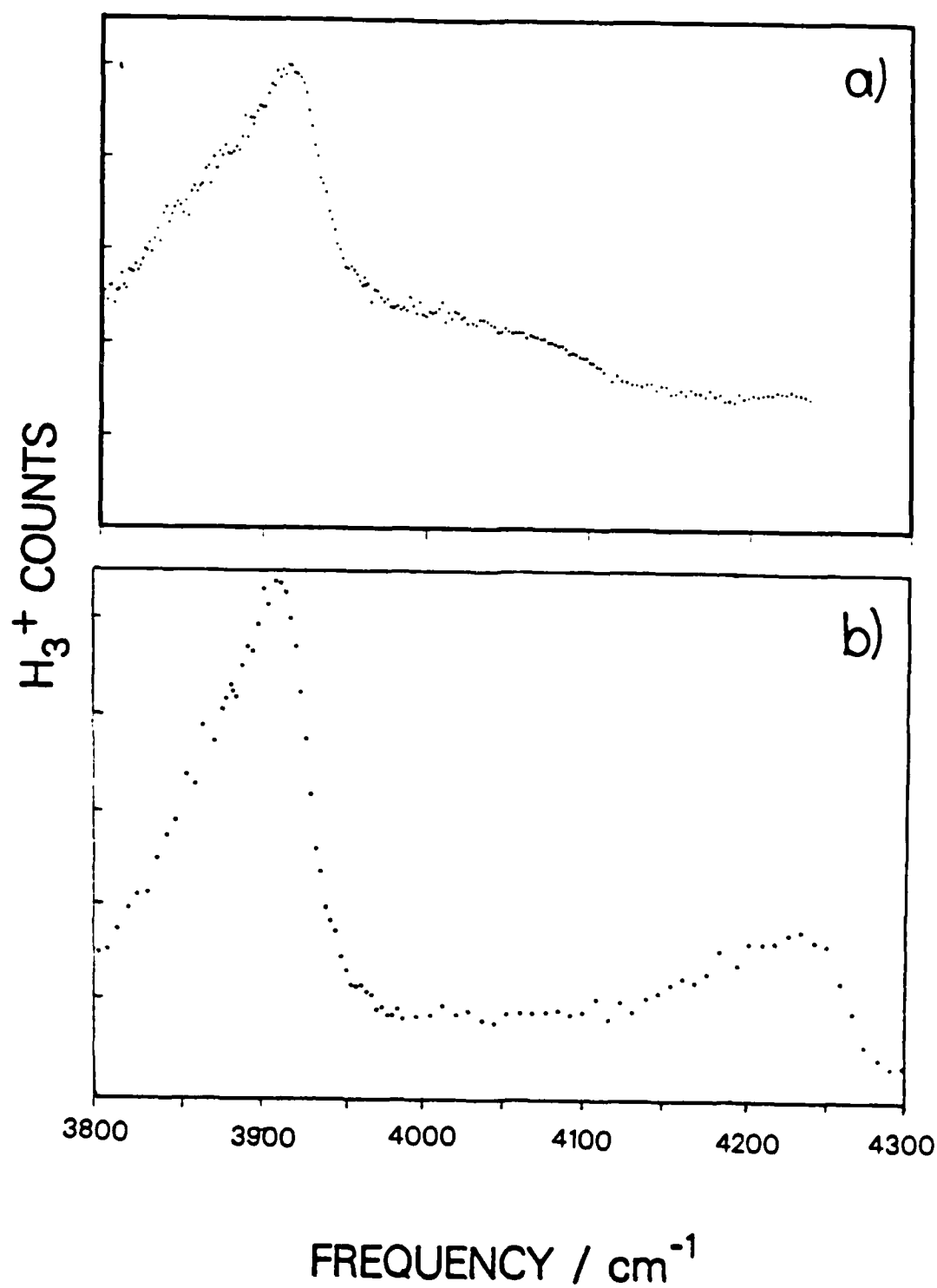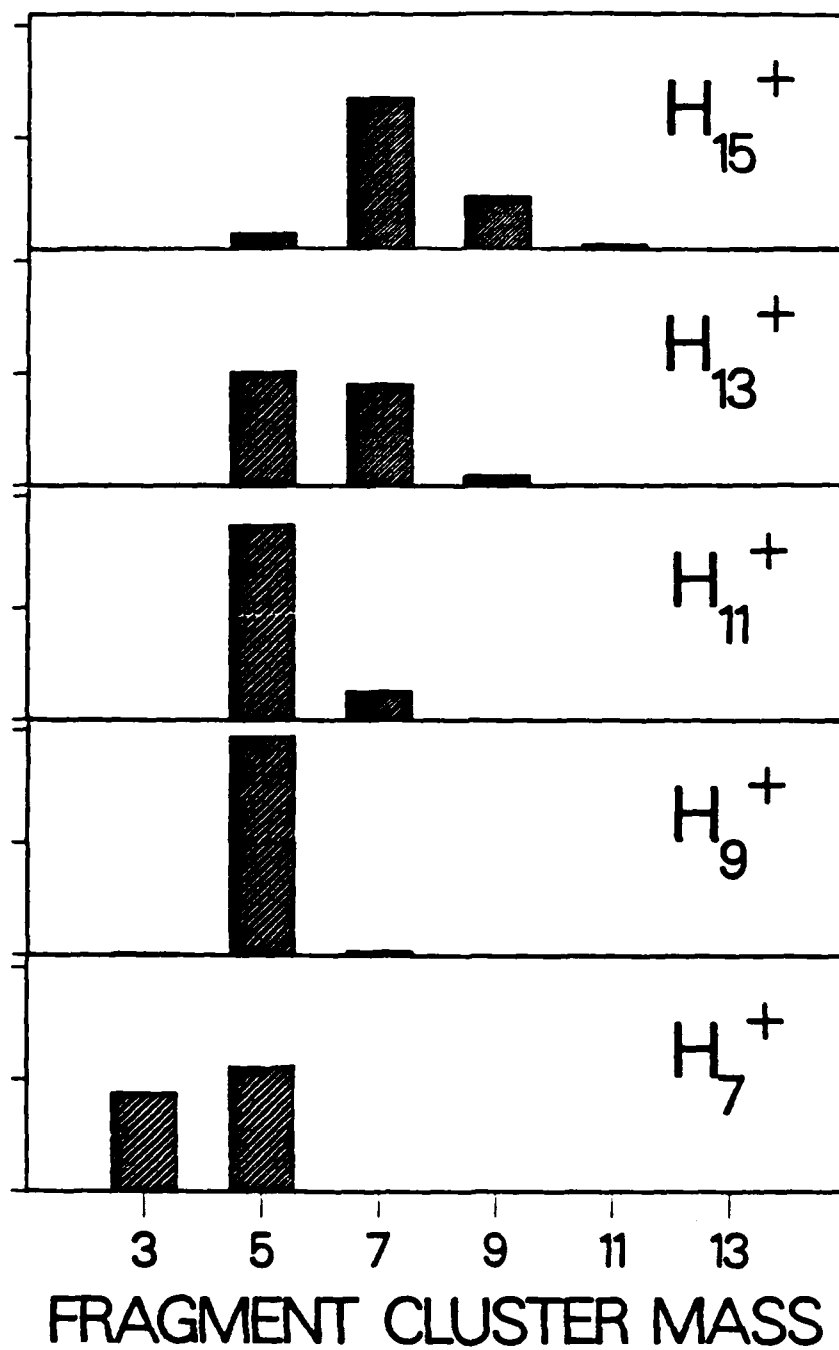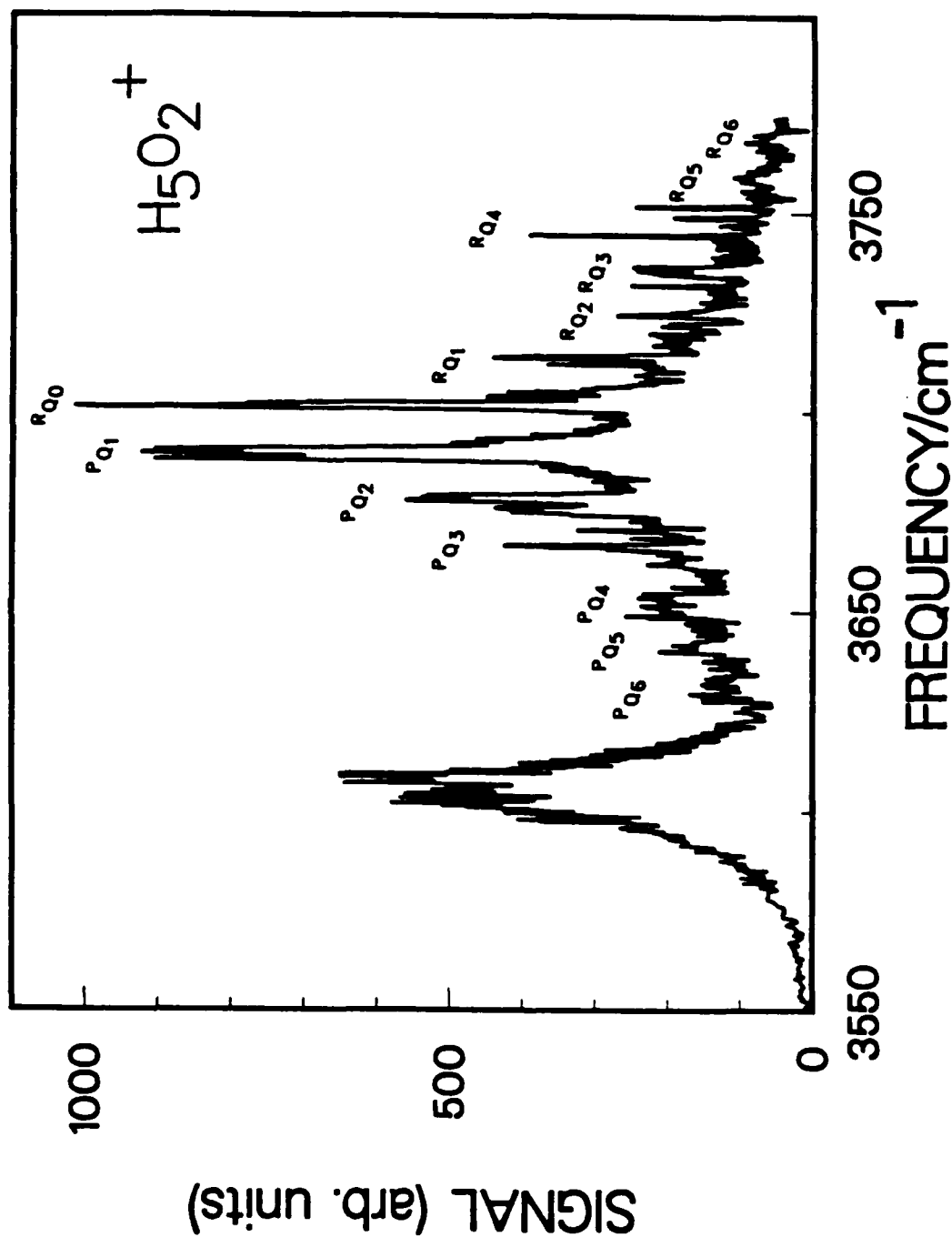
Fig. 7

XBL 873-1347

J. B. A. Mitchell

The Role of Electron-Ion Recombination in Bulk Antimatter Production

THE ROLE OF ELECTRON-ION RECOMBINATION IN BULK ANTIMATTER PRODUCTION

J.B.A. Mitchell
Department of Physics
and
Centre for Chemical Physics
The University of Western Ontario
London, Ontario, Canada. N6A 3K7

ABSTRACT

The differences between the recombination of electrons with atomic ions and molecular ions is outlined. Methods for studying recombination processes experimentally are described. A discussion is given of how electron ion recombination must be optimized in order to maximize the production of antimatter cluster ions.

INTRODUCTION

Electron-Ion, (Positron-anti-ion) recombination processes play a central role in the schemes for bulk antimatter production discussed elsewhere in this volume. The neutralization of anti-protons to form antihydrogen is a crucial step in the process of constructing antihydrogen cluster ions which are envisaged as the most useful form in which to store antimatter. This neutralization process will most probably involve the two body radiative recombination of antiprotons with positrons.

Once formed, the antihydrogen can combine with other antipro-protons to form $\bar{H}_2^-$ and then on to $\bar{H}_3^-$, $\bar{H}_5^-$ - - - - $\bar{H}_n^{-*}$. At each step positrons can recombine with the molecular ions leading to their neutralization and fragmentation.

It is very important to understand the magnitudes of these recombination processes and their detailed mechanisms in order to optimize bulk antimatter production. The following discussion will be given in terms of normal matter interactions therefore electron-ion recombination will be emphasized.

Energy must be delivered to an atom or a molecule in order to ionize it. For electron-ion recombination to occur at least some of this energy must be disposed of. The rate of the recombination process depends critically upon the ability of an ion to release this energy.

The collision between a thermal electron and an ion takes place in a time of $\sim 10^{-15}$ secs. If the ion is a bare nucleus such as a proton then the excess energy in a binary electron-ion collision can only be released by photon emission. The process is known as Radiative Recombination.

*Note: The analogous normal matter ions are H_2^+, H_3^+, H_5^+ --- H_n^+.

$$e + A^+ \rightarrow A + h\nu \; - - - \tag{1}$$

The problem here lies in the fact that typical times for photon emission are $\sim10^{-9}$ seconds. Thus the likelihood of the electron-ion pair losing energy via photon emission during the collision time is very small. Hence radiative recombination at thermal energies has a very small rate, i.e. the cross section for the process is very small. Calculations of radiative recombination cross sections are given in Bethe and Salpeter, (1957).

If the ion has at least one bound electron then it is possible for the incoming electron to excite this electron and in the process be itself captured into a high lying state. The resulting atom has then two excited electrons neither of which has sufficient energy to escape. This intermediate state will usually decay via autoionization, i.e. the outer electron will be ejected. This will occur within a typical timescale of $\sim10^{-13}$ secs. If, however, the inner electron drops back to its original state during the existence of the intermediate state, then the outer electron will be left permanently bound and so the recombination is stabilized. This process is illustrated in Figure 1.

$$e + A^+ \rightarrow A^{**} \rightarrow A^* + h\nu \; - - \tag{2}$$

The problem however is that again the typical time for radiation is $\sim10^{-9}$ secs. Because the effective time of electron-ion interaction has been increased by about a factor of 100, the cross section for this process which is known as Dielectronic Recombination will be enhanced. It can be seen however from Figure 1 that the doubly excited states into which the electron can be captured are discrete and so dielectronic recombination is a resonant process which displays large cross sections at specific electron energies only. Nevertheless dielectronic recombination plays a very important role in the areas of stellar astrophysics and thermonuclear fusion research. A series of reviews of dielectronic recombination research has recently been compiled by Nayfeh and Clarke, (1985).

Electron molecular ion recombination also occurs via an initial capture into an autoionizing state which lies above the ionization potential for the molecule. Such a state is illustrated in Figure 2. The difference here is that the intermediate molecular state can be repulsive and if this is so then when the potential energy has dropped below the ionization potential of the molecule, the state can no longer autoionize and the recombination is stabilized. The lifetime of the intermediate state is again $\sim10^{-13}$ sec. but the time taken for dissociation is also $\sim10^{-13}$ secs. This means that the stabilization is very efficiently accomplished and so molecular ion recombination typically exhibits very large cross sections. This process is known as Dissociative Recombination and has been reviewed by Mitchell (1987). (See also enclosed references.)

146

MEASUREMENTS OF ELECTRON ION RECOMBINATION

A recent review of the techniques used for studying electron molecular ion recombination has been given by Mitchell and McGowan (1983). Studies of electron-atomic ion recombination are reviewed in Nayfeh and Clarke, 1985. The major problem with measuring dissociative recombination in the laboratory is the fact that the cross section is large only for collision energies less than 1eV. For this reason most experimental measurements have involved the study of the decline of the electron concentration in a plasma as a function of time. Of particular note are the studies of Biondi's group at Pittsburgh. In these experiments a microwave discharge is created in a vessel at a pressure of a few torr, Figure 3. The microwave generator is then turned off and the decay of the electron density in the afterglow is examined by studying the scatter of a low power microwave beam produced from a second generator. Provided losses due to ambipolar diffusion are properly accounted for the rate coefficient can be determined from the electron decay rate. The identity of the principal ion species responsible for the recombination can be determined using a quadrupole mass spectrometer.

In certain cases the identity of the recombination products has been determined spectroscopically but generally the afterglow method is most useful for simply determining the recombination rate. The temperature of the electrons in the afterglow can be varied using microwave heating and this technique does not increase the temperature of the ions.

The vibrational state of the recombining ions has been determined in some cases using laser induced fluorescence (Zipf 1980). Generally, however, it is expected to be low for most molecular ions because of the high pressures used in the experiment.

The other major approach to the study of electron ion recombination involves the use of intersecting electron and ion beams. This area has been reviewed by Mitchell and McGowan (1983) and discussions concerning the technology of intersecting beam experiments have been given by Auerbach et al (1977), Claeys and Brouillard (1983) and by Dolder (1969). Only the merged beam technique where the intersection angle between the beams $\theta \approx 0°$, is capable of achieving very low centre of mass collision energies. The Merged Electron-Ion Beam Experiment at The University of Western Ontario is illustrated in Figure (4).

An electron beam generated from a thermionic cathode is made to merge with an ion beam from a 400 KeV Van de Graaff accelerator using a trchoidal analyzer. This device uses crossed electric and magnetic fields to shift the beam from its original path to a parallel but offset path which coincides with that of the ion beam. The beams intersect over a distance of about 10 cms before being demerged using a second trochoidal analyzer. The electron beam is collected and measured using a faraday cup. The ion beam is deflected using electrostatic condensor plates and it too is collected and measured using a second faraday cup. The neutral atoms resulting from electron ion recombination and background gas collisions are detected using a surface barrier detec-

tor. Electron beam modulation and gated counting techniques are used to separate true recombination signals from background signals. The beams are scanned in the intersection region to determine the effective collision area.

The recombination cross section is given in terms of experimental parameters by: -

$$\sigma = \frac{C_n e^2 F}{I_e I_i L} \left| \frac{v_e v_i}{v_e - v_i} \right| - - \qquad (I)$$

where v_i v_e I_i I_e are the ion and electron velocities and currents respectively, L is the length of the collision region, e is the electronic charge, F is the effective collision area (see Keyser et al 1979) and C_n is the count rate for the neutral products of the recombination. Since all the necessary parameters are measured experimentally, absolute cross sections can be determined with this technique.

If one defines a reduced ion energy thus

$$E_+ = \frac{E_i M_e}{M_i} - - \qquad (II)$$

then the centre of mass collision energy in a merged beam experiment is given by: -

$$E_{CM} = E_+ + Ee - 2(E_+ Ee)^{\frac{1}{2}} \cos \theta. - - \qquad (III).$$

A discussion of the energy resolution in a merged beam experiment has been given by Auerbach et al (1977), who showed that at low centre of mass energy, the spread in the interaction energy is dominated by the uncertainty in the intersection angle. Thus to achieve very low interaction energies it is vital that the beams be perfectly merged and that transverse energies of the electron beam, (caused by for example thermal spread, space charge effects and electrostatic focussing) be minimized.

NEUTRALIZATION CHEMISTRY

In terms of recombination processes the formation of bulk antimatter can be seen to comprise four stages.

(a) The neutralization of antiprotons.

The formation of antihydrogen from antiprotons may be accomplished via radiative recombination with positrons. As pointed out earlier, however, because of the disparity between collision time and the time for radiation emission, the cross section for this process is small.

An experiment is currently being planned to use a Merged beam approach at the CERN Low Energy Antiproton Ring (LEAR) to study this capture. The details of this experiment are given in a recent paper by Neumann et al (1983). In an effort to increase the cross section it is proposed to use a laser to stimulate the stabilizing photon emission transition.

148

The problem is that once formed the antihydrogen can be re-ionized by the laser beam. Because of this it is estimated that the maximum achievable enhancement of the cross section can be of the order of 110.

The cross section for radiative recombination is proportional to E^{-1} at low energies. Bethe and Salpeter, 1957. One might suppose therefore that the merged beam approach would offer the ability to enhance the antihydrogen yield by reducing the interaction energy to very small values. It can be seen however by inverting equation (I) that the neutral count rate for a merged beam experiment is proportional to $L(v_i-v_e)$ where L is the length of the collision region, v_i and v_e are the ion and electron velocities. What this means in physical terms is that as the difference between the ion and electron velocities becomes small the effective collision length becomes much shorter. Hence the ability for the apparatus to manufacture antihydrogen atoms will be correspondingly reduced even though the capture cross section increases. This effect has been demonstrated by Auerbach et al (1977).

There are at least two alternative approaches to antihydrogen production which are being considered. One is to trap antiprotons and positrons together in a hybrid trap and to give them time to interact together. This is probably a better approach although it will require a careful engineering design to ensure that the positrons and antiprotons actually occupy the same regions in space.

The second approach is to collide antiprotons with positronium and to capture positrons via a straight forward charge transfer process.

$$p^- + e^+e^- \rightarrow \bar{H} + e^- \quad - - \qquad (3)$$

In this case the electron carries away the excess energy and so this process probably has a larger cross section.

Positronium can be produced by collisions of positrons with a solid target with production efficiencies as high as 50% (P.J. Schultz, 1987, Private Communication). The lifetime of singlet positronium is 0.125 ns whilst that of the triplet state is 140 ns. The relative populations of these two states is 1:3. This approach certainly deserves further study.

(b) The formation of small molecules

Once antihydrogen has been formed then it is possible to form $\bar{H}_2$ and $\bar{H}_3$ via the reactions.

$$p^- + \bar{H} \rightarrow \bar{H}_2^- + h\nu \quad - - \qquad (4)$$

$$\text{and } \bar{H} + \bar{H}_2^- \rightarrow \bar{H}_3^- + h\nu \quad - - \qquad (5)$$

These molecules might then be destroyed via positron-anti-ion recombination.

$$\text{i.e.} \qquad \bar{H}_2^- + e^+ \rightarrow \bar{H} + \bar{H} \qquad - - \qquad (6)$$

$$\bar{H}_3^- + e^+ \rightarrow \bar{H} + \bar{H} + \bar{H} \quad - - \qquad (7a)$$

149

$$\rightarrow \overline{H}_2 + \overline{H} - - \qquad \text{(7b)}$$

If the neutral products are free to leave the trap then these processes will present a serious loss mechanism if their rate coefficients are large and if positrons are present in the trap.

With regard to the recombination of H_2^+ with electrons it can be seen from Figure 2 that provided the H_2^+ ions are in a vibrational state $v \geq 2$, direct capture into a repulsive doubly excited intermediate state is likely and therefore the process will have a large cross section. Indeed this is the case as has been shown by Peart & Dolder (1973) and by Auerbach et al 1977 (Figure 5). For H_2^+ ($v \leq 1$) however a low energy electron cannot excite the H_2^{**} state directly. It is possible however for the electron to be captured into a vibrationally excited autoionizing rydberg state which can then make a subsequent transition to the repulsive H_2^{**} state through which the recombination will be stabilized, i.e.

$$e + H_2^+ \rightarrow H_2^R \rightarrow H_2^{**} \rightarrow H + H.$$
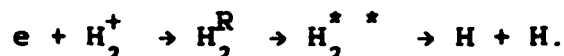
This process has been examined theoretically by Giusti et al (1983), Takagi and Nakamura (1986) and most recently by Hickman (1987).

The results of these calculations are compared in Figures 6. It can be seen that despite the poor overlap with the resonant state, the recombination cross section is still large at low energies for H_2^+ ($v = 0$ and 1). Experimental measurements of vibrationally cold H_2^+ ions are currently in progress using the merged beam technique.

It is more likely however that the $\overline{H}_2^-$ ions formed via reaction 4 will be vibrationally excited. Since $\overline{H}_2^-$ does not have a dipole moment the radiative lifetime of these states is ~10^7 secs. and since there will be no collisional de-excitation of the ions in the trap, the recombination cross sections shown in Figure 5 will be more appropriate.

The recombination of $\overline{H}_2^-$ may not be a serious problem however for the following reason. In order to produce $\overline{H}_2^-$, hydrogen atom trapping techniques, (See Phillips this volume) will be required to keep the H atoms mixed with the $\overline{p}^+$ in the ion trap. The $\overline{H}$ atom products from the recombination of $\overline{H}_2^-$ will also therefore be trapped.

Overall this will slow the rate of formation of $\overline{H}_3^-$ somewhat, but the antimatter itself though chemically changed is not lost.

Once $\overline{H}_3^-$ is formed via reaction 5 then it too can recombine with positrons according to reaction 7. This is particularly interesting since channel 7b produces $\overline{H}_2$. Once molecular $\overline{H}_2$ is available then a wide range of reactions opens up as described by Stwalley (this volume). Mitchell et al (1983) have measured the branching ratio for the dissociative channels following H_2^+ recombination. Figure 7. As can be seen the channel leading to $H_2 + H$ appears to be about a factor of 2 less favoured than that producing $H + H + H$. However, more than 60% of H_2^+ ions used in this study were vibrationally excited.

Unlike H_2^+, the vibrationally excited states of H_3^+ will radiatively decay in a time of a few msec. Oka (1981). For vibrationally cold, H_3^+ ions, it has been predicted (Michels and Hobbs, 1984a) and possibly observed experimentally (Adams et al 1983) that the recombination rate will drop to a very low value. The reason for this can be seen from Figure 8. The resonant state through which the recombination will proceed intersects the H_3^+ curve at an energy about 1eV above the zero point level. This rules out the possibility of direct dissociative recombin- ation from low lying vibrational states. Michels and Hobbs (1984b) have also predicted that indirect recombination should also be very slow. Again this reaction is currently being studied using the merged beam technique.

(c) Small cluster formation

Following the formation of the small hydrogen molecules $\bar{H}_2$ $\bar{H}_2^-$ and $\bar{H}_3^-$, condensation reactions to form higher clusters such as $\bar{H}_5^-$, $\bar{H}_7^-$, $\bar{H}_9^-$, etc. should begin to proceed fairly rapidly. See Stwalley (this volume). Cluster ion recombination processes have been reviewed by Smirnov (1977) and Biondi (1975). The recom- bination rates for these ions are expected to be at least an order of magnitude higher than that for vibrationally excited H_3^+. Biondi's group have used the microwave afterglow technique to study H_3^+ recombination with electrons, Leu et al (1973a), MacDonald et al (1984), and their most recent results are shown in Figure 9.

Rates for higher hydrogen clusters have not been measured. Figure 10 shows the rates for the recombination of water cluster ions $H_3O^+.(H_2O)_n$. It can be seen (Leu et al (1973b)) that the rate rises linearly with increasing n. This is in agreement with theoretical predictions of Bottcher (1978).

(d) Large cluster formation

At some point the complexity of the cluster will be such that the recombination energy can be absorbed in the vibrational- rotational motions of the molecule and so dissociative stabili- zation will no longer dominate. It is not known at what size this will occur.

This is a very important parameter because a large neutral cluster will leave the trap and be lost since the laser frequencies used for trapping the H and H_2 molecules will presumably not trap these clusters. Again this is a fertile area of study.

SUMMARY

In conclusion it is clear that (a) recombination processes are important to bulk antimatter production and (b) a great deal of work must be done before we have a clear understanding of these phenomena.

REFERENCES:

1. Adams, N.G., Smith, D. and Alge, E., J. Chem. Phys. 81, 1778, 1984.
2. Auerbach, D., Cacak, R., Caudano, R., Gaily, T.D., Keyser, C.J., McGowan, J.Wm., Mitchell, J.B.A., Wilk, S.F.J., J. Phys. B., 10, 3797, 1977.
3. Bethe, H. and Salpeter, E: Quantum Mechanics of one- and two-electron systems. In: Handbuch der Physik. Vol. 35, p. 88. Springer; New York, 1957.
4. Biondi, M.A., Comments At. Mol. Phys. 5, 85, 1975.
5. Bottcher, C., J. Phys. B, 11, 3887, 1978.
6. Brouillard, F. and Claeys, W. in Physics of Ion-Ion and Electron-Ion Collisions. NATO ASI, Baddeck, Canada, 1981, (eds. F. Brouillard and J.Wm. McGowan), Plenum Press, N.Y., 1983, p. 415.
7. Dolder, K.T. in Case Studies in Atomic Collision Physics (eds. E. W. McDaniel and M.R.C. McDowell), North-Holland, Amsterdam, 1969. p. 249.
8. Giusti-Suzor, A., Bardsley, J.N. and Derkits, C., Phys. Rev. A. 28, 682, 1983.
9. Hickman, P., J. Phys. B. (submitted for publication).
9a. Keyser, C.J., Froelich, H.R., Mitchell, J.B.A. and McGowan, J. Wm., J. Phys. E. 12, 316, 1979.
10. Leu, M.T., Biondi, M.A. and Johnsen, R., Phys. Rev. A8, 413, 1973a.
11. Leu, M.T., Biondi, M.A. and Johnsen, R., Phys. Rev. A7, 292, 1973b.
12. MacDonald, J.A., Biondi, M.A. and Johnsen, R., Planet Space Sci. 32, 651, 1984.
13. Michels, H.H. and Hobbs, R.H., AIP Conf. Proceed. No. 111, 1984. p. 118.
14. Michels, H.H. and Hobbs, R.H. Ap. J. 286, L27, 1984.
15. Mitchell, J.B.A. and McGowan, J.Wm. in Physics of Ion-Ion and Electron-Ion Collisions. NATO ASI, Baddeck, Canada, 1981, (Eds. F. Brouillard and J.Wm. McGowan), Plenum Press, N.Y., 1983, p.279
16. Mitchell, J. B. A., Forand, J. L., Ng, C. T., Levac, D.P., Mitchell, R.E., Mul, P.M., Claeys, W., Sen, A. and McGowan, J.Wm., Phys. Rev. Lett. 51, 885, 1983.
17. Mitchell, J. B. A., Ng, C. T., Forand, J. L., Levac, D.P., Mitchell, R.E., Sen, A., Miko, D.B. and McGowan, J.Wm., Phys. Rev. Lett. 50, 335, 1983b.
18. Mitchell, J.B.A. in Physics of Electron-Ion and Ion-Ion Collisions NATO ASI, Han-sur-Lesse, Belgium, 1985. Eds. F. Brouillard and P. Defranie, Plenum Press, N.Y., 1987.
19. Nayfeh, M.H. and Clark, C.W.: Atomic Excitation and Recombination in External Fields", Gordon & Breach, New York, 1985.
20. Neumann, R., Poth, H., Winnacker, A., Wolf, A., J. Phys. A., 313, 253, 1983.
21. Oka, T.K., Phil. Trans. R. Soc. A303, 543. 1981.
22. Peart, B. and Dolder, K.T., J. Phys. B., 7, 236, 1974.
23. Smirnov, B.M., Sov. Phys-Usp 20, 119, 1977.
24. Takagi, H. and Nakamura, H., J. Chem. Phys. 84, 2431, 1986.
25. Zipf, E., J. Geophys. Res. 85, 4232, 1980.
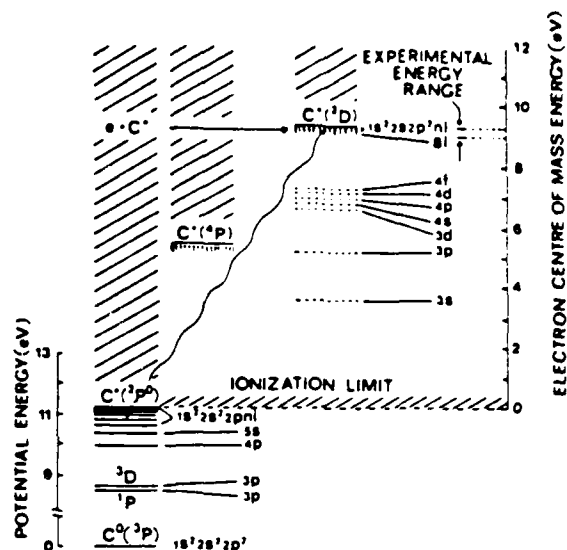
Fig.1. Dielectronic recombination of an atomic ion such as C$^+$ proceeds via the resonant electron capture into a bound, doubly excited state of C^0 lying in the ionization continuum. This state can then decay either via autoionization or via radiation emission. The latter process stabilizes the recombination. Radiative re-combination involves a direct transition from the ionization continuum to a bound state of C^0 via photon emission. (Reprinted from Mitchell et al, 1983b).
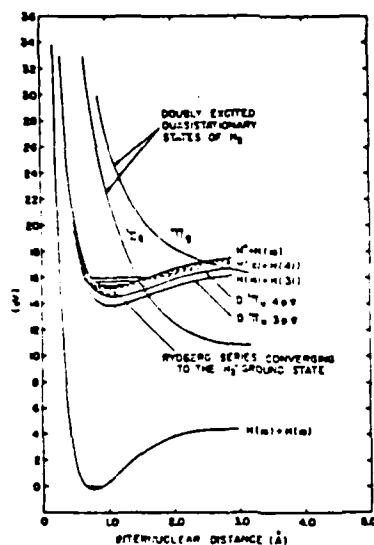
Fig.2. Dissociative recombination of a molecular ion such as H$_2^+$ proceeds either directly via a transition to a doubly excited repulsive state of H$_2$ or indirectly via initial resonant capture into a vibrationally or rotationally excited rydberg state, (dotted curves), which subsequently decay by making a transition to a repulsive state. (Reprinted from Mitchell and McGowan 1983).
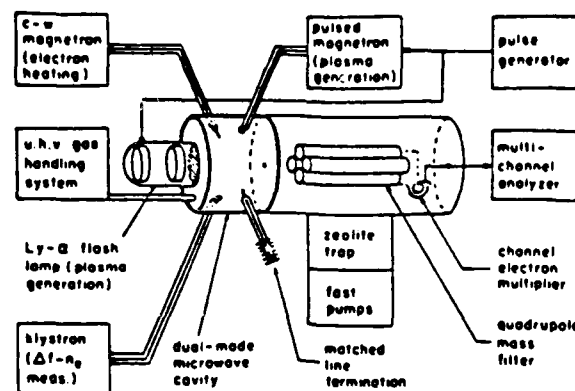
Fig.3. Schematic diagram of Biondi's Microwave Afterglow Apparatus. (Reprinted from Mehr and Biondi, 1969).
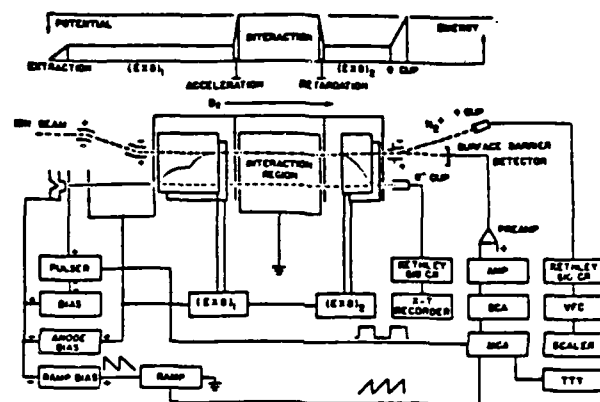
Fig.4. Schematic of the Merged Electron Ion Beam Experiment, MEIBE, described in the text. (Reprinted from Auerbach et al, 1977).
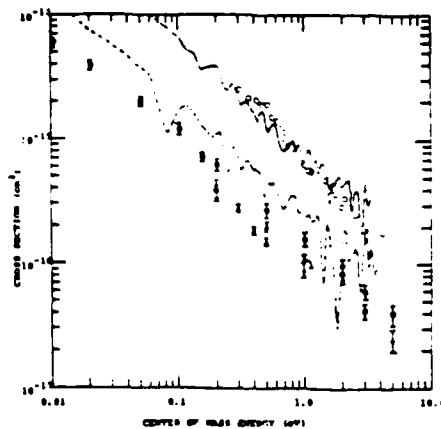
Fig.5. Cross sections for the dissociative recombination of H_2^+ with electrons. O Peart and Dolder, 1974. —Auerbach et al, 1977, (Ions produced using pure H_2 source gas). ——— Auerbach et al, 1977. (Ions produced from a H_2/He mixture). ●, ■ Recent unpublished results obtained using an rf trap ion source to produce the ions. The presence of He in the ion source destroys excited H_2^+ ions with v>2. Complete removal of higher states has not as yet been accomplished in these results. This work is currently in progress.
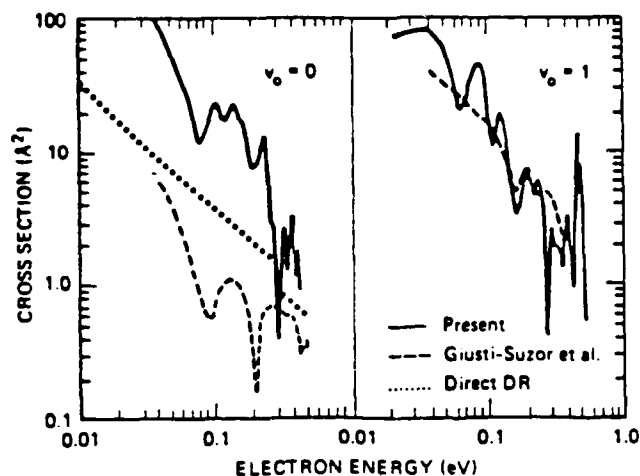
Fig.6. Calculated cross sections for the dissociative
recombination of H_2^+ for v=0 and v=1 states.
—— Hickman, 1987 – – Giusti-Suzor et al, 1983.
These calculations include indirect recombination
via rydberg states. ··· Direct recombination only.
(Reprinted from Hickman, 1987).
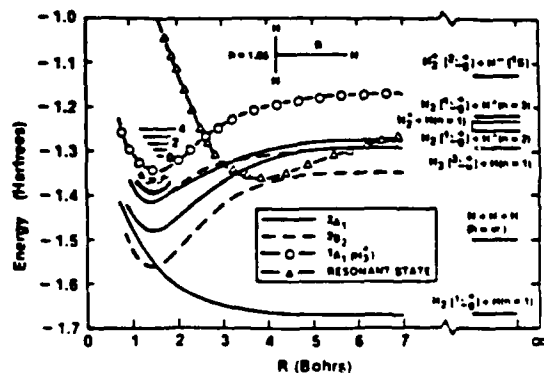
Fig.7. Potential energy curves for H_3^+ and H_3 showing
the intersection with the dissociative curve
responsible for e-H_3^+ recombination.
(Reprinted from Michels and Hobbs,1984)
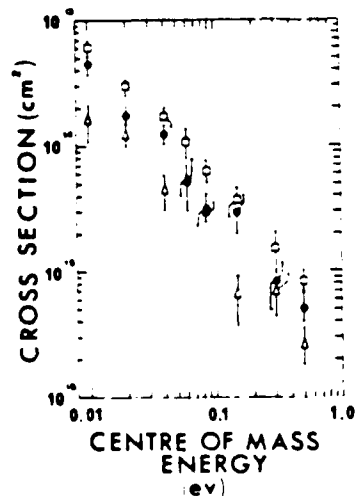
Fig.8. Cross sections for the dissociative recombination
of H_3^+ with electrons leading to the individual
channels, H+H+H (Circles) and H_2+H (Triangles).
Squares show the total recombination cross section.
(Reprinted from Mitchell et al,1983a).

155
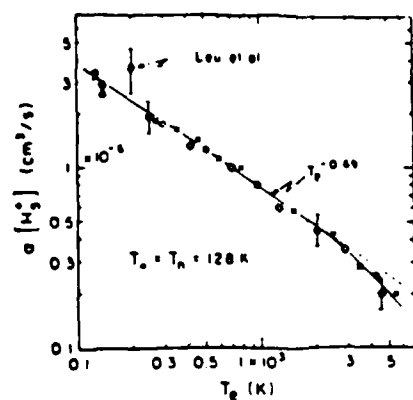
Fig.9. Rate coefficient vs Temperature for e - H_5^+
recombination. (Reprinted from MacDonald
et al, 1984).
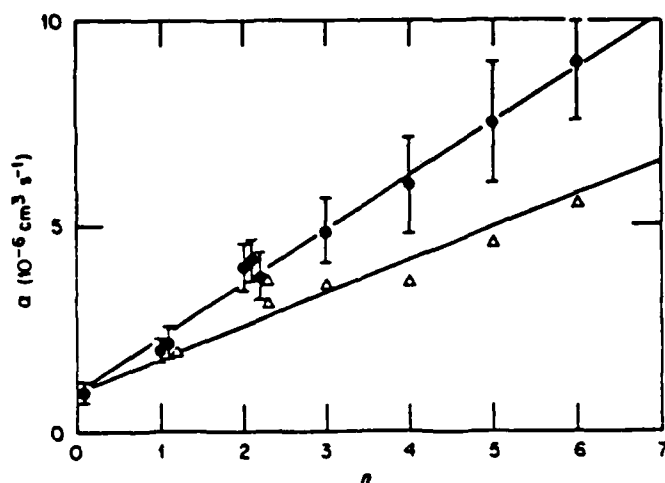
Fig.10. Rate coefficients for the dissociative recombination
of water cluster ions $(H_3O^+).(H_2O)_n$ as a function of
n as measured by Leu et al, (1973). The full circles
are measured data. The open triangles are the same
data normalised to a temperature of 540K assuming
a variation according to $T^{-\frac{1}{2}}$. (Reprinted from
Bottcher, 1978).

156

William D. Phillips, Phillip L. Gould, and Paul D. Lett

Electromagnetic Manipulation of Atomic Hyrdrogen

ELECTROMAGNETIC MANIPULATION OF ATOMIC HYDROGEN

William D. Phillips, Phillip L. Gould*, and Paul D. Lett

Electricity Division, National Bureau of Standards,
Gaithersburg, MD 20899

ABSTRACT

The production of atomic antihydrogen and its condensation into molecules and clusters is likely to involve various techniques of laser cooling, electromagnetic trapping, and other kinds of electromagnetic manipulations. We review some of the possibilities for electromagnetic manipulation as they apply to atomic hydrogen.

INTRODUCTION:

The precise ways in which the electromagnetic manipulation of atomic antihydrogen will be needed in production of bulk antimatter will depend upon the specific schemes which are used for the production of the antihydrogen and the formation of bulk antimatter from it. Nevertheless, we can identify some general concerns which probably apply to any such set of schemes.

Highly effective electromagnetic confinement of the antimatter will be needed because: (1) antimatter is costly to produce and losses must be minimized; (2) rates of formation of atoms, molecules and clusters are likely to be low, so long storage times will be needed to allow such reactions to go to completion; (3) storage in ordinary material containers is out of the question for antimatter.

Electromagnetic cooling will be important because the processes of atom, molecule and cluster formation are enabled or enhanced when the kinetic energy of the reactants is low. Furthermore, low kinetic energy may be a requirement for confinement in some shallow electromagnetic traps.

Electromagnetic transfer of antimatter from one location to another is also likely to be important. For example, the environment in which atoms are formed may not be ideal for the formation of molecules and clusters. Transfer of atoms may involve acceleration, deceleration and focussing of atomic beams.

While the confinement, cooling and manipulation of antiprotons, positrons, antihydrogen, and clusters of antihydrogen may be important, we will consider in this paper the manipulation of neutral atoms. For simplicity, the discussion

will concern hydrogen, with the understanding that the techniques will work as well for antihydrogen.

LASER DECELERATION AND COOLING OF ATOMIC BEAMS

Laser deceleration of an atomic beam was first demonstrated in our laboratory in 1982[2]. Since that time about a half dozen other groups have succeeded in slowing and stopping atomic beams of sodium, cesium and rubidium, and the technique is now well established. The techniques for laser deceleration and the experiments performed through mid-1985 have been reviewed in ref 3. The techniques for deceleration and velocity compression can be used just as effectively to accelerate atoms. A combination of acceleration and deceleration could be used for transferring atoms from one place to another.

Intense radiation at Lyman-α (121.6 nm) is needed to accelerate hydrogen. The technique for generation of the Lyman-α is discussed elsewhere in these proceedings [4]. An important feature of Lyman-α generation is that for high efficiency production, achieved by frequency multiplication from the visible or near-visible, the radiation must be pulsed. Therefore, we have analyzed the acceleration properties of a train of pulses.

Consider a train of identical π-pulses of length τ, separated by T, incident on a beam of two-level atoms. Assuming that the pulse length is short compared to the lifetime, $1/\gamma$, and that it simply inverts the population of the two-level system, we find that the average fraction of time spent in the excited state is

$$f = \frac{\tanh(T\gamma/2)}{T\gamma} .$$

The rate of photon absorption is the same as the rate of emission and is given by $f\gamma$. The acceleration is the absorption rate times the velocity change per photon absorption, $\hbar k/M$ where k is the photon wavevector and M is the atomic mass. Thus the acceleration is given by $a = f\gamma\hbar k/M$. The maximum possible acceleration, obtained when $T \to 0$, is identical to the acceleration with continuous excitation at very high light intensity and is given by $a_{max} = \hbar\gamma k/2M$. For $T\gamma \gg 1$, $a = 2a_{max}/T\gamma$. When $T\gamma = 3$, $a \approx 0.6\ a_{max}$ which is about the acceleration achieved with continuous excitation on resonance with a Rabi frequency equal to the decay rate.

We conclude that even with pulse spacings of several lifetimes, accelerations near the maximum are obtained. Furthermore, it can be shown that when the accelerating pulses are obtained by n^{th} harmonic generation so that the peak

intensity in the harmonic goes as the nth power of the intensity in the fundamental, then for $n > 2$ more acceleration is achieved with a pulse train than with the same average intensity used for continuous harmonic generation.

The cw light intensity required to saturate the strongest transition of the 1S → 2P manifold in hydrogen is about 15 W/cm². Here, saturation means that $\Omega = \gamma$ where Ω is the Rabi frequency in radians/second and γ is the decay rate of the population of the excited state. The ratio of peak power needed for a π pulse of length τ to the cw saturation power is $(\pi/\gamma\tau)^2$, so a 100 ps π-pulse requires about 35 kW/cm² peak power.

When $T\gamma > 3$, each π-pulse transfers about a photon momentum $\hbar k$ to the atom, with a resulting velocity kick of 3.3 m/s to the hydrogen atom. Thermal velocity hydrogen atoms at 300 K, having a velocity of 2.7×10^3 m/s, would require about 850 such kicks to be stopped, and 4.2 K atoms would require 100. For $T\gamma = 3$ the time and distance required to stop the atoms would be about 4.5 µs and 6.1 mm at 300 K and 0.5 µs and 0.08 mm at 4.2 K. To accomplish such deceleration, the frequency of the laser must be chirped to compensate for the changing Doppler shift as the atomic velocity changes. Also, heating due to transverse radiation of photons will occur if additional transverse cooling is not provided. This heating will result in a transverse momentum equivalent to that of the square root of the total number of scattered photons.

COLLIMATION, FOCUSSING, AND OPTICAL MOLASSES

The transverse heating experienced by an atomic beam undergoing laser deceleration or acceleration must be compensated by collimation or focussing in order to prevent loss of atoms as the beam diverges. Such collimation, or transverse cooling, has been demonstrated using both spontaneous [5] and stimulated [5] forces. Since stimulated cooling requires very high saturation parameters, it is likely that application to hydrogen will come first from spontaneous cooling.

In its simplest conception transverse cooling is achieved by crossing the atomic beam at right angles with a pair of counterpropagating lasers beams tuned slighlty below resonance. Atoms with a velocity component transverse to the atomic beam axis will have that component damped by the laser beam directed in the opposing direction, as the Doppler shift of that beam puts it closer to resonance. A similar pair of transverse laser beams orthogonal to the first provides complete transverse cooling.

If in addition the opposed laser beams are diverging as they cross the atomic beam axis, atoms off the axis will feel a restoring force resulting in a focussing of the atomic beam onto

the axis [7]. A combination of focussing and collimation will result in an atomic beam concentrated on the axis, with a transverse energy spread of approximately $\hbar\gamma$. For hydrogen this corresponds to a velocity of about 9 m/s or a temperature of 5 mK.

If the average longitudinal velocity is brought near zero, the transverse cooling can be extended to three dimensions with three pairs of mutually orthogonal laser beams forming what is known as optical molasses[38]. Here, damping of the atomic velocity occurs in all directions, resulting in a small total velocity, as well as a sort of atomic Brownian motion leading to long diffusion times for the atoms compared to the relatively short transit time which would be implied by their ballistic velocities.

ELECTROMAGENTIC TRAPS

The low kinetic energies achievable with laser cooling enable atoms to be confined in electromagnetic traps. Many types of traps for atoms have been proposed, but all of the stable traps are quite shallow, having energy depths on the order of about a kelvin or less (see ref. 3 for a review of types of electromagnetic traps.)

The first electromagnetic trapping of neutral atoms was accomplished using a magnetostatic trap for sodium atoms [9]. A magnetostatic trap works for atoms having a permanent magnetic dipole moment, exerting forces on the atom by virtue of an inhomogeneous magnetic field. Since a configuration of magnetic field with an absolute maximum in field magnitude is not possible [10], such traps must have absolute minima and therefore can trap only those states of an atom whose energy increases in increasing magnetic field.

The depth of a magnetostatic trap is the difference in interaction energy of the magnetic moment with the magnetic field from the lowest to the highest field in the trap. For a magnetic moment of a Bohr magneton, as in the ground state of hydrogen, the depth of a 5 T trap would be about 3.5 K. The first magnetic trap for Na was only 17 mK deep and was loaded with laser cooled atoms [9].

Since a magnetostatic trap can only hold states whose energy increases with field, one must avoid any transitions to non-trapping states. For slowly moving atoms, non adiabatic or Majorana transitions are rare and will not be much of a problem [9], especially if regions of low field are avoided. Laser irradiation, however, may change the atomic state, making laser cooling more difficult. Some of these problems can be avoided by using magnetodynamic [11] traps which work in a manner analogous to rf traps for ions. Such traps work independently of the

direction of the magnetic moment of the atom, so all states are trapped, but the well depth is reduced compared to a static trap with the same field.

The only other form of neutral trap yet demonstrated is the laser dipole trap. This trap works by virtue of the energy of interaction (ac Stark shift) between the atom and an inhomogeneous light field. The first such trap [12] had a depth of 5 mK, a volume of 10^{-7} cm^3, and was loaded with sodium atoms in optical molasses. Other kinds of laser traps have been proposed[13] which rely on the ordinary radiation pressure force (scattering force) rather than the dipole force. Such traps may be deeper and larger than dipole traps and require less laser power.

Magnetic and laser traps each have their own advantages and disadvantages for storing antimatter. Magnetic traps may be more stable because, apart from collisions, the stored atoms neither gain nor lose energy. Laser traps constantly heat the atoms, but at the same time can cool them, establishing an equilibrium temperature. On the other hand, laser cooling is difficult in magnetic traps. Magnetic traps may be easily made in quite large volumes, while laser traps will be smaller. Laser traps are easier to load because of the damping provided by laser cooling.

CONCLUSIONS

The tools for electromagnetic manipulation of atoms are well established and based soundly on experiment. Application to hydrogen and antihydrogen requires the extension of presently available laser manipulation techniques to the use of trains of Lyman-α pulses.

ACKNOWLEDGEMENTS

REFERENCES

* NRC Postdoctoral Fellow
[1] J. Weiner, these proceedings.
[2] W. Phillips and H. Metcalf, Phys. Rev. Lett., 48, 596 (1982).
[3] W. Phillips, J. Prodan, and H. Metcalf, J. Opt. Soc. Am. B2, 1751 (1985).

[4] T. McIlrath, these proceedings.

[5] V.I. Balykin, V. S. Letokhov, and A. I. Sidorov, JETP Lett. 40, 1026 (1984).

[6] A. Aspect, et al., Phys. Rev. Lett., 57, 1688 (1986).

[7] V. I. Balykin, et al., JETP Lett., 43, 217 (1986).

[8] S. Chu, et al., Phys. Rev. Lett. 55, 48 (1985).

[9] A. Migdall et al., Phys. Rev. Lett. 54, 2596 (1985).

[10] W. Wing, Prog. Quantum Electron. 8, 203 (1984).

[11] R. Lovelace et al., Nature 318, 30 (1985).

[12] S. Chu et al., Phys. Rev. Lett., 57, 314 (1986).

[13] D. Pritchard et al., Phys. Rev. Lett. 57, 310 (1986).

G. Gabrielse

First Capture of Antiprotons in an Ion Trap and the
Possibility of Antihydrogen

First Capture of Antiprotons in an Ion Trap
and the
Possibility of Antihydrogen[*]

G. Gabrielse

Department of Physics, FM-15
University of Washington
Seattle, Washington 98195

Abstract

The motivations and prospects for a measurement of the inertial mass of the antiproton are discussed. Prospects for such a measurement are now excellent since our TRAP Collaboration actually captured antiprotons in a Penning trap only several months ago. An overview of ways to cool particles within the trap is provided and brief speculations upon the possibility of producing antihydrogen in a trap are included.

A. The Antiproton Mass

Measurements of the antiproton mass[1,2,3,4] are represented in Fig. 1. All of these are deduced from measurements of the energy of x-rays radiated from highly excited exotic atoms. For example. if an antiproton is captured in a Pb atom. it can make radiative transitions from its $n = 20$ to $n = 19$ state. The antiproton is still well outside the nucleus in this case, so that nuclear effects can be neglected. The measured transition energy is essentially proportional to the reduced mass of the nucleus and hence the antiproton mass can be deduced by comparing the measured values with theoretical values. corrected for QED effects. The most accurate quoted uncertainty is 5×10^{-5} and is consistent with the much more accurately known proton mass. indicated by the dashed line. It looks like it would be difficult to extend the accuracy realized with the exotic atom method. It might be possible. however, that proton and antiproton masses could be compared directly in a storage ring. from the spatial separation of counter propagating beams of protons and antiprotons at comparable or somewhat improved accuracies.[5]

Based upon precisions obtained with trapped electrons, positrons and protons. it seems very likely that the measurement uncertainty in the ratio of antiproton to proton masses could be reduced by more than 4 orders of magnitude. to order 10^{-9} or better. A major question. however. is whether or not one should bother. The widely accepted assumption of CPT invariance would insure that antiproton and proton masses are equal. Fig. 2 shows the current status of experimental tests of CPT invariance. taken from the Particle Data Group compilation[6] with several updates. Since CPT invariance implies that a particle and antiparticle have the same magnetic moment (with opposite sign). the same inertial mass and the same mean life. the tests are so grouped. The fractional accuracy is plotted. and baryons, mesons and leptons are distinguished. The neutral kaon system provides a test of CPT invariance of striking precision. Equally striking. however. is that only 3 other tests exceed 1 part per million in accuracy. and these involve leptons only. In fact. there is not even a single precision test of CPT invariance with baryons. The widespread faith in CPT invariance is clearly based upon the success of field theories in general and not upon a dearth of precision measurements.

We note here that it is even conceivable that proton and antiproton masses could be different without a violation of CPT invariance. Precisely stated. CPT invariance relates the mass of a proton in a matter universe to an antiproton in an antimatter universe. A long range coupling to baryon number would not affect the kaon system

[1] A. Bamberger. et. al.. Phys. Lett. **33B**. 233 (1970).

[2] Hu. et.al.. Nucl. Phys. **A 254**. 403 (1975).

[3] P.L. Roberson. et. al.. Phys. Rev. C **16**. 1945 (1977).

[4] B.L. Roberts. Phys. Rev. D. **17**. 358 (1978).

[5] S. van der Meer. private communication.

[6] Particle Data Group. Rev. Mod. Phys. **56**. S1 (1984).

but could shift differently the proton and antiproton masses, given the preponderance of baryons in our apparatus and universe.

The scarcity of precise tests of CPT invariance makes the case for a precise comparison of proton and antiproton masses seem to be very strong to me, especially since no precise test at all involves baryons. Such a measurement also satisfies several additional criteria.

1. A big improvement in accuracy is involved, somewhere between four and five orders of magnitude.

2. A simple, basic system is involved.

3. The technique used will be convincing if the masses are found to differ.

4. The measurement will involve a reasonable effort.

5. It will be fun.

The last two criteria are more subjective than the others, but important nonetheless.

B. First Slowing and Capture of Antiprotons in an Ion Trap

As you well know, antiprotons are created at energies of several GeV. Precision experiments in Penning traps take place at millielectron volts (meV). An experimental difficulty, then, is to reduce the antiprotons kinetic energy by approximately 12 orders of magnitude, as illustrated in Fig. 3. The first slowing, from GeV energies down to MeV energies takes place within LEAR. The unique capabilities of this machine are well known here, so I will not discuss them further.

I am delighted to report that in the last several months the TRAP Collaboration (PS196) has taken 21.3 MeV antiprotons from LEAR (200 MeV/c) and slowed them down to below 3 keV. At this energy they were caught in the small volume of an ion trap and help up to ten minutes. Members of the TRAP Collaboration are listed in Fig. 4. I should point out that this effort succeeded despite incredible time pressure. The capture of antiprotons, for example, occured during a single 24 hour period.

The experiments went in two stages. In May, we used a simple time-of-flight apparatus to measure the energy distribution of antiprotons emerging from a thick degrader. Since we have not yet finished our analysis, I present in Fig. 5 only a preliminary result taken on line during the May run. The upper graph shows transmitted antiproton intensity versus thickness of the degrader. As degrader thickness is increased, the number of antiprotons drops as more of them are stopped in the degrader. The degrader thickness at the half intensity point is very close to the proton range which is compiled in standard tables. All energies of transmitted antiprotons are included and most of these antiprotons have energies above 3 keV which is the highest energy we could trap.

The lower curve in Fig. 5 is more crucial. Here the number of antiprotons which emerge from the degrader with low kinetic energies (along the beam axis) between 2

and 8 keV is plotted versus degrader thickness. The low energy flux is clearly peaked at the half intensity point of the upper curve. Approximately 1 in 10^4 of the incident antiprotons emerges from the degrader with below 3 keV. These are the particles available for trapping.

In July we returned to LEAR for a 24 hour attempt to actually catch antiprotons in the small volume of an ion trap. An account of our success has just been published,[7] so I will only briefly summarize. The trap is very simple as is indicated in Fig. 6. The slowest antiprotons leaving the thick degrader are confined in 2 dimensions to field lines of the 6T superconducting magnet (dotted lines in Fig. 6) and are so guided through the series of 3 trap electrodes. As the antiprotons enter the trap, the first ring-shaped trap electrode (the entrance endcap) and the main ring electrode are both grounded. The third cylindrical electrode (exit endcap) is at -3 kV so that negative particles with energy less than 3 keV turn around on their magnetic field lines and head back towards the entrance of the trap. Approximately 300 ns later, before the antiprotons can escape through the entrance, the potential of the entrance endcap is suddenly lowered to -3kV, catching them within the trap. The potential is switched in 15 ns with a kryton circuit developed for this purpose and is applied to the trap electrodes via an unterminated coaxial transmission line.[8] The 3 keV potentials and 15 ns rise times contrast sharply with the several volt potentials and the 100 ns switching times used recently to capture Kr^+ in a few eV well.[9]

After antiprotons are held in the trap between 1 ms and 10 minutes, the potential of the exit endcap is switched from -3 kv to 0 volts in 15 ns, releasing the antiprotons from the trap. The antiprotons leave the trap along respective magnetic field lines and annihilate at a beam stop well beyond the trap. The high energy charged pions which are released are detected in a 1 cm thick cylindrical scintillator outside the vacuum system. A multiscaler started when the potential is switched records the number of detected annihilations over the next $6\mu s$ in time bins of $0.4\mu s$. A second multiscaler records the pion counts over a wider time range with less resolution to monitor backgrounds. This time-of-flight method is similar to but less refined than that used on very low energy electrons and protons ejected from a Penning trap with a 6 volt potential well.[10]

Fig. 7 shows a time-of-flight spectrum for antiprotons kept in the trap for 100s. The spectrum includes 31 distinctly counted annihilations which corresponds to 41 trapped particles when the detector efficiency is included. We carefully checked that these counts are not electronic artifacts. When the high voltage on the exit endcap is switched to release antiprotons from the trap, a single count (occasionally two) is observed in the multichannel scalers. We take this to be time $t = 0$ and always remove

[7] G. Gabrielse, X. Fei, K. Helmerson, S.L. Rolston, R. Tjoelker, T.A. Trainor, H. Kalinowsky, J. Haas, W. Kells, Phys. Rev. Lett. 57, 2504 (1986)

[8] X.Fei, R.Davisson and G.Gabrielse, Rev. of Sci. Inst. (in press).

[9] Schnatz, et.al., Nucl. Inst. and Meth. (in press)

[10] G. Graff, H. Kalinowsky and J. Traut, Z. Phys. 297, 35 (1980)

a single count from the measured spectra. Otherwise, the background is completely negligible. When the potential of the entrance endcap is switched on just 50 ns before 3 keV antiprotons arrive in the trap, when the magnetic field is off, or when the -3 keV on one of the electrodes is adiabatically turned off and then back on during a 100s trapping time to release trapped antiprotons, no counts are observed.

The potential on the exit endcap is lowered quickly compared to the transit time of particles in the trap in order to maximize the detection efficiency. Even a small number of trapped particles can be observed above possible background rates in the $6\mu s$ window. For trapping times shorter than 100s, however, we actually released so many trapped antiprotons that our detection channel is severely saturated. For a 1 ms trapping time, we conservatively establish that more than 300 antiprotons are trapped out of a burst of 10^8, which corresponds to trapping 3×10^{-6} of the antiprotons incident at 21.3 MeV and 3% of the antiprotons slowed below 3 keV in the degrader. We observe that 5 particles remain in the trap after 10 minutes. This is actually based upon only two trials (since we were reluctant to use up our short time at LEAR holding antiprotons for long times), but both of these trials used a burst of antiprotons from LEAR of comparable intensity to that used for the 41 trapped particles of the 100s spectra in Fig. 7. If a simple exponential decay describes the number of particles trapped between 100 a and 10 minutes, the decay time is 240 seconds. An extrapolation back to the loading time $t = 0$, however, would then indicate that only 62 particles are initially trapped. We clearly observe many more for a trapping time of 1 ms, suggesting that antiprotons are lost more rapidly at earlier times.

A key point here is that the rate of cooling and annihilation via collisions with background gas will decrease with decreasing pressure. The background pressure can be made lower by orders of magnitude compared to the present vacuum by cooling a completely sealed vacuum enclosure to 4.2K. We thus expect a very significant increase in achievable trapping times.

C. Cooling Particles Within the Trap

If, as we suspect, we will soon be able to hold antiprotons in a trap for times much longer than 10 minutes, we feel rather confident that we will be able to cool them from approximately 1 keV down to of order meV. When the background pressure is greatly reduced, electron cooling seems to be the most promising method of cooling trapped antiprotons from keV to eV energies. In fact, electrons are probably already confined in the present trap, under the assumption that each antiproton emerging from the degrader liberates several electrons and many of them are trapped. A 1 keV antiproton traveling through a cloud of 1 eV electrons with density of $10^8/cm^3$ loses energy exponentially with a time constant of 1 s or less, which is much shorter than the time antiprotons were held. Although such a calculation of electron cooling rates

within a trap was only done recently,[11] and the possibility of spatial separation of trapped electrons and antiprotons must be investigated,[12] such cooling is quite well understood both experimentally and theoretically insofar as cold electron beams have often been used to cool various particle beams traveling along the same axis with the same velocity.[13]

We presently prefer electron cooling as a first step because no resonant frequencies are involved and it thus promises to be the quickest cooling scheme. Once the amplitude of the oscillation along the magnetic field line is sufficiently reduced, the oscillation frequency of this oscillation will become increasingly independent of amplitude. It then should be possible to couple to a resistor such as that used to detect induced currents using a tuned circuit to cancel out the trap capacitance on resonance. The induced current dissipates power in the resistor. This removes energy from the axial oscillation, cooling the axial motion to the temperature of the resistor. Resistor cooling is a well established technique which has been used for many years.

D. Antihydrogen Production

While I would prefer to wait until we have completed a more detailed study which is under way, I think it would be unfortunate if some thoughts about antihydrogen production in traps were not part of this discussion. If one could make antihydrogen in a particle trap, this would impact LEAR itself very much less than the merged beams approach. Many years ago, we mentioned the possibility of putting positrons and antiprotons into a radio frequency trap at the same time in order to make antihydrogen.[14] At that time, there was no promising proposal for getting antiprotons in a trap, but this of course is no longer the case. More recently, we mentioned the possibility which we have been studying for some time, of using a nested pair of Penning traps to simultaneously capture positrons and antiprotons.[15]

To provide a concrete starting estimate, consider a cloud of positrons of volume density n in thermal equilibrium at 4.2 K. For simplicity, we will assume the positrons are each moving with the average speed $\bar{v} = 10^6 cm/sec$. If we now simultaneously fill the same volume with N antiprotons, with energies below 1 ev, the relative velocity

[11] W. Kells, G. Gabrielse and K. Helmerson, Fermilab-Conf.-84/68 E (1984).

[12] D.J. Larson, J.C. Berquist, J.J. Bollinger, W.M. Itano and D.J. Wineland, Phys. Rev. Lett. **57** 70 (1986)

[13] F.T. Cole and E.E. Mills, Ann. Rev. Nucl. Sci. **31**. 295 (1981)

[14] H. Dehmelt, R.S. Van Dyck, Jr., P.B. Schwinberg and G. Gabrielse, Bull. Am. Phys. Soc. **24**. 757 (1979).

[15] G.Gabrielse, K. Helmerson, R. Tjoelker, X. Fei, T. Trainor, W. Kells, H. Kalinowsky, in Proceedings of the First Workshop on Antimatter Physics at Low Energy, edited by B.E. Bonner and L.S. Pinsky, April 1986, Fermilab.

between antiprotons and positrons is the positron velocity $\bar{v}$. since antiprotons are much heavier. The antiproton production rate is thus approximately given by

$$R \approx N n \sigma \bar{v}. \tag{1}$$

The cross section for radiative recombination to any antihydrogen bound state is well known[16] so that

$$\sigma \approx \frac{1}{10}\sigma_B \approx 10^{-17} cm^2 \tag{2}$$

for $\bar{v} = 10^6 cm/sec$. where σ_B is the Bohr cross section. Suppose we take $N = 10^4$ which is larger than we have already achieved by a factor of 10 but looks to be a realistic expectation. We further assume that $n = 10^8$ positrons/cm^3 can be placed in a trap at in thermal equilibrium at 4.2K. Together this gives a production rate

$$R \approx 10/sec. \tag{3}$$

This rate could possibly be made larger by stimulation with a laser as suggested for a merged beams experiment,[17] perhaps by a factor of 10, depending upon how small the interaction region can be made. Our favorite scheme is to stimulate to $n = 3$ or higher. perhaps even with a diode laser. However, the effective rate is actually lower owing to the duty cycle involved in loading a trap with antiprotons from LEAR.

Such low rates might be sufficient to observe antihydrogen for the first time. When antihydrogen is formed in an ion trap. the neutral atoms will no longer be confined and will thus quickly strike the trap electrodes. Resulting annihilations of the positron and antiprotons could be monitored. However. it is very clear that the very low rate will make further experiments with antihydrogen to be very different than experiments with copious amounts of hydrogen. and much more difficult.

For me. the most attractive way around this difficulty would be to capture the antihydrogen in a neutral particle trap such as has been used for neutrons[18] and neutral atoms[19,20] The objective would be to then study the properties of a small number of atoms confined in the neutral trap for a long time. To capture an antihydrogen atom directly into a neutral trap would require a neutral trapping well depth of order 4.2 K or 3×10^{-4} eV This unfortunately is many orders of magnitude deeper than what is being realized. Thus. laser cooling and optical molasses techniques would be required. with Ly α lasers. The technologies which would need to converge in order to permit

[16] H. Bethe. E. Saltpeter. *Quantum Mechanics of One and Two Electron Atoms.* in Handbuch fur Physik. **35**. 88 (Springer. Springer. 1957).

[17] R. Neumann. H. Poth. A. Winnacker. A. Wolf. Z. Phys.**313**. 253 (1983).

[18] K.J. Kugler. W Paul and U. Trinks. Phys. Lett. **72B**. 422 (1978).

[19] A.L. Migdall. J V. Prodan. W.D. Phillips. T.H. Bergeman. H.J. Metcalf. Phys. Rev. Lett. **54**. 2596 (1985).

[20] S. Chu. J.E. Bjorkholm. A. Ashkin and A. Cable. Phys. Rev. Lett. **57**. 314 (1986).

the study of antihydrogen in a neutral trap is rather imposing, but may be possible. It would also be necessary to minimize the rather strong interactions of the atom and the neutral trap in order cto meaningfully study the properties of antihydrogen.

Since I am speculating in this section, let me make several comments relevant to the discussions about gravity which are part of this school. I find the possibility of measuring the acceleration due to gravity for a antiproton to be very appealing, if it can be done. Another group is presently endeavoring to demonstrate that such a measurement can be done with charged particles.[21] We are investigating a different approach, to see whether such a measurement could possibly be done instead with neutral antihydrogen, in order to reduce the extreme sensitivity to stray charges.

Finally, to avoid the small cross sections involved in radiative capture. it has been proposed to send positronium into a cloud of trapped antiprotons.[22] The cross section is several orders of magnitude larger, but because the positronium can not be confined in the same volume as the antiprotons for a long time, the rate seems to be lower than considered here. There are nonetheless attractive features to this approach and we are studying it further.

[21] Beverini. et. al. CERN/PSCC/86-2PSCC 'P94. 1986.

[22] B.I. Deutch. A.S. Jensen. A. Miranda and G.C. Oades. in Proceedings of the First Workshop on Antimatter Physics at Low Energy. edited by B.E. Bonner and L.S. Pinsky. April 1986. Fermilab.
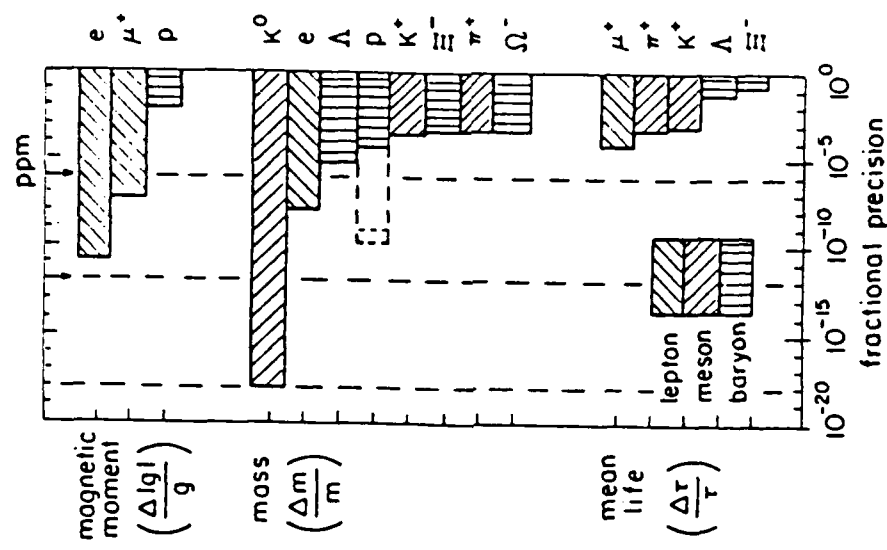
Fig. 2. Fractional accuracy in experimental tests of CPT invariance.
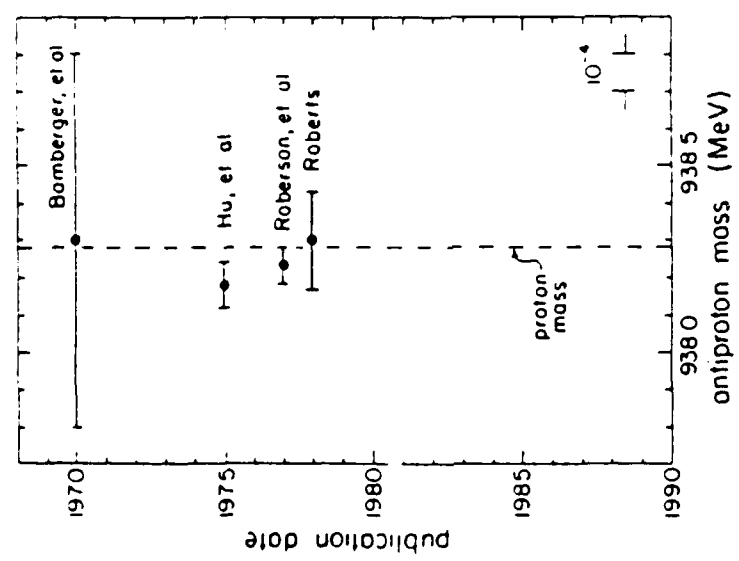
Fig. 1. Antiproton mass measurements.

175

TRapped AntiProton Collaboration

(TRAP Collaboration)

University of Washington

G. Gabrielse

X. Fei

K. Helmerson

S.L. Rolston

R. Tjoelker

T.A. Trainor

University of Mainz

H. Kalinowsky

J. Haas

Fermi National Accelerator Laboratory

W. Kells

Fig. 4. TRAP collaboration.
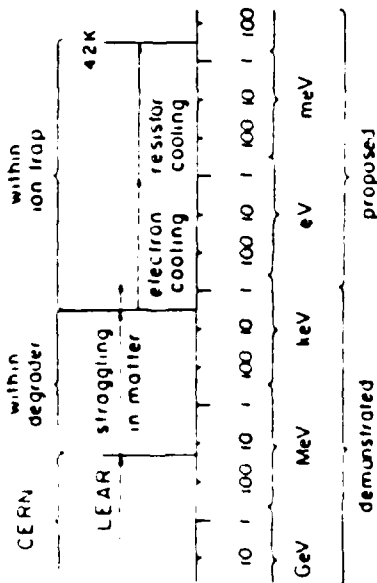
Fig. 3 Antiprotons produced at several GeV energies must be slowed to below a meV for a high precision mass measurement.

Fig. 7. Time of flight spectra, started when antiprotons were released from the trap.

Fig. 6. Ion trap in which first capture of antiprotons took place.

Fig. 5. Transmission of antiprotons through material versus effective thickness of Be.

D. J. Wineland

Ion Traps for Large Storage Capacity

ION TRAPS FOR LARGE STORAGE CAPACITY*

D. J. Wineland
Time and Frequency Division
National Bureau of Standards
Boulder, Colorado 80303

ABSTRACT

Ion storage in Penning-type or rf (Paul)-type traps is discussed.
Emphasis is given to low-energy, long-term confinement of high densities and
large numbers of ions. Maximum densities and numbers are estimated using a
low-temperature, static model of the ion plasmas in the traps. Destabilizing
mechanisms are briefly discussed.

INTRODUCTION

The following notes are concerned with the storage of large densities and
numbers of charged particles or ions in electromagnetic traps. Certainly,
this is a small part of the problem concerned with the accumulation, storage,
and manipulation of antimatter. However, this particular problem appears to
be interesting by itself and may have interesting applications elsewhere.[1-3]
Devices such as tokamaks and tandem-mirror machines for fusion plasmas are not
discussed because we concentrate on long-term, low-energy confinement which is
desirable for antimatter storage. For brevity, only Paul (rf) and Penning-
type traps[4,5] are discussed. Maximum densities and maximum numbers of ions
for one or a mixture of species with different charge to mass ratio are
investigated.

GENERAL CONSIDERATIONS

We will assume that thermal equilibrium of the stored ion sample has been
achieved. This condition may not always be achieved or desirable. For
example, antihydrogen might best be made by passing antiprotons through
positrons without thermal equilibrium between these two species being
achieved. For long term storage, however, thermal equilibrium appears likely.

If we assume that the ion trap has symmetry about the z axis, the thermal
equilibrium distribution function for the ith species can be written[5-9]

$$f_i = n_i \left(\frac{m_i}{2\pi k_B T}\right)^{3/2} \exp[-(H_i - \omega \ell_{z i})/k_B T]. \tag{1}$$

m_i is the ion mass, k_B is Boltzmann's constant, T is the ion temperature, and ω and n_i are constants (determined below). If a magnetic field is superimposed along the z axis ($\vec{B} = B\hat{z}$), then

$$H_i = m_i v_i^2/2 + q_i \phi(x) \tag{2}$$

is the ion energy and

$$\ell_{zi} = m_i v_{\theta i} r_i + q_i A_{\theta}(\vec{x}) r_i /c \tag{3}$$

is the ion canonical angular momentum. q_i and $\vec{v}_i$ are the ion charge and velocity, and $v_i = |\vec{v}_i|$. $v_{\theta i}$ and $A_{\theta i}$ are the θ components of the velocity and the vector potential, and r_i is the radial coordinate of the ion in cylindrical coordinates. $\phi = \phi_I + \phi_T + \phi_{ind}$ is the total potential, which is written as the sum of the potential that is due to ion space charge ϕ_I, the applied trap potential ϕ_T, and the potential, ϕ_{ind}, that is due to the induced charges on the trap electrodes.[9] We choose the symmetric gauge where $\vec{A}(\vec{x}) = \vec{B} \times \vec{x}/2$, so that $A_{\theta i} = Br_i/2$. We can therefore write the distribution function as

$$f_i(\vec{x},\vec{v}) = n_i(\vec{x}) \left(\frac{m_i}{2\pi k_B T}\right)^{3/2} \exp[-\tfrac{1}{2}m_i(\vec{v}_i - \omega r_i \hat{\theta})^2/k_B T], \tag{4}$$

where $n_i(\vec{x})$ is the ion density given by

$$n_i(\vec{x}) = n_i \exp\{-[q_i \phi(r,z) + \tfrac{1}{2}m_i \omega(\Omega_{ci} - \omega)r_i^2]/k_B T\}. \tag{5}$$

We assume that the trap potential is adjusted to make $\phi = 0$ at the origin, in which case n_i is the ion density at the center of the trap for a single ion species. From Eq. 4, we see that the ion cloud, or non-neutral ion plasma, rotates at frequency ω. $|\Omega_{ci}| = |q_i|B/m_i c$ is the cyclotron frequency. The signs of ω and Ω_{ci} indicate the sense of circulation where we use the right-hand rule. For example, Ω_{ci} is negative for positive ions ($q_i > 0$) and is positive for $q_i < 0$.

In the limit $T \to 0$, we must have $q_i \phi - m_i \omega(\omega - \Omega_{ci})r_i^2/2 \to 0$ for f_i to be well behaved. This condition and Poisson's equation imply that the charge density, ρ, at the position of the ions be given by

$$\rho = -\rho_i' + m_i \omega(\Omega_{ci} - \omega)/(2\pi q_i), \tag{6}$$

where ρ_i' is a fictitious charge density arising for rf traps since the pseudopotential does not satisfy Poisson's equation[9] (see below). By low temperature, we mean that the Debye length, λ_D, for the plasma given by[5-9]

$$\lambda_D^2 = k_B T/(4\pi n_i q_i^2), \tag{7}$$

is short compared to the plasma dimensions. From Eq. 7, we can write

$$\lambda_D \simeq 6.9(T/n_i)^{\frac{1}{2}}/Z \text{ cm},\tag{8}$$

where T is expressed in kelvin, n_i is expressed in cm^{-3}, and Z is the ion charge in units of the proton charge. For $T = 4$ K, $Z = 1$, and $n_i = 10^8/cm^3$, $\lambda_D = 14$ μm. Therefore, for the low temperatures desired for long term storage, the $T\rightarrow 0$ limit will usually be valid.

PENNING TYPE TRAPS

By Penning-type trap, we will mean that the trap is formed by a static magnetic field $\vec{B} = B\hat{z}$ and an axially symmetric electric trap potential, ϕ_T, of the form (in spherical coordinates)

$$\phi_T = \sum_k C_k r^k P_k(\cos\theta),\tag{9}$$

where C_k are constants and P_k is a Legendre polynomial of order k. Axial symmetry is particularly important for the Penning trap. If the trap is not axially symmetric, angular momentum can be coupled into the ions and they will diffuse out of the trap. If the trap is axially symmetric, angular momentum is a constant of the motion and stable ion clouds are maintained.[10] For spectroscopy,[4,5] particularly mass spectroscopy,[5,11,12] we desire $\phi_T \propto r^2 P_2(\cos\theta)$ as indicated in Fig. 1. This is because the ion motions (neglecting relativistic effects) will be harmonic. A fourth order trap where $\phi_T \propto r^4 P_4(\cos\theta)$ would look something like that in Fig. 2.
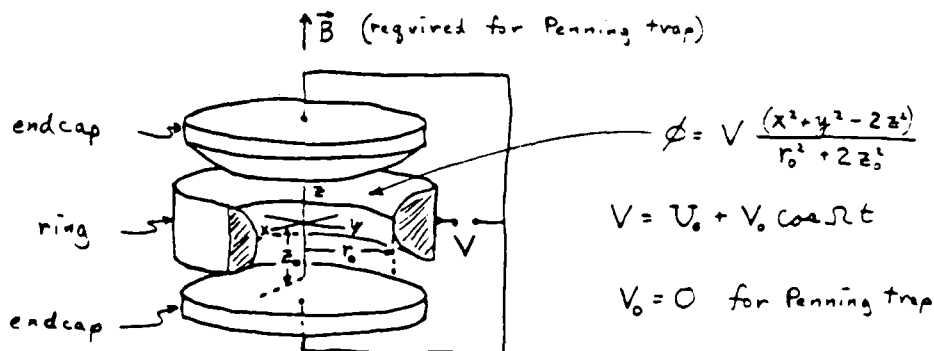
Fig. 1. Electrode configuration for the quadrupole rf (Paul) or Penning trap. Inner surfaces of electrodes are assumed to be equipotentials of ϕ, and the effect of truncating the electrodes is neglected. r_0 is the inner radius of the ring electrode and $2z_0$ is the endcap to endcap spacing.
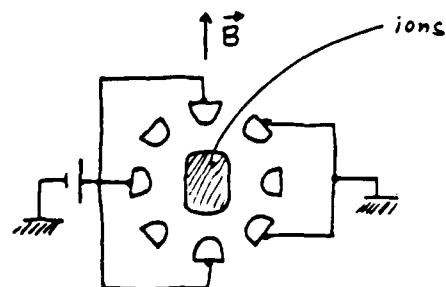
Fig. 2. Sketch of fourth order Penning-type trap for positive ions. The view shown is a cross section in the y-z plane.

An experimentally convenient geometry[1] might be a "cylinder trap" as shown in Fig. 3.
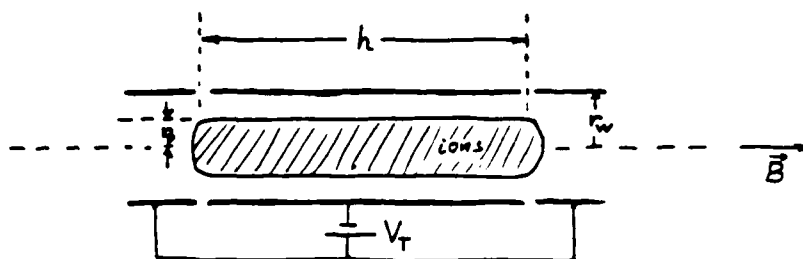
Fig. 3. Sketch of cylinder Penning-type trap for positive ions.

With $\rho_i'=0$, Eq. 6 can be written

$$n_i = m_i \omega (\Omega_{ci} - \omega)/(2\pi q_i^2).$$ (10)

Therefore, if we assume axial symmetry, n_i is independent of ϕ_i. Because of this, we will assume throughout that we are using the experimentally convenient geometry of the cylinder trap (Fig. 3). n_i is maximum for $\omega = \Omega_{ci}/2$, which is called the Brillouin limit.[6] ω may be determined by initial loading conditions or may be altered as discussed below. If we assume a single ion species and drop the indices,

$$n(\max) = B^2/(8\pi mc^2) = 2.7 \times 10^9 \, B(T)^2/M,$$ (11)

where $B(T)$ is the magnetic field in tesla and M is the ion mass in u (atomic

mass units). $n(max)$ is independent of Z. From Fig. 3 and Eq. 11, the maximum number of ions, $N(max)$, is given by

$$N(max) \simeq 8.4 \times 10^9 \ r_p^2 h B(T)^2/M, \tag{12}$$

where r_p and h are the plasma radius and height in cm, respectively. The potential, ϕ_c, at the center of the plasma (assuming the central cylinder is grounded as in Fig. 3) is easily calculated to be[1]

$$\phi_c(V) \simeq 1.4 \times 10^{-7} \ NZ(1+2\ell n(r_w/r_p))/h, \tag{13}$$

where ϕ_c is given in volts. The magnitude of V_T must be higher than the magnitude of this potential to confine ions along the z axis. If we eliminate N from Eqs. 12 and 13, we obtain

$$r_p^2 = 8.3 \times 10^{-4} M\phi_c/(B(T)^2 Z(1+2\ell n r_w/r_p)). \tag{14}$$

For $\phi_c = 30$ kV, $B = 10T$, $r_p/r_w = 0.5$, and $Z = 1$, we find $r_p^2 \simeq M/10$.

A few examples of $n(max)$ and $N(max)$ for these values of ϕ_c, B, and r_p/r_w are illustrated in table I. From the above considerations and table I, large mass storage would favor ions with large values of M.

Table I. Example parameters for a cylinder Penning-type trap. Fig. 3 applies with $V_T > \phi_c = 30$ kV, $B = 10$ T, $r_p/r_w = 0.5$, and $Z = 1$.

M(u)	h(cm)	r_p(cm)	$n(max)(cm^{-3})$	N
1	500	0.32	2.7×10^{11}	$4.3\times10^{13} \simeq 0.7\times10^{-7}$mg
1000	500	10	2.7×10^8	$4.3\times10^{13} \simeq 0.7\times10^{-4}$mg
1/1836	500	0.0075	5.0×10^{14}	4.3×10^{13}

rf(PAUL) - TYPE TRAPS

Paul or rf - type traps provide trapping of charged particles in oscillating, spatially-nonuniform electric fields. It is also possible to use static electric fields to alter the trapping geometry somewhat,[4,5] but for simplicity, we assume trapping in pure oscillating fields here. If the trapping potential is given by

$$\phi_T = \phi_0(\vec{r}) \cos\Omega t, \tag{15}$$

then, for Ω sufficiently high (defined below), ions are confined in a pseudo potential, ϕ_{p}, given by[4]

$$\phi_{pi} \simeq q_i |\vec{\nabla}\phi_0(\vec{r})|^2/(4m_i\Omega^2). \tag{16}$$

The fictitious charge density is given by $\nabla^2\phi_{pi} = -4\pi\rho_i'$. For spectroscopy, the usual choice is the quadrupole rf trap where $\phi_0 \propto r^2 P_2(\cos\theta)$ (spherical coordinates).[4,5] This makes the trap pseudopotential harmonic in all directions. In this case, Ω sufficiently high means[4,5]

$$q_{zi} = \frac{8|q_i|V_0}{m_i\Omega^2(r_0^2+2z_0^2)} \lesssim 1. \tag{17}$$

V_0 is the magnitude of the rf voltage applied between ring end endcaps whose dimensions are indicated in Fig. 1.

If we assume that the "secular" motion in the pseudopotential well of Eq. 16 can be cooled, and if we assume $\omega = 0$, the density of ions for a single species is determined by space charge repulsion and is given by [4,5] (dropping the subscripts)

$$n = 8.3 \times 10^8 \ q_z V_0(kV)/(Z(r_0^2+2z_0^2)). \tag{18}$$

If we neglect ϕ_{ind}, the shape of the ion plasma is a spheroid of revolution.[9] If we also assume $r_0 = 2z_0$, and assume that the dimensions of the ion cloud are equal to inner trap dimensions, the maximum number of ions is given by

$$N(\max) = 2.3 \times 10^9 \ q_z \ z_0 V_0(kV)/Z. \tag{19}$$

From Eq. 17, we have

$$\Omega/2\pi(MHz) = 5.7(V_0(kV)Z/(Mq_z))^{\frac{1}{2}}/z_0. \tag{20}$$

From Eqs. 18-20, we tabulate a few example parameters in table II.

Table II. Example parameters for a quadrupole rf trap.

M	V_0(kv)	q_z	Z	r_0(cm)	n(cm^{-3})	N	$\Omega/2\pi$(MHz)
1000	10	0.5	1	1	2.8×10^9	5.8×10^9	0.81
1	"	"	"	"	"	"	25
1/1836	"	"	"	"	"	"	1100
"	"	0.005	"	"	2.8×10^7	5.8×10^7	11 GHz
M	"	0.5	"	20	6.9×10^6	1.2×10^{11}	$1.3/M^{\frac{1}{2}}$

We note the independence of n and N(max) on M. For electrons and positrons, the practical limits on n and N(max) may be due to the required large values of Ω.

For higher order rf traps, $\phi_0(\vec{r})$ might take the form given by Eq. 9. Perhaps a more useful form of ϕ_0 is given by the potential (in cylindrical coordinates)

$$\phi_0(r,\theta,z) = V_0 r^{k+1} \cos[(k+1)\theta]/r_0^{k+1}, \tag{21}$$

where θ is the azimuthal angle and k is an integer. A sketch of such a trap for k=2 is given in Fig. 4. Ideally, the electrode surfaces are equipotentials of Eq. 21; in Fig. 4, they are shown as cylindrical rods for simplicity. k=1 describes the Paul quadrupole mass filter. The ends of the trap could be closed off by bending the rods in towards the axis of the trap or using endcaps with appropriate static potentials thereby making a cylinder rf-type trap. Alternatively, the individual rods could be connected end-on-end to make a kind of race track.[13]
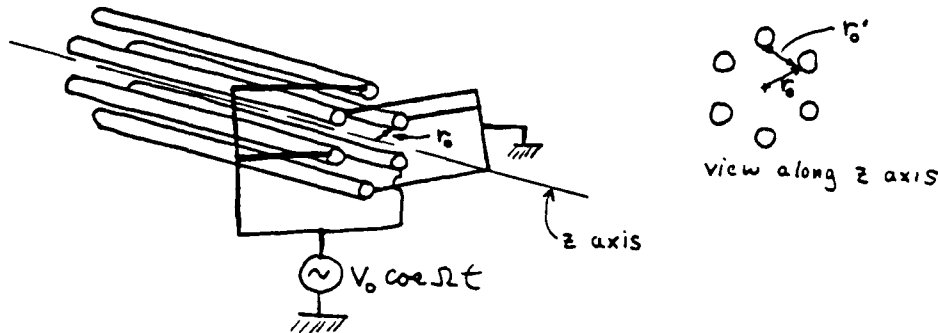
Fig. 4. Sketch of cylinder rf-type trap for k = 2.

Experimental examples of higher order traps are given in refs. 14 and 15. From Eqs. 16 and 21,

$$\phi_{pi} = C_{ki} r^{2k}, \tag{22}$$

where

$$C_{ki} = q_i V_0^2 (k+1)^2/(4 m_i \Omega^2 r_0^{2(k+1)}). \tag{23}$$

ϕ_{pi} is cylindrically symmetric.

From Gauss's law, the density of stored ions is determined by space charge repulsion and is given by (if we assume $\omega = 0$)

$$n_i(r) = k^2 C_{ki} r^{2(k-1)}/(\pi q_i). \tag{24}$$

Therefore, for $k \gg 1$, the ions tend to form cylindrical shells near the inner edge of the trap electrodes where $r - r_0$. If the ions occupy the space out to $r - r_0$, integration of Eq. 24 gives

$$N(\text{max}) = \frac{k(k+1)^2}{32} \frac{V_0 h}{q_i} \left(\frac{r_0'}{r_0}\right)^2 q_{xi} , \tag{25}$$

where q_{xi} is the stability parameter analogous to Eq. 17, and r_0' is defined in Fig. 4. We have

$$q_{xi} = 8 \ V_0 q_i / (m_i \Omega^2 r_0'^2) . \tag{26}$$

For $k - 1$, $r_0'/r_0 - \sqrt{2}$ and $q_{xi} \sim 1$ for stability. For $k - 1$, the ratio of $N(\text{max})$ for the cylinder rf - trap to $N(\text{max})$ for the rf quadrupole trap of Eqs. 15 - 20, is equal to $3h/(4z_0)$ where h is the length of the plasma column as in Fig. 3. For $k \gg 1$, we have

$$N(\text{max})_k / N(\text{max})_{k-1} \sim k\pi^2/8 , \tag{27}$$

where we have assumed that the required value of the trap stability parameter, q_x, is independent of k. Thus, $N(\text{max})$ increases approximately as kh/z_0.

ION MIXTURES

For brevity, we consider only two ion species, with charge-to-mass ratios $q_1/m_1 \neq q_2/m_2$. The results are easily generalized to more species. When $q_1/q_2 > 0$, we consider only cylinder-type traps for simplicity. However the qualitative aspects of the results apply to other geometries.

Cylinder Penning-type trap, $(q_1/q_2 > 0)$

In Eq. 6, with $\rho' - 0$ for the Penning-type trap, ρ can be single valued only if the two ion species occupy different spatial regions. Qualitatively, since thermal equilibrium implies that ω is the same for all ions, if $q_1 - q_2$ and $m_2 > m_1$, species 2 is forced to larger radii than species 1 because of the larger centrifugal force acting on it. This separation has been theoretically and experimentally studied.[16,17] In the $T - 0$ limit, the separation should be complete with a gap between the species. If we look along the z axis of the trap, the spatial distributions appear as in Fig. 5.

The ion densities are still given by Eq. 10. The maximum density of the outer species is again given by $\omega - \Omega_{c2}/2$. Using this value of ω, we can find the corresponding value of n_1. The separation of the plasmas is given by solving the equation of motion for the rotation motion of species 2 at the radius a_2. We find

$$a_2/b_1 - (\rho_1/\rho_2)^{\frac{1}{2}} . \tag{28}$$

188

For $a_2 - b_1 > \lambda_D$, we expect the thermal contact between the two species to be reduced.[17]

$$q_1/m_1 > q_2/m_2$$
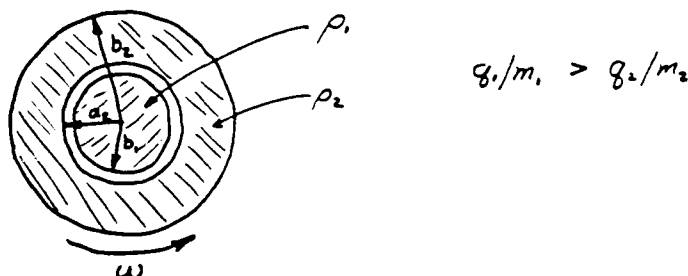
Fig. 5. Centrifugal separation of ion species in cylinder Penning or rf-type trap. The view is along the z axis, $\vec{B}$ is into the paper, and q_1, $q_2 > 0$.

A possible configuration for maintaining cold trapped positrons[3] in a Penning trap might be the following. Consider simultaneous trapping of positrons and $^9Be^+$ ions. The $^9Be^+$ ions would form a hollow cylinder around the central e^+ column. Using laser cooling, the $^9Be^+$ ions and therefore the positrons could be cooled to temperatures much less than 1 K.[17] In addition, angular momentum can be imparted to the ions in the laser cooling process to prevent radial diffusion of both species.[17] In this way, a stable, low temperature positron sample could be maintained. It is likely that ω would be limited to the value for maximum $^9Be^+$ density; that is $\omega(max) = \Omega_c(^9Be^+)/2$. If we assume $B = 10$ T this would limit the maximum positron density to $n(e^+) \approx 5.9 \times 10^{10}/cm^3$.

It would be nice to realize a similar scheme for antiprotons; unfortunately, negative ions suitable for laser cooling do not seem to be available. Cooling of antiprotons by thermalized electrons should work[1,18-20]. In the condition of thermal equilibrium, the antiprotons form a hollow cylinder around the electrons. In order to prevent radial diffusion, angular momentum of the appropriate sign might be imparted to the ions by particle beams,[21] positive or negative feedback on the ion motion[21,22] or angular momentum transfer from plasma waves.[23,24]

Cylinder rf-type trap ($q_1/q_2 > 0$)

For the rf-type trap, assumming $\omega = 0$, separation of the species with $q_1/m_1 \neq q_2/m_2$ occurs because the pseudopotential wells are unequal. This phenomenon has been investigated[25] for the quadrupole trap configuration. A simpler case to analyze is that of the cylinder rf-type trap where ϕ_0 is given by Eq. 21. If we assume $q_1/m_1 > q_2/m_2$, Fig. 5 again applies. Ion densities are still given by Eq. 24 and the separation of species can be easily determined by noting that at $r = a_2$, the space-charge electric field outward from species 1 is just equal to the pseudopotential field inward acting on species 2. We find

$$\frac{a_2}{b_1} = \left(\frac{Z_1 M_2}{Z_2 M_1} \right)^{\frac{1}{2k}} . \qquad (29)$$

Low order traps (e.g., k = 1 (quadrupole trap)) can give rise to a significant separation of the species.

Penning-type traps ($q_1/q_2 < 0$)

Simultaneous trapping of charges of opposite sign is particularly interesting in the context of this meeting. An important example is the simultaneous trapping of positrons and antiprotons for the production of antihydrogen by radiative recombination.

For the Penning-type trap, simultaneous trapping of charges of opposite sign is precluded because it is impossible to simultaneously trap both species along z. Therefore, to achieve a mixture of positive and negative ions, one species must be injected through the other. A possible arrangement might be to stack Penning traps for charges of opposite sign along the z axis in a "nested" arrangement as suggested in ref. 26. If positrons are stored in the central trap, antiprotons could be passed back and forth between traps adjacent to the central trap. Angular momentum transfer would tend to spread the positrons, but this might be overcome as described in the previous section.

rf - type traps ($q_1/q_2 < 0$)

In the pseudopotential approximation, it is apparent that if $N_1 q_1 = N_2 q_2$ the ions shrink to a point! The practical limit would appear to be due to rf heating which tends to keep the ions very hot. This problem is accentuated for simultaneous storage of positive and negative ions since they can come very close together due to Coulomb attraction and the rf micromotions[4,5] are 180° out of phase for the two species. Some experimental work has been reported in ref. 27, where Tl^+ and I^- ions were simultaneously stored in a quadrupole rf trap. In this work, an increase in density over the maximum value for a single stored species was observed, but overall densities were still fairly low. Clearly more work needs to be done on this interesting possibility.

Penning - rf trap combinations

An example of such a combined trap might be an rf type trap for positrons superimposed on a Penning-type trap for antiprotons. Such a scheme appears valid for small numbers of positrons in an antiproton sample. When the number of positrons exceeds the number of antiprotons, trapping is more likely to occur because the positrons are held by the rf trap pseudopotential and antiprotons are held by the attractive space charge of the positron sample.

PROBLEMS

The analysis in this paper has considered only the static properties of nonneutral ion plasmas held in Penning-type or rf-type traps. The calculated maximum densities and numbers will be reduced by various effects which we might classify as plasma instabilities.

Penning-type traps

The most serious problem appears to be due to asymmetry induced transport. Radial transport can also occur due to ion collisions with background gas, but at very high vacuum, this process is negligible. The basic idea of asymmetry induced transport is that if the trap is not axially symmetric, angular momentum can be coupled into the ions which causes them to spread radially in the trap. Eventually, the ions will strike the electrodes and be lost. During this spreading process, the electrostatic space-charge energy will be converted to heat. In a cylinder Penning-type trap, spreading rates proportional to $(h/B)^2$ have been observed,[28] where h is the plasma length (Fig. 2). Although the spreading mechanism is not understood, one possibility might be resonant particle transport.[9,28,29] Resonant particle transport might occur if the trap geometric axis and magnetic field axis are misaligned. As the ion density increases, ω becomes larger. As the temperature becomes lower, the individual ion axial frequency, ω_z', defined as the mean axial velocity, v_z, divided by h/π, becomes smaller. When $\omega_z' \approx \omega$, a coupling exists[9,29] which can simultaneously heat the axial motion and increase the ion radii. At the densities required for this condition, ω_z' becomes less well defined due to collisions, but the same mechanism may still apply. For $\omega - \omega_z'$, the densities may be considerably less than the maximum density given by Eq. 11. For small samples, some experimental evidence for such a resonant effect exists.[9]

Independently of the mechanism, such transport is likely caused by trap asymmetries. Conversely, if axial symmetry is preserved, angular momentum is a constant of the motion and confinement is assured.[10] Therefore, axial symmetry in the Penning-type traps appears to be at a premium.

rf-type traps

Historically, the mechanism of rf heating[30] has prevented the attainment of low temperatures and long confinement times in the rf traps. Therefore, attainable densities have typically been less than those dictated by space charge limitations (Eqs. 18 and 24). Cooling with a buffer gas allows the space-charge limited densities to be obtained, but this option seems to be precluded for antimatter storage.

The basic mechanism for ion-ion rf heating is that the rf driven micromotion can impart energy to the secular motion, that is, the motion in the pseudopotential well. In many experiments, this has limited the ion kinetic energy to a value of about 1/10 of the well depth of the trap due to evaporation.[4,5,30] This problem is often accentuated since it is desirable to operate the trap with large q_z values (Eq. 17) in order to obtain deep well depths. For the quadrupole rf trap (Eqs. 15-20), the relation $\omega_z/\Omega - q_z/(2\sqrt{2})$ holds, where ω_z is the single ion secular frequency.[4,5,30] Therefore, for

191

large values of q_z, ω_z approaches Ω and subharmonic excitation of the secular motion becomes more likely.

For stored ions of the same sign of charge, it would appear that rf heating could be made less by using much lower values of q_z ($q_z < 0.01$). This reduces the ion micromotion amplitude at a given distance from the center of the trap and it increases the mean spacing between ions. Both of these effects would reduce the rf heating mechanism and thereby allow the space charge density limit to be approached. Unfortunately, reducing q_z also reduces n (Eq. 18), so that a reasonable compromise would have to be met to achieve maximum stored numbers.

ACKNOWLEDGEMENTS

192

REFERENCES

1. C.F. Driscoll, Low Energy Antimatter, Ed. by D.B. Cline, (World Scientific, Singapore, 1986), p. 184. This paper summarizes the work of J.H. Malmberg, T.M. O'Neil, Driscoll and their colleagues. It addresses some of the same issues of this paper.

2. L.R. Brewer, J.D. Prestage, J.J. Bollinger and D.J. Wineland, in Strongly Coupled Plasma Physics, ed. by F.J. Rogers and H.E. DeWitt, Plenum, 1986, to be published; J.J. Bollinger and D.J. Wineland, Phys. Rev. Lett. 53, 348 (1984).

3. C.M. Surko, M. Leventhal, W.S. Crane and A.P. Mills, Jr., H. Kugel, and J. Strachan, in Positron Studies of Solid Surfaces and Atoms, ed. by K.F. Canter, W.S. Crane and A.P. Mills, Jr. (World Scientific, Singapore, 1986), p. 221.

4. H.G. Dehmelt, Adv. At. Mol. Phys. 3, 53 (1967) and 5, 109 (1969).

5. D.J. Wineland, W.M. Itano, and R.S. Van Dyck, Jr., Adv. At. Mol. Phys. 19, 135 (1983).

6. R.C. Davidson, Theory of Nonneutral Plasmas (Benjamin, Reading, MA, 1974), p. 4.

7. T.M. O'Neil and C.F. Driscoll, Phys. Fluids 22, 266 (1979).

8. S.A. Prasad and T.M. O'Neil, Phys. Fluids 22, 278 (1979).

9. D.J. Wineland, J. J. Bollinger, W.M. Itano, and J.D. Prestage, J. Opt. Soc. Am. B2, 1721 (1985).

10. T.M. O'Neil, Phys. Fluids 23, 2216 (1980).

11. R.S. Van Dyck, Jr., F.L. Moore, D.L. Farnham, and P.B. Schwinberg, Int. J. Mass Spectrom. and Ion Processes 66, 327 (1986).

12. D.J. Wineland, W.M. Itano, J.C. Bergquist, J.J. Bollinger, and J.D. Prestage, in Atomic Physics 9, R.S. Van Dyck, Jr., and E.N. Fortson, eds., (World Scientific, Singapore, 1985), p. 3.

13. D.A. Church, J. Appl. Phys. 40, 3127 (1969).

14. E. Teloy and D. Gerlich, Chem. Phys. 4, 417 (1974); A. Sen and J.B.A. Mitchell, J. Phys. B: At. Mol. Phys. 19, L545 (1986).

15. M. Okumura, L.I. Yeh, D. Normand, and Y.T. Lee, J. Chem. Phys. 85, 1971 (1986).

16. T.M. O'Neil, Phys. Fluids 24, 1447 (1981).

17. D.J. Larson, J.C. Bergquist, J.J. Bollinger, W.M. Itano, and D.J. Wineland, Phys. Rev. Lett. 57, 70 (1986).

18. H.G. Dehmelt et al., Bull, Am. Phys. Soc. 24, 757 (1979); G. Torelli, in Proceedings of the Fifth European Symposium on Nucleon Anti-Nucleon Interactions, Bressanone, Italy, 23-28 June 1980, edited by M. Cresti (Istituto Nazionale di Fisica Nucleare, Padua, Italy, 1980), p. 43.

19. G. Gabrielse, H. Kalinowsky, and W. Kells, in Physics with Antiprotons at LEAR in the ACOL Era, edited by U. Gastaldi et al. (Editions Frontieres, Gif-sur-Yvette, France, 1985), p. 665; W. Kells, IEEE Trans. Nucl. Sci. 32, 1770 (1985).

20. M.H. Holzscheiter, in Low Energy Antimatter, Ed. by D. B. Cline, (World Scientific, Singapore, 1986).

21. D.J. Wineland, R.E. Drullinger J.C. Bergquist, and W.M. Itano, Bull. Am. Phys. Soc. 24, 1185 (1979).

22. W.D. White, J.H. Malmberg, and C.F. Driscoll, Phys. Rev. Lett. 49, 1822 (1982).

23. D.L. Eggleston, T.M. O'Neil, and J.H. Malmberg, Phys. Rev. Lett. 53, 982 (1984).

24. J.D. Crawford, T.M O'Neil, and J.H. Malmberg, Phys. Rev. Lett. $\underline{54}$, 697 (1985).
25. L. S. Cutler, private communication.
26. G. Gabrielse, K. Helmerson, R. Tjoelker, X. Fei, T. Trainor, W. Kells, and H. Kalinowsky, in Proc. of 1st Workshop on Antimatter Physics at Low Energy, B.E. Bonner and L.S. Pinsky eds., Fermilab, Apr. 1986, p. 211.
27. F.G. Major and J.P. Schermann, Bull. Am. Phys. Soc. $\underline{16}$, 838 (1971).
28. C.F. Driscoll, K.S. Fine, and J.H. Malmberg, Phys. Fluids $\underline{29}$, 2015 (1986).
29. C.F. Driscoll and J.H. Malmberg, Phys. Rev. Lett. $\underline{50}$, 167 (1983).
30. D.A. Church and H.G. Dehmelt, J. Appl. Phys. $\underline{40}$, 3421 (1969); H.G. Dehmelt, in Advances in Laser Spectroscopy, F.T. Arecchi, F. Strumia, and H. Walther eds., Plenum, 1983, p. 153.

Thomas J. McIlrath

Long Duration Coherent Lyman-Alpha Sources

195

LONG DURATION COHERENT LYMAN-ALPHA SOURCES

THOMAS J. MCILRATH

University of Maryland, College Park, Maryland, 20742 and
National Bureau of Standards, Gaithersburg, Maryland 20899

ABSTRACT

Resonant radiation at 1215.56 Å for cooling and trapping of
atomic hydrogen can be produced by parametric upconversion of
visible laser outputs. Several gases and vapors have been shown
to be suitable for generating 1215 Å radiation with verified
conversion efficiencies of $>10^{-4}$. A scenario for producing long
pulse ($(2 \times 10^{-6}$ sec) outputs of $\gtrsim 10$ W power using proven tech-
niques is discussed.

I. INTRODUCTION

Trapping, cooling and manipulating atomic hydrogen by
optical means requires an intense source of laser radiation at
the Lyman-alpha resonance line (1215.56 Å). Coherent generation
of Lyman-alpha radiation can be achieved in several ways. Direct
generation between 1232 Å and 1274 Å has been demonstrated with
an Ar_2 excimer laser[1] and the tuning range is expected to
extend[2] below 1215 Å. However, contamination of the discharge by
H due to dissociation of H_2O and hydrocarbon contaminants makes
lasing at 1215.56 Å itself difficult and unreliable. In
addition, optics for this region are sparse and easily damaged
which makes it difficult to obtain narrow band operation. Gain
media at 1215.56 Å seem most appropriate as amplifiers for low
power, narrow band sources.

The absence of direct laser sources at 1215.56 Å is not,
however, a serious problem for laser cooling. Lyman-alpha radia-
tion can be readily obtained by frequency upconversion of longer
wavelength laser outputs. This has the advantage that all of the
laser generation and control can be done in the familiar and
convenient visible portion of the spectrum and only the final up-
conversion need be done in vacuum. As we will show below,
sources based on this technique have now been tried and proven
and are sufficiently powerful to satisfy the requirements for
cooling atomic hydrogen from room temperature to the low values
associated with atomic traps. We will devote this paper to dis-
cussing upconversion sources.

II.   PARAMETRIC UPCONVERSION

A.   Introduction

The only efficient way to generate coherent 1215.56 Å radiation is by upconversion of visible radiation.[2] The process of upconversion is a parametric process whereby fundamental driving waves at frequencies ω_1, ω_2, and ω_3 simultaneously drive a nonlinear medium which in consequence produces a polarization wave at ω_4 with

$$\omega_4 = \omega_1 + \omega_2 + \omega_3$$

There can be any odd number of driving waves for an isotropic nonlinear medium. Two or more frequencies can be the same and the frequencies can be positive or negative. In the case shown here, the process is termed four-wave mixing since a total of four electromagnetic waves are involved, three driving waves and one product wave. If all three driving frequencies are the same then the process is that of frequency tripling. The characteristic of a parametric process is that the nonlinear medium is in exactly the same state before and after the process, it acts as a catalyst. Thus no energy absorbed by the medium and the energy of the final wave is completely determined by that of the driving wave. In addition, the linewidth of the final beam is determined by the linewidth of the driving beams. Since the driving beams are from visible lasers, all of the beam generation and control occurs in the visible where we have a wide variety of techniques and instrumentation. Single mode lasers can be used and frequencies monitored with Fabry-Perot interferometers. Vacuum techniques do not need to be incorporated until the final stage when the parametric generation occurs. The only suitable, transparent, nonlinear materials are gases which are isotropic so we are limited to an odd number of driving waves and the lowest order process is frequency tripling or four-wave mixing. In frequency tripling the driving waves are at 3646.68 Å which can be produced by frequency doubling 7293.36 Å using con ventional crystals. The generation of visible or near infrared radiation is accomplished using dye lasers or tunable solid state lasers such as Alexandrite.[3]

B.   Nonlinear Susceptibilities

In order to understand the potentials and limitations of upconversion we must consider the process more carefully. When a material medium is subject to a driving electric field $E(t)$ there is a resultant polarization $P(t)$ generated in the medium. The polarization is related to the driving field by a power series

$$P(t) = \chi^{(1)} E(t) + \chi^{(3)} E^3(t) + \ldots$$

where only odd powers of the driving field are present due to the isotropy of the gaseous medium. The driving field is the sum of all the optical waves present so higher order terms contain all the sum and difference frequencies.

The first term gives an incoherent wave representing Rayleigh scattering and a forward, coherent wave which interferes with the driving wave to give the refractive index of the material. The higher order terms give the parametric processes of tripling and sum and difference generation. Efficient generation of the parametric wave requires a coherent superposition of the radiation from the spatially distinct components of the bulk material and the resulting output is a collimated, forward directed wave with a mode structure reflecting the mode structure of the driving wave.

C.   Phase Matching

The polarization wave $P(t)$ travels in the medium with a phase velocity determined by the phase velocity of the driving waves. The generated wave at ω_4 travels with a phase velocity characteristic of its frequency. In order to achieve a coherent superposition of the generated waves from the different portions of the bulk medium it is necessary that the phase velocity of the polarization and the generated waves be the same (or just slightly different to compensate for the effects of focusing). This requirement is called phase matching. The normal behavior of transparent materials is to increase their refractive index monotonically with frequency. This normal dispersion precludes phase matching. The phase matching requirement is overcome by using a material with a strong absorption line between the driving and generated frequencies. The anomalous real dispersion associated with passing through a resonance reduces the high frequency refractive index to allow phase matching. The requirement of phase matching restricts the available materials for upconversion in the case of gases just as it does with crystals used in the visible.

D.   Resonant Enhancement

The nonlinear susceptibility for four-wave processes, $\chi^{(3)}$, is resonantly enhanced whenever the intermediate or final processes can proceed through a real level while conserving energy. Upconversion by frequency summing represents the absorption of a quantum of energy at each of the driving frequencies and emitting a photon at the product frequency. The susceptibility is large if there is a real level which can be reached by absorption of one of the driving frequencies, or by absorbing the generated frequency. Either of these resonances also entail large losses in the medium. However, in four-wave

mixing the susceptibility is also enhanced if there is an intermediate resonance corresponding to the absorption of two of the three driving frequencies, i.e. an intermediate resonance part way up the ladder. The enhancement is just as efficient as one photon or product photon resonances in increasing the susceptibility. However, the associated system loss is much reduced because of the low rate associated with two photon absorption processes.

III. CURRENT SYSTEMS FOR LYMAN-ALPHA GENERATION

A. Materials for upconversion

Several gaseous media have been shown to be capable of producing Lyman-alpha radiation by four wave mixing. The materials fall into the two categories of metal vapors and room temperature gases. Among metal vapors, Lyman-alpha generation has been reported using Hg, Be and Mg^2 and there is no reason to doubt that many more metals could be used. Both Hg and Mg have low susceptibilities at 1215 Å compared with their susceptibilities at nearby frequencies and Be is extremely difficult to handle at high vapor pressures. All of the metal vapor systems exhibit substantial challenges in attempting to operate at high vapor pressures. The metals also have low lying excited states and exhibit abundant resonances with visible and ultraviolet radiation which substantially enhances their susceptibility. An inevitable associated property is that they break down or saturate at relatively low incident fluxes. Thus the metal vapors are very useful systems for obtaining reasonable efficiencies at modest laser energies but lose many of their advantages when used with high energy systems.. The disadvantages associated with working with metal vapors remain at high energies.

Room temperature gases include molecular gases such as NO or CO and the rare gases He, Ne, Ar, Kr and Xe. Efficient generation has been achieved in NO between 1500 Å and 1300 Å but ionization occurs below ~1250 Å and the reported conversion efficiency at 1215 Å is very low. The rare gases have proven to be extremely convenient materials for generation of radiation from ~1700 Å to as short as 380 Å. The major disadvantage of the rare gases is that resonance enhancement requires driving radiation at 2500 Å or below. It is possible to satisfy the resonance condition using driving radiation produced from visible laser combined with mixing in efficient crystals.^{3} Furthermore, found that for high energy systems the limiting efficiency of nonresonant systems is comparable to that for resonant but at larger output energies.

B. Limiting Conversion Efficiencies

The conversion efficiency of parametric limited by several physical processes in ulation by multiphoton absorption, se
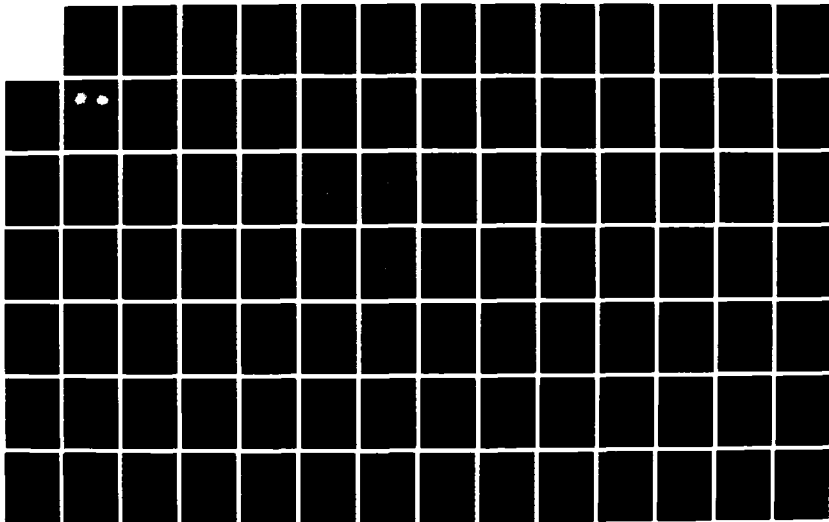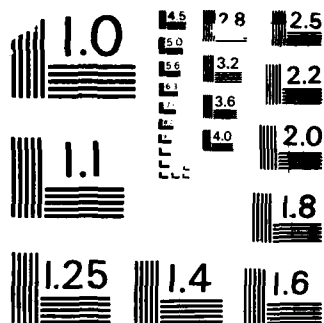
MICROCOPY RESOLUTION TEST CHART

NATIONAL BUREAU OF STANDARDS-1963

ing. For unconversion in the rare gases the efficiency is limited by stark induced refractive index changes which preclude maintaining the phase matched condition during the full intensity range of a high energy pulse. In the laboratory the highest conversion efficiency observed to date for generation of 1216 Å radiation is 1.4×10^{-4}. This was achieved by Langer, Puell and Rohr[4] using non-resonant upconversion in a high pressure mixture of Ar and Kr. The efficiency was limited by breakdown and an analysis of the results indicated that under optimized condition a conversion efficiency of 10^{-3} could be achieved. An efficiency of 10^{-4} or 5×10^{-5} is accepted as a reasonable goal with modest effort. Higher efficiencies will presumably follow from new materials and fully optimized experiments.

C.   Lyman-Alpha Generation using Current Systems

Experiments on generation of Lyman-alpha radiation by parametric upconversion in rare gases have shown conversion efficiencies of 10^{-4} with an incident pulse of 3648 Å radiation of 10^{-8} s duration focused to a power density of 5×10^9 W cm^{-2}. A 50 cm focal length lens was used to give a confocal beam parameter b=0.16 cm. Output powers of 5 to 10 W have been produced in this and other experiments and coherently generated Lyman-alpha radiation has been used to probe atomic hydrogen in the prepulse of a Tokamak by resonant scattering.[5]

The requirement for cooling atomic hydrogen by Lyman-alpha radiation is that a sufficient number of photons be scattered to absorb the momentum of the hydrogen atom. For hydrogen initially at room temperature this requires $\approx 10^3$ scatters. Since one can incoherently scatter at most one photon per spontaneous lifetime, the laser pulse must last $> 10^3$ atomic lifetimes or 1.6×10^{-6} s. The required power depends on the beam area but an energy of 10^{-9} J per spontaneous lifetime would allow saturating the atoms in a beam with a cross-section of ≈ 0.1 cm^{-2}.

There are several possible ways by which such Lyman-alpha outputs can be obtained. One straightforward scenario would be based on a mode locked, cw pumped Nd:YAG laser, YAG amplifiers and dye lasers. By Q-switching the mode locked oscillator with an actively controlled cavity gain, the energy stored in the YAG would be spread over $> 10^3$ mode locked pulses of $\approx 10^{-9}$ s. The energy per pulse would be at least $\approx 10^{-7}$ J. This could be amplified in a bank of Nd:YAG rods. The use of three rods in parallel would allow amplification to ≈ 2mJ per pulse extracting ≈ 666mJ per amplifier rod. These numbers are in line with conventional operation of Nd:YAG systems.

The second and third harmonics of the 1.064u Nd:YAG output at 5320 Å and 3547 Å could be efficiently generated with non-linear crystals. The output of a synchronously pumped dye laser oscillator operating at 6070 Å could be amplified in pulsed dye laser amplifiers pumped by the 5320 Å beam. This would produce ≈ 150 uj per pulse at 6070 Å. This output can in turn be summed

with the remaining 1.064 µ radiation in a nonlinear crystal to yield 350 µJ of 3547 Å radiation and 50 µJ of 3865 Å radiation. This would produce a power in the driving waves for the parametric up conversion of 5.3×10^5 W which has been shown sufficient to achieve conversion efficiencies of 10^{-4}. This efficiency for upconversion in a high pressure Kr/Ar cell would give a train of 10^3 pulses at 1215.67 Å with ~10nJ per pulse. The output could be nearly transform limited both spatially and temporally. This would be sufficient for cooling a beam of atomic hydrogen initially at room temperature.

The scenario outlined above is intended only to show that the required power levels and durations of Lyman-alpha radiation for cooling atomic hydrogen can be achieved by non-heroic methods with tested technologies. There are other approaches which might prove more desireable after preliminary studies. Lasers based on Alexandrite rods are tunable over a wide region including 7296 Å. The second harmonic of this output could be tripled in Kr to generate Lyman-alpha radiation. Alexandrite lasers are high energy systems currently under rapid development. The 7296 Å region is near the edge of the gain profile and the attainable output at this wavelength would need to be studied to see if the required long train of pulses could be produced.

Upconversion as discussed so far has involved a single pass of the Kr/Ar cell with low conversion efficiencies. Recent work on high reflectivity mirrors has produced reflectivities >0.9995. It should be possible to produce a cavity with a finesse of $>10^2$ to enhance the driving fields. A Brewster plate in the cavity could be used to extract the resultant 1216 Å radiation.

IV.   SUMMARY

The problem of laser cooling of atomic hydrogen is difficult due to the short wavelengths involved but the problem is made considerably easier by the high momentum per photon and the low mass of the hydrogen atoms. Direct generation of Lyman-alpha radiation is difficult and until fundamentally new techniques are developed does not represent a practical approach to narrow band, long duration Lyman-alpha sources. On the other hand, techniques for generation of coherent Lyman-alpha by nonlinear mixing in gases are well developed. They have been shown to produce intense pulses of narrow band radiation with wavelength control derived entirely by control of the visible driving lasers. It is seen that demonstrated techniques can produce outputs which are sufficient to cool a beam of atomic hydrogen initially at room temperature. There are several alternative approaches which promise to enhance both the efficiency and simplicity of the generation process.

V.   REFERENCES

1.   W. G. Wrobel, H. Röhr and K. H. Steuer, Appl. Phys. Lett.
      36, 113 (1980).

2.   See J. F. Reintjes, Nonlinear Optical Parametric Processes
      in Liquids and Gases (Academic Press, Orlando, 1984).

3.   K. D. Bonin and T. J. McIlrath, J. Opt. Soc. Am. B 2, 527
      (1985).

4.   H. Langer, H. Puell and H. Röhr, Opt. Commun. 34, 137
      (1980).

5.   R. W. Dreyfus, P. Bogen and H. Langer in Laser Techniques
      for Extreme Ultraviolet Spectroscopy, T. J. McIlrath and
      R. R. Freeman eds. (AIP, New York, 1982).

Richard Lovelace, Dave Thompson, and Dave Lee

Magnetic Traps for An Anti-Hydrogen Gas

MAGNETIC TRAPS FOR AN ANTI-HYDROGEN GAS

Richard Lovelace,
Dave Thompson, and
Dave Lee

Department of Applied Physics, and
Laboratory of Atomic and Solid State Physics
Clark Hall, Cornell University,
Ithaca, New York 14853

Abstract

Magnetic traps are described for the confinement of a dense, collisional gas of spin-polarized anti-hydrogen.

INTRODUCTION

We consider the magnetic confinement of a dense, collisional gas of anti-hydrogen atoms. The confinement is a result of the interaction of the magnetic moments of the gas atoms with a magnetic field which includes a component which oscillates rapidly in the reference frame of an atom.

Spin-polarized atomic hydrogen gas can be formed by collecting atoms in the two low energy hyperfine Zeeman states (the "a" and "b" states, where the electron magnetic moment is parallel to the magnetic field with the spin anti-parallel) in a strong magnetic field at low temperatures.[1] For anti-hydrogen, the "a" and "b" states have the positron magnetic moment parallel to the magnetic field with the spin also parallel. Atoms in these two states are forced towards regions of stronger magnetic field, while atoms in the two high energy hyperfine states (the "c" and "d" states, where the magnetic moment is anti-parallel to the magnetic field) are forced towards low field regions. That is, the "a" and "b" state atoms are strong-field-seekers while the "c" and "d" state atoms are weak-field-seekers. The "a" state is a mixed state whose wavefunction includes a small admixture of the electronic spin-up state causing recombination of atoms to molecules in three-body, singlet interaction collisions. As a consequence, the sample loses its "a" state population as time progresses, leaving only the pure "b" state atoms whose nuclei and electrons are polarized parallel to one another (and therefore, have a triplet interaction). Because of the long longitudinal relaxation time (T_1) between the "b" and "a" state the resulting doubly polarized sample would be long lived[2,3] and thus ideal to produce a high density sample needed for storage were it not for the three-body dipole recombination which becomes important at densities above 10^{18} cm^{-3} (Refs. 4-7). One possible solution is to go to temperatures below 10 mK, where the needed gas phase densities are less than 10^{17} cm^{-3}.

The influence of surfaces is removed by constructing three-dimensional magnetic traps.[8-11] Static magnetic field minimum traps are possible, but only for the "c" and "d" state atoms which are low-field seekers. One could inject a "b" state gas and use electron spin resonance to flip the electron spins so that the resulting "c" state atoms would be magnetically confined. However, dipole-dipole interactions are predicted[4] to cause a rapid flipping of the electron spins and this would lead to a rather rapid loss of the sample.

Here, we discuss three dimensional <u>dynamic magnetic traps</u> where the magnetic field includes a "fast" time-dependent component. The dynamic trap must provide containment in the presence of frequent collisions. (Thus, one can rule out confinement in a rotating magnetic mirror field where the possible stable single particle motion is analogous to that of the Trojan asteroids.) A simple AC dynamic trap which is viable in the presence of collisions can be made by passing an alternating current through a circular wire loop located with its axis parallel to a strong, uniform static magnetic field.[12] This magnetic field oscillates between a mirror and an anti-mirror configuration and it provides containment for the high field seeking "a" and "b" state atoms (as well as for the "c" and "d" state atoms). In the following, we first analyze the collisionless confinement of a single atom. Secondly, we investigate the influence of collisions using the Boltzmann transport equation and a Monte-Carlo code for the numerical evaluation of particle orbits including collisions. Finally, we describe a storage ring for neutral atoms.[13] This trapping method has the important advantage that it avoids the Ohmic dissipation associated with the AC fields. Both the AC trap and the storage ring suffer from viscous heating at high densities (corresponding to a total number of trapped atoms $\sim 10^{16}$ for systems of size <50 cm).[12,13] For the storage of anti-hydrogen this heating would need to be counteracted by cooling with a Lyman-Alpha laser.[14]

SINGLE PARTICLE MOTION

The envisioned temporal variations of $\underline{B}(\underline{x},t)$ are very much slower than the electron spin precession period. Thus, the potential describing the interaction of the atom with the magnetic field is

$$V(\underline{x},t) = -\mu |\underline{B}(\underline{x},t)| \quad .$$

where μ is the magnetic moment of the atom. For the case of spin-polarized atomic hydrogen, $\mu \approx \hbar e/(2m_e c) \approx 0.93 \times 10^{-20}$ erg/Gauss (or 0.93×10^{-23} J/T). Note that the magnetic moment is parallel to $\underline{B}$ for the "a" and "b" states of atomic hydrogen so that $\mu > 0$. For the "c" and "d" states it is anti-parallel and $\mu = -|\mu|$. In the absence of collisions, the equation of motion for an atom of mass m is

$$m \frac{d^2 \underline{x}}{dt^2} - \underline{\nabla} V \quad . \tag{1}$$

In a static $\underline{B}(\underline{x})$ field, a spin-polarized atom with μ parallel to $\underline{B}$ (the "a" or "b" states of hydrogen) tends to move towards regions of maximum $|\underline{B}|$. There are, of course, no isolated maxima of $|\underline{B}|$ in free space (Earnshaw's theorem).

The magnetic field $\underline{B}(\underline{x},t)$ is considered to consist of a uniform, time-independent component $B_0 \hat{z}$ (with $B_0 > 0$), and the time-dependent field $\underline{b}(t)$ of one or more circular wire loops with axes coinciding with the z-axis. We first consider the case of a single wire loop of radius R. We assume $\underline{b}^2 \ll B_0^2$ so that $|\underline{B}| = B_0 + b_z$. In the vicinity of the center of the loop we have

$$b_z = b_0(t)\left\{ 1 + \frac{3}{4}\left[\frac{R}{r}\right]^2 - \frac{3}{2}\left[\frac{z}{R}\right]^2 + \cdots \right\} \quad ,$$

where $r^2 = x^2 + y^2$, $b_0(t) = 2\pi I(t)/(cR)$ in Gaussian units [or $\mu_0 I/(2R)$ in MKS units], and I is the current in the wire loop. For $b_0 < 0$ the field configuration corresponds to a mirror field, whereas for $b_0 > 0$ it is an anti-mirror configuration. The Taylor expansion simplifies the immediate discussion; the exact field of a circular loop is used subsequently. From equation (1),

$$\frac{d^2 x}{dt^2} = -\alpha(t)\, x \quad , \quad \frac{d^2 y}{dt^2} = -\alpha(t)\, y \quad , \quad \frac{d^2 z}{dt^2} = 2\alpha(t)\, z \quad , \tag{2}$$

where $\alpha(t) \equiv (3/2)\,[\mu b_0(t)/(mR^2)]$. Evidently, the sign of μ is irrelevant if $b_0(t)$ is an oscillatory function with an average value of zero.

Exact solutions to equations (2) exist for the case where $b_0(t)$ or $\alpha(t)$ has a square wave dependence, that is, $\alpha(t) = \alpha_0$ $\text{sign}[\sin(\omega_e t)]$, and α_0 and ω_e are constants. This case is evidently the temporal analogue to an alternating-gradient or strong-focusing synchrotron.[15] The motion in the x, y, or z directions can be written down explicitly during the intervals in which $\alpha(t)$ is positive or negative. We have stability for

$$\alpha_0 < 0.177\, \omega_e^2 \quad . \tag{3}$$

That is, the rate of switching between the mirror and anti-mirror configurations must be rapid compared with the "natural" frequency in the mirror field $(\alpha_0)^{1/2}$.

Equations (2) with $\alpha(t) = \alpha_0 \sin(\omega_e t)$ can be solved approximately in the limit where $\alpha_0 \ll \omega_e^2$ (Ref. 16): Let $\underline{x} = \underline{X} + \underline{\zeta}$, where $\underline{X}(t)$ is slowly varying on the time scale $1/\omega_e$, and $\underline{\zeta}(t)$ is rapidly varying. Notice that $\underline{X}(t)$ is analogous to the guiding center position of a charged particle in a magnetic field while $\underline{\zeta}$ represents the rapid gyration. Then, $d^2\zeta_x/dt^2 = -\alpha_0 \sin(\omega_e t) X_x$ or $\zeta_x \approx (\alpha_0/\omega_e^2) \sin(\omega_e t)X_x$ and $d^2X_x/dt^2 \approx -\langle\alpha\zeta_x\rangle \approx -(1/2)(\alpha_0/\omega_e^2)^2X_x$, where the angular brackets denote a time average over the interval $2\pi/\omega_e$. Similar formulae describe the y and z motion. Hence, the angular frequency for the slow motion is $\Omega_x = \alpha_0/(\omega_e\sqrt{2})$, $\Omega_y = \alpha_0/(\omega_e\sqrt{2})$, or $\Omega_z = \alpha_0\sqrt{2}/\omega_e$, for the x, y, or z motion. For the guiding center motion,

$$d^2X_j/dt^2 = -\partial V_e/\partial X_j \ ,$$

where

$$V_e(\underline{X}) = \frac{1}{4}\left[\frac{\alpha_0}{\omega_e}\right]^2 (X_x^2 + X_y^2 + 4X_z^2) \tag{4}$$

is an effective potential, and $j = x$, y, or z.

Equations (2) and (4) can readily be generalized to account for the full spatial dependence[17] of the magnetic field $b_z(r,z)$ of one or more coaxial wire loops for $b_0^2 \ll B_0^2$. In place of equation (2), we write

$$\frac{d^2x_j}{dt^2} = \alpha(t)F_j(\underline{X}) \ , \tag{5}$$

for $j = x$, y, or z. Here, $\alpha(t) = \alpha_0 \sin(\omega_e t)$ with α_0 defined as before below equation (2), and $F_j = R^2\nabla_j\{2b_z(r,z,t)/[3b_0(t)]\}$. An approximate solution is again obtained by letting $\underline{x} = \underline{X} + \underline{\zeta}$, where $d^2\zeta_j/dt^2 = \alpha(t)F_j(\underline{X})$ or $\zeta_j \approx -(\alpha/\omega_e^2) F_j(\underline{X})$. The slow, guiding center motion obeys the equation

$$\frac{d^2 X_j}{dt^2} = \Sigma_i [\partial F_j(\underline{X})/\partial X_i] \langle \alpha \xi_i \rangle = -\partial V_e /\partial X_j \qquad (6a)$$

where

$$V_e(\underline{X}) = (1/4)(\alpha_0/\omega_e)^2 [\underline{F}(\underline{X})]^2 \qquad (6b)$$

is the effective potential.

Figure 1 shows a contour plot of $V_e(r,z)$ obtained from equation (6b) and the actual field $b_z(r,z)$ of a single circular coil of radius R. The lowest values of the effective potential are seen to occur along the z-axis where the effective potential is $V_e(0,z) = (\alpha_0/\omega_e)^2 z^2 [1 + (z/R)^2]^{-5}$. Thus, the "top" of the effective potential, the separatrices of V_e, occur at $z = \pm R/2$ where $\max(V_e) \approx 0.0819 (\alpha_0 R/\omega_e)^2$.

INFLUENCE OF COLLISIONS

Here, we consider the "equilibrium" of a magnetically confined classical collisional gas in an oscillating mirror/anti-mirror field [$\alpha = \alpha_0 \sin(\omega_e t)$] in equation (5)]. Of course, the equilibrium will not be a simple Maxwell-Boltzmann distribution. For the present purposes the equilibrium can be described by the single particle distribution function (or phase space density) $f(\underline{X}, \underline{V}, t)$ which satisfies the Boltzmann equation

$$Df/dt \equiv \partial f/\partial t + (\underline{v} \cdot \underline{v})f + (\underline{a} \cdot \underline{v}_v)f = C(f,f) \quad , \qquad (7)$$

where $C(f,f)$ is the Boltzmann collision integral, and $a_j = \alpha(t) F_j(\underline{X})$. A dimensionless measure of the "strength" of the scattering is R/λ_0. Here, $\lambda_0 \equiv [n(0)\sigma_{tot}]^{-1}$ is the mean-free path at the center of the trap [at which point the number-density is $n(0)$]; σ_{tot} is the total scattering cross-section; and R is the radius of the current loop (which is larger than the radius of the trapped gas). For the case of spin-polarized atomic hydrogen the scattering at low temperatures is predominantly the isotropic (S wave) scattering of identical ("b" state) particles so that $\sigma_{tot} = 4\pi a_s^2$, where $a_s \approx 0.72 \times 10^{-8}$ cm (Ref. 18). Thus, $\lambda_0 \approx 1.6$ cm $[10^{15}$ cm$^{-3}/n(0)]$.

Approximate solutions to (7) can be developed utilizing the smallness of two parameters: $\epsilon \equiv \alpha_0/\omega_e^2 \ll 1$ and $\delta \equiv \epsilon R/\lambda_0 < 1$. We let $f = f_0 + f_1 + f_2 \cdots$, where the zeroth approximation is

$$f_0(\underline{x},\underline{v},t) = K \exp(-H_0/T) \quad , \tag{8}$$

with

$$H_0(\underline{x},\underline{v},t) \equiv \frac{1}{2}[\underline{v} - \underline{u}(\underline{x},t)]^2 + V_e(\underline{x}) \quad .$$

Here, K = constant; $T \equiv k_B T_0/m$, with T_0 the usual absolute temperature; V_e is given in equation (6b); and $\underline{u} \approx d\underline{\xi}/dt$ is a time and space dependent flow-velocity with $\underline{\xi}$ the above mentioned rapid component of the single particle motion. Specifically, we take $u_j = -(d\alpha/dt)F_j(\underline{x})/\omega_e^2$. Therefore, $\underline{u}$ differs from $d\underline{\xi}/dt$ by a fractional amount of order ϵ; and $\underline{v} \times \underline{u} = 0$ and $\underline{v} \cdot \underline{u} = 0$ in that F_j is proportional to $v_j b_z$ and $v^2 b_z = 0$. Thus, $\underline{v} = d\underline{X}/dt + \underline{u} + 0(\epsilon)$. Consequently, $H_0 = 1/2(d\underline{X}/dt)^2 + V_e(\underline{X}) + 0(\epsilon)$ is an approximate constant of the single particle motion.

We have numerically determined the orbits of test particles in an oscillating mirror/anti-mirror magnetic field including, via a Monte-Carlo method, collisions (S-wave scattering) of the test particle off of the background distribution function given by equation (8). Projections of a sample orbit are shown in Figure 2. In terms of the physical variables, the conditions for confinement that we find can be expressed as

$$I < 1400 \text{ A-turn}\left[\frac{R}{1 \text{ cm}}\right]^3 \left[\frac{f_e}{10^3 \text{ Hz}}\right]^2 \quad , \tag{9a}$$

and

$$I > 2700 \text{ A-turn}\left[\frac{T_0}{1 \text{ mK}}\right]^{1/2} \left[\frac{R}{1 \text{ cm}}\right]^2 \left[\frac{f_e}{10^3 \text{ Hz}}\right] \quad , \tag{9b}$$

where I is the number of ampere-turns of the circular coil and $f_e = \omega_e/2\pi$. In order for equations (9a) and (9b) to be compatible we need $f_e > 1.9 \text{ kHz}(T_0/1 \text{ mK})^{1/2}(1 \text{ cm}/R)$. The Ohmic dissipation from these large AC currents represents a non-trivial problem for the system design.

STORAGE RINGS FOR NEUTRAL ATOMS

A spatial analogue of the AC dynamic trap can be obtained by having the atoms circulate toroidally along a strong DC toroidal magnetic field while passing through periodically spaced DC current loops[13] as shown in Figure 3. The current loops act as lenses for the poloidal (r,z) motion of the atoms. The average toroidal motion of an atom gives rise to a time-dependent component of the magnetic field which has the role of $\underline{b}(t)$ in the AC trap.

The particle dynamics in the storage ring can be more easily understood for a straightened-out system. The magnetic field can then be written as

$$\underline{B}(\rho,z) = \sum_{n=-\infty}^{\infty} \underline{B}_\ell(\rho, z-n\ell), \qquad (10)$$

where $\underline{B}_\ell$ is the field of a single loop, ℓ is the distance between loops, and $\rho^2 = x^2 + y^2$. The potential for the single particle motion, $V = -\mu|\underline{B}|$, is periodic in z so that

$$V(\rho,z) = \sum_{n=0}^{\infty} U_n(\rho)\cos(2\pi zn/\ell) \quad , \qquad (11)$$

with $U_n = c_n + d_n\rho^2 + \cdots$. As in the above treatment of the AC trap, we may separate the particle motion into slow and rapid components, $x = X + \zeta_x$, $y = Y + \zeta_y$, and $z = Z + \zeta_z$. In contrast with the AC trap, we now have $Z = \langle v_z \rangle t$. As before, $\langle x \rangle = 0$, $\langle y \rangle = 0$, and $\langle \zeta_z \rangle = 0$. For the storage ring, the average angular frequency at which a particle passes through the loops, $\omega_\ell = 2\pi\langle v_z \rangle/\ell$, is the analogue of the driving frequency ω_e of the AC trap. Following the methods used for the AC trap, an effective potential for the transverse guiding center motion (X,Y) can readily be derived.

Table 1 summarizes the results of a large number of particle orbit calculations in different toroidal-storage ring geometries. The storage ring magnetic field is entirely DC so that superconducting coils can be used. This represents an important advantage over the AC trap.

REFERENCES

1. Silvera, I. F., and Walraven, J. T. M. Phys. Rev. Lett. 44, 164-168 (1980).

2. Statt, B. W., and Berlinsky, A. J. Phys. Rev. Lett. 45, 2105-2108 (1980).

3. Cline, R. W., Greytak, T. J., and Kleppner, D. Phys. Rev. Lett. 47, 1195-1198 (1981).

4. Kagan, Y., Vartanyantz, I. A., and Shlyapnikov, G. V. Zh. Eksp. Teor. Fiz. 81, 1113-1140 (1981) [Soviet Physics JETP, 54, 590-604 (1982)].

5. Sprik, R., Walraven, J. T. M., and Silvera, I. E. Phys. Rev. Lett. 51, 479-482 (1983).

6. Hess, H. F., Bell, D. A., Kochanski, G. P., Cline, R. W., Kleppner, D., and Greytak, T. J. Phys. Rev. Lett. 51, 483-486 (1983); See also, Hess, H. F., Bell, D. A., Kochanski, G. P., and Greytak, T. J. Phys. Rev. Lett. 52, 1520-1523 (1984).

7. Tommila, T., Jaakkola, S., Krusius, M., Salonen, K., and Tjukanov, E. in Proceedings of the 17th International Conference on Low Temperature Physics, Part I, eds V. Eckern, A. Schmid, W. Weber, and H. Wuhl, pp. 453-454 (North Holland, Amsterdam, 1984).

8. Pritchard, D. E. in Proceedings of Workshop on Spectroscopic Applications of Slow Atomic Beams: Laser Cooled and Trapped Atoms, pp. 103-111 (National Bureau of Standards, Gaithersburg, 1983).

9. Wing, W. H. Ibid, pp. 74-92.

10. Metcalf, H. J. Ibid, pp. 59-67.

11. Hess, H. F. Bull. Am. Phys. Soc. 30, 854 (1985).

12. Lovelace, R. V. E., Mehanian, C., Tommila, T. J., and Lee, D. M. Nature 318, 30-36 (1985).

13. Thompson, D., Lovelace, R. V. E., and Lee, D. M. "Storage Rings for Spin-Polarized Hydrogen," Cornell University preprint (1987).

14. McIlrath, T. "Long Duration Lyman-Alpha Sources for Atomic Hydrogen Cooling," in these proceedings (1987).

15. Persico, E., Ferrari, E., and Segre, S. E. Principles of Particle Accelerators, Chapter 6 (Benjamin, New York, 1968).

16. Landau, L. D., and Lifshitz, E. M. Mechanics, pp. 93-95 (Pergamon Press, Oxford, 1960).

17. Landau, L. D., and Lifshitz, E. M. Electrodynamics of Continuous Media, pp. 124-125 (Pergamon Press, Oxford, 1982).

18. Friend, D. G., and Etters, R. D. J. Low Temp. Phys. 39, 409-415 (1980).
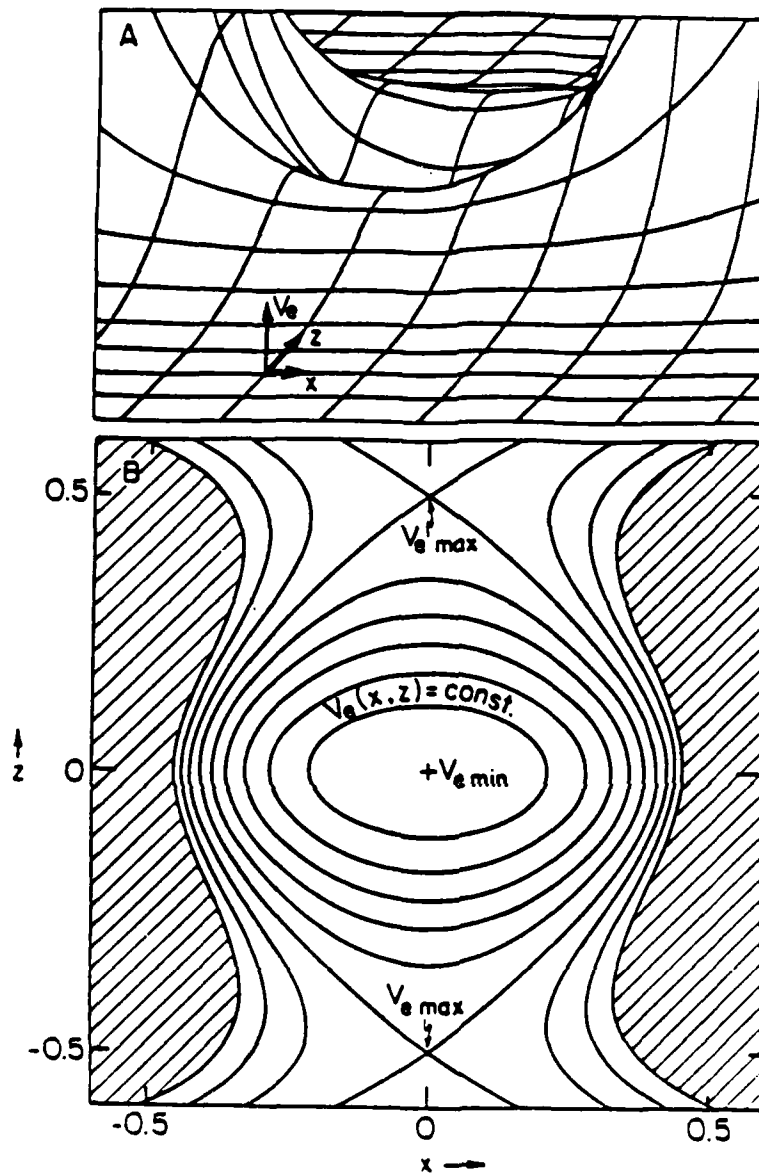
Figure 1. Representations of the effective potential from equation (7b) for the case where the b field is due to a single circular wire loop of unit radius in the (x,y) plane. An isometric view of the potential is shown in A, and the equi-potentials are shown in B. The two points denoted by V_m are separatrices. The trapped particles occupy the region $V_e \le V_{max} = 0.0819 \ (\alpha_0/\omega_e)^2 R^2$. The equi-potential contours are uniformly spaced with $\Delta V_e = V_{max}/6$.
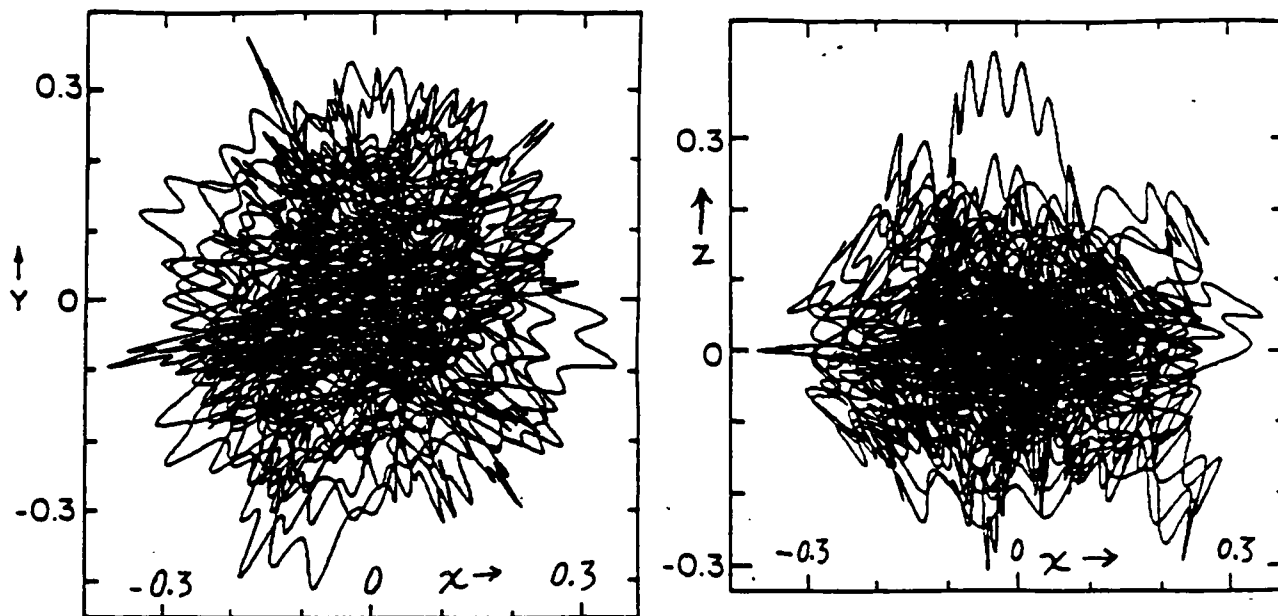
Figure 2: Projections of the trajectory of a test particle for the conditions where $\hat{T} = 3 \times 10^{-3}$ and $\epsilon = 0.076$. The **b** field is due to a single circular loop. This trajectory corresponds to an elapsed time of $10^3 \, t_e$. During this interval 490 collisions occurred.
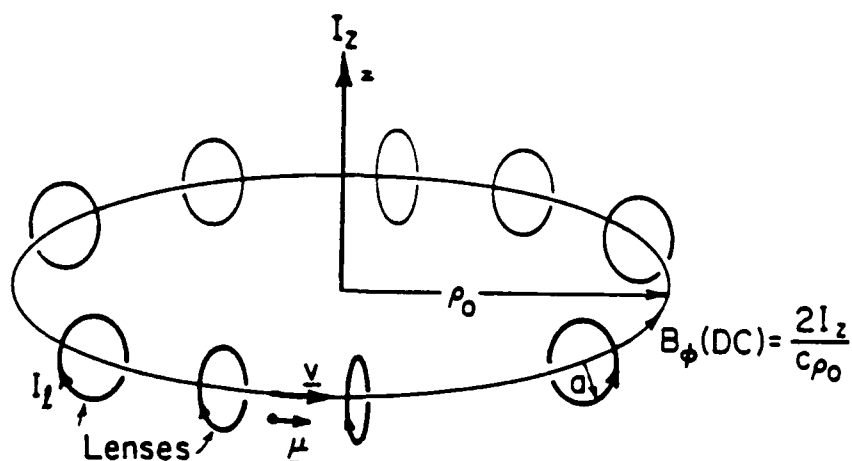
Figure 3: Geometry of the storage ring.

ρ_0 (cm)	N_l	I_ℓ (A)	a (cm)	Δv_s (m s^{-1})	Δv_x (m s^{-1})	Δv_y (m s^{-1})
25	12	8000	1	3	4	
25	20	8000	1	6	9	10
25	24	8000	1	10		12
25	28	8000	1	9		12
25	32	8000	1	12		≥ 14
20	12	8000	1			
10	12	8000	1	6		12
5	12	8000	1	no stable orbits found		
5	6	8000	1	6		12

Table 1:   A summary of the single particle simulations of the storage rings,   listing: ρ_0 the major radius; N_ℓ the number of current-loop lenses; I_ℓ the current through one of the current loops, a the radius of the current loops; Δv_s the longitudinal passband for zero initial transverse velocity; Δv_x the transverse passband in the plane of the ring; and Δv_y the transverse passband perpendicular to the plane of the ring. Blank spaces in the passband columns indicate that no attempt was made to explore that passband. Only one simulation, which was stable, was run for the $\rho_0 = 20$ cm, $N_\ell = 12$ ring.

The average toroidal velocity is 100 m/s, and the DC toroidal magnetic field is 1.8 T at the major radius.

J. T. Bahns

Key Problems and Hydrogen Atom Formation

Key Problems
and
Hydrogen Atom Formation

J. T. Bahns
UDRI
AFAL/LKCS/MS24
EAFB, Ca. 93523-5000

Abstract

This paper is divided into two parts: First, key problem areas in the cluster ion approach to containerless condensation are reviewed. In the second part, problems and strategies involving the first step in the overall synthesis (H atom formation) are discussed.

I Key Problems

As a result of the Workshop and analysis to date on the "Cluster Ion Approach," a number of problem areas have been identified:

A. Problems with cluster ion synthesis:

It has been known since the HCISG meetings that the "bottleneck" to the overall synthesis involves the smallest hydrogen cluster fragments: H, H_2^+, H_2, H_3^+, H_4^+..., H_c^+, where H_c^+ is a critically sized "seed" cluster ion that possesses enough internal degrees of freedom to withstand collisions (without fragmentation) with a suitable reactant (say H or H_2 etc.). It has been estimated by Tardy (see appendix) that the threshold cluster ion size for $H_2(v=0, j=0)$ addition (M^+) is at around $c=29$. The threshold cluster size for the A^+ path is not known and there have been no attempts to determine if it exists. It is understood that the synthesis of small cluster ions will be slow as well as difficult, but one may argue that once the seed cluster ion(s) exist, the growth rates will be limited to how fast the reactant can be produced (hence the ideal reactant is likely the one that can be produced the fastest).

The most desirable synthetic path (A^+), utilizes H as a reactant and is thus limited by H atom formation rates. If the H atoms must be in the ground (1S) state, the cluster ion growth rates may be rather seriously limited. However, the rates should be larger if Rydberg atoms (that is, association through excited states) can be used. It seems clear in any event that H atom formation is of central importance to the cluster ion approach and will be discussed as a separate topic.

One key problem currently being studied theoretically is the A^+ path involving the production of an odd cluster ion (from an even one, where n is the number of protons in the cluster):

$$H_n^+ \text{ (even) } + H = H_{n+1}^+ \text{ (odd) } + h\nu.$$

This reaction is exoergic by roughly 4.5 eV, and will likely proceed via the elimination of H_2. Is it possible to perform this step in a way that does not deposit excessive amounts of energy into the cluster ion? The reaction to produce an even cluster ion,

$$H_n^+ \text{ (odd) } + H = H_{n+1}^+ \text{ (even) } + h\nu,$$

is much less exoergic (a few tenths of eV's), with correspondingly less tendency to fragment the cluster ion. A number of other questions are closely related:
- What are the radiative cooling rates of the hydrogen cluster ions in the ground states?
- Are there viable pathways involving excited states?
- What steps can be stimulated, and how?
- What are the relative radiative vs. unimolecular decomposition rate constants as a function of cluster ion size?
- How does the association exoergicity couple to the degrees of freedom of a cluster ion?
- What wavelengths and photon fluxes will cluster ions tolerate without photofragmentation?
- Is there vapor pressure data on hydrogen cluster ions?
- Are there unstable cluster ions (e.g. H_{11}^+)?
- Are there significant advantages to clustering about larger nuclei (e.g. deuterium or helium ions)?

A critical issue in the formation of small cluster ions is the formation of cold reactants (see reports by Sando and Weiner). Since small cluster ions have binding energies of only a few tenths of eV's and possess relatively few states, it is vital (with the possible exception of H_2^+ formation) that the association reactions through the ground state manifolds be done with no excess energy. Hence the reactants must be vibrationally, rotationally, and translationally cold. Both H_2^+ and H_2 present difficulties in this regard since neither have dipole allowed transitions in their ground states. This problem might be circumvented by utilizing deuterium or helium nuclei.

B. Other problems

1.   The elimination of background gas is considered an engineering problem.

2.   The cooling of H atoms seems to be an unavoidable task; hence there is a real need for laser cooling (see report by W. Phillips). The development of an efficient, quasi-continuous laser at the Lyman-alpha wavelength has been considered in this Workshop (see report by T. McIlrath). Recent advances in the development of VUV sources and McIlrath's analysis imply that this problem may well be solved in the near future.

3.   Large volume storage of cluster ions will likely be needed. This is a very worthy problem that has been considered in detail by D. Wineland (these proceedings).

4.   Clustering about larger nuclei has not been considered in this workshop so a brief discussion will be included here. The production rates of antideuterium and antihelium-3 nuclei are currently large enough (1) to justify a detailed analysis of these pathways. Low temperature, 13 K, reactions of He^+ with H_2 in ion traps have been studied recently by Barlow, (2) who has also reviewed the extensive literature on this system.

The clustering pathways for the buildup of mixed hydrogen/deuterium cluster ions are the same as for those using only hydrogen. However, one obvious advantage in using deuterium is that radiative transitions in the ground state of HD are dipole allowed. This means that if the M^+ process is required, the production of internally cold reactant molecules becomes easier.

Certainly the radiative properties of cluster ions that are mixtures of H and D will be different. The ground state radiative rates of the mixed cluster ions should exceed those of the pure cluster ions. It has been found in the photodissociation studies (see report by Yeh) that the peripheral H_2 molecules belonging to cluster ions larger than 13 do not radiate (or absorb) in the infrared; hence the addition of HD could be a significant advantage in the build up of cluster ions beyond this size. Thus, studies should be conducted to determine critical cluster ion sizes for the A^+ and M^+ pathways involving mixed clusters.

Antihelium-3 presents an interesting variation to the problem of containerless condensation. HeH^{++} is not bound in the ground state, and the larger dipositive cluster ions are probably not stable. Likewise, the negative cluster ions are probably not stable and will be dismissed at this time. The singly charged positive cluster ions should all be stable (HeH^+ is bound by 1.8 eV). HeH_2^+ has been observed experimentally and is bound by 0.2 eV relative to $H_2 + He^+$ (2). Although no information on the larger ions (or their radiative properties) is at hand, they will likely be bound by tenths of eV's via the ion-induced dipole force. Because He^{+1} has a 1s electron, the number of states available to a collision complex with this ion is increased, and this should increase its lifetime and diminish the probability of unimolecular decomposition. This would be a noticeable advantage in the bottle neck region (particularly reaction b, below), where condensation is made difficult by the general lack of available internal states. Presumably, the analogous A^+ clustering pathway should proceed via:

a. $He^{++} + e = He^+ + h\nu$,
(or) $He^{++} + H = He^+ + H^+$
b. $He^+ + H = HeH^+ + h\nu$
c. $HeH^+ + H = HeH_2^+ + h\nu$ ...
d. $HeH_n^+ + H = HeH_{n+1}^+ + h\nu$.

Because the first ionization potential of He exceeds that of H (by 11 eV), the charge on these cluster ions beyond N=3 will reside primarily as H_3^+ (rather than as He^+), and the neutral He will likely be ejected from the cluster ion and lost. The M^+ and A^+ pathways would be analogous to the pure hydrogen case.

224

The lack of stable nuclei at mass 5 and the very low probability of producing ^{6}Li (and larger) nuclei tends to preclude the possibility of their use. This topic is reserved for a later date.

II H Atom Formation

The H atom formation problem is rather serious since the spontaneous recombination rate of electrons and protons is likely the rate limiting step in the prescribed condensation.

The recombination of electrons and protons has been understood for a long time (3) and numerous formulae are in the literature that allow one to calculate accurate cross sections and rate constants (4-7). The rate constant for spontaneous radiative recombination is 10^{12} cm^3 s^{-1} (@ $E_{c.m.}$=0.2 eV). If one assumes a minimum production rate of 1 mg of antimatter per year (=10^{14} s^{-1}) as reasonable, an effective volume is implied. If the ion density is (space charge limited) 10^7 cm^{-3}, the rate of H atom formation is 10^2 cm^{-3} s^{-1}. But one must condense at 10^{14} s^{-1}, so the effective volume becomes,

$$V = (10^{14} \text{ s}^{-1})/(10^2 \text{ cm}^{-3} \text{ s}^{-1}) = 10^{12} \text{ cm}^3 = 10^6 \text{ M}^3.$$

A similar calculation can be performed if one considers the effective volume resulting from the finite cooling rate of cluster ions. If one assumes that the radiative cooling rate of a given cluster ion (in a single radiative association that increases its mass by 1 AMU) is 0.1 s^{-1}, then

(10^{15} cluster) X (0.1 assoc./s cluster) X (10^7 s/year)=10^{21} assoc./yr.

If, in addition, the cluster ion density is limited to 10^7 cm^{-3}, the storage volume becomes only10^2 M^3, implying that H atom formation (rather than radiative rates) is the more serious probem.

One possibility for improving recombination rates is to reduce the temperature of the electrons. Using simplified rate constant formulae for the capture of low-energy electrons by stationary protons for thermal Maxwellian and "flattened" Maxwellian distributions (8):

$$\alpha \text{ (Maxwell)} = 3.79 \ (kT)^{-0.678} \ X \ 10^{-13} \ cm^3 \ s^{-1}$$

$$\alpha \text{ (flattened)} = 7.88 \ (kT)^{-0.645} \ X \ 10^{-13} \ cm^3 \ s^{-1}$$

(where kT is the energy in eV), one can estimate the effect of electron cooling on the effective volume (the quoted accuracy is <10% for kT<.01 eV).

kT (eV)	α (flattened) ($cm^3 \ s^{-1}$)	Volume (M^3)
10^{-3}	$9 \ X \ 10^{-12}$	$1 \ X \ 10^5$
10^{-4}	$4 \ X \ 10^{-11}$	$2 \ X \ 10^4$
10^{-5}	$2 \ X \ 10^{-10}$	$5 \ X \ 10^3$
10^{-6}	$7 \ X \ 10^{-9}$	$1 \ X \ 10^3$

At the present time, obtaining a source of electrons with microvolts of kinetic energy would be difficult so one is led to consider the possibility of laser stimulated recombination. This was suggested some time ago by Forward (9) and has been considered in detail recently by Neumann et al. (10) who have proposed a concept for the production of anti-H atoms at LEAR (fig.1).
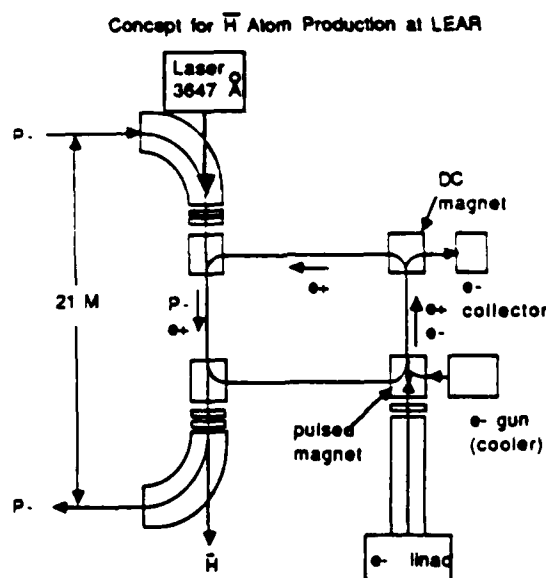

Figure 1. Diagram of proposed anti-H atom production scheme at LEAR.

As shown, an electron-cooled beam of positrons is merged with the main beam of antiprotons. A laser, operating at 3647 Angstroms stimulates free-bound transitions to the $n=2$ level of the anti-H atoms. This transition is saturated (rate of photoionization equals stimulated radiative association) at a laser intensity of about 18 MW/cm^2, and the estimated maximum gain factors for spherical and flattened electron distributions were found to be,

$$G_s max = 7.2$$
$$G_f max = 110.$$

There was found to be a factor of 15 (G_f/G_s) increase in recombination rate for the flattened electron distribution, implying the use of merged beams. However, it has been pointed out by Mitchell et al. (11) that although very low center of mass velocities can be achieved in merged beams, the recombination coefficients do not continue to increase with decreasing electron temperature as implied in the above table due to interaction length, angle, and energy resolution limits imposed in the laboratory.

The rate of spontaneous recombination in a merged beam arrangement is given by,

$$R = \eta \, r^{spont} N_i / \zeta^{*2},$$

where η is the fractional overlap of the two storage rings, r^{spont} is the spontaneous recombination rate for the flattened distributions, N_i is the number of recirculating ions, and $\zeta^{*2} = 1/(1-b^{*2})$ is a relativistic correction factor for obtaining the recombination rate in the laboratory reference frame. Using this formula with

$N_i = 10^{10}$ particles
$r^{spont} = \alpha \, n_e = 2.2 \times 10^{-12} \, cm^3 \, s^{-1} \times 10^8 \, e/cm^3 = 2.2 \times 10^{-4} \, s^{-1}$
$b^{*2} = .47$
$\eta = 0.02$

gives: $R = 10^4$ H atoms s^{-1}. The rate should be increased by a factor of 100 from laser stimulation yielding an H atom

recombination rate of only 10^6 s^{-1}, far less than the 1 mg/year rate of 10^{14} s^{-1}.

As mentioned briefly in the first section, Rydberg atom formation (12, 13) may be an attractive possibility provided that these can somehow be used directly in the condensation.

A final possibility worth mentioning is the use Positronium or Protonium:

a. $\qquad\qquad\qquad e^+e^- + P^- = H + e^-$

b. $\qquad\qquad\qquad P^+P^- + e^+ = H + P^+$.

Reaction (a) seems more useful, at first glance, based on the longer lifetime for Positronium.

In conclusion, the H atom recombination rates are in drastic need of improvement (if one relies upon radiative processes). H atom formation likely be achieved in practice by using:

a. Merged beams (providing flattened distributions).
b. Ion traps using cold electrons and protons in ultra-low energy (center of mass) n-body collision arrangements.
c. Maximum ion densities.
d. Stimulated radiative recombination.

References

1.   Prokoshkin Y. D., "Particles of Antimatter," Die Naturwissenschaften, 59, 281 (1971).

2.   Barlow, S. E., "The Dynamics of Stored Ions and Low Temperature Ion-Molecule Reactions," PhD. Thesis, University of Colorado, Boulder, Colo..

3.   Bates D. R., Buckingham R. A., Massey H. S. W., and Unwin J. J., "Dissociation, Recombination and Attachment Processes in the Upper Atmosphere II: The Rate of Recombination," Proc. Roy. Soc., 170, 322 (1939).

4.   Byron S., Stabler R. C., and Bortz P. I., "Electron-Ion Recombination by Collisional and Radiative Processes," Phys. Rev. Lett. 8, 376 (1962).

5.   Johnson L. C. and Hinnov E., "Ionization, Recombination, and Population of Excited States in Hydrogen Plasmas," J. Quant. Spectrosc. Radiat. Transfer., 13, 333 (1973).

6.   Massey H. S. W., and Gilbody H. B., "Electronic and Ionic Impact Phenomena," Oxford at the Clarendon, Vol 4 (1974).

7.   Stevefelt J., Boulmer J., and Delpech J. F., "Collisional-Radiative Recombination in Cold Plasmas," Phys. Rev. A, 12, 1246 (1975).

8.   Bell M. and Bell J. S., "Capture of Cooling Electrons by Cool Protons," Particle Accelerators, 12, 49 (1981).

9.   Forward R. L., "Antiproton Annihilation Propulsion," AFRPL Special Publication, F04611-83-C-0046/UDR-TR-85-55, (Sept 1985).

10.   Neumann R., Poth H., Winnacker A., and Wolf A., "Laser-Enhanced Electron-Ion Capture and Antihydrogen Formation," Z. Phys. A-Atoms and Nuclei, 313, 253 (1983).

11.   Auerbach D., Cacak R., Caudano R., Gaily T. D., Keyser C. J., McGowan J. Wm., Mitchell J. B. A., and Wilk S. F. J., "Merged Electron-Ion Beam Experiments I. Method and Measurements of (e-H_2^+) and

(e-H$_3^+$) Dissociative-Recombination Cross Sections," J. Phys. B: Atom. and Molec. Phys., 10, 3797 (1977).

12. Haroche S. and Raimond J. M., "Radiative Properties of Rydberg States in Resonant Cavities," Advances in Atomic and Molecular Physics, Academic Press, 20, 347 (1985).

13. Gallas J. A. C., Leuchs G., Walther H., and Figger H., "Rydberg Atoms: High Resolution Spectroscopy and Radiation Interaction-Rydberg Molecules", Advances in Atomic and Molecular Physics, Academic Press, 20, 413 (1985).

R. L. Forward

Production of Heavy Antinuclei: Review of Experimental Results

PRODUCTION OF HEAVY ANTINUCLEI: REVIEW OF EXPERIMENTAL RESULTS

Dr. Robert L. Forward
Senior Scientist
Hughes Research Laboratories
3011 Malibu Canyon Road
Malibu, California 90265 USA

23 April 1987

PRODUCTION OF HEAVY ANTINUCLEI: SUMMARY OF EXPERIMENTAL RESULTS

Dr. Robert L. Forward
Hughes Research Laboratories
Malibu, California 90265 USA

ABSTRACT

Antinuclei heavier than antiprotons, such as antideuterons, antitritons, antihelium-3, and larger antinuclei, might be useful in the initial phases of the nucleation and growth of antihydrogen cluster ions from antiprotons and antielectrons (positrons). The heavier antinuclei could possibly be used as seed catalysts to initiate the growth of a cluster ion, or to broaden or increase the number of infrared emission lines for radiation cooling purposes, or to break the symmetry of the smaller cluster ions, thus changing the large difference in binding energy between clusters with even versus odd numbers of atoms. There also may be other uses for heavy antinuclei, antiatoms and excited antiatom species that will be discovered once it is realized that small quantities can be obtained using variations on present antiproton production, capture, and trapping techniques. This paper summarizes the experimental work to date on the production of antideuterium, antitritium, and antihelium nuclei, and the prospects for production of heavier antinuclei such as antilithium. The general experimental trend is that the ratio of production of antideuterons to antiprotons is 10^{-4}, antitritium and antihelium-3 to antiprotons is 10^{-8}, and each added baryon lowers the production rate by another factor of 10^{-4}. A typical facility using high energy protons striking metal targets can produce about 10^{15} antiprotons per day (about a nanogram), of which only 0.1% or 10^{12} (about a picogram) is captured. Thus, if special collection apparatus were used to separate out these heavier antiparticles and the collection efficiency was the same as that for antiprotons (0.1%), then along with the 10^{12} antiprotons being captured there would be 10^8 antideuterons, 10^4 antitritons and antihelium-3 nuclei, and 1 antihelium-4 nuclei. In addition, there are alternative proposals for producing antideuterium through colliding beams of antiprotons that may ultimately prove to be more effective in producing significant quantities of captured antideuterons. Extension of these techniques to colliding beams of heavy antinuclei may even allow fabrication of small amounts of very heavy antinuclei that are not feasible using the straight proton-target production approach.

234

INTRODUCTION

The availability of small numbers of heavy antinuclei may be useful in certain scientific and technological areas. Some examples would be the use of antideuterium and antitritium in the initial phases of antihydrogen cluster ion nucleation and growth, or the use of antihelium or antilithium with their multiple ionization states as a catalyst for antihydrogen cluster ion or antihydrogen ice crystal growth. Muon catalyzed fusion of antideuterium and antitritium to produce antihelium and an antineutron could also be attempted to search for any anomalous results from the use of antiparticles.

This paper is a brief review of the experimental results reported in the literature on the relative formation rates of heavy antinuclei. Most of this work was done in the 1970s, soon after the particle accelerator energies were sufficient to produce heavier antiparticles than antiprotons. After a brief flurry of papers, interest in production of heavy antinuclei dropped off and later papers only mention the production of heavy antinuclei in passing with the major emphasis being on searches for more exotic particles with approximately the same masses.

The threshold for production of antiprotons in pp collisions is 5.6 GeV, for antideuterons it is 15 GeV, for antitritium and antihelium-3 it is 28 GeV, for antihelium-4 it is 45 GeV, etc. For the efficient production of antinuclei it is necessary that the incident proton energy be considerably greater than these threshold values. For example, as the incident particle energy is increased from 30 to 70 GeV, the yield of antideuterons increases by more than an order of magnitude.

The production rate of heavy nuclei varies with a large number of parameters, the incident particle type and energy, the target type, and the output heavy antinuclei type, energy (momentum), and production angle. The variations with incident particle type, target nuclei type, and production angle turn out to be small ($<50\%$). Even e^+e^- beam collisions give almost the same rates as proton-target interactions at the same center of mass energy. The major variation in production rate is the variation with output antiparticle type, with the antiproton production rate being a few percent of the pion production rate, the antideuteron production rate being 10^{-4} of the antiproton production rate, and succeeding antinuclei being down another factor of 10^{-4} for each additional antibaryon.

The simple model[1] that seems to fit the data is that it is necessary that several antinucleon-nucleon pairs be produced simultaneously, and that the antinucleons travel off in nearly the same direction at the same speed so they are close enough to "stick" together to form an antinucleus.

Most of the experimental measurements surveyed are reported as a ratio of the production of the heavy antinuclei at a given

momentum and production angle compared to the number of negative pions with the same momentum and production angle, because this is an easy measurement to make. Sometimes this ratio is (or can be) converted to the number of heavy antinuclei at a given momentum and production angle compared to the number of antiprotons at the same momentum and production angle. Less seldom the absolute production rate of pions is also determined (or estimated) and an absolute production cross section for the heavy nuclei from the given target nucleus is given. There are small but significant differences in production rates from different target materials.

HEAVY ANTINUCLEI EXPERIMENTAL RESULTS

The first report of the production of antideuterons seems to have been in 1965 at the Alternating Gradient Synchrotron (AGS) at Brookhaven National Laboratory by a team from Columbia University[1]. They used the 30 Gev (BeV in 1960s notation) proton beam from the AGS on a beryllium target. About 200 heavy antinuclei events were reported and the ratio of antideuterons to negative pions at this low energy was only 5.5×10^{-8}. No firm evidence was found for antitritium. This team barely beat out another group in Europe[2] who also observed antideuterons using the 19.2 GeV/c proton beam from the CERN Proton Synchrotron. Their antideuteron to negative pion production ratio was 8×10^{-9}. In 1969 an IHEP-CERN Collaboration[3] made measurements at incident proton energies of 43, 52, and 70 GeV, and a number of antideuteron energies and production angles. This was followed in 1971 by further measurements at low antideuteron momenta by an IHEP team[4], again using 70 GeV protons on aluminum targets. The results of all the IHEP experimental measurements at 70 GeV is shown in Figure 1. At the peaks of the 70 GeV production curves, which occurred around 13 GeV/c secondary particle momentum, the ratio of antiprotons to pions was about 3×10^{-2}, and the ratio of antideuterons to pions was about 3×10^{-6}, giving a ratio of antideuterons to antiprotons of about 10^{-4}.

The same IHEP team[5,6] also reported in 1971 the first observation of antihelium-3 from 70 GeV protons on aluminum. A total of five antihelium-3 particles were observed out of 2.4×10^{11} particles (mostly negative pions) passing through the apparatus. The ratio of the differential cross section for the production of doubly ionized antihelium-3 nuclei at a momentum of 20 GeV/c compared to the negative pion at a momentum of 10 GeV/c was measured as 2×10^{-11}. In 1974, essentially the same group[7] reported the production of four antitritium nuclei with 70 GeV protons on aluminum. The production ratio of antitritons to negative pions was about 10^{-11}. Although the statistics of the heavier nuclei are bad, it is possible to draw a trend curve of the relative production ratio. The (sparse) data for 70 GeV proton on aluminum production ratios of antideuterons, antitritons, and antihelium-3 nuclei with respect to antiprotons (instead of negative pions) is shown in Figure 2.
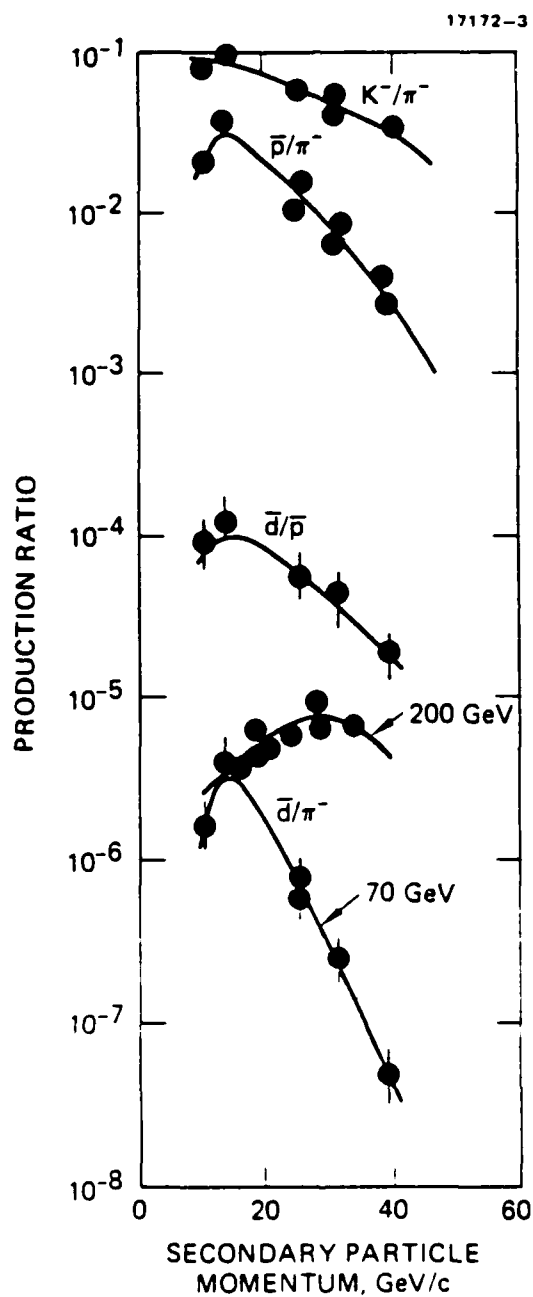
Figure 1 - Secondary particle production ratios as a function of
secondary particle momentum for 70 GeV protons[3,4] and 200 GeV
protons[3] on aluminum targets.

Figure 2 - Heavy antinuclei production ratio compared to the antiproton production ratio as a function of secondary antinucleus baryon number.

238

With the advent of the 200 GeV SPS machine at CERN, experiments were initiated in 1978 that produced copious quantities of antideuterons, ten antihelium-3 nuclei, and three antitritium nuclei[8]. The production ratio of antideuterons to negative pions was measured as a function of the secondary particle momentum and as shown in Figure 1, a broad peak was found at 30 GeV/c compared to the 13 GeV/c for antideuterons produced by 70 GeV protons. Later experiments[9] in 1979 increased the number of heavier antinuclei to 99 antitritons and 94 antihelium-3 nuclei. From this data the relative production ratio compared to negative pions is 3×10^{-2} for antiprotons, 4.6×10^{-6} for antideuterons, 1.3×10^{-9} for antitritium, and 3×10^{-10} for antihelium-3. This is also plotted in Figure 2 with the heavier antinuclei production ratios given as the production rate with respect to antiprotons rather than negative pions. At that time all the available data[1-12] on the production of antideuterons at low transverse momentum seemed to show a smooth trend as shown by the open data points in Figure 3 taken from Bozzoli, et al.[8] There was an increase in antideuteron production rate with increasing incident proton energy, leveling off at about 5×10^{-6} antideuterons per negative pion above 200 GeV. The solid line drawn through the data points is the square of the production ratio for antiprotons to negative pions at half the antideuteron momentum, as a simple model for the antideuteron production ratio.

Measurements in 1978 of the ratio of production of deuterons to antideuterons in proton-proton beam collisions at the CERN ISR Collider[12] at a center-of-mass energy of 53 GeV (1400 Gev equivalent p->N energy) gave a value of 3.8 deuterons to antideuterons, which is close to the square of the ratio of protons to antiprotons. This gives credence to the simple model[1] that if (anti)deuterons are produced as the result of the overlap of two produced (anti)nucleons, then the deuteron to antideuteron ratio should equal approximately the square of the ratio of protons to antiprotons at the same transverse momentum per (anti)nucleon.

Later experiments in 1985 that included correction factors for relative absorption of negative pions and antideuterons gave a value of 5.8×10^{-6} antideuterons per negative pion[13]. Then more data points were generated by other experiments with the highest energies being reached by experiments that involved protons colliding with protons. The data for the antideuteron to negative pion production ratio as a function of the equivalent incident beam momentum in many different experiments with different targets and different secondary momentum is shown as the filled spots in Figure 3 taken from Thron, et al.[13] The smooth trend with a leveling off above 200 GeV is now not so clear, and there could be a possibility that the production ratio of antideuterons (and presumably the heavier antinuclei) is increasing with increasing production energy above 200 GeV.
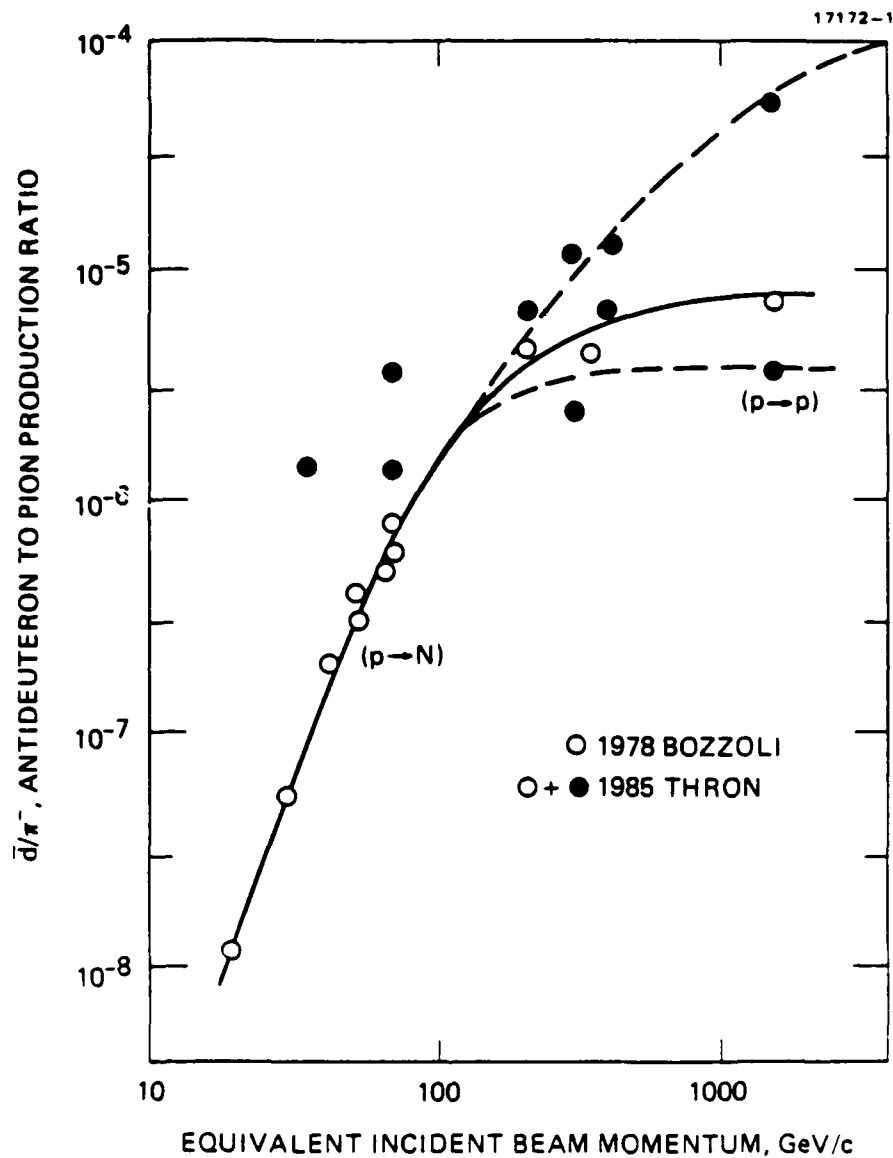
Figure 3 - Antideuteron to negative pion production ratio as a
function of effective incident proton beam momentum.

Antideuterons have also been observed in electron-positron annihilation collisions at 10 GeV center-of-mass energy in the ARGUS detector at the DORIS II storage ring at DESY in Hamburg, Germany[14]. A total of six candidates passed the selection criteria for antideuterons. The production rate for antideuterons was about 2×10^{-5} per hadronic event compared to a production rate for antiprotons of 2×10^{-1} per hadronic event, or a ratio of antiprotons to antideuterons of 10^{-4}, similar to that observed in proton-proton or proton-target interactions.

PRODUCTION CROSS SECTIONS

A few production cross sections have been given in some of the papers. To convert production cross sections per target nucleus (usually ^{27}Al or ^{9}Be) to production cross sections per nucleon, the accepted procedure is to divide by $A^{2/3}$, which is 9 for Al and 4.33 for Be.

For 30 GeV/c protons on Be:[1]
antideuterons at 5 GeV/c 7×10^{-33} cm^2/sr•(GeV/c)•Be

For 70 GeV/c protons on Al:[4]
antideuterons at 13 GeV/c 3×10^{-30} cm^2/sr•(GeV/c)•Al
antitritons at 25 GeV/c $1.0 \pm 0.6 \times 10^{-35}$ cm^2/sr•(GeV/c)•Al
antihelium-3 at 20 GeV/c 2.0×10^{-35} cm^2/sr•(GeV/c)•Al

For 200 GeV/c protons on Be:[9]
antihelium-3 at 21 GeV/c $1.3 \pm 0.3 \times 10^{-34}$ cm^2/sr•(GeV/c)•Be
antihelium-3 at 47.4 GeV/c $1.9 \pm 0.3 \times 10^{-34}$ cm^2/sr•(GeV/c)•Be
antitritons at 23.7 GeV/c $7.6 \pm 0.9 \times 10^{-34}$ cm^2/sr•(GeV/c)•Be

SUMMARY OF EXPERIMENTAL RESULTS

If we extrapolate the data to date on the production of heavy antinuclei as shown in Figure 2, we can predict that at machine energies above 200 GeV, that for 10^{12} antiprotons captured (roughly one day's production at CERN or Fermilab) we could expect to capture 10^3 antideuterons, 10^5 antitritons, 10^4 antihelium-3 nuclei, and 1 antihelium-4 nuclei. Antilithium will have to wait for higher machine energies, greater beam currents, and especially better collection efficiencies.

Since machines exist that make large numbers of antiprotons using proton-target interactions, it is relatively simple to consider the installation of a diverter and a collection ring after the target and focusing lens to capture other particles than antiprotons. It might even be possible to make such an installation without significantly affecting the collection of antiprotons. It was estimated[15] in 1982 that the Antiproton Accumulator could store 2 antideuterons per production pulse at 3.5 GeV/c. At 7 GeV/c this number would be increased by a factor of 40. Another factor of 80 could be gained in the production rate if antideuteron beams of 30 GeV/c were produced from 200 GeV

primary protons. Thus, for planning purposes, it is probably best to assume that if antideuterons or heavier antinuclei are urgently needed for some critical scientific experiments or to overcome some bottleneck in the development of antimatter technology, that they can be obtained using the same machines that are presently producing antiprotons. There are alternate methods for producing heavy antinuclei, however, and they may have some advantages.

ALTERNATE HEAVY ANTINUCLEI PRODUCTION CONCEPTS

Since cooled antiproton beams are now available at low energy at CERN and high energy at Fermilab, it is possible to consider using these beams for the production of antideuterons through the reaction $\bar{p} + \bar{p} \rightarrow \bar{d} + \pi^-$. The process occurs in 8% of all $\bar{p}\bar{p}$ reactions. The details of arranging the reactions and capturing the resulting deuterons are discussed in two papers[15,16]. In principle the reaction could be iterated to produce antihelium ions and perhaps heavier antinuclei, although there have been no publications discussing this concept in any detail.

It is also well known that negative muons can be used as a catalyst to initiate fusion of a DT molecule to produce He^4 and an energetic fusion neutron. Once we have copious amounts of trapped neutral antihydrogen molecules with a large component of antitritium and antideuterium nuclei, we could attempt the formation of antihelium-4 by subjecting the trap to a positive muon beam.

ACKNOWLEDGMENTS

REFERENCES

[1] D.E. Dorfman, J. Eades, L.M. Lederman, W. Lee, and C.C. Ting, "Observation of Antideuterons", Physical Review Letters 14, 1003-1006 (14 June 1965).

[2] T. Massam, Th. Muller, B. Righini, M. Schneegans, and A. Zichichi, "Experimental Observation of Antideuteron Production", Il Nuovo Cimento 39, 6574-6578 (1 September 1965).

[3] F. Binon, P. Duteil, V.A. Kachanov, V.P. Khromov, V.M. Kutyin, V.G. Lapshin, J.P. Peigneux, Yu.D. Prokoshkin, E.A. Razuvaev, V.I. Rykalin, R.S. Shuvalov, V.I. Solianik, M. Spighel, J.P. Stroot, and N.K. Vishnevsky, "Production of Antideuterons by 43 GeV, 52 GeV, and 70 GeV Protons", Physics Letters 30B, 510-513 (24 November 1969).

[4]Yu.M. Antipov, N.K. Vishnevskii, Yu.P. Gorin, S.P. Denisov, S.V. Donskov, F.A. Ech, A.M. Zaitsev, V.A. Kachanov, V.M. Kut'in, L.G. Landsberg, V.G. Lapshin, A.A. Lebedev, A.G. Morozov, A.I. Petrukhin, Yu.D. Prokoshkin, E.A. Razuvaev, V.I. Rykalin, V.I. Solyanik, D.A. Stoyanova, V.P. Khromov, and R.S. Shuvalov, "Production of Negative Particles with Low Momenta by 70-BeV Protons", Yad. Fiz. **13**, 135-138 (January 1971) [English translation: Soviet Journal of Nuclear Physics **13**, 78-79 (July 1971)]; essentially the same data and graphs also appeared in: Yu.M. Antipov, S.P. Denisov, S.V. Donskov, Yu.P. Gorin, V.A. Kachanov, V.P. Khromov, V.M. Kutjin, L.G. Landsberg, V.G. Lapshin, A.A. Lebedev, A.G. Morozov, A.I. Petrukhin, Yu.D. Prokoshkin, E.A. Razuvaev, V.I. Rykalin, V.I. Solyanik, D.A. Stoyanova, R.S. Shuvalov, N.K. Vishnevskii, F.A. Yetch, and A.M. Zaytzev, "Production of Low Momentum Negative Particles by 70-GeV Protons", Physics Letters **34B**, 164-166 (1 February 1971).

[5]Yu.M. Antipov, N.K. Vishnevskii, Yu.P. Gorin, S.P. Denisov, S.V. Donskov, F.A. Ech, G.D. Zhilchenkova, A.M. Zaitsev, V.A. Kachanov, V.M. Kut'in, L.G. Landsberg, V.G. Lapshin, A.A. Lebedev, A.G. Morozov, A.I. Petrukhin, Yu.D. Prokoshkin, E.A. Razuvaev, V.I. Rykalin, V.I. Solyanik, D.A. Stoyanova, V.P. Khromov, and R.S. Shuvalov, "Observation of Antihelium 3", Yad. Fiz. **12**, 311-322 (August 1970) [English translation: Soviet Journal of Nuclear Physics **12**, 171-172 (February 1971)].

[6]Yu.D. Prokoshkin, "Particles of Antimatter", Die Naturwissenshaften **59**, 281-284 (1972).

[7]N.K. Vishnevskii, M.I. Grachev, B.I. Rykalin, V.G. Lapshin, V.I. Solyanik, Yu.S. Khodyrev, V.P. Khromov, B.Yu. Baldin, L.S. Vertogradov, Ya.V. Grishkevich, Z.V. Krumshtein, R. Leiste, Yu.P. Merekov, V.I. Petrukhin, D. Pose, A.I. Ronzhin, I.F. Samenkova, V.M. Suvorov, G. Cheminitz, N.N. Khovanskii, B.A. Khomenko, M. Szawlowski, G.A. Shelkov, and J. Schuler, "Observation of antitritium nuclei", Yad. Fiz. **20**, 694-708 (October 1974) [English translation: Soviet Journal of Nuclear Physics **20**, 371-378 (April 1975)].

[8]W. Bozzoli, A. Bussiere, G. Giacomelli, E. Lesquoy, R. Meunier, L. Moscoso, A. Muller, R. Rimondi, and S. Zylberajch, "Production of d, t, ^{3}He, anti-d, anti-t, and anti-^{3}He by 200 GeV Protons", Nuclear Physics **B144**, 317-328 (1978).

[9]W. Bozzoli, A. Bussiere, G. Giacomelli, E. Lesquoy, R. Meunier, L. Moscoso, A. Muller, D.E. Plane, R. Rimondi, and S. Zylberajch, "Search for Long-Lived Particles in 200 GeV/c Proton-Nucleon Collisions", Nuclear Physics **B159**, 363-382 (1979).

[10]J.A. Appel, M.H. Bourquin, I. Gaines, L.M. Lederman, H.P. Parr, J.-P. Repellin, D.H. Saxon, J.K. Yoh, B.C. Brown, and J.-M. Gaillard, "Heavy Particle Production in 300 GeV/c Proton/Tungsten Collisions", Physical Review Letters **32**, 428-432 (25 February 1974).

[11]M.G. Albrow, D.P. Barber, P. Benz, B. Bosnjakovic, J.R. Brooks, C.Y. Chang, A.B. Clegg, F.C. Erné, P. Kooijman, F.K. Loebinger, N.A. McCubbin, P.G. Murphy, A Rudge, J.C. Sens, A.L. Sessoms, J. Singh, and J. Timmer, "Search for Stable Particles of Charge >1 and Mass > Deuteron Mass", Nuclear Physics **B97**, 189-200 (1975).

[12]W.M. Gibson, A. Duane, H. Newman, H. Ogren, S. Henning, G. Jarlskog, R. Little, T. Sanford, S.L. Wu, H. Bøggild, B.G. Duff, K. Guettler, M.N. Prentice, and S.H. Sharrock, "Production of Deuterons and Antideuterons in Proton-Proton Collisions at the CERN ISR", Lettere Al Nuovo Cimento **21**, 189-194 (11 February 1978).

[13]J.L. Thron, T.R. Cardello, P.S. Cooper, L.J. Teig, Y.W. Wah, C. Ankenbrandt, J.P. Berge, A.E. Brenner, J. Butler, K. Doroba, J.E. Elias, J. Lach, P. Laurikainen, J. MacLachlan, J.P. Marriner, E.W. Anderson, A. Breakstone, and E. McCliment, "Search for Heavy Charged Particles and Light Nuclei and Antinuclei Produced by 400-GeV Protons", Physical Review **D31**, 451-463 (1 February 1985).

[14]ARGUS Collaboration, "Observation of Antideuteron Production in Electron-Positron Annihilation at 10 GeV Center of Mass Energy", Physics Lett. **157B**, 326-332 (18 July 1985).

[15]D. Möhl, K. Kilian, H. Pilkuhn, and H. Poth, "Production of Antideuterons in Antiproton Rings", Nuclear Instruments and Methods **202**, 427-430 (1982).

[16]H. Koch, K. Kilian, D. Möhl, H. Pilkuhn, and H. Poth, "Antideuterons at LEAR", pp. 877-880, Proceedings Workshop on Physics at LEAR with Low-Energy Cooled Antiprotons", Erice, Italy (9-16 May 1982).

APPENDIX

Proceedings of the Hydrogen Cluster Ion Study Group

Sponsored by
The University of Dayton Research Institute

Conducted at
The Iowa Laser Facility
University of Iowa

J. T. Bahns, K. M. Sando, D. C. Tardy, and W. C. Stwalley
June 30, 1986 – July 11, 1986

TABLE OF CONTENTS

LIST OF PARTICIPANTS

Dr. John T. Bahns
University of Dayton Research Institute
Dayton, Ohio 45469
(805) 275-5540

    Mailing Address:
    AFRPL/LKCS/MS24
    Edwards AFB, Ca. 93523-5000

Prof. William C. Stwalley
Department of Physics and Chemistry
Director, Iowa Laser Facility
(319) 335-1299

    Mailing Address:
    Iowa Laser Facility
    Department of Chemistry CB111
    University of Iowa
    Iowa City, Iowa 52242

Prof. Kenneth M. Sando
Department of Chemistry
University of Iowa
(319) 353-3788

    Mailing Address:
    Department of Chemistry
    University of Iowa
    Iowa City, Iowa 52242

Prof. Dwight C. Tardy
Department of Chemistry
University of Iowa
(319) 353-5497

    Mailing Address:
    Department of Chemistry
    University of Iowa
    Iowa City, Iowa 52242

ABSTRACT

A Hydrogen Cluster Ion Study Group (HCISG) meeting, sponsored by the University of Dayton Research Institute, was held at the University of Iowa (June 30-July 11, 1986) with a twofold purpose: First, to consider the problem of "containerless" condensation of protons, electrons, and hydrogen atoms (and possibly molecules) to form bulk matter (as a simulant for the condensation of bulk antihydrogen). In a closely related task, the participants were also asked to critically analyze the "Cluster Ion Approach" to the problem. Second, to determine and then examine individual aspects of the problem in detail. The greatest difficulty was found to involve the condensation to form the small hydrogen cluster ions (N<30) since condensation of these may necessarily involve the production of cold (translationally, vibrationally, and rotationally) H_2 molecules. The "Cluster Ion Approach" was found to be an acceptable solution. The participants recommended that a workshop be conducted to examine the issues (see individual reports) more closely prior to any lengthy theoretical or experimental investigations.

For simplicity, the discussions presented in this document refer to "normal matter" hydrogenic species.

THE CLUSTER ION APPROACH TO THE CONDENSATION, AND STORAGE OF ANTIHYDROGEN

J. T. Bahns

ABSTRACT

The problem of concentrating antiprotons and positrons into a high energy density form is analyzed from the viewpoint of "the containerless" condensation of hydrogen cluster ions in traps using ion-neutral association. The constraints that lead to the proposed method and the available ion-neutral association channels are discussed. It is found that the condensation method should (if possible) avoid the use of neutral hydrogen dimers. It is concluded that the condensation to produce the first seed (critically sized) cluster ions need only be done once to surmount the main problems associated with "containerless" condensation.

INTRODUCTION

The central problem is the "containerless" assembly of subatomic, atomic, and molecular fragments into bulk antimatter, in this case solid antihydrogen (1). It is necessary to condense antimatter into this form to achieve favorable mass payload fractions when it is used as a fuel for propulsion as well as have a new means of high-energy density storage, when it is used for energy storage. Since this condensation has not been done before and must be done under "containerless" conditions, severe restrictions are placed on the methods to be used. Fortunately, normal matter can be used in all aspects of the investigation since the only relevant difference in the two forms of matter (in this case) is the sign of the charge. Hence, this discussion will refer to normal hydrogen. Because the process by which antiprotons are produced involves relativistic velocities (kinetic energy much greater than interatomic and intermolecular potential energy), the antiprotons must have virtually all of this translational energy removed before condensation. In addition, the process of condensation also requires the removal of significant amounts of chemical energy. The primary emphasis is with the condensation of precooled (this includes kinetic, electronic, vibrational, and

3

rotational) hydrogen fragments in devices such as ion traps
(2-20) to ultimately achieve the large cluster ions of hydrogen.

The problem of laser cooling hydrogen atoms is reasonably
well understood (21-30); the primary task here is the
construction of an appropriate vacuum ultraviolet laser of high
average, and peak power. In recent years six methods have
been used to construct Lyman-Alpha lasers (31-38) that have the
right wavelength (121.57 nM) to cool hydrogen atoms. Laser
manipulation (cooling, deflecting etc.) of neutral molecules of
hydrogen (Figure 1) involves the development of a multiline
cooling laser resembling hundreds of Lyman-Alpha sources. This
is unavoidable for these systems due to redistribution among
numerous available states. However, none of these laser systems
comes close to meeting the power and duty cycle requirements.
At present no such cooling laser exists, although there are
plans to build a free electron laser (39) at Los Alamos, NM
within the next several years that will likely be capable of
cooling hydrogen atoms. However, the development of a cooling
laser for hydrogen atoms will not solve fundamental problems
associated with condensation and storage. It is clear that research
is needed to investigate the character and manipulation of
cluster ions, positively and negatively charged leading to a
definite antimatter synthetic, or condensation, method. This
will be necessary to answer the question of what to do with
cold hydrogen atoms after they have been produced.

DISCUSSION

Since no appropriate condensation method exists, it is
necessary to devise one. There are five primary constraints
that the method or process must employ to be feasible
with present and near future technology. The resulting product
must be in high-energy density, or mass density form implying
clusters. The product should be chemically stable, implying
cluster ions. The process must at all times confine the

LASER-COOLING OF MOLECULES
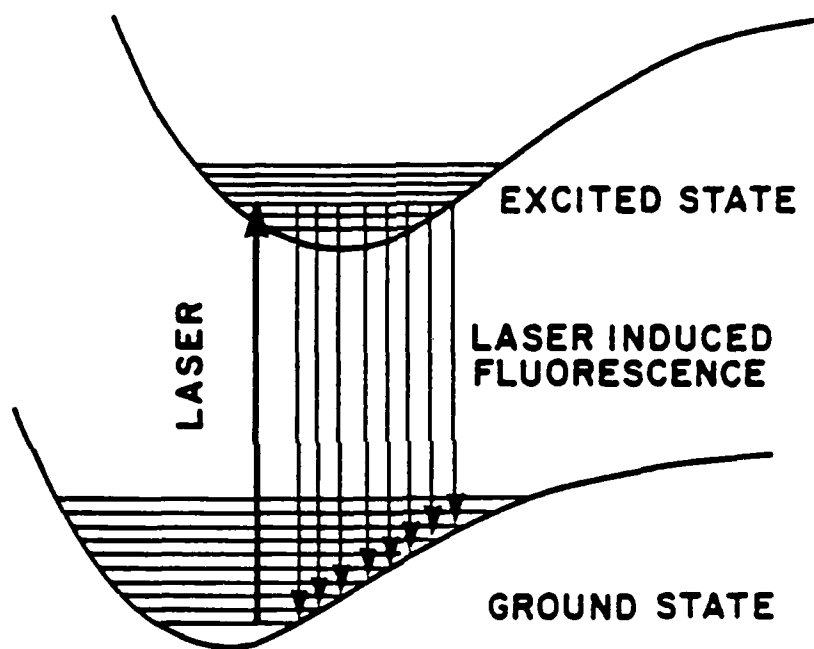
PROBLEM REDISTRIBUTION OF STATES

Figure 1. Schematic of laser-induced fluorescence between two electronic states of a diatomic molecule. Because the minima of the curves seldom coincide, there is efficient redistribution among the lower vibronic states.

antimatter in a tight "containerless" environment that is stable for very long times (months or years), implying ion traps. It must allow for storage in a near perfect vacuum such that annihilation with normal matter is minimized. To achieve such a near-perfect vacuum ($<10^7$ cm^{-3}) environment, it will be necessary to maintain the system, as well as the product cluster ions, at very low temperatures ($<2K$). It is thus concluded that ion clusters of hydrogen (40-54) used in conjunction with ion traps are capable of satisfying these constraints. The resulting "cluster ion approach" has become the first comprehensive plan for the containerless condensation (and confinement) of antimatter into a high-energy density form.

The primary consequences of satisfying the given constraints are: First, the method will be limited to low densities (10^7-10^{10} cm^{-3}). Second, the association rates will also be low ($<10^5$ cm^{-3} s^{-1}). These two difficulties can only be overcome by using large volumes and/or times respectively, or large cluster ions.

Research is needed to understand interactions between hydrogen cluster ions and laser fields such that, upon collision, chemical energy may be released through stimulated or spontaneous emission of a photon, or the ejection of some small fragment. Because wall collisions and expansions cannot be used, special condensation techniques using available third-bodies are necessary. The primary goal is to obtain a detailed understanding of the available association channels. The simultaneous requirements of the association reactions are: release of energy, conservation of momentum, and generation of a larger cluster ion. Generally, the association pathways may be categorized as radiative, for example,

$$H_2^+ + H_2^* = H_4^+ + h\nu,$$

or dissociative,

6

$$H_2^+ + H_2 = H_3^+ + H$$

or

$$H_4^+ + H_2 = H_5^+ + H \quad \text{etc.},$$
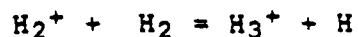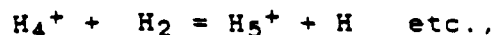
where the (*) denotes an electronically excited state. In the
first case a larger cluster ion is obtained because the channel
allows the excess energy (kinetic, electronic, etc.) to be
radiated as a photon. In the second case the excess energy is
released in the form of kinetic energy of the ejected atom
(certain channels may exist that involve both processes
simultaneously). Furthermore, the channels may involve only
ground state reactants, or have one in an electronically excited
state. As with radiative association; for example, in a cluster
ion containing N hydrogen atoms, there are N-1 possible radiative
photoassociation channels (Figure 2). Currently, the radiative
association channels to form H (55,56) and H_2+ (57-60) are
known. For the larger cluster ions only the channel that
involves H_2 plus a smaller cluster ion has been studied and only
with odd-numbered hydrogen cluster ions (43,45,51,52). Both the
odd (40,53,54) and even-numbered (61-63) positive hydrogen
cluster ion ground state surfaces have been calculated (to
N=11). The odd-numbered negative hydrogen cluster ion ground
states have been calculated (64,65) and H_3- has been observed
(66). Also, in the case of the odd-numbered negative hydrogen
cluster ions, only the ground states have been calculated (65)
(for N<5).

There are many pathways by which ion-neutral association
reactions may proceed, three of which are illustrated
schematically in Figure 3, see also report by W. C. Stwalley).
Path (a) uses the addition of neutral molecules by radiative
association to ions and uses only odd-numbered cluster ions, path
(b) uses the addition of neutral atoms to ions (via radiative
association) producing alternately odd-and even-numbered cluster

$$T^* \quad H + H^+ = H_2^+ + h\nu$$

$$* \quad H_2 + H^+ = H_3^+ + h\nu$$
$$H + H_2^+$$

$$T \quad H_2 + H_2^+ = H_4^+ + h\nu$$
$$H_3 + H^+$$
$$H + H_3^+$$

$$* \quad H_2 + H_3^+ = H_5^+ + h\nu$$
$$H_4 + H^+$$
$$H_3 + H_2^+$$
$$H + H_4^+$$

$$* \quad H_2 + H_4^+ = H_6^+ + h\nu$$
$$H_5 + H^+$$
$$H_4 + H_2^+$$
$$H_3 + H_3^+$$
$$H + H_5^+$$

$$* \quad H_2 + H_5^+ = H_7^+ + h\nu$$
$$H_6 + H^+$$
$$H_5 + H_2^+$$
$$H_4 + H_3^+$$
$$H_3 + H_4^+$$
$$H + H_6^+$$
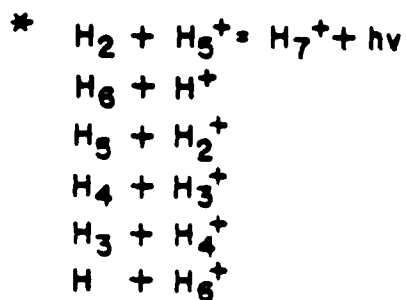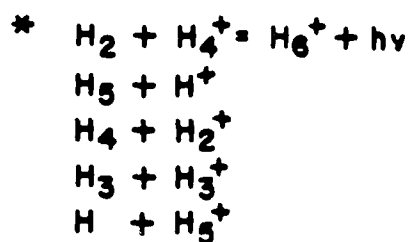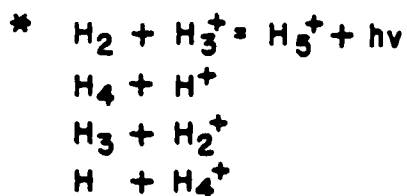
Figure 2.   Hydrogen cluster ion ground state radiative association channels through H_7^+. Known channels are indicated with (*) for experimental and (T) for theoretical studies.

8

Figure 3. Hydrogen cluster ion synthetic pathways involving ground states. The solid (open) circles represent odd (even) positive hydrogen cluster ions.

ions, path (c) uses the addition of neutral molecules to even numbered cluster ions (resulting in the production of either the next larger even or odd cluster ion depending upon the use of the radiative or dissociative channel respectively). The figure also shows the enthalpies involved in the synthesis of small (N<11) hydrogen cluster ions. The small cluster ions are the most important to study because they involve the release of more chemical energy, per step upon condensation, relative to product binding energies, than the larger cluster ions. It is noteworthy that the energy released in each step decreases rapidly in going to larger cluster ions and the overall process proceeds exothermically all the way to the bulk limit.

Figure 4 shows the enthalpies for the ion-molecule association pathway. The diagram is divided into four regions in which different association reactions (see Table 1) may be necessary, or allowed. In the first region the association reactions are limited to the three-body process. This is therefore, presumably the rate limiting regime. The second region uses ion-molecule 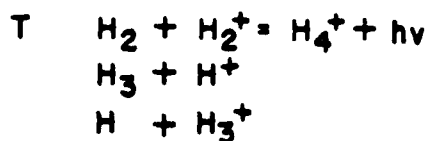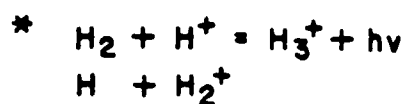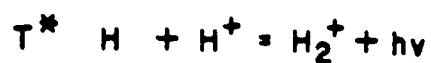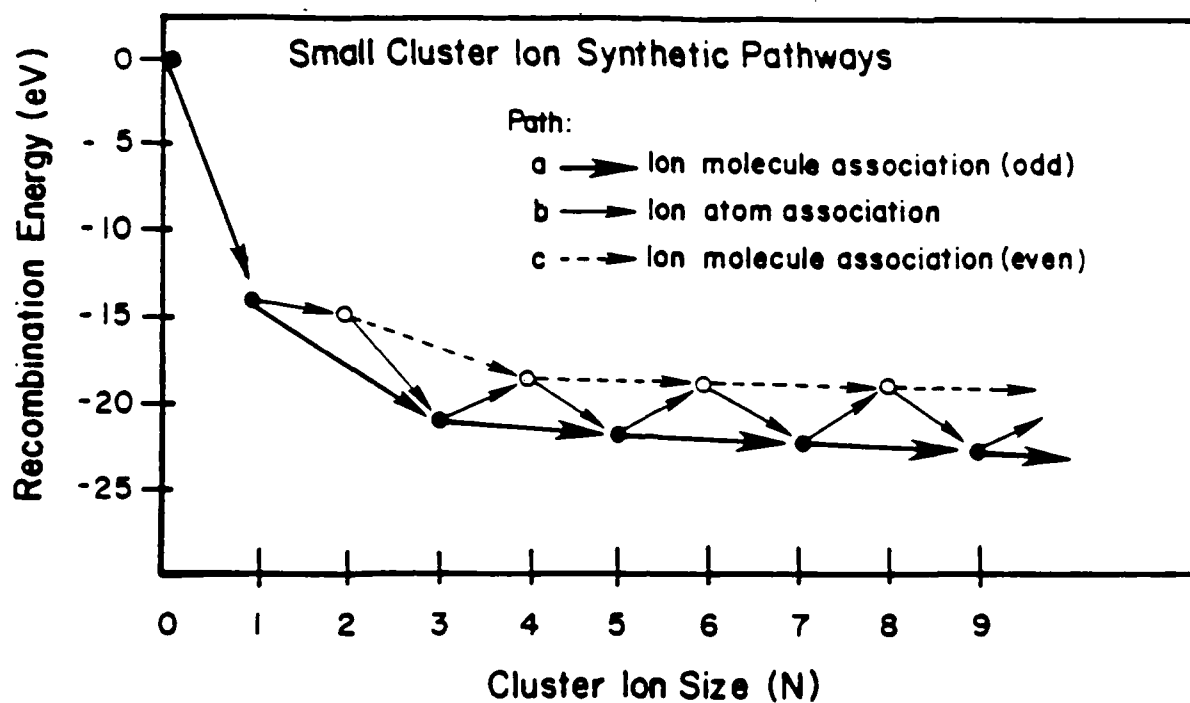association through the ground state manifold. As mentioned, the use of molecules is not desirable; see also report by K. M. Sando. This region is currently believed to extend from N≈30 (see report by D. C. Tardy) to N≈600. At the threshold of this region the reaction,

$$H_2 \ (Ke,V,J) + H_{n=29}^+ \quad \text{<->} \quad (H_{31}^+)^\ddagger = H_{31}^+ \ (Ke,V,J) + h\nu$$
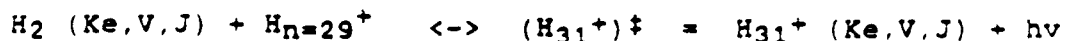
where (*) denotes a vibrationally excited state, proceeds to the right via radiative stabilization. The third region uses the desirable ion-atom association mechanism. Current estimates imply that the critical size positive hydrogen cluster for this association reaction is $N_c(H)$-600 (atoms/cluster). Figure 5 shows an estimate of $N_c(H)$ for ion-atom association using an empirically defined unimolecular dissociation rate (RRK theory) and assumes a radiative rate, in the ground state manifold of $10^3 \ s^{-1}$. The fourth region uses ion-ion association. This

10
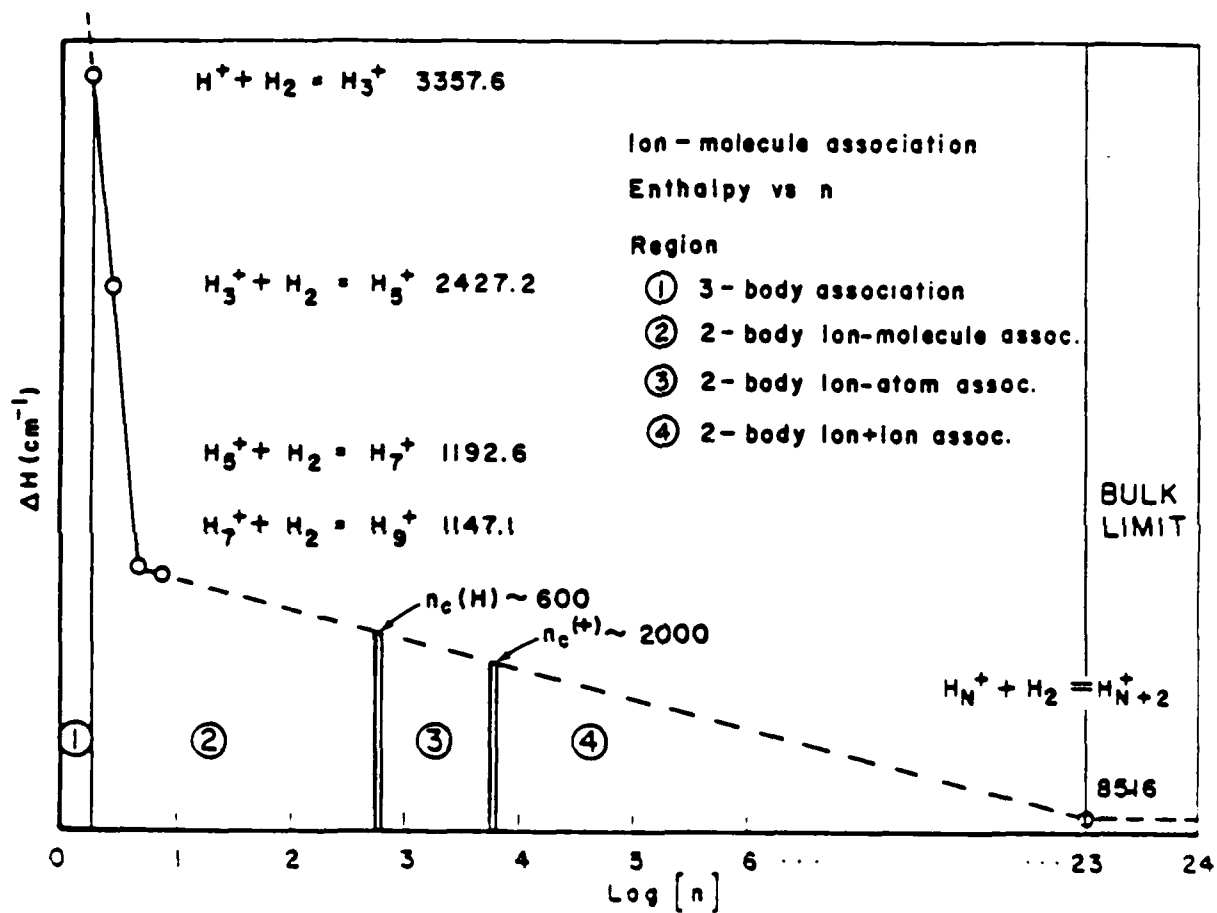
Figure 4. Plot of enthalpy of reaction versus cluster ion size
for ion-molecule association, with extrapolation to
the bulk limit. The bulk limit is taken to be the
work function for H_2 from uncharged solid hydrogen.
The four ideal synthetic reaction zones are also indi-
cated (see text).

11

Table 1. Reactions.

<u>REGION:</u>

   (1) 3-BODY ASSOCIATION

$$H^+ + e^- + h\nu_1 = H + h\nu_2 \qquad\qquad 13.6\ ev$$

$$H + H + h\nu_1 = H_2 + h\nu_2 \qquad\qquad 4.6$$

$$H^+ + H + h\nu_1 = H_2 + h\nu_2 \qquad\qquad 2.6$$
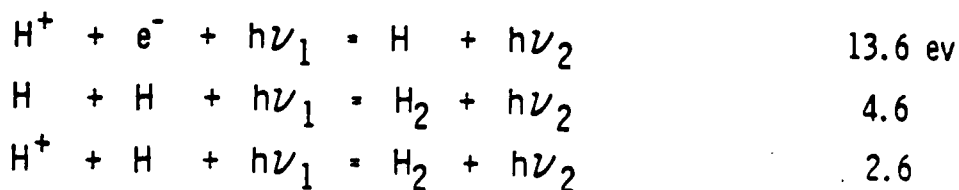
   (2) 2-BODY ION-MOLECULE ASSOCIATION (ODD CLUSTER IONS ONLY!)

$$H^+ + H_2 = H_3^+ \qquad\qquad 4.1$$

$$H_3^+ + H_2 = H_5^+ \qquad k = 1.6 \times 10^{-9}\ \frac{cm^3}{S} \qquad .416$$

$$\vdots \qquad\qquad .301$$

$$\vdots$$

$$H_{n_c(H)-2}^+ + H_2 = H_{n_c(H)}^+$$
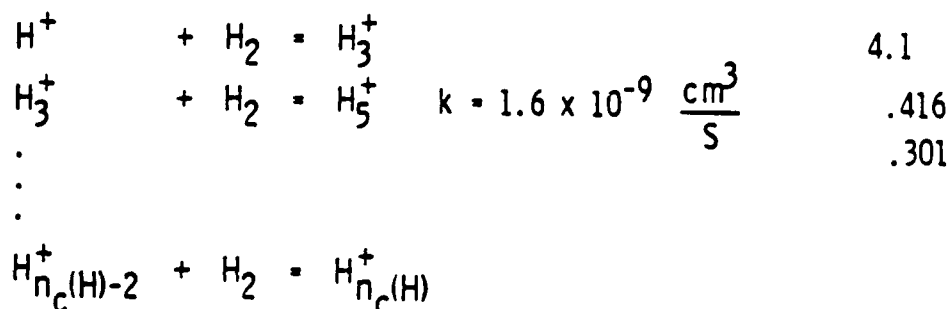
   (3) 2-BODY ION-ATOM ASSOCIATION $n_c(H) \simeq 600$

$$H_{n_c(H)}^+ + H = H_{n_c(H)+1}^+$$

$$H_{n_c(H)+1}^+ + H = H_{n_c(H)+2}^+$$

$$\vdots \qquad\quad \vdots \qquad\quad \vdots$$

$$H_{n_c(+)-1}^+ + H = H_{n_c(+)}^+$$
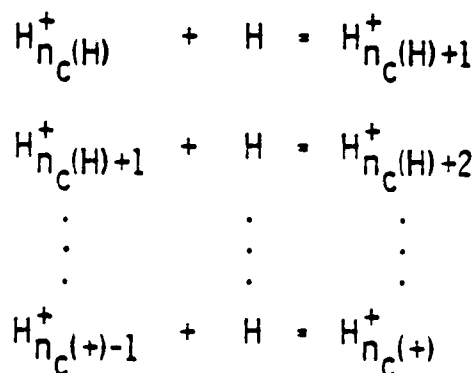
   (4) 2-BODY ION-ION ASSOCIATION $n_c(+) \simeq 2000$

$$H_{n_c(+)}^+ + H_{n_c(+)}^+ = H_{2n_c(+)}^{+2} \qquad q/m = CONST.!$$

$$\vdots \qquad\quad \vdots \qquad\quad \vdots$$
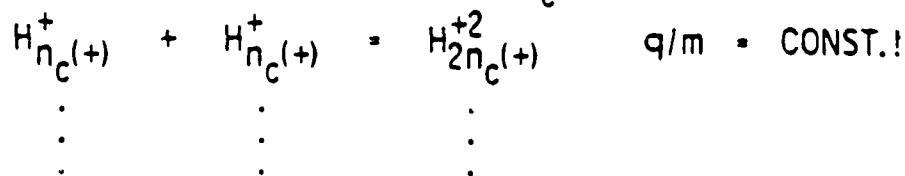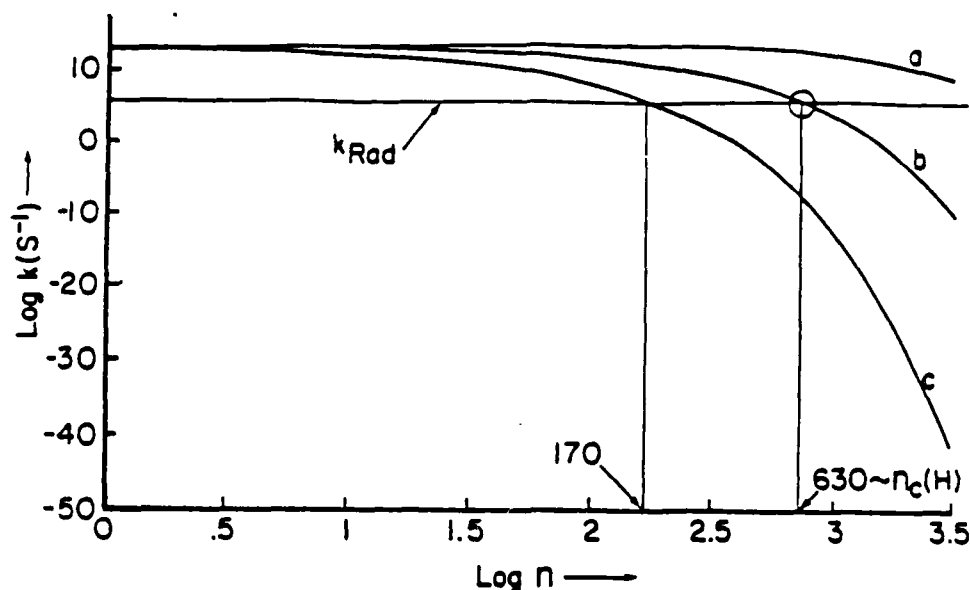
$$\text{(a)} \quad \nu \cdot \left[\frac{D_e(H_2) - 70}{D_e(H_2)} \right]^{2n-3}$$

$$\text{(b)} \quad \nu \cdot \left[\frac{D_e(H_2) - (70 + W(n))}{D_e(H_2)} \right]^{2n-3}$$

$$\text{(c)} \quad \nu \cdot \left[\frac{D_e(H_2) - (70 + 3\,W(n))}{D_e(H_2)} \right]^{2n-3}$$

$$k_{Rad} \simeq 10^3 - 10^4 \qquad\qquad W(n) = \frac{3530}{n^{1/3}} \quad cm^{-1}$$

Figure 5.   Plot of unimolecular decay rates and radiative stabil-
ization rates versus cluster ion size.   Simple RRK
theory was used for the unimolecular decay of the
activated cluster ion-molecule complex.   The radiative
rates were assumed to be constant with cluster size.
W (n) is the assumed form of the (H_2-cluster ion)
binding energy.

13

process becomes possible for sufficiently large cluster ions $(Nc(+) \approx 2000)$. Figure 6 shows an estimate of this parameter and predicts the critical cluster size to be $Nc(+) \approx 2000$. The ion-ion association process is particularly desirable for use in ion traps because the products have the same mass-to-charge ratio (m/q) as the reactants and thus all fragments experience the same trap potential field.

Because of reduction in the space-charge effect, due to the shielding effect of hydrogen dimers surrounding the charged core of cluster ions one may expect larger ion densities in ion traps with increase in the average cluster ion size.

The maximum ion-molecule association cross sections, assuming unit probability of association upon collision, σ (N), have been considered as a function of cluster ion size. In Figure 7 the Langevin cross section for ion-molecule association has been plotted with the gas kinetic cross-section as a function of N. As can be seen the Langevin function decreases with cluster ion size while the gas kinetic (or hard sphere) function increases. Note also that the two functions cross at $N=40$ where the total cross section is about $100A^2$; the total cross section is of course the sum of the two functions. The rate constant $(k(N))$ of bimolecular collisions is related to the cross section by

$$k(N) = \sigma(N) \cdot V$$

where V is the center of mass velocity. Table 2 shows the calculated bimolecular rate constants (particles^{-1} cm^3 s^{-1}) as a function of cluster ion size for collisions at 10 K. Note that the total rate constant is large, even for the smallest clusters, and increases with N due to the gas kinetic cross section. Hence, once large cluster ions (say, $N > 10^4$) are obtained, the rate constants cease to be a concern.

Table 3 shows the corresponding rates (cm^{-3} s^{-1}) for the case of a dilute gas (10^7 cm^{-3}) of cold hydrogen molecules condensing on a dilute (10^7 cm^{-3}) gas of cluster ions.

14

ESTIMATION OF $n_c(+)$ ...
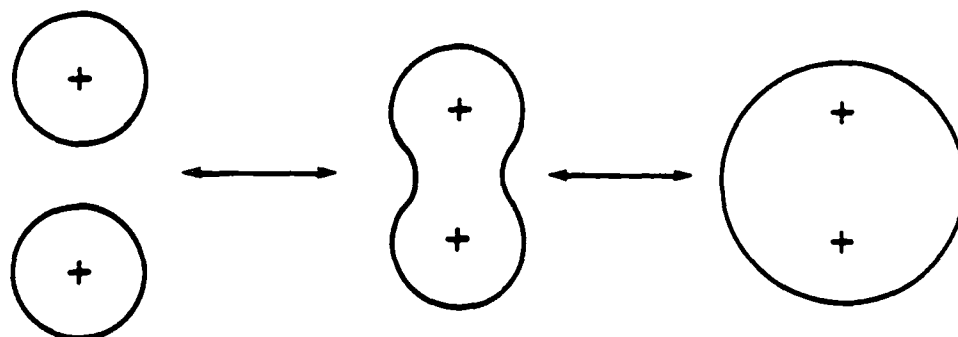
$$V_R(n) = \frac{q^2}{4\pi\epsilon r} \approx E_b(n)$$

$$\frac{51347}{n^{1/3}} = 28\, n^{2/3}\ (cm^{-1})$$

SIMPLE MODEL PREDICTS: $n_c^{(+)} \approx 1830$

EXPT.: $n_c^{(+)} \approx 2000 - 8000$

Figure 6.   A simple electrostatic model calculation of the mini-
mum sized, stable, doubly charged hydrogen cluster
ion (or $N_c(+)$). This also indicates roughly where
the lower bound of the mass-to-charge ratio is for
stable dipositive ground state hydrogen cluster ion.
Thus ion traps will not need to operate for cluster
ions with m/q much larger than a few thousand.
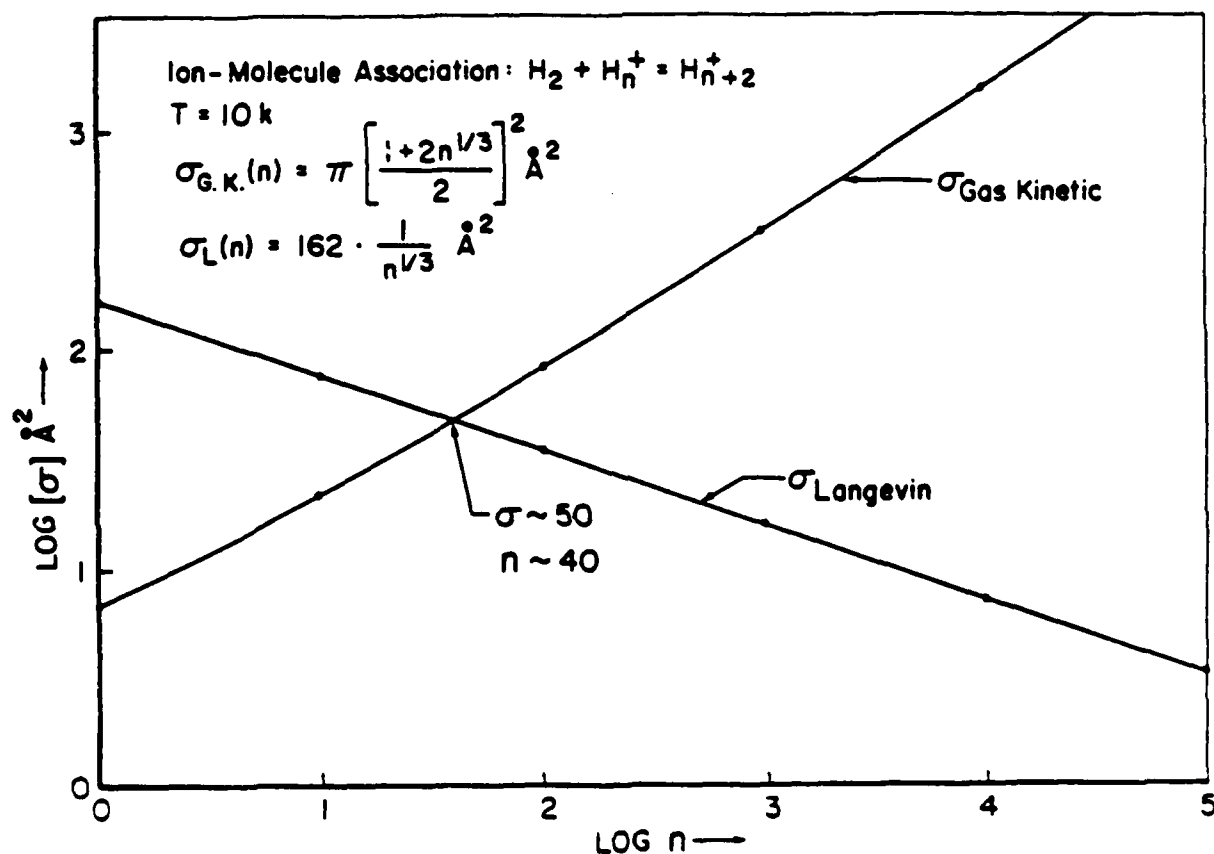
Figure 7. Ion-molecule collision cross-sections versus cluster ion size. The Gas Kinetic model represents collisions of hard spheres while the Langevin model represents the ion-induced dipole interaction. The Langevin cross-section decreases due to shielding of H_3^+ by H_2; here it was assumed that the charge on the cluster ion was immobile, in the center of the cluster.

Table 2. Collision Rate Constants.

$$k \quad vs. \quad n \quad \{FOR\ H_2 + H_n^+\}$$

$$k = \sigma V \quad \left\{\frac{cm^3}{s}\right\}$$

$$T = 10K$$

LOG n	V (n, 10K)	HARD SPHERE $k_{G.K.}$ (n, 10)		LANGEVIN k_{LANG}(n, 10)	
0	7.25×10^5	5.1×10^{-10}		1.17×10^{-8}	
1	5.92×10^4	1.31	-10	4.45	-10
2	4.23×10^4	3.51	-10	1.46	-10
3	4.19×10^4	1.45	-9	6.78	-11
4	4.18×10^4	6.39	-9	3.15	-11
5	4.18×10^4	2.89	-8	1.46	-11
6	4.18×10^4	1.33	-7	6.78	-12
∞	4.18×10^4	---		---	

A critical issue in the overall scheme is the mean free path associated with the described condensation (Table 4). As shown, the expected mean free paths (given in miles) are very large for the small cluster ions and decreases with N. This implies the use of either recirculating reactants, perhaps in rings, or of large volume trap arrangements.

Ion traps are well suited for the proposed condensation. Figure 8 shows a calculation of the expected trap depths in the axial (D(Z)) and radial (D(R)) directions as a function of cluster ion size. The parameters for the RF or Paul trap were held constant and yield a spherical potential of about 12 eV for cluster ions with m/q equal to 200, where the two curves cross. Notice that the heavier cluster ions that might be produced in such a trap experience an ever-decreasing trap depth in the axial direction while the well depth in the radial direction remains rather constant. This would be of practical value for the growth, separation, and transfer of the larger "in trap" grown cluster ions, through the end cap electrodes to other "resonant" traps where they may be stored. Figure 9 shows the corresponding stability diagram. Note that the larger cluster ions remain in stable orbits while clusters with N much less than 100, in this case, are lost.

Hydrogen cluster ions (both positive and negative) are known to be stable. Most work so far has been done on the positive cluster ions, both theoretically and experimentally. In the case of the positive hydrogen cluster ions singly charged clusters have been observed experimentally at sizes beyond 10^6. Figure 10 shows some of the distributions obtained by various research groups (45,46,47,49). Notice that the even-numbered cluster ions are not observed for sizes much below N≈200 (47). It is known that this is due to conditions used in the plasma expansion and that the small even numbered clusters have binding energies comparable to neighboring odd ones (62,63). Also, certain hydrogen cluster ions (magic numbers) exist that have

19

Table 4. Ion-Molecule Association Vs. Mean Free Path.

$$\Delta X = \frac{1}{\sigma \rho} \qquad \frac{1}{10^7 \cdot \sigma}$$

LOG n	HARD SPHERE ΔX (MILES)	LANGEVIN ΔX (MILES)
0	878.00	38.3
1	281.00	82.6
2	74.80	178.0
3	17.90	383.0
4	4.07	.
5	0.89	.
6	0.19	3835.0
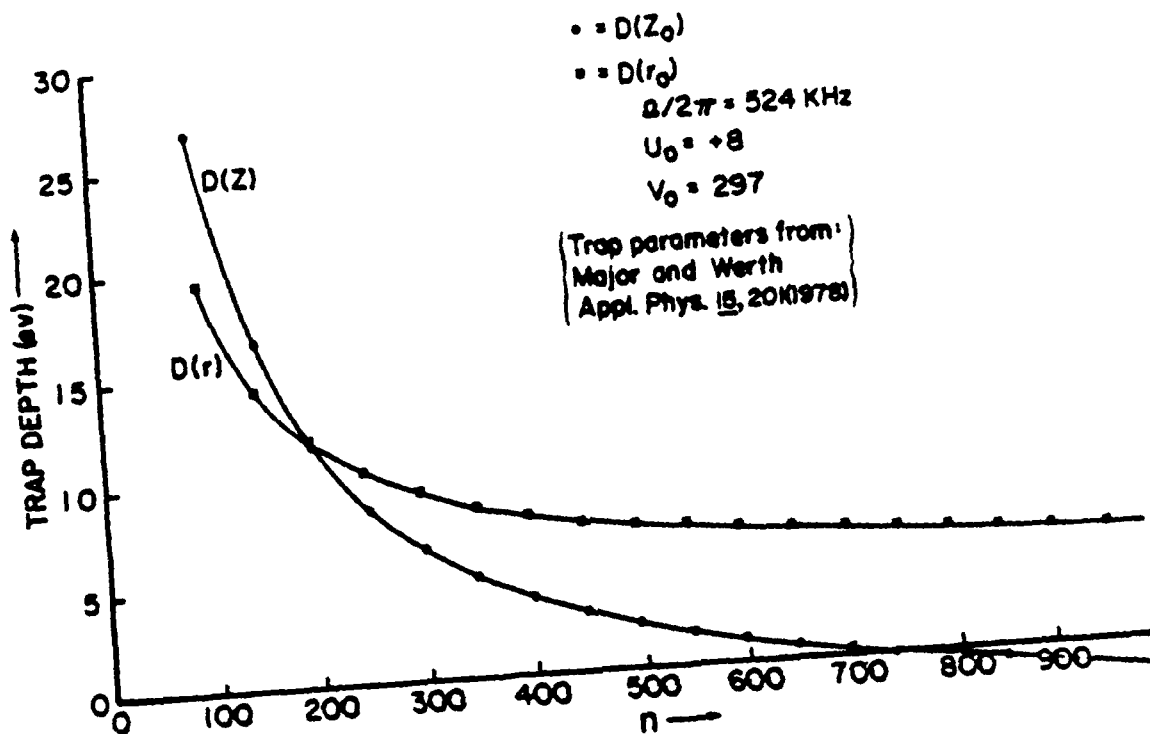
Figure 8. Radio frequency quadrupole trap depth in the axial and radial direction versus mass to charge ratio. The parameters of this trap give a spherical potential for m/q=200. Notice that if cluster ions were grown inside such a device, the largest m/q clusters would drift in the axial but not in the radial directions.
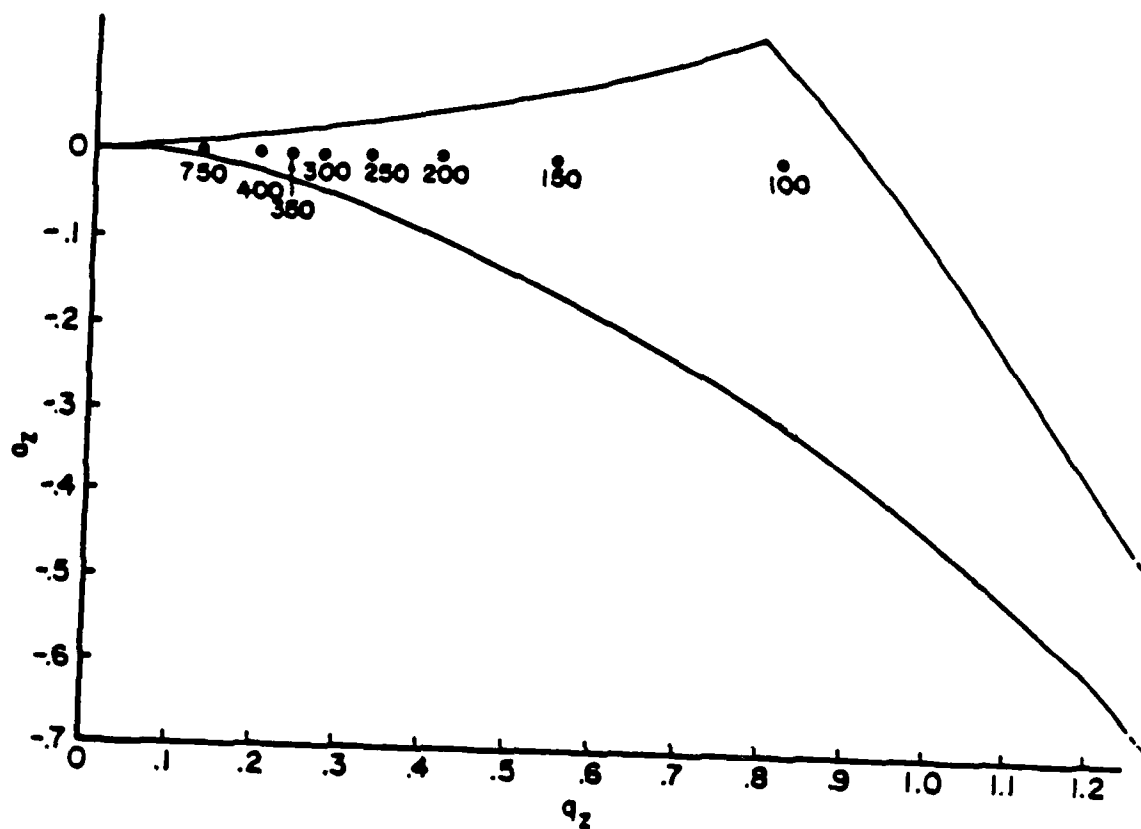
Figure 9.   Stability diagram of the same radio frequency ion
            trap. Notice that charged fragments with m/q much
            less than 100 would escape but that the larger m/q
            cluster would tend to remain in stable orbits.
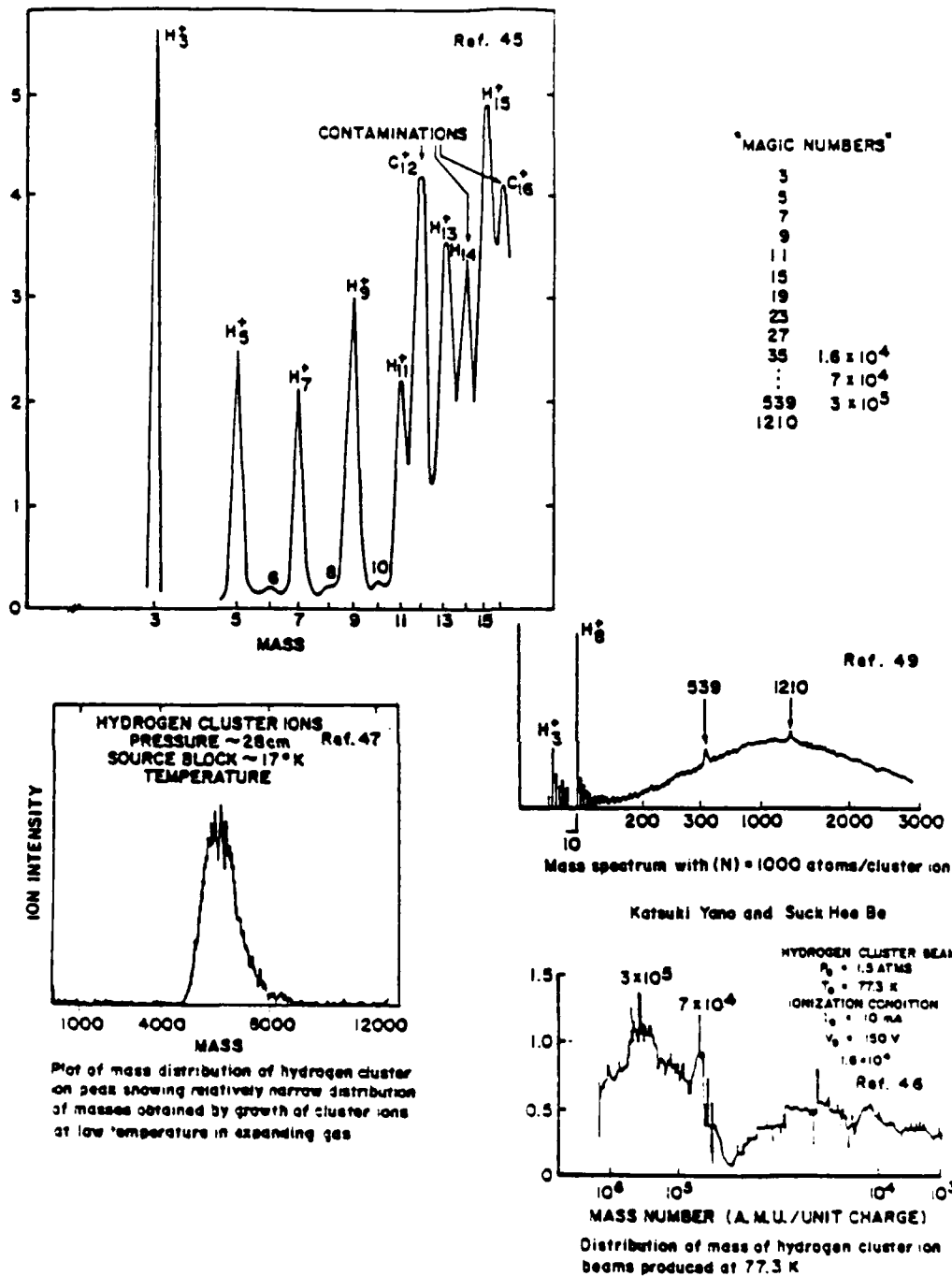
Figure 10. Experimentally reported hydrogen cluster ion mass to charge ratio distributions from the literature. The lack of even-numbered cluster ions, is not due to lack of stability but instead to conditions in the discharge and expansion. Also shown is a list of currently known "magic number" cluster ions.

23

enhanced stability. This behavior is an active area of research and it is currently believed that it is due to packing structures (such as icosahedra) in the case of weakly bound (Van der Waals) clusters.

Finally, the energy that can be stored in an ion trap in the form of antihydrogen cluster ions has been considered. Table 5 shows the volume needed to store one milligram of cluster ions of a given size, assuming an ion trap limited maximum ion density of 10^7 cm^{-3}. Notice that if cluster ions of size $N=10^7$ are used, one milligram can be stored in a trap volume of only 6 M^3 (or less). Table 6 is included to show the potential energy density achievable with antihydrogen cluster ions in a one-gram, one cm3, ion trap. Note that these crude calculations indicate that for cluster ions of $N>10^7$ the energy density (in Kj per gram of trap + fuel) may exceed condensed spin-polarized hydrogen (in Kj per gram of fuel). It should be pointed out that these are conservative estimates and do not take into account space charge shielding or density increases due to laser cooling techniques, or to improvements in ion-trap design.

Table 5. Cluster Ion Storage Volume – 1 mg @ 10^7 cm-3.

Log n	VOLUME (M^3)
0	6×10^7
1	6×10^6
2	6×10^5
3	6×10^4
4	6×10^3
5	6×10^2
6	6×10^1
7	6×10^0
8	6×10^{-1}
9	6×10^{-2}

Table 6. Anti Cluster Ion Energy Density In An Ion Trap:
— Assume 1 cm^3, 1g Trap, $\rho_{ion\ cloud}$ = 10^7 cm^{-3}.

MEAN CLUSTER ION SIZE	J/kg (TRAP)	J/TRAP
10^0	3×10^1	3×10^{-3}
10^1	3×10^2	3×10^{-2}
10^2	3×10^3	3×10^{-1}
10^3	3×10^4	3
10^4	3×10^5	3×10^1
10^5	3×10^6	3×10^2
10^6	3×10^7	3×10^3
10^7	3×10^8	3×10^4
10^8	3×10^9	3×10^5
10^9	3×10^{10}	3×10^6

COMPARISON	J/kg (FUEL)
O_2/H_2	1.5×10^7
(CBES LIMIT) ⟶ H/ H/	2.2×10^8
FISSION	8.2×10^{13}
FUSION	3.9×10^{14}
$P + \bar{P}$	9.0×10^{16}

26

CONCLUSION

This analysis, in its current state of development, concludes that cluster ion synthesis in ion traps is a highly desirable method within the confines of near-term technology and may be of significant value in the synthesis and confinement of antihydrogen in high-energy density form. The method is able to satisfy all of the critical constraints and at the same time is capable of incorporating the reaction of laser cooled atoms (or cold molecules) with trapped ions resulting in association to form large, well-confined cluster ions. It is found that the initial reactions to form H and H_2^+ are known and have been demonstrated experimentally (in reverse via photodissociation) and are rate limiting due to three-body kinetics (67,68). Association pathways to produce cluster ions larger than N=3 under the conditions imposed by the proposed method are not known. An analysis of the relevant potential energy surfaces (ground and excited) in search of radiative and dissociative channels resulting in larger cluster ions is currently underway, with specific emphasis on 3<N<11. In addition, it was found that for the case of ion-atom association through the ground state manifold, there are critical cluster ions sizes associated with a given channel that result from competition between unimolecular decomposition and radiative stabilization. Channels through the electronically excited states are not known. It is also clear that the difficulty in producing the first large "seed" cluster ion(s) will be great, will only need to be done once, and will govern the condensation rate!

REFERENCES

1.   Forward, R., "Antimatter Annihilation Propulsion," AFRPL
      Special Publication, F04611-83-C-0046/UDR-TR-85-55,
      September 1985.

2.   Wineland, D., "Trapped Ions, Laser Cooling, and Better
      Clocks," Science 226, p. 395, 1984.

3.   Brown, L. and G. Gabrielse, "Geonium Theory: Physics of a
      Single Electron or Ion in a Penning Trap," Rev. Mod. Phys.
      58, p. 233, 1986.

4.   Gabrielse, G., "Detection, Damping, and Translating the
      Center of the Axial Oscillation of a Charged Particle
      in a Penning Trap with Hyperbolic Electrodes," Phys.
      Rev. A 29, p. 462, 1984.

5.   Larson, D., J. Bergquist, J. Bollinger, W. Itano, and D.
      Wineland, "Sympathetic Cooling of Trapped Ions: A
      Laser-Cooled Two-Species Nonneutral Ion Plasma," submitted
      to Phys. Rev. Lett., 1986.

6.   Javanainen, J., and S. Stenholm, "Laser Cooling of Trapped
      Particles I: The Heavy Particle Limit," Appl. Phys. 21,
      p. 283, 1980.

7.   Wineland, D., R. Drullinger, and F. Walls, "Radiation
      Pressure Cooling of Bound Resonant Absorbers," Phys. Rev.
      Lett. 40, p. 1639, 1978.

8.   Itano, W., D. Wineland, H. Hemmati, J. Bergquist, and J.
      Bollinger, "Time and Frequency Standards Based on Charged
      Particle Trapping," IEEE Trans. on Nucl. Sci. NS-30,
      p. 1521, 1983.

9.   Dehmelt, H., "Radiofrequency Spectroscopy of Stored Ions I
      Storage," Advances in Atomic and Molecular Physics 3,
      NY, Academic Press, 1967.

10.   Dehmelt, H., "Radiofrequency Spectroscopy of Stored Ions II
      Spectroscopy," Advances in Atomic and Molecular Physics
      5, NY, Academic Press, 1967.

11.   Itano, W. and D. Wineland, "Laser Cooling of Ions Stored in
      Harmonic and Penning Traps," Phys. Rev. A 25, p.35, 1982.

12.   Nagourney, W., G. Janik, and H. Dehmelt, "Linewidth of Single
      Laser-Cooled $^{24}Mg^+$ Ion in Radiofrequency Trap," Proc. Natl.
      Acad. Sci. 80, p. 643, 1983.

13. Schwinberg, P., R. Van Dyck Jr., and H. Dehmelt, "New Comparison of the Positron and Electron g Factors," Phys. Rev. Lett. $\underline{47}$, p. 1679, 1981.

14. Neuhauser, N., M. Hohenstatt, and P. Toschek, "Optical-Sideband Cooling of Visible Atom Cloud Confined in Parabolic Well," Phys. Rev. Lett. $\underline{41}$, p. 233, 1978.

15. Neuhauser N., M. Hohenstatt, and P. Toschec, "Preparation, Cooling, and Spectroscopy of Single, Localized Ions," Laser Spectroscopy $\underline{4}$, Berlin, Springer-Verlag, 1979.

16. Church D. and H. Dehmelt, "Radiative Cooling of an Electrodynamically Confined Proton Gas," J. Appl. Phys. $\underline{40}$, p. 3421, 1969.

17. Eckstrom P. and D. Wineland, "The Isolated Electron," Sci. Am. August, p. 105, 1980.

18. Lakkaraju H. and H. Schuessler, "Motional Side-band Resonances in the Microwave Spectrum of Stored Ions," J. Appl. Phys. $\underline{53}$, p. 3967, 1982.

19. Neuhauser W., and M. Hohenstatt, and P. Toschek, "Localized Visible Ba^+ Mono-ion Oscillator," Phys. Rev. A $\underline{22}$, p. 1137, 1980.

20. Prior M. and R. Knight, "Fluorescence of Optically Pumped Trapped Ions," Opt. Comm. $\underline{35}$, p. 54, 1980.

21. Phillips W., "Laser-cooled and Trapped Atoms," Proceedings of the Workshop on Spectroscopic Applications of Slow Atomic Beams held at the National Bureau of Standards, Gaithersburg, MD, April 1983.

22. Blatt R., W. Ertmer, and J. Hall, "Laser-Cooled and Trapped Atoms," Ed. by W. D. Phillips, National Bureau of Standards (U.S.) Special Publication 653, June 1983.

23. Phillips W. and H. Metcalf, "Laser Deceleration of an Atomic Beam," Phys. Rev. Lett. $\underline{48}$, p. 596, 1982.

24. Wineland D. and W. Itano, "Laser Cooling of Atoms," Phys. Rev. A $\underline{20}$, p. 1521, 1979.

25. Prodan, J., A. Migdall, W. Phillips, I. So, H. Metcalf, J. Dalibard, "Stopping Atoms with Laser Light," Phys. Rev. Lett. $\underline{54}$, p. 992, 1985.

26. Phillips W. and J. Prodan, "Cooling Atoms with a Frequency Chirped Laser," Coherence and Quantum Optics 5, NY, Plenum Press, 1978.

27. Ashkin, A., "Stable Radiation-Pressure Particle Traps using Alternating Light Beams," Opt. Lett. 9, p. 454, 1984.

28. Ashkin, A., "Trapping of Atoms by Resonance Radiation Pressure," Phys. Rev. Lett. 40, p. 729, 1978.

29. Ashkin, A and J. Gordon, "Cooling and Trapping of Atoms by Resonance Radiation Pressure," Opt. Lett. 4, p. 161, 1979.

30. Djeu, N., "Laser Cooling of Gases by Radiation at Higher Frequency Transitions," Opt. Comm. 26, p. 354, 1978.

31. Tompkins F. and R. Mahon, "Generation of Continuously Tunable Narrow-band Radiation from 1220 to 1174 Angstroms in Hg Vapor," Opt. Comm. 7, p. 304, 1982.

32. Himeno, S., et al., "Generation of Coherent Lyman-Alpha Radiation with an Alexandrite Laser for Diagnostics of Neutral Hydrogen Density," J. Nuclear Materials 128-129, p. 974, 1984.

33. Caro, R., et al., "Generation of 121 nm Radiation by Resonant Up-conversion of Raman-shifted KrF Laser Radiation in Mg," J. Phys. D 18, p. 1291, 1985.

34. Jamroz, W., et al., "Generation of Continuously Tunable Coherent Vacuum-ultra Violet Radiation (140 to 106 nm) in Zinc Vapor," Opt. Lett. 7, p. 617, 1982.

35. Mahon, R. and Y. Yiu, "Generation of Lyman-Alpha Radiation in Phase-matched Rare-gas Mixtures," Opt. Lett. 5, p. 279, 1980.

36. Mahon R., et al., "Four-wave Sum Mixing in Beryllium around Lyman-Alpha," Opt. Lett. 4, p. 360, 1979.

37. Kajiwara, T., et al., "Measurements of Density, Surface Recombination Coefficient, and Diffusion Coefficient of Hydrogen Atoms by Lyman-Alpha Laser Fluorescence Spectroscopy," Rev. Sci. Instrum. 56, p. 2213, 1985.

38. Kajiwara, T., et al., "Determination of Atomic Hydrogen Density by Lyman-Alpha Laser Fluorescence Spectroscopy," Jap. J. of Appl. Phys. 24, p. 870, 1985.

39. LaSala, J., et al., Proceedings of the Third Topical Meeting on Short Wavelength Coherent Radiation: Generation and Applications," Monterey, CA. March 1986.

40. Yamaguchi, Y., J. Gaw, and H. Schaefer III, "Molecular Clustering about a Positive Ion. Structures, Energetics, and Vibrational Frequencies of the Protonated Hydrogen Clusters H_3^+, H_5^+, H_7^+, and H_9^+," J. Chem. Phys. 78, p. 4074, 1983.

41. Carrington, A., J. Buttenshaw, and R. Kennedy, "Observation of the Infrared Spectrum of H_3^+ at its Dissociation Limit," Mol. Phys. 45, p. 753, 1982.

42. Carrington, A. and R. Kennedy, "Infrared Spectrum of the H_3^+ Ion," J. Chem. Phys. 81, p. 91, 1984.

43. Okumura, M., L. Yeh, and Y. Lee, "The Vibrational Predissociation Spectroscopy of Hydrogen Cluster Ions," J. Chem. Phys. 83, p. 3705, 1985.

44. Kutina, R., A. Edwards, R. Pandolfi, and J. Berkowitz, "UV Laser Photodissociation of Molecular Ions," J. Chem. Phys. 80, p. 4112, 1984.

45. Chanut, Y., J. Martin, R. Salin, and H. Moser, "Production and Beam Analysis of Energetic Small Hydrogen Cluster Ions for Study of their Interactions with Targets and of Their Structure," Surface Science 106, p. 563, 1981.

46. Yano, K. and S. Bee, "Mass Analysis of Cluster Ion Beams by Wien Filter," Jap. J. of Appl. Phys. 19, p. 1019, 1980.

47. Beuhler R. and L. Friedman, "Cluster Ion Formation in Free Jet Expansion Process at Low Temperatures," Ber. Bunsenges. Phys. Chem. 88, p. 265, 1984.

48. Beuhler, R. and L. Friedman, "Hydrogen Cluster Ions," Phys. Rev. Lett. 48, p. 1097, 1982.

49. Henkes, P. and U. Pfeiffer, "Interaction of Accelerated Cluster Ions of Hydrogen with Gas Targets," Ber. Bunsenges Phys. Chem. 88, p. 258, 1984.

50. Moser, H., "Time of Flight Spectroscopy of Sub-Mev Cluster Ions in the Mass Range $1-10^6$ Atoms Per Charge," Rev. Sci. Instrum. 55, p. 1914, 1984.

51. Beuhler, R., S. Ehenson, and L. Friedman, "Hydrogen Cluster Ion Equilibria," J. Chem. Phys. 79, p. 5982, 1983.

52. Hiraoka, K. and P. Kebarle, "A Determination of the Stabilities of H_5^+, H_7^+, H_9^+, and H_{11}^+ from Measurement of the Gas Phase Ion Equilibria $H_n^+ + H_2 = H_{n+2}^+$ (n=3,5,7,9)," J. Chem. Phys. 62, p. 2267, 1975.

53. Yamabe, S., K. Hirao, and K. Kitaura, "Theoretical Study on the Stability and Structure of H_n^+(n=3,5,7,9,11)," Chem. Phys. Lett. 56, p. 546, 1978.

54. Huber, H., "Geometry Optimization in Ab Initio SCF Calculations. The Hydrogen Clusters H_n^+ (n=7,9,11,13)," Chem. Phys. Lett. 70, p. 353, 1980.

55. Bell M. and J. Bell, "Capture of Cooling Electrons by Cool Protons," Particle Accelerators 12, p. 49, 1982.

56. Neumann R., et al., "Laser-enhanced Electron-ion Capture and Antihydrogen Formation," Z. Phys. A - Atoms and Nuclei 313 p. 253, 1983.

57. Ozenne, J., D. Pham, and J. Durup, "Photodissociation of H_2^+ by Monochromatic Light with Energy Analysis of the Ejected H^+ Ions," Chem. Phys. Lett. 17, p. 422, 1972.

58. van Asselt, N., J. Maas, and J. Los, "Laser Induced Photodissociation of H_2^+ and D_2^+ Ions," Chem. Phys. 5, p. 429, 1974.

59. Kutina, R., A. Edwards, R. Pandolfi, and J. Berkowitz, "UV Laser Photodissociation of Molecular Ions," J. Chem. Phys. 80, p. 4112, 1984.

60. Ozenne, J., J. Durup, R. Odom, C. Pernot, A. Tabche-Fouhaille, and M. Tadjeddine, "Laser Photodissociation of the Isotopic Hydrogen Molecular Ions. Comparison between Experimental and Ab Initio Computed Fragment Kinetic Energy Spectra," Chem. Phys. 16, p. 75, 1976.

61. Wright, L. and R. Borkman, "Ab Initio Studies on the Stabilities of Even- and Odd- Membered H_n^+ Clusters," J. Chem. Phys. 77, p. 1938, 1982.

62. Kirchner, N., J. Gilbert, and M. Bowers, "The First Experimental Observation of Stable H_4^+ Ions," Chem. Phys. Lett. 106, p. 7, 1984.

63. Jungen, M. and V. Staemmler, "Rydberg States of H_4," Chem. Phys. Lett. 103, p. 191, 1983.

64. Garcia, R., A. Rossi, A. Russek, "Dissociating States of the H_3^- System," J. Chem. Phys. 70, p. 5463, 1979.

65. Sapse, A., M. Rayez-Meaume, J. Rayez, and L. Massa, "Ion-Induced Dipole H_n Clusters," Nature 278, p. 332, 1979.

66. Aberth, W., R. Schnitzer, and M. Anbar, "Observations of Diatomic and Triatomic Hydrogen Negative Ions," Phys. Rev. Lett. 34, p. 1600, 1975.

67. Johnson, R., C. Huang, and M. Biondi, "Three-body Association Reactions of H^+ and H_3^+ Ions in Hydrogen from 135 to 300 K," J. Chem. Phys. 35, p. 1539, 1976.

68. Viggiano, A., "The Temperature Dependence of Ion-molecule Association Rate Coefficients in the Low Pressure Limit," J. Chem. Phys. 84, p. 244, 1986.

Analysis of "Containerless" Condensation of
Poly-Atomic Hydrogen Ions, with emphasis on H_3^+, -
Association Channels and a Future Workshop
to Study Related Topics

W. C. Stwalley

William C. Stwalley
7/11/88
Revised 8/25/88

Analysis of 'Containerless' Condensation of Polyatomic

Hydrogen Ions, with Emphasis on H_5^- Association

Channels and a Future Workshop to Study Related Topics

The Air Force has identified antimatter propulsion as a possible "enabling" technology for a wide variety of important propulsion applications. As a result, it has begun funding of research aimed at the ultimate goal of an antiproton propulsion system. For such a system, antiprotons must be produced, slowed to low energy and condensed to a high density form suitable for propulsion, all the while maintaining "containerless" (indeed "collisionless') conditions; i.e. there must be no contact with walls of ordinary matter (or even with background gas molecules) to avoid catastrophic matter-antimatter annihilation. Such high energy density antimatter may, of course, have other important applications besides propulsion.

As a result, it now appears that a significant number of antiprotons and positrons can be produced and that, after being slowed to low energy, they can be laser-stimulated to recombine into antihydrogen atoms via the 2p state. Moreover, antihydrogen atoms can presumably in turn be cooled, moved and trapped using laser beams. It also appears that condensed antihydrogen (say micro- or milligrams) will be used if it can be conveniently stored in a 'containerless" fashion. The question then is how to go from cold antiprotons, positrons and antihydrogen atoms to bulk antihydrogen.

A leading concept to span this gap from atom to the bulk is the cluster ion approach formulated by Dr. John T. Bahns of the University of Dayton, with my assistance on a number of topics. Because ion traps are a relatively well defined technology (the new generation of "atomic clocks' employs them), the bulk trapping should be feasible. It is this concept that led to the conve-

ning of a study group at the University of Iowa these past two weeks.

For simplicity, I shall discuss ordinary matter rather than antimatter in what follows. Hence our goal is to formulate a "containerless" procedure to "grow" $H_n^\pm$ ($n \geq 10^{17}$) starting from the raw materials H^-, e^- and H. I note in passing that hydrogen cluster ion technology may in itself be of significant importance: as a stable high mass beam for directed energy or laser amplifier applications; as the precursor ion for a H_n neutral beam for directed energy or magnetic or inertial confinement fusion applications; and as the precursor ion for chemically bound excited states of interest as advanced propellants (e.g. H_4, H_{10}, ...).

The possible growth processes considered by the Cluster Ion Study Group are as follows:

1. A^+ $H_n^- + H \rightarrow H_{n+1}^-$

2. M^- $H_n^- + H_2 \rightarrow H_{n+2}^-$ or $H_{n+1}^- + H$

3. A/M^- $H_{n_{odd}}^- + H \rightarrow H_{n_{odd}+1}^-$
   $$H_{n_{odd}+1} + H_2 \rightarrow H_{n_{odd}+2}^- + H$$

4. A^+ $H_n^- + H \rightarrow H_{n+1}^-$

5. M^- $H_n^- + H_2 \rightarrow H_{n+2}^-$ or $H_{n+1}^- + H$

6. A/M^- $H_{n_{odd}}^- + H \rightarrow H_{n_{odd}+1}^-$
   $$H_{n_{odd}+1}^- + H_2 \rightarrow H_{n_{odd}+2}^- + H$$

Each process suggests at least one important concern. All processes except 1. and 4. involve production of translationally, rotationally and especially vibrationally cold H_2 molecules, certainly a challenging and difficult task. Let us first examine therefore the $A^\pm$ processes.

The first process, A^+, involves first the formation of H_2^+ and then H_3^+. H_2^+ could be formed by radiative association of H and H^+ either free ($^2\Sigma_u^+$) $\rightarrow$ bound ($X^2\Sigma_g^+$) or free ($X^2\Sigma_g^+$) $\rightarrow$ bound ($^2\Lambda_u$) $\rightarrow$ bound ($X^2\Sigma_g^+$), the latter process seeming preferable at first glance. Both processes have the disadvantage of

38

producing a variety of vibrational-rotational levels of the ground electronic state. These levels will have a very long radiative lifetime, so cannot be quickly cooled internally under 'containerless' conditions. Cooling with cold H, H^- or e^- would be possible. However, the process

$$H_2^- + H \rightarrow H_2 + H^-$$
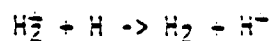
would quickly occur. Unfortunately, this is ~2 eV exoergic, so a high internal excitation of the H_2 produced is expected. It might be possible to avoid this using transition state spectroscopy, i.e. stimulating free-free emission from $H_2^- + H$ to $H^- + H_2$ ($v = 0$):
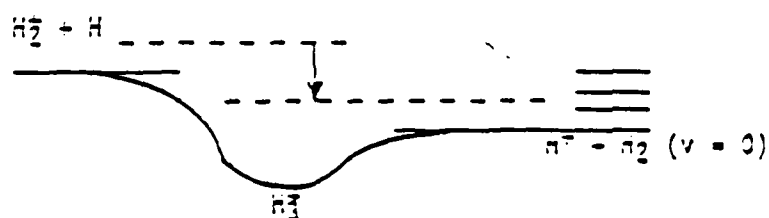
Figure 1

The sketched process should be studied, especially in comparison with free-free absorption. This diagram suggests a second possibility, namely free-bound-bound spontaneous radiative association via electronically excited $(H_3^-)^*$.
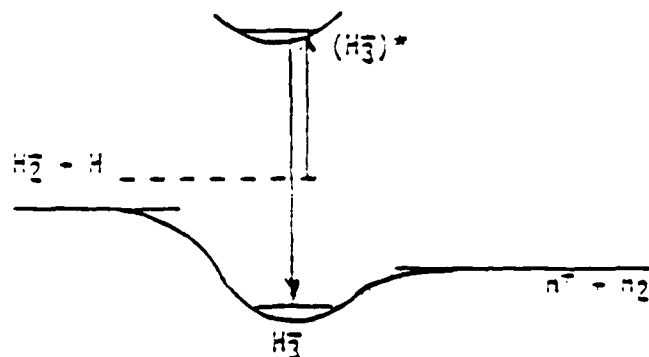
Figure 2

The simple molecular orbital argument for H_3^- indicates the ground state corresponds to $(a_1')^2$ (two electrons in strongly bonding orbitals). The lowest allowed excited singlet state corresponds to (a_1') (e') (one orbital strongly bonding, one orbital weakly antibonding) and thus may be bound (rather than repulsive). Ab initio calculations of this excited state and its radiative

39

transitions are needed.

The next process $H_3^+ + H \rightarrow H_4^+$ which is ~0.1 eV excergic, may also proceed by radiative association via the $(H_4^+)^*$ electronically excited state. Again excited state calculations are needed.

The process

$$H_4^+ + H \rightarrow H_5^+$$

is more problematical, since the competing process

$$H_4^+ + H \rightarrow H_3^+ + H_2$$

occurs rapidly. Again radiative control is the method of choice, but calculations are needed.

In general for the A^+ synthesis, it appears that the

$$H_{n_{even}}^+ + H \rightarrow H_{n_{even}+1}^+$$
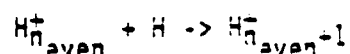
is the critical step because of competition from

$$H_{n_{even}}^+ + H \rightarrow H_{n_{even}-1}^+ + H_2.$$
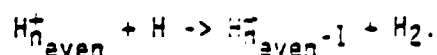
Can radiative association via electronically excited states be used here? The answer is no one yet knows and calculations (and ultimately experiments) are needed.

For significantly larger n ($>10^3$?), the process of ground electronic state radiative association

$$H_n^+ + H \rightarrow H_{n+1}^+ + h\nu$$
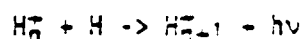
becomes competitive, and thus very large clusters ($n > 10^4$?) may be able to sustain multiple collisions with H atoms by this process.

The A^- synthesis is much more problematic. In particular, H_2^- is not stable, so

$$H^- + H \rightarrow [H_2^-] \rightarrow H_2 + e^-$$
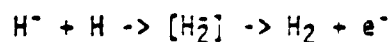
will occur. Perhaps H_2^- resonances are sufficiently long-lived that

$$[H_2^-] + H \rightarrow H_3^-$$
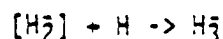
can occur, but it seems unlikely. It appears that H_3^- can only be produced by

40

three-body collisions, and even H^- may be difficult to form (perhaps $e^- + H_2$ -> $H + H^-$ is the best method). Finally, there is no evidence for the existence of H_4^-, H_6^-, etc., presumably because

$$H_4^- \rightarrow H_2 + H_2 + e^-$$
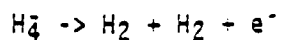
and similar decays may be exoergic. Clearly calculations are needed. If H_4^-, H_6^-, etc. are unstable, the A^- process is ruled out.

The other processes involve first the formation of cold H_2. Such formation is by no means easy. Even population of $B^1\Sigma_u^+$, $v = 0$, $J = 1$ H_2 or $C^1\Pi_u$, $v = 0$, $J = 1$ H_2 leads to only ~12% and ~18% emission to $X^1\Sigma_g^+$ $v = 0$, $J = 0$, 2 H_2. Such population could be obtained with $3v^*$ vacuum ultraviolet lasers, where v^* is the highest ground electronic state vibrational level significantly populated, in the case that only $J = 0$ and 2 H_2 levels are populated. A detailed consideration of cooling H_2 is needed.

Given cold H_2, the synthesis M^+ appears to be the most attractive of the four remaining. In particular, H_5^+, H_7^+, H_9^+, etc. correspond to the binding of successive H_2 molecules to an H_3^+ core. A third body such as H might carry away the excess energy.
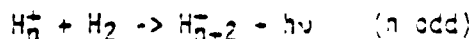
For large n ($n \geq 27$ in Figure 3, attached, based on Professor Tardy's preliminary calculations), the fairly slow ($k_{rad} \sim 10^{-1}$ sec^{-1}) process of ground state radiative association

$$H_n^+ + H_2 \rightarrow H_{n+2}^+ + h\nu \quad (n \text{ odd})$$

becomes competitive with unimolecular decomposition ($k_{threshold}$ in Figure 3). It should be noted that if the species H_n^+ contains only 1000 cm^{-1} of internal energy, the unimolecular decomposition becomes much faster ($k_{+1000cm^{-1}}$ in Figure 3) and one must go to larger clusters ($n \geq 37$) before radiative stabilization of H_{n+2}^+ is competitive with unimolecular decomposition. The numbers 27 and 37 quoted above are of course uncertain because of the simplicity of the model used, but are probably the right order of magnitude.

41

Figure 3. Rate constants of unimolecular decomposition of the species H_{n-2}^-
with threshold vibrational energy for decomposition to $H_n^- + H_2$
($k_{threshold}$) and with 1000 cm^{-1} of vibrational energy in excess of
threshold ($k_{+1000\ cm^{-1}}$). Also shown is the estimated rate constant
for photon emission (k_{rad}) which appears to reach a limiting value
of $\sim 10^{-1}$ s^{-1} as $n \rightarrow \infty$.
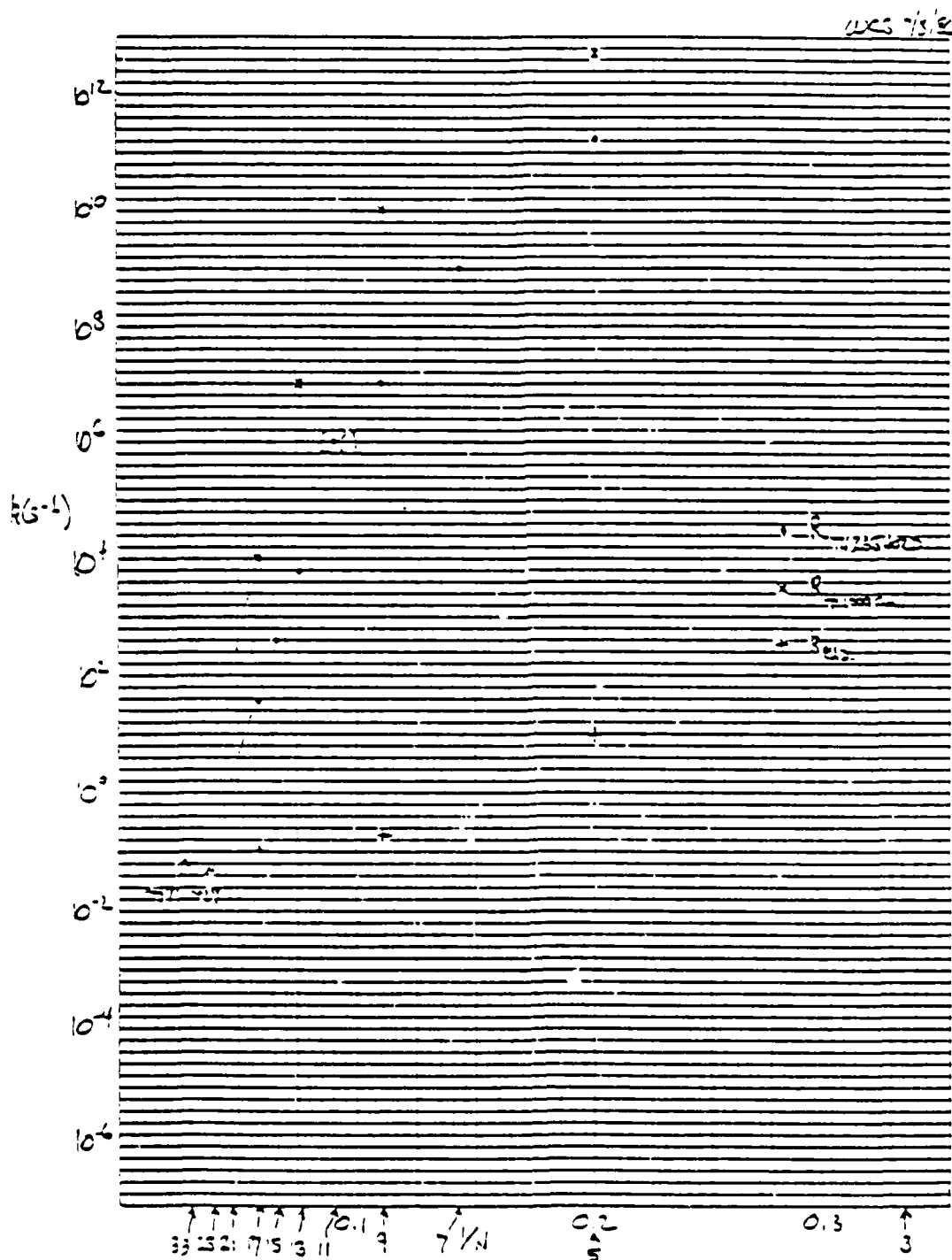
Similar arguments apply to the M^- synthesis. The A/M^- synthesis allows one to avoid the difficult

$$H_{n_{even}}^+ + H \to H_{n_{even}-1}^- + H_2$$
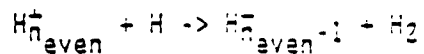
process. The A/M^- process is ruled out if the H_4^-, H_6^-, ... molecules are unstable.

It is with the above background, especially the set of synthetic routes, that the November Workshop has been planned by Dr. John T. Bahns with my assistance. His report will contain our detailed recommendations.

Small Molecule and Small Cluster Ion Formation
in a Low-Density, Containerless Mixture
of Electrons, Protons, and Hydrogen Atoms

K. M. Sando

SMALL MOLECULE AND SMALL CLUSTER ION FORMATION IN A LOW-DENSITY,

CONTAINERLESS MIXTURE OF ELECTRONS, PROTONS, AND HYDROGEN ATOMS

[signature]

The purpose of this study is to investigate the possibility and means

of producing condensed antimatter. There is, however, no chemical

difference between antimatter and matter and initial experiments will be

done with matter for reasons of cost and availability. Therefore, in this

discussion terms relating to matter will be used throughout.

The formation of large cluster ions has been shown to be a promising

method of producing bulk antimatter in a containerless environment. The

production of cold anti- electrons, protons and hydrogen atoms has been

discussed elsewhere, and is believed to be feasible. The chemical process

of producing large cluster ions from medium sized (about 30 atoms) ions has

also been discussed and is believed to be feasible. Therefore, this

discussion is limited to the production of small to medium-sized cluster

ions from electrons, protons, and hydrogen atoms. Cold hydrogen molecules

may be more effective for increasing the size of a cluster ion than hydrogen

atoms. Because there is no known method for producing cold hydrogen

molecules in a low-density, containerless environment, some discussion of

hydrogen molecule formation is also given.

PREMISES.

In a medium to high density environment with walls, the

formation of larger molecules or cluster ions from smaller ones may occur

via collisions with a third body or with walls to remove the excess energy

due to binding of the fragments. In the low-density, containerless

environment, wall collisions are strictly prohibited and third body colli-

sions are rare. The third body is restricted to be a photon, an electron, a

47

proton, a hydrogen atom, or (as the synthesis proceeds) a molecule or cluster ion. Because of the low probability of 3-body collisions, reactions that produce two products, so that the energy of reaction can be more effectively dissipated, will dominate those that produce only one. For reactions beneficial to cluster growth, the second product will be small (H atom or a photon). Reactions that produce a photon as a product can in some cases be stimulated. A careful analysis of the kinetics is required because, of course, if the forward reaction is stimulated, the reverse reaction is also stimulated. In the event that a third body is required, long-lived resonances in the collision complex of the reactants will enhance the probability of a three-body collision.

To avoid wall collisions, all matter must be confined. Electric and magnetic fields are used as "traps" for confinement. Existing methods provide ion traps that are energetically much deeper than traps for neutrals. Therefore, neutral atoms and molecules are difficult to contain and will eventually reach the walls. Neutrals escaping the reaction zone must be photoionized and the resulting electrons and positive ions must be re-trapped and cooled.

REACTIONS INVOLVING H_2^+

The hydrogen molecular ion can be a valuable reactant for subsequent steps in small cluster ion formation. Ideally, it should be vibrationally, rotationally, and translationally cool.

A hydrogen ion and a hydrogen atom can approach on two potential energy curves corresponding to the $^2\Sigma_u$ and $^2\Sigma_g$ molecular states.
The potential curves are shown schematically, below.
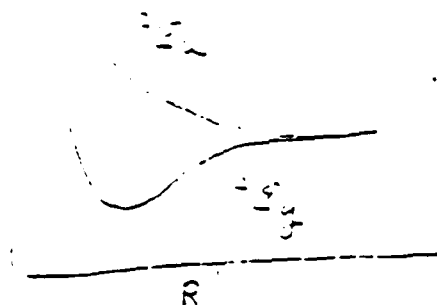
Reactions involving the $^2\Sigma_u$ curve are

$$H^- + H \rightleftharpoons H_2^-(^2\Sigma_u) \overset{\text{radiative association}}{\rightleftharpoons} H_2^+(^2\Sigma_g) + h\nu$$

$$\Big\updownarrow$$
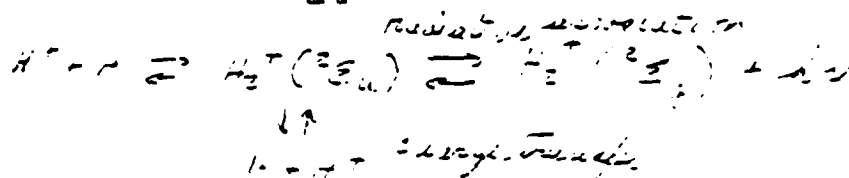
$$H + H^+ \quad \text{charge transfer}$$

The charge transfer reaction is harmless unless energetic hydrogen ions are involved. In which case energetic hydrogen atoms are produced that will quickly escape the reaction zone and must be photoionized so that they can be re-trapped. The radiative association reaction will produce bound H_2^+, but in a distribution of vibrational states that favors high vibrational quantum numbers, except for highly energetic collisions. The actual distribution of bound states produced can be readily calculated as a free-bound process because the potential curves and transition moments for H_2^+ are well known.

Question: What is that distribution as a function of collision energy? Is it in the literature? If not, is it important enough to calculate?

The radiative association can, perhaps, be stimulated. Because the process is reversible, the product H_2^+ must be removed. Because relaxation processes will be slow, the only practical removal process seems to be physical removal. Ion trap technology could, perhaps be used to selectively

49

remove H_2^+ from the reaction zone. The advantages in stimulating the process are to enhance the rate and to enhance population of lower vibrational levels.

Production of low vibrational levels of H_2^+ is favored by high collision energies. This means energetic H^+ because the H is cold. High collision energies, however, means the production of hot H atoms via charge transfer.

It is probable that the use of hot H^+ and the sweeping out of H_2^+ formed will prove impractical. Therefore, reactions of H^+ with H on the $^2\Sigma_u$ surface will produce vibrationally excited H_2^+ at a slow rate. The overall rate can be calculated from the results of Bates. Level-specific rates can be easily calculated as a free-bound process if they are not available in the literature.

Under low density conditions, reaction of H^+ with H on the $^2\Sigma_g$ surface will not occur unless a collisional resonance (quasibound state) is formed. The lifetime of the resonance must be sufficiently long to allow a third body to remove the collision energy and bring the molecule to a true bound state. The result will be formation of H_2^+ in a vibrationally excited state at a slow rate.

From the above discussion it can be predicted that the formation of H_2^+ in low vibrational levels from H^+ and H will require effective removal of vibrational energy by means of a third body. That third body cannot be a photon (unless some very tricky methods are used) because H_2^+ has no dipole moment. More will be said later on the use of a third body for vibrational relaxation.

The most important reaction of H_2^+ with H is

$$H_2^+ + H \rightarrow H^+ + H_2$$

50
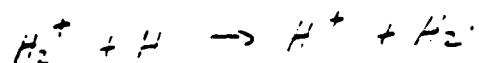
Because this reaction is exoergic and involves the formation of two products, it will occur readily under the reaction conditions considered. The H_2 will be formed in vibrationally excited states.

Question: For this reaction, what is the overall rate and what is the branching ratio into various vibration-rotation levels of product H_2 as a function of collision energy and initial H_2^* excitation?

Even though a photon is not normally a product of this reaction, it is possible it could occur radiatively

$$H_2^- + H \rightleftharpoons H_3^{-*} \longrightarrow H_2 + H^- + h\nu$$

Here H_3^{-*} is a vibrationally excited exciplex in either the ground electronic state or in the excited state that also dissociates to a ground state H atom and a ground state H_2^- molecular ion. The second step can be effectively stimulated because it is not reversible. The advantage in stimulating this step is that it may be possible to select low vibrational levels of product H_2 by selecting the laser wavelength. High laser powers would be required to overcome the high rate expected for the non-radiative reaction.

Question: Is this a viable process for making vibrationally cold H_2? If so, is vibrationally cold H_2^- required as a reactant?

The most important reaction between H_2^- and H_2 is

$$H_2^- + H_2 \longrightarrow H_3' + H$$
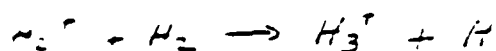
This reaction is also exoergic and involves the formation of two products.

so it will be very favorable under the reaction conditions considered. The cross-section for this reaction is known to be large. The H_2^- will likely be formed in a vibrationally excited state, but (in contrast to H_2 and H_2^-) H_3^- can lose its excess energy radiatively (See Carney and Porter) via infrared radiation.

Question: How does the cross-section depend upon the vibrational states of the reactant molecules?

REACTIONS INVOLVING H_2

Neutral molecular hydrogen could be a valuable reactant for the growth of cluster ions. The production and the confinement of cold H_2 are, however both major problems. The confinement of H_2 is probably not practical. Therefore, it must be regarded as a transient species that either reacts soon after its production or is photoionized as it leaves the reaction zone.

Question: What are the most efficient methods of photoionizing H_2? Single photon and resonantly enhanced multiphoton processes should be considered. Production of vibrationally cold product H_2^+ is preferable.
See (for example) Cornaggia, et al. Phys. Rev. A $\underline{34}$, 207 (1986).

One method for producing H_2 has been discussed above (the reaction of H_2^+ with H). Another method will be discussed here. It has been shown that hydrogen molecules can be formed efficiently in a high pressure environment by the association of two H atoms in a collisional resonance (quasibound

state) followed by relaxation via a third body. That process is possible here. also. but it is likely to be slow and lead to only highly vibrationally excited H_2. Here. the possibility of enhancing the process by using laser excitation is discussed. The processes considered are

$$H + H \rightleftharpoons H_2 (X\,^1\Sigma_g^+)^* \quad (resonance)$$

$$H_2 (X\,^1\Sigma_g^+)^{**} + h\nu \rightleftharpoons H_2 (B\,^1\Sigma_u^+ \text{ or } C\,^1\Pi_u)$$

$$H_2 (B\,^1\Sigma_u^+ \text{ or } C\,^1\Pi_u) \longrightarrow H_2 (X\,^1\Sigma_g^+) + h\nu$$
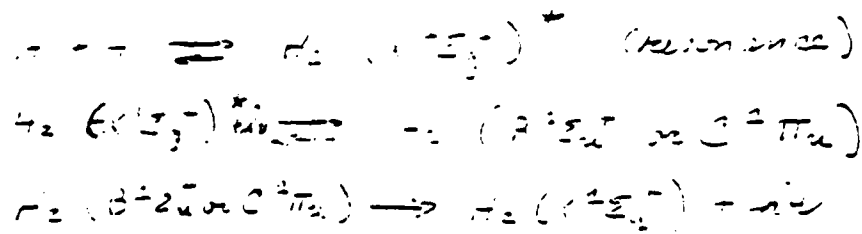
The most likely candidates for resonances are $J=4$. $v=14$ ($E = 4.5$ cm^{-1}, $\Gamma = 0.006$ cm^{-1}) and $J=5$. $v=14$ ($E = 44.7$ cm^{-1}, $\Gamma = 6.0$ cm^{-1}). The $J=4$ resonance is the most appealing because of its low energy. and its long lifetime (6×10^{-9} sec). Its narrow width means. however. that only a small fraction of collisions will have a collision energy needed to form the resonance. For radiative assistance. absorption into a vibrational level of the B or C state followed by spontaneous emission into a distribution of levels of the X-state was considered. Einstein A and B coefficients for all relevant transitions were calculated (a table is available). A promising sequence is absorption from $v=14$. $J=4$ of the ground state to $v=6$. $J=3$ of. the B-state ($B = 1 \times 10^4$ cm/J. $\lambda = 162.139$ nm) followed by spontaneous emission back to the ground state. Some A-coefficients are given in the table below.

All transitions from v=8, J=3 of the B-state. Units 10^8 sec^{-1}

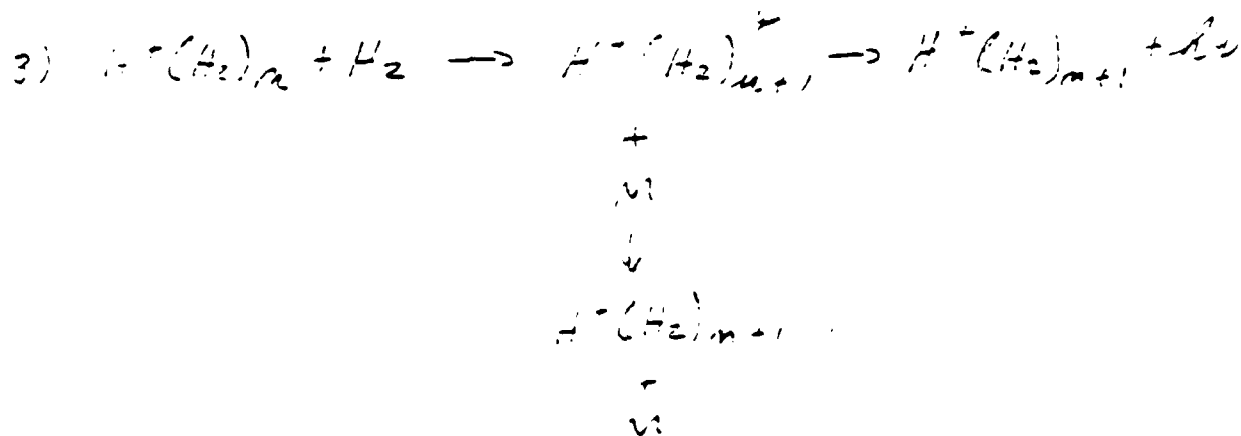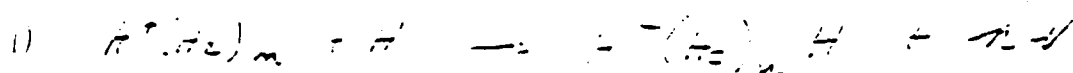| v	J=2	J=4
0	1.7 (102.50 nm)	1.2 (103.50 nm)
1	0.74	0.59
2	0.05	0.18
3	1.1	0.50
4	0.02	0.10
5	1.1	1.1
6	0.02	0.0007
7	0.99	1.05
8	0.10	0.000003
9	0.07	1.05
10	0.05	0.002
11	1.02	0.89
12	0.68	1.4
13	3.3	2.2
14	0.41	0.26

In addition to these bound-bound transitions, there will also be bound-free transitions leading to dissociation. It is clear that through the spontaneous emission, a small, but significant number of molecules will end up in v=0, J=2 or 4. If molecules in higher vibrational levels can be selectively photoionized, a small population of vibrationally cold H_2 can be maintained. The laser power required to make the process proceed efficiently can be estimated by requiring the absorption rate to be equal to the spontaneous emission rate (note that the rate of decay of the resonance, 1.7×10^8 sec^{-1}, is also comparable to the spontaneous emission rate). The units of B are chosen such that if it is multiplied by the integral of the product of the line-shape functions (in cm^{-1}) of the laser and of the transition and by the laser power in watts/cm^2 a transition rate in sec^{-1} is obtained. For the sake of definiteness, assume the laser line shape is much narrower than 0.006 cm^{-1}, in which case the integral of the product of normalized line-shape functions is simply $1/\pi\Gamma$, where Γ is the width of the resonance (0.006 cm^{-1}). We then want $B \cdot \pi\Gamma \times P = 2.0 \times 10^8$. This gives us a laser power required of $P = 400$ Watts/cm^2. Given a translational energy distribution for the reactant H atoms, an overall rate for the

54

production of H_2 molecules in each vibrational state could be calculated as a function of laser power from the numbers given above.

Question: What are the rates of competing processes, such as two-photon ionization?

REACTIONS TO FORM LARGER CLUSTER IONS

Many possible reactions have been discussed for getting from H_3^+ to larger cluster ions. In this section, the notation $H^-(H_2)_n$ will be used for odd cluster ions and $H^+(H_2)_nH$ for the even cluster ions. Three of the more promising are listed below

1) $H^+(H_2)_m + H^- \longrightarrow H^-(H_2)_m H + H_2 + H$

2) $H^+(H_2)_m H + H_2 \longrightarrow H^-(H_2)_{m+1} + H$

3) $H^-(H_2)_n + H_2 \longrightarrow H^-(H_2)_{m+1} \longrightarrow H^-(H_2)_{m+1} + H_2$

$$+$$
$$\downarrow$$
$$\psi$$
$$H^-(H_2)_{m+1}$$
$$\rightarrow$$
$$\psi$$

The rates of none of these processes is known. In the first process, approach can be on the ground state surface, the excited state surface that correlates with ground state reactants, or a more highly excited state

55

surface if the H is initially excited. The second process should be very favorable if vibrationally cold H_2 is used. The third process is important because it allows the growth of larger clusters with only one reactant (H_2), albeit a difficult one to handle. The reaction will be enhanced by the numerous resonances that probably exist (by analogy with H_3^+). The central question is: What are the relative lifetimes of the resonances toward dissociation as compared to their lifetimes toward radiative (infrared) relaxation or relaxation via a third body?

Question: If H_2 and H_3^+ collide in a single collision environment, will any stable H_5^+ be formed? If the H_2 is initially vibrationally excited, how will that affect the outcome? Will the vibrational energy of the H_2 be rapidly transferred to the cluster, thus causing it to fragment; will the charged cluster induce a dipole in the H_2 allowing it to radiate before the excess energy can cause fragmentation; or will the energy gradually leak into the cluster at a rate that can be radiated away?

RELAXATION BY A THIRD BODY

For all the processes discussed here, it would obviously be advantageous to have a third body available for relaxation processes. It has been assumed above that the environment is at low density. This is because the proposal for anti-matter condensation involved ion traps and a neutral hydrogen atom laser-cooled "molasses." Each of these is limited to low density (about 10^7 for the ion trap and perhaps 10^{11} cm^{-3} for the molasses). Three-body collisions are then infrequent, even if resonances are used.

Question: Are there alternative methods that would yield higher densities so that three-body collisions will be effective in removing the energy of reaction resulting from the exoergicity of cluster ion formation? Can a cold plasma be used? What happens in a tokomak or other plasma confinement device when the energy is lowered? Are cluster ions produced?

57

The Formation of Hydrogen Cluster Ions
from Ion-Molecule Association Utilizing H_2

D. C. Tardy

Tardy's summary (7/17/86)

The formation of H_{2n+1}^+ clusters from the association reaction

$$H_2 + H_{2n-1}^+ \quad ---> \quad H_{2n+1}^+(E)$$
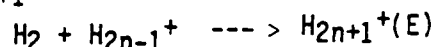
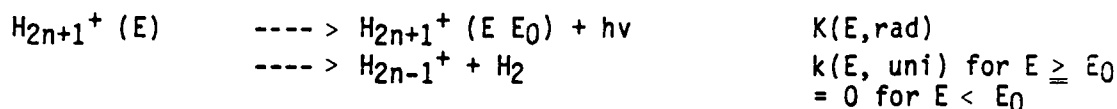has a minimum excergicity of approximately 2000 cm^{-1} which is distributed between the internal degrees of freedom of H_{2n+1}^+, if this energy is not removed, then the association complex will undergo unimolecular elimination of H_2 (the critical energy E_0, for this process is just the minimum excergicity for the association reaction). In competition with the H_2 elimination is collisional or radiative (infrared emission) stabilization; at low pressures radiative emission is dominant. Thus the probability for observing H_{2n+1}^+ from the association reaction, P(E), is given by

$$k(E,rad)/(k(E,rad) + (k(E,uni))$$

where the pertinent processes are:

$$H_{2n+1}^+ (E) \quad ----> \quad H_{2n+1}^+ (E\ E_0) + hv \qquad K(E,rad)$$
$$----> \quad H_{2n-1}^+ + H_2 \qquad k(E, uni) \text{ for } E \geq E_0$$
$$= 0 \text{ for } E < E_0$$

If the association energy is not coupled to the internal modes of the cluster, then elimination will occur in a time comparable to the vibrational period (i.e., 10^{13} seconds) and further associations will not be possible. However with strong coupling the lifetime relative to elimination is substantially increased as the energy can be partitioned between more vibrational modes. In a similar fashion the radiative lifetime will be affected. If the energy is statistically distributed, then k(E,uni) can be computed from RRKM theory and an average radiative lifetime can be computed by using statistical vibational mode population distribution and Einstein coefficients for each vibrational energy level (an effective Einstein coefficient is calculated). Since these rate constants have different dependences on the vibrational frequency pattern, it is important to know how the stabilization probability depends upon cluster size.

A group of six frequencies (4516, 373, 343, 114, 114, 63) which correlate with the six degrees of freedom of H_2 was determined from Schaefer's vibrational frequencies for H_7^+ and H_9^+. An integral multiple of this group was added to the frequencies of H_9^+ to simulated H_{2n+1}^+. The activated complex frequencies were identical to the ion except that the 373 mode was chosen as the reaction coordinate (373 ---> 0) and the four modes, 343, 114, 63) correlating with rotation and translation were reduced by a factor of two. This provided a consistent pattern to simulate vibrational frequencies for clusters larger than H_9^+. The absolute rate constants for these clusters may have large errors (<10) but the error in the relative change of the rate constant when H_2 is added should be small.

Average Einstein coefficients, k(E,rad), were computed assuming that the Einstein coefficient scales as v^3 and m (where v is the vibrational frequency and m is the vibrational energy level in units of hv). An average Einstein coefficient of 2 x 10^{-1} sec^{-1} was computed when a 4000 cm^{-1} mode was assumed to have an Einstein coefficient of 10^3 sec^{-1}; this average value was relatively independent of cluster size for n 9.
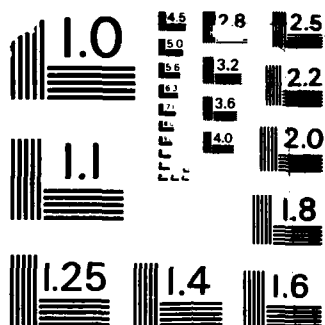
MICROCOPY RESOLUTION TEST CHART

NATIONAL BUREAU OF STANDARDS-1963-A

Rate constants, $k(E,uni)$, were calculated at two total energies, E_0 and $E_0 + n/2 * 4000$ corresponding to the total available internal energy being the complex dissociation energy and the complex dissociation energy plus 4000 cm^{-1} for each H_2 moiety (each H_2 have 1 quantum of vibrational energy). The results are:

n		$k(E_0,uni)$		$K(<E>,uni), <E>$		$P_n(E_0)$	
4	H_9^+	8.8	10^6	7.4 10^{12} :	8000	2.2	10^{-8}
5	H_{11}^+	1.7	10^5	5.8 10^{12} :	10000	1.2	10^{-6}
6	H_{13}^+	6.7	10^3	4.9 10^{12} :	12000	2.9	10^{-5}
8	H_{17}^+	3.5	10	3.9 10^{12} :	16000	5.6	10^{-3}
10	H_{21}^+	5.5	10^{-1}	3.5 10^{12} :	20000	2.7	10^{-3}
12	H_{25}^+	1.7	10^{-2}	3.1 10^{12} :	24000	0.91	
14	H_{29}^+	8.2	10^{-4}	2.9 10^{12} :	28000	1.00	
16	H_{33}^+	5.6	10^{-5}	2.9 10^{12} :	32000	1.00	

Two points are clear from these calculations:

i.   any internal energy in excess of the dissociation energy (i.e., that due to internal energy of H_2 or H_{2n-1}^+ and relative translational or rotational energy of the collisions partners) will substantially decrease the elimination lifetime so that radiative stabilization will not be competitive

ii. clusters larger than H_{29}^+ (the critical size) are quantitatively stabilized by radiative emission.

Hence the bottleneck for the formation of large clusters is the stabilization of the small clusters. Once the critical cluster size is reached, the only constraints for further addition are that the increase in the rate constant due to an increase in internal energy is offset by the decrease in the rate constant due to the increase in the number of vibrational frequencies. With the proper dependence of $k(E,uni)$ on E and the number of vibrational frequencies the association rate (addition of H_2) may be increased so that there still is a low probability for H_2 elimination; this seems feasible for clusters larger than the critical size.

It is critical that radiative lifetimes be obtained and unimolecular rate constants are verified. If the association excergicity does not couple to the internal degrees of freedom of H_{2n+1}^+, then $k(E,uni)$ will not decrease with cluster size and stabilization will be an extremely improbable event; a critical size where $P_n(E)=1$ will not exist. The above rate constant calculations will be an upper limit if the true density of vibrational states is larger than we have assumed; spectroscopic results of Carrington indicate that this may be the case.

Recommendations for a Workshop on the Cooling, Condensation and Storage of Hydrogen Cluster Ions

J. T. Bahns and W. C. Stwalley

July 11, 1986

The purpose the proposed workshop is to analyze specific problems associated with the condensation of antihydrogen into a high density form. Detailed planning of the University of Dayton sponsored Workshop on the Cooling Condensation and Storage of Hydrogen Cluster Ions (CCSHCI) is currently in progress. This report outlines the detailed recommendations for this workshop as determined in the HCISG meetings.

The workshop will, at the onset, make three basic assumptions: First, that the basic building blocks for the "containerless" condensation can be produced in unlimited amounts and consist entirely of the cold (translationally as well as internal degrees of freedom where this applies) particles H, H^+, e^-, and possibly H_2. Unlimited amounts of photons (from VUV to IR) are also presumed available, and are preferred as a third body. Second, that it is in fact possible to synthesize large ($N > 10^7$), cold hydrogen cluster ions by some "containerless" method(s). Third, it is assumed that these large clusters ions are useful; see report by W. C. Stwalley, p. 2.

The CCSHCI workshop will be held at the Stanford Research Institute, Menlo Park, CA. on January 8-9, 1987. It will feature at least 10 participants with outstanding qualifications in the task-relevant fields of hydrogen cluster ions, ion traps, and laser cooling (total attendance shall be less than 30. Besides specific tasks, the participants will:

1. Identify and outline specific condensation pathways to $N=11$.

2. Examine the validity of the cluster ion concept as a sound approach.

63

3. Outline a plan including relevant experimental and theoretical issues.

4. Identify areas of uncertainty and suggest solutions to "problem areas."

Each participant will provide oral and written presentation of a relevant topic in his field of expertise. The written reports will be compiled to form the Proceeding of the CCSHCI Workshop. Among the topics to be covered are:

1. The even-and odd-numbered positive hydrogen cluster ions.

2. The even-and odd-numbered negative hydrogen cluster ions.

3. Radiative and dissociative recombination pathways using hydrogen cluster ions.

4. Hydrogen cluster ion electronically excited states.

5. Hydrogen cluster ion transition state spectroscopy.

6. The synthesis, condensation, and confinement of antihydrogen in ion traps.

7. Laser cooling of many-state systems.

8. Laser photofragmentation studies of hydrogen cluster ions.

9. The infrared, visible, and ultraviolet spectroscopy of the hydrogen cluster ions.

10. Hydrogen atom formation.

The participants under consideration include (* indicates
those assigned in the itinerary):

*	R. Forward	Hughes Research
	L. Friedman	Brookhaven National Laboratory
*	G. Gabrielse	University of Washington
*	H. Helm	Stanford Research Institute
	D. Konowalow	State University of New York (Binghamton)
*	Y. Lee	University of California, Berkeley
	H. Michels	United Technologies Research
*	B. Miller	University of California, Berkeley
	B. Mitchell	University of W. Ontario
	J. Muckerman	Brookhaven National Laboratory
*	T. Oka	University of Chicago
	W. Phillips	National Bureau of Standards (Gaithersburg)
	K. Sando	University of Iowa
*	R. Saxon	Stanford Research Institute
	R. Saykally	Stanford Research Institute
*	H. Schaefer II	University of California, Berkeley
*	W. Stwalley	University of Iowa
	D. Tardy	University of Iowa
	D. Wineland	National Bureau of Standards (Boulder)

65

AGENDA
1/8/87

Topic/Activity	Participant	Time
Introduction to Antimatter Propulsion/Hot to Cold Antiprotons and Positrons	R. L. Forward	8:00-8:45
Large Hydrogen Cluster Ions	W. C. Stwalley	9:00-9:30
Ion traps	G. Gabrielse	9:45-10:15
Laser Cooling of H and H_2	W. Phillips	10:30-11:15
Cluster Ion Synthesis	J. T. Bahns	11:30-12:15
Lunch	----------	12:30-1:30
Positive and Negative Cluster Ion Energetics	H. Helm	1:30-2:00
Ion-Molecule Processes: Radiative Stabilization Photofragmentation Photodetachment	H. Schaefer III	2:15-2:45
Atom and Molecule and Alternate Additions (Positive and Negative) Associative Pathways	Y. Lee	3:00-3:45
Discussion: Review and Key Problems	(J. T. Bahns)	4:00-6:00

66

Introduction: Key Problems	J. T. Bahns	8:00-8:30
H_3^+ Transition State: Stimulated (Vis-IR)	W. Miller	8:45-9:15
H_3^+ Transition State: Spontaneous (UV-Vis)	R. Saxon	9:30-10:00
H_n^+ IR Spectroscopy and A. Carrington's Paper	T. Oka	10:30-11:00
Discussion	(J. T. Bahns)	11:15-12:30
Lunch	----------	12:00-1:30
Research Strategy and Discussion (Theory and Experiment)	(J. T. Bahns)	1:30-4:00
Prospects for Funding	H. Weichel or J. Prince	4:00-4:30
Closing Comments	J. T. Bahns	4:30-?

SUMMARY

From the analysis presented here, the "cluster ion approach" to the problem of "containerless" condensation seems valid. The most basic assumption of the study was that the low energy reagents (<.1eV) (beams of protons, electrons, and hydrogen atoms) will eventually become available resulting in an unlimited supply of reagents (a large assumption since these sources do not yet exist). The results of this study seem to justify research leading to the development of these sources. Although calculations exist, there have been no experimental studies that we are aware of to measure the hydrogen atom recombination rates, densities, and energy dependences; this seems surprising for such a fundamentally simple system consisting of a proton an electron, and a third body, which may be another proton, electron, or photon. Another assumption, perhaps serious, is that the laser sources needed for cooling hydrogen atoms or for stimulating recombination will also become available. A cooling laser for molecules is not considered desirable or feasible. If the proposed method of condensation is possible, the results suggest the need for large volume hybrid ion trap devices compatible with cold reagent beams. Research involving ion-atom radiative association of the smallest positive hydrogen cluster ions, beginning with the formation of atoms, is thought to be of highest priority.

With the above assumptions the study group analysis has focused primarily on the radiative formation of hydrogen cluster ions ranging in size from N=2 to the bulk limit. It was found that H_2^+ can be radiatively formed but the added constraint of having it vibrationally cold is difficult, it should be possible to calculate the production rates if they are not available. The production and manipulation of H_2 is difficult and should be avoided if possible; theoretical studies are probably sufficient at this time. Transition state calculations and experiments should be performed on the next larger

systems H_3^+ and H_4^+ to determine if they can be produced by
radiative processes, and the rates, branching ratios, and energy
dependences measured. For the synthesis of larger cluster ions
from ion-molecule association on the ground state manifold, a
simple model predicted that for energies near threshold
radiative stabilization should be competitive with unimolecular
decomposition for cluster ions $N \approx 30$. This radiative association
process is of course limited by the radiative lifetimes; these
need to be measured. The threshold cluster ion size for the
corresponding ion-atom association is not known but is likely
$N > 600$.

It is recommended that the CCSHCI Workshop be held and that
calculations of the radiative properties of the H_3^+ and H_4^+
systems be done, followed by experimental verification. More
fundamentally, the rates, densities, and energy dependences
should be measured for hydrogen atom formation via three-body
recombination.

END
DATE
FILMED

4-88
DTIC